# THE DEVELOPMENT AND MODELING OF AN ETHANOL PRODUCTION BIOCATALYTIC SYSTEM WITH CELL RETENTION

*by*

**Thapelo Mokomele**

Thesis presented in partial fulfillment
of the requirements for the Degree
of

Master of Engineering
(Chemical Engineering)

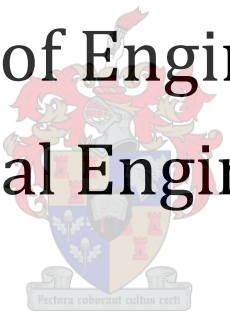

in the Faculty of Engineering
at Stellenbosch University

**Supervisor:**

Prof. K.G.Clarke

**Co-Supervisor:**

Dr. L.H. Callanan

December 2014

# DECLARATION

By submitting this thesis electronically, I declare that the entirety of the work contained therein is my own, original work, that I am the sole author thereof (save to the extent explicitly otherwise stated), that reproduction and publication thereof by Stellenbosch University will not infringe any third party rights and that I have not previously in its entirety or in part submitted it for obtaining any qualification.

**Thapelo Mokomele** **2014**

…… ……..

Signature Date

# ABSTRACT

Ethanol produced from renewable sources such as lignocellulosic biomass has been touted as a promising solution to the finite supply of energy from fossil fuels; its economical production via an environmentally benign process being the ultimate goal .Conventional cellulosic ethanol production strategies have focused on the fermentation of sugars obtained from lignocellulosic biomass, with yeasts used as the fermentation biocatalysts.

Lignocellulosic materials are primarily composed of cellulose, hemicellulose and lignin. The cellulose carbohydrate is a glucose homopolymer, whilst the hemicellulose fraction is composed of the hexose sugars glucose, mannose, and galactose, and pentoses xylose and arabinose. Although the relative proportions of the available monomeric sugars in lignocellulosic materials are dependent on the raw material and the efficacy of the biomass chemical and/or enzymatic hydrolysis, glucose and xylose typically constitute the greatest quantity of the fermentable sugars. Yet, whilst wild-type yeast strains are capable of metabolizing hexose sugars they are unable to ferment xylose which is a major constituent of the pentose fraction. Hence, for improving process economics, the conversion of xylose and glucose become imperative for cost-effective ethanol production processes.

Wild type *Zymomonas mobilis* has been demonstrated to exhibit superior ethanol production kinetics from glucose-based substrates over *Saccharomyces cerevisiae,* suggesting significant promise of this organism as a vehicle for renewable energy production. Genetically modified *Z. mobilis* 8b has demonstrated immense promise towards the efficient conversion of glucose and xylose with enhanced stability and retention of native activity for producing hexose and pentose fermenting enzymes. Moreover, in view of its GRAS status, *Z. mobilis* 8b is one of the most promising engineered fermentation biocatalysts to date.

To this end, the principle objective of this research was to study the biological performance of *Z. mobilis* ZM4 and *Z. mobilis* 8b in batch culture, and subsequently evaluate its performance in continuous culture. Two continuous culture strategies were evaluated, i.e. continuous culture (without cell recycle) and continuous culture with cell recycle via a cross-flow membrane cell (or membrane recycle bioreactor (MRB)). The ultimate viability of the batch, continuous culture (without cell recycle), and MRB was evaluated based on their overall performance as indicated by the ethanol volumetric productivity, ethanol yield and final ethanol concentration. The research approach undertaken in this work involved the division of the project into four main segments, i.e. the optimization of the fermentation conditions in batch culture, the design and characterization of a microfiltration unit for cell separation and recycling, the quantification of the kinetics of *Z. mobilis* in continuous culture (with and without cell recycle) and the kinetic modeling of the continuous culture and cell recycle system.

The optimization of the fermentation conditions in batch culture was performed using two 3-level 2-factor ($3^2$) full statistical designs in view of finding the optimal combination of temperature and initial fermentation pH that led to an optimum volumetric productivity and ethanol yield. The first $3^2$ full factorial statistical design accounted for the fermentation of a 50g.$L^{-1}$ glucose substrate by wild-type *Z. mobilis* ZM4. The optimum fermentation temperature and pH for *Z. mobilis* ZM4 corresponded with literature default values of 30 $^oC$, pH = 6-5.5. The second factorial design considered the co-fermentation of glucose and xylose in a xylose-rich substrate (37g.$L^{-1}$ xylose, 13g.$L^{-1}$ glucose) by *Z. mobilis* 8b (a ZM4 derivative). The optimum fermentation temperature and pH for *Z. mobilis* 8b were at 33.5 $^oC$, pH = 6.5-6. These results showed that the optimum fermentation temperature and pH for mixed-sugar hydrolyzate fermentation is dependent on the sugar composition and the fermentative microorganism strain. Moreover, presence of glucose was shown to have an indirectly positive impact on the overall rate of xylose consumption through its rapid but preferential consumption rate. However, the presence of glucose did not have a significant effect on the specific xylose consumption rate nor the ethanol yield from xylose.

The microfiltration unit was characterized by evaluating the filtration performance of cell-free fermentation media in response to changes in the operating hydrodynamic conditions. It was found that increasing the cross-flow velocity (CFV) and decreasing the substrate concentration resulted in an increase in both the membrane permeability and the membrane critical flux. Moreover, internal fouling by the fermentation media generally increased with an increase in the substrate concentration.

A central composite design (CCD) was used to quantify the significant process operating parameters on the pseudo-steady state permeate flux rate in view of selecting the operating conditions that permitted high flux rates. The ensuing ANOVA analysis revealed that the cell concentration, trans-membrane pressure (TMP), cross-flow velocity (CFV) and the TMP-cell concentration interaction all had a significant effect on the pseudo-steady state permeate flux through the microfiltration unit. Moreover, a quadratic mathematical model fitted by non-linear regression to the CCD experimental data was sufficient to predict the pseudo-steady state permeate flux as a function of the TMP, CFV and cell concentration. Permeate flux recovery though periodic membrane back flushing did not have a significant effect on recovering the permeate flux of cell-containing fermentation media.

The process performance of the batch, continuous culture (without cell retention) and MRB process strategies was performed and compared for the fermentation of a 50-50g.$L^{-1}$ glucose-xylose synthetic substrate with *Z. mobilis* 8b as the ethanologen. Considering this substrate composition and concentration, it was found that the optimal volumetric productivity from batch and continuous culture (without cell retention) was 1.42 and 4.58 g EtOH.$L^{-1}$.$h^{-1}$ (at D = 0.11$h^{-1}$) respectively. The optimal volumetric productivity of the latter was limited by the decrease in the ethanol concentration below the minimum concentration of 40.g. $L^{-1}$ (or 4% (w/v)) at dilution rates greater than D = 0.11$h^{-1}$. The minimum concentration has been reported in many techno-economic ethanol

production publications to be significant towards the minimization of energy and economic requirements for ethanol recovery by distillation.

At the same feed substrate composition, the volumetric productivity of the MRB fermentation strategy was limited to 1.15 g $EtOH.L^{-1}.h^{-1}$ whilst operating the microfiltration unit at a TMP of 100kPa and a CFV of $0.433m.s^{-1}$. The volumetric productivity of the MRB system was limited by severe membrane fouling in the microfiltration unit and the subsequent the low hydraulic dilution rate obtained from the system. As a result, it was concluded that the volumetric productivity of the MRB system was not limited by the rate of ethanol production but by the system hydraulic dilution rate (i.e. rate of ethanol removal from the system). The improvement of the hydrodynamic conditions was touted as a potential area for increasing the viability of the MRBprocess strategy.

Nevertheless, in comparing the continuous culture (without cell retention) to the MRB process strategy at the same dilution rate and feed substrate composition, it was determined that the volumetric productivity of both systems was indeed the same.

Kinetic modeling of the MRB fermentation strategy was performed using a mass balance around the system and simulating the subsequent ordinary differential equations (ODEs) in Excel™. The 4th order Runga-Kutta numerical method was used to solve the system of ODEs within the initial values estimated using the experimental data obtained during the start-up period. Fitting the system of ODEs to the experimental data was achieved by defining a goal term i.e. the total residual sum of squares ($RSS_{total}$). Parameter estimation was achieved by using Excel™'s Solver function as the goal-attaining tool for minimizing $RSS_{total}$ by varying the kinetic parameters. The adjusted correlation coefficient ($R^2_{adj}$) and the minimized $RSS_{total}$ were used as comparative indications of the goodness of the model fit.

Considering the co-fermentation of a 50-50 $g.L^{-1}$ glucose-xylose substrate, the MRB kinetic model accurately predicted the CDW, glucose, xylose, acetate and ethanol concentrations. The high degree of model fit was highlighted by adjusted correlation coefficients consistently greater than 0.98 and the minimized $RSS_{total}$ being smaller than 0.09. The MRB kinetic model achieved similar results for 25-75 $g.L^{-1}$ and 75-25 $g.L^{-1}$ glucose-xylose substrate co-fermentations. Moreover, using the pseudo-steady state statistical model, it was projected that a minimum of eight membranes would be required to meet the minimum ethanol concentration and exceed the volumetric productivity of the continuous culture (without cell retention) fermentation strategy.

In light of the principle objective, this work demonstrated that the MRB system performance was highly dependent on controlling and/or minimizing membrane fouling on the microfiltration unit. Hence, under its current operating apparatus and conditions, the potential of the current MRB system for the co-fermentation of a synthetic glucose-xylose substrate was limited. However, through the improvement of the microfiltration operating hydrodynamic conditions and/or

increasing the microfiltration unit surface area, the potential for this fermentation strategy can be maximized.

# OPSOMMING

Die produksie van etanol vanaf hernieubare bronne word beskou as 'n belowende oplossing vir die beperkte voorraad van fossielbrandstowwe. Vir onwikkeling van die proses is die ekonomiese produksie deur 'n omgewingsvriendelike proses die belangrikste doelwit. Konvensionele etanol produksie strategieë het tot dusver gefokus op die fermentasie van suikers, afkomstig van lignosellulose wat lignien, hemi-sellulose en sellulose bevat. Gisse, wat as biokataliste dien, word gebruik in die proses. Xilose en glukose is belangrike komponente van lignosellulose biomassa, wat verkry word deur die ensimatiese of chemiese hidroliese van onderskeidelik hemisellulose en sellulose. Waar wilde-tipe gis variasies heksose suikers kan metaboliseer, is hulle egter nie in staat daartoe om xilose, 'n belangrike komponent van die pentose fraksie, te fermenteer nie. Gevolglik word die omskakeling van xilose en glukose uiters belangrik vir die ontwikkeling van 'n ekonomiese etanol produksie proses.

Daar is voorheen getoon dat wilde-tipe *Zymomonas mobilis* beter reaksie kinetika lewer vir die produksie van etanol as *Saccharomyces cerevisiae.* Hierdie feit is belowend vir die gebruik van hierdie organisme vir hernieubare energie produksie. Geneties veranderde *Z. mobilis* 8b het die potensiaal om beide xilose en glukose tot naby aan hulle teoretiese opbrengs te fermenteer. Verder, in die lig van sy GRAS status, is *Z. mobilis 8b* tans een van die mees belowende fermentasie biokataliste wat tot dusver ontwikkel is.

Vir hierdie rede is die hoof doelwit van hierdie studie die ontwikkeling, modellering en assesering van die gebruik van 'n membraan bioreaktor (MRB) vir die omskakeling van 'n sintetiese glukose-xilose substraat na etanol met die doel om die volumetriese produktiwiteit van die fermentasie proses te verbeter. Die finale bruikbaarheid van die MRB fermentasie proses is evalueer deur die etanol volumetriese produktiwiteit en die etanol opbrengs relatief tot die van konvensionele stategieë, insluitende 'batch' en kontinue reaktors. Die navorsings strategie van die studie behels die verdeling van die projek in vier dele: die optimisering van fermentasie kondisies, die ontwerp en karakterisering van 'n mikrofiltrasie eenheid, die kwantifisering van die MRB fermentasie kinetika en die kinetiese modellering van die MRB sisteem.

Die optimisering van die fermentasie kondisisie is uitgevoer deur twee 3-vlak, 2-faktor volle statistiese ontwerpe met die doel om die kombinasie van temperatuur en aanvanklike fermentasie pH te vind wat lei tot 'n optimale volumetriese produktiwiteit en etanol opbrengs. Vir glukose substraat fermentasie vergelyk die optimale fermentasie temperatuur en pH vir *Z. mobilis* ZM4 goed met algemene literatuur waardes van 30°C en pH = 6-5.5. Vir 'n xilose-ryk substraat is die optimale waardes vir *Z. mobilis* 8b egter 33.5°C en 'n pH van 6.5-6. Hierdie resultate toon dat die optimale fermentasie temperatuur en pH vir gemengde suiker 'hydrolyzate' fermentasie afhanklik is van die

suiker komposisie en die tipe fermentasie mikro-organisme wat gebruik word. Verder is daar getoon dat die teenwoordigheid van glukose indirek die algemene tempo van xilose gebruik positief beïnvloed deur sy vinnige, maar voorkeur, benuttingstempo. Die teenwoordigheid van glukose het egter nie 'n merkwaardige effek gehad op die spesifieke xilose gebruik of die etanol opbrengs vanaf xilose nie.

Die karakterisering van die mikrofiltrasie eenheid is gedoen deur die evaluering van die filtrasie vermoeë van selvrye fermentasie media in reaksie op veranderinge in die hidrodinamiese kondisies. Daar is bevind dat 'n toename in die dwarsvloei snelheid en 'n afname in substraat konsentrasie gelei het tot 'n toename in beide die membraan deurlaatbaarheid en kritiese vloeitempo van die membraan. Verder het die interne aangroei van die fementasie media in die algemeen vermeerder met 'n toename in die substraat konsentrasie.

Die bedryfsparameters met 'n merkwaardige invloed op die pseudo-gestadigde deurlatings vloeitempo is identifiseer deur 'n sentrale saamgestelde ontwerp, met die mikpunt om bedryfskondisies te kies wat hoë deurlatings vloeitempos toelaat. Die ANOVA analise toon dat die selkonsentrasie, trans-membraan druk, dwarsvloei snelheid en die trans-membraan druk-selkonsentrasie interaksie almal 'n merkbare invloed het op die pseduo-gestadigde deurlatingstempo van die mikrofiltrasie eenheid. Verder is 'n kwadratiese wiskundige model, gepas deur regressie, instaat daartoe om die die pseudo-gestadige konsentrasie te voorspel as 'n funksie van die sel konsentrasie, trans-membraan druk en dwarsvloei snelheid. Die herwinning van deurlatingsvloei deur periodiese membraan terugvloei het nie 'n merkwaardige effek gehad op die herwinning van die deurvloei van sel bevattende fermentasie media nie.

Die kinetiese prestasie van die MRB is ondersoek en vergelyk met 'batch' en kontinue 'culture' (met behoud van selle) proses strategieë, uitgevoer met eenderse eksperimentele kondisies met 'n 50-50g.$L^{-1}$ glukose-xilose sintetiese substraat. Deur hierdie substraat komposisie en konsentrasie te beskou is daar gevind dat die optimale volumetriese produktiwiteit vir 'batch' en kontinue 'culture' onderskeidelik 1.42 en 4.58 g EtOH.$L^{-1}$.$h^{-1}$ (by D = 0.11$h^{-1}$) was. Die optimale volumetriese produktiwiteit van die laasgenoemde is beperk deur die afname in die etanol konsentrasie tot onder die minimum konsentrasie van 40.g. L-1 (of 4% (w/v)) by verdunnings tempos van groter as D = 0.11$h^{-1}$. Hierdie minimum konsentrasie is noodsaaklik vir die minimalisering van energie en die ekonomiese vereistes vir etanol herwinning deur distillasie.

Die volumetriese produktiwiteit van die MBR is beperk tot 1.15 g EtOH.$L^{-1}$.$h^{-1}$, met dieselfde substraat komposisie in die voer, as die mikrofiltrasie eenheid bedryf is teen 'n trans-membraan druk van 100kPa en 'n dwarsvloei snelheid van 0.433m.$s^{-1}$. Die volumetriese produktiwiteit van die MRB is beperk deur ernstige membraan aangroeiing in die mikrofiltrasie eenheid en die lae hidroliese verdunningstempo wat dit tot gevolg het. Gevolglik is die gevolgtrekking gemaak dat die volumetriese produktiwiteit van die MRB nie beperk word deur die tempo van etanol produksie nie, maar deur die sisteem se hidroliese verdunningstempo (dit is die tempo van etanol verwydering uit

die sisteem). Die verbetering van die hidrodinamiese kondisies word dus aanbeveel as die beste area waardeur die prestasie van die MRB strategie verbeter kan word.

Ongeag hiervan is daar getoon dat die volumetriese produktiwiteit van die twee sisteme dieselfde is met dieslefde verdunningstempo en substraat komposisie in die voer.

Kinetiese modelering van die MRB is uitgevoer deur gebruik te maak van 'n massa balans oor die MRB sisteem en deur die ordinêre differensiaal vergelykings wat volg in Excel™ te simuleer. Die MRB kinetiese model het die CDW, glukose, xilose, asetaat en etanol konsentrasies goed voorspel by 'n fermentasie met 'n substraat van 50-50g.$L^{-1}$ glukose-xilose. Die goeie passing van die model is getoon deur aangepaste korrelasie koeffisiënte ($R^2_{adj}$) deurlopend groter as 0.98. Die MRB kinetiese model het soortgelyke resultate gelewer by 25-75.$L^{-1}$ en 75-25.$L^{-1}$ glukose-xilose substrate. Verder is daar voorspel deur die pseudo-gestadigde statistiese model dat 'n minimum van 8 membrane benodig sou word om die minimum etanol konsentrasie te bevredig en die volumetriese produktiwiteit van die kontinue 'culture' fermentasie strategie te oorskry.

In die lig van die primêre doel van die studie is daar getoon dat die werksverrigting van die MRB sisteem hoogs afhanklik is van die beheer en/of minimalisering van membraan aangroeiing op die mikrofiltrasie eenheid. Gevolglik is die potensiaal van die MRB sisteem vir die ko-fermentasie van sintetiese glukose-xilose substrate beperk by die huidige apparatuur en kondisies. Deur die mikrofiltrasie hidrodinamiese bedryfskondisies te verbeter en/of die mikrofiltrasie eenheid oppervlaksarea te vergroot kan die potensiaal van hierdie fermentasie strategie egter gemaksimeer word.

# ACKNOWLEDGEMENTS

Throughout the two years required to complete this research, there have been a number of individuals and entities who have a positive influence on the completion of this work. I hope to express my sincere gratitude to the following people for their unwavering contributions towards the completion of this work:

- ✓ For unrelenting passion, never-ending source of encouragement and for technical and theoretical assistance, thank you **Prof. K.G. Clarke** and **Dr. L.H. Callanan**. Without your guidance, support and contribution, this thesis would not be possible.
- ✓ For sponsoring the project, I would like to thank the Centre of Excellence. My unparalleled appreciation goes to the **Centre of Renewable and Sustainable Energy Studies** (CRSES) and to the **Stellenbosch University merit bursary scheme** for bursary support.
- ✓ For assistance and valuable discussions with regards to statistical analysis and model validation, I would like to convey a big thank you to **Dr. Lidia Auret**.
- ✓ For assistance with HPLC sample analysis, thank you **Manda Rossouw**. Moreover, for fermentation media viscosity measurements, thank you **Hanlie Botha**.
- ✓ I am also grateful to the **workshop staff** at the **Department of Process Engineering** (Stellenbosch University) for realizing my thoughts and ideas and subsequently manufacturing all my experimental apparatus.
- ✓ For moral support, friendship and never-ending evening but invaluable conversations, I would like to acknowledge my study colleagues**: Andre, Peter, Travis, Suandrie, Dietmar, Louise, Angelo, Jannean, Fran, Royston, Herman, Henri, James, Jamie**.
- ✓ To **my mother**, my pillar of strength and endless source of wisdom and encouragement, thank you for always believing in me. I have matured to the man I am today because of you and the conversation we had when I was a mere seven year old boy.
- ✓ To the **rest of my family and friends**, thank you for enduring and bearing with me.
- ✓ **Mpati Tsuebeane**, for being a constant source of support, love and patience, thank you.
- ✓ Lastly, I would like to give thanks to my **Father in Heaven** who is the giver of life and wisdom, for spiritual guidance and for paving the way for me to complete this thesis.

# TABLE OF CONTENTS

# LIST OF FIGURES

# LIST OF TABLES

# NOMENCLATURE

## *Symbols*

| | | |
|---|---|---|
| $A_{membrane}$ | Membrane area | $[m^2]$ |
| b | Fouling index | |
| $C_i$ | Initial concentration of species i | $[mol.l^{-1}]$ |
| $C_r$ | Concentration of species i in the retenate | $[mol.L^1]$ |
| $C_p$ | Concentration of species i or product in the permeate | $[mol.L^1]$ |
| $C_{so}$ | Initial glucose or xylose concentration | $[mol.L^{-1}]$ |
| $D_{eff}$ | Effective diffusivity | $[m^2/s]$ |
| $D_{Si}$ | Diffusion coefficient of the substrate solution | $[m^2/s]$ |
| $d_{pore}$ | Mean pore diameter | [m] |
| $F_x$ (P) | Extent of ethanol inhibition on cell growth | $[h^{-1}]$ |
| $F_p$(P) | Extent of ethanol inhibition on ethanol production | $[h^{-1}]$ |
| $G_x$ (S) | Extent of substrate inhibition on cell growth | $[h^{-1}]$ |
| $G_p$ (S) | Extent of substrate inhibition on ethanol production | $[h^{-1}]$ |
| J(t) | Permeate flux at time t | $[L.m^{-2}.h^{-1}]$ |
| $J_{cs}$ | Strong-form of the critical permeate flux | $[L.m^{-2}.h^{-1}]$ |
| $J_{cw}$ | Weak-form of the critical permeate flux | $[L.m^{-2}.h^{-1}]$ |
| $K_{sx}$ | Saturation constant | $[mol.L^{-1}]$ |
| $K_{ix,1}$ | Threshold substrate concentration for cell growth | $[g.L^{-1}]$ |
| $k_d$ | Mortality factor | $[h^{-1}]$ |
| $M_B$ | the molecular weight of the solvent | [g/mol] |
| $m_i$ | Maintenance energy coefficient | $[h^{-1}]$ |
| $M_{si}$ | Molecular weight of the substrate | [g/mol] |
| VP | volumetric productivity of ethanol | $[g.L^{-1}h^{-1}]$ |
| $p_{i,x}$ | Threshold ethanol concentration for cell growth | $[g.L^{-1}]$ |
| $p_{i,p}$ | Threshold ethanol concentration for ethanol production | $[g.L^{-1}]$ |
| $p_{,mx}$ | Maximum ethanol concentration for cell growth | $[g.L^{-1}]$ |
| $p_{,mp}$ | Maximum ethanol concentration for ethanol production | $[g.L^{-1}]$ |
| $q_{pmax}$ | Specific ethanol production rate | [g EtOH produced/h] |
| $q_{smax,\ glucose}$ | Specific glucose uptake rate | [g glucose consumed /h] |
| $q_{smax,xylose}$ | Specific xylose uptake rate | [g xylose consumed /h] |

| | | |
|---|---|---|
| $r_s$ | Rate of substrate utilization | [g substrate consumed/L/h] |
| $r_p$ | Rate of ethanol production | [g ethanol produced/L/h] |
| $R^2_{adj}$ | Adjusted correlation coefficient | |
| $s_i$ | Threshold substrate concentration | [$g.L^{-1}$] |
| $V_{tot}$ | Total reactor volume | [$m^3$] |
| $V_i$ | initial volume containing species i | [L] |
| $V_p$ | collective permeate volume | [L] |
| x | Biomass concentration | [mg $cells.L^{-1}$] |
| $Y_{p/s}$ | Overall product yield (ethanol) | [g EtOH produced/ g substrate consumed] |
| $Y_{x/s}$ | Overall biomass yield | [g cells produced/ g substrate consumed] |

***Greek Letters***

| | | |
|---|---|---|
| $\gamma$ | the dynamic viscosity of the solvent | [cP] |
| $\mu_{max}$ | the maximum specific growth rate | [$h^{-1}$] |
| $\Delta P$ | Pressure change between state 1 and state 2 | [kPa] |
| $\beta$ | Bleeding rate fraction | |
| $\alpha$ | glucose-xylose fermentation proportionality constant | |
| $\eta_0$ | fuid viscosity | [Pa.s] |

***Acronyms***

| | |
|---|---|
| ATCC | American Type Culture Collection |
| ED | Enter-Douroroff |
| EMP | Embden-Meyerhof-Parnas |
| MRB | Membrane Recycle Bioreactor |
| MWCO | Molecular Weight Cut-Off |
| NREL | National Renewable Energy Laboratory |
| ODE | Ordinary Differential Equation |
| OD | Optical Density |
| RSS | Residual Sum of Squares |
| SSF | Simultaneous Saccharification and Fermentation |
| SSCF | Simultaneous Saccharification and Co-Fermentation |
| TMP | Trans-Membrane Pressure |

# CHAPTER 1

# INTRODUCTION

*Biotransformation of lignocellulosic biomass into ethanol remains an essential component of the global initiative of minimizing the consumption of the diminishing fossil fuels and utilizing renewable sources for energy supply. In addition to the physio-chemical pre-treatment of lignocellulosic biomass, the co-fermentation of glucose and xylose is a critical step for the economic production of ethanol as an alternative biofuel. In this work, the co-fermentation of glucose and xylose, with Zymomonas mobilis as the biocatalyst, in cell retention systems is investigated with the ultimate goal being the maximization of the volumetric productivity of ethanol.*

## 1.1 BACKGROUND

Due to the diminishing fossil fuel reserves, the demand for an alternative fuel source has increased significantly in the last three decades. Moreover, concerns related to environmental security, economic stability, and more recently global warming; have aggravated the demand for an alternative fuel source. One particular area of interest has been the production of liquid transportation fuels from biomass with the main focus on alcohols as alternative fuel sources (Feltenstein, 1983; Lawford 1988). Biofuels such as ethanol produced from renewable energy sources have been widely considered as potential successors or as petroleum extenders (in blend form) for fossil fuel based petroleum fuels (Deanda et al. 1996; Dien *et al.,* 2003; Chander *et al.,* 2011).

In developing countries such as South Africa, the use of biomass such as corn as feedstock for the production of relatively low value biofuels (such as ethanol) becomes a debatable socio-economic issue due to the scarcity of water and food. Therefore, the production of biomass or feedstock materials for energy production should not compromise the availability of resources required for basic human needs. Second-generation ethanol production from the low-cost, non-edible, vastly available and renewable energy-source, lignocellulose, has attracted vast interest due to the the demand for alternative fuel sources (Lin and Tanaka 2006; Chander *et al.*, 2011; Davison and Scott 1988).

Glucose and xylose constitute the largest quantity of monomer sugars obtained from lignocellulosic biomass through enzymatic or chemical hydrolysis of the hemicellulose and cellulose fractions

respectively. As a result, the efficient bioconversion of both the glucose and xylose to ethanol is of central importance in the pursuit of cost-effective cellulosic ethanol production.

## 1.2 RESEARCH MOTIVATION

### 1.2.1 *Z. MOBILIS AS THE ETHANOL-PRODUCING BIOCATALYST*

The ethanologic microbe *Z. mobilis* has been reported to exhibit superior ethanol production kinetics relative to *S. cerevisiae* with respect to ethanol productivity, ethanol tolerance and sugar uptake, thereby suggesting significant promise of this microorganism as a vehicle for renewable energy production (Karsch *et al.,* 1983). Nonetheless, like yeasts, naturally occurring strains of *Z. mobilis* are incapable of metabolizing pentose sugars to ethanol (Swings and De Ley 1977; Gunasekaran and Chandra 1999; Chander *et al.,* 2011; Liu 2010; Bothast *et al.,* 1999; Mohagheghi *et al.,* 2002; M. Zhang *et al.,* 1995; Lawford and Rousseau 2002). However, the genetically engineered strain *Z. mobilis* 8b has demonstrated immense promise towards the efficient conversion of glucose, mannose, xylose and arabinose with enhanced stability and retention of native activity for producing hexose and pentose fermenting enzymes (Mohagheghi *et al.,* 2002; Mohagheghi *et al.,* 2004; Mohagheghi *et al.,* 2006; Chander *et al.,* 2011).

### 1.2.2 *POTENTIAL FOR CELL RETENTION IN BIOPROCESSING*

The economic feasibility of bioprocesses is largely dependent on the capability of the process for maximizing the product selectivity, maintaining stable and high volumetric productivity and the continuous removal of the product and inhibitory metabolic by-products from the fermentation broth (Dhariwal, 2007). To this end, continuous culture with membrane cell retention systems have shown significant promise for biological processes by facilitating effective cell-liquid separation, high cell densities within the bioreactor and increasing the potential for enhancing the process volumetric productivity and commercial appeal (Rogers *et al.,* 1980; Daubert *et al.,* 2003; Mercier-bonin *et al.,* 2001)

Nonetheless, Mercier-bonin *et al.,* (2001) noted that continuous culture with cell recycle via a membrane cell separation unit (or membrane recycle bioreactor (MRB)) generally encounter two obstacles. First, in aerobic bioprocesses, as the cell density increases within the bioreactor, the oxygen transfer capacity limits the achievable capacity of the microbial population (Mercier-bonin *et al.,* 2001; Daubert *et al.,* 2003). However, the anaerobic nature of both wild-type and recombinant *Z. mobilis* facilitate the metabolization of hexose and pentose sugars through the Entner-Douroroff pathway, which does not require an oxygen source during the fermentation process.

Secondly, the hydraulic dilution rate from the system is severely limited by the decline of the membrane permeate flux as a function of the biomass concentration and the duration of the culture. To this end, a major area of exploration for the evaluation of MRBs as alternative fermentation

process strategies is the understanding of operational approaches required for minimizing membrane fouling such as optimized hydrodynamic conditions (operating at sub-critical flux trans-membrane pressures and/or high cross-flow velocities) and periodic membrane back-flushing (Belfort et al., 1994; Carrère et al., 2001; Mercier-bonin et al., 2001; Pearce et al., 2011).

Considering the necessities for stable, continuous, highly productive bioprocesses; continuous culture cell retention systems provide an attractive alternative fermentation approach relative to conventional batch and fed-batch bioprocesses where product accumulation in the bioreactor may lead to a decline in the activity of the biocatalysts and a decrease in productivity.

### 1.2.3 Ethanol Production through Cell Retention

Lawford (1988) predicted that ethanol fermentation in closed-type continuous culture systems (operating at high cell densities due to total cell-recycle or retention) have the potential to be associated with 35-40% reduction in capital costs of fermentation equipment, 10-15% saving in product recovery through distillation, and 3-7% reduction in the overall production costs.

Rogers *et al.,* (1980) obtained the highest reported volumetric productivity for the fermentation of a synthetic glucose medium in a continuously stirred tank reactor (CSTR) with *Z. mobilis* ZM4 as the biocatalyst and with cell retention achieved through a cross-flow microfiltration unit. Their work demonstrated that ethanol concentrations of 60-65g.$L^{-1}$ can be maintained at high productivities at the reported cell densities of 30-60g.$L^{-1}$. At quasi steady-state, the optimum volumetric productivity of 120-200 g.$L^{-1}$.$h^{-1}$ (at 90% substrate conversion) was reported (Rogers *et al.,* 1980).

Based on their preliminary findings, cell retention through an external cross-flow unit demonstrated significant promise for ethanol production from a glucose substrate. Expanding from the work performed by Roger *et al.,* (1980), this work aims to investigate the fermentation of a glucose/xylose substrate within a cell retention system with a single channel external cross-flow microfiltration unit and using wild-type and recombinant strains of *Z. mobilis* as the biocatalysts. Whilst many fermentation strategies have been developed for the conversion of glucose based substrates to ethanol, no work has been published for the fermentation of a glucose-xylose substrate using *Z. mobilis* 8b as the biocatalyst.

## 1.3 Global Objective and Scope

The global objective of this work to study the biological performance of *Z. mobilis* ZM4 and *Z. mobilis* 8b in batch culture, and subsequently evaluate its performance in continuous culture fermentation strategies. Two continuous culture strategies were evaluated, i.e. continuous culture (without cell recycle) and membrane recycle bioreactor MRB. The ultimate viability of the batch, continuous culture (without cell recycle), and MRB was evaluated based on their overall performance as indicated by the ethanol volumetric productivity, ethanol yield and final ethanol concentration.

The scope of this research encompasses the use the wild-type strain *Z. mobilis* ZM4 to develop an ex-situ cell retention system with the design objectives being to facilitate the fermentation of a glucose based sugar substrate to ethanol. The system will thereafter be extended to facilitate the fermentation of a glucose-xylose substrate with the aid of the genetically engineered biocatalyst *Z.*

*mobilis* 8b. Due to the fundamental nature of this study, synthetic sugar mixtures were used as the substrate with effects of hydrolyzate inhibitory compounds such as HMF and furfural not included.

In light of the project scope, the principal aims of this work were to:

- ✓ statistically define optimum fermentation conditions, in terms of the fermentation temperature and pH, in view of maximising the volumetric productivity and ethanol yield in free-cell batch fermenter,
- ✓ design and characterization of a biocompatible microfiltration module for the effective retention of *Z. mobilis*,
- ✓ design a bioprocess consisting of a continuously operating bioreactor coupled with a cross-flow microfiltration membrane cell (i.e. MRB) and subsequently quantify the MRB fermentation kinetics relative to batch and continuous culture (without cell retention) at the same operational conditions,
- ✓ develop and validate a kinetic model for the prediction of the expected MRB process performance at various substrate compositions.

## 1.4 THESIS OUTLINE

An overview of the thesis layout is illustrated in *Figure 1*. This flowchart highlights the approach of this work into determining the viability and limitations of the batch, continuous culture and MRB fermentation strategies for ethanol production.

**Chapter 2** presents a critical literature survey on the potential of *Zymomonas mobilis* for ethanol production from the fermentation of sugars extracted from pre-treated lignocellulosic materials. Moreover, this chapter delves into the use of continuous culture with cell retention systems in bioprocessing and highlight areas of exploration within literature for the potential of MRBs for high productivity ethanol production. Lastly, the design considerations for the development of biocompatible microfiltration units and characterizing membrane fouling were underlined in **Chapter 3**.

**Chapter 4** provides the backbone of this work through the development of the project hypotheses and the fundamental project objectives. The subsequent chapters were based on the validation or rejection of these hypotheses.

**Chapter 5** delivers a detailed description of the methods implemented for preparing the fermentation cultures and the analytical techniques employed for the analysis of the glucose, xylose, ethanol and any other metabolic by-product concentrations. Moreover, the design of the experimental system and the experimental design are subsequently discussed. A stepwise development of a kinetic model for the prediction of the transient substrate, cell, and ethanol concentration profiles is derived in **Chapter 6**.

**Chapter 7** presents a detailed discussion of the results obtained from the following project segments: (1) the optimization of the of the fermentation conditions at shake flask level, (2) design and characterization of the microfiltration unit, (3) the quantification of the kinetics of *Z. mobilis* in continuous culture, and (4) the kinetic modelling of the developed process. The primary output from

this section was the quantification of the kinetics of *Z. mobilis* in batch, continuous culture (without cell retention) and continuous culture with cell recycle (MRB) fermentation strategies. The viability of each fermentation strategy was quantified by the ethanol yield, volumetric productivity and final ethanol concentration as performance indicators. Finally, **Chapter 8** presents a reconciliation of the key research objectives and a subsequent summary of the research outputs pertaining to the validation of whether these objectives have been met or not.

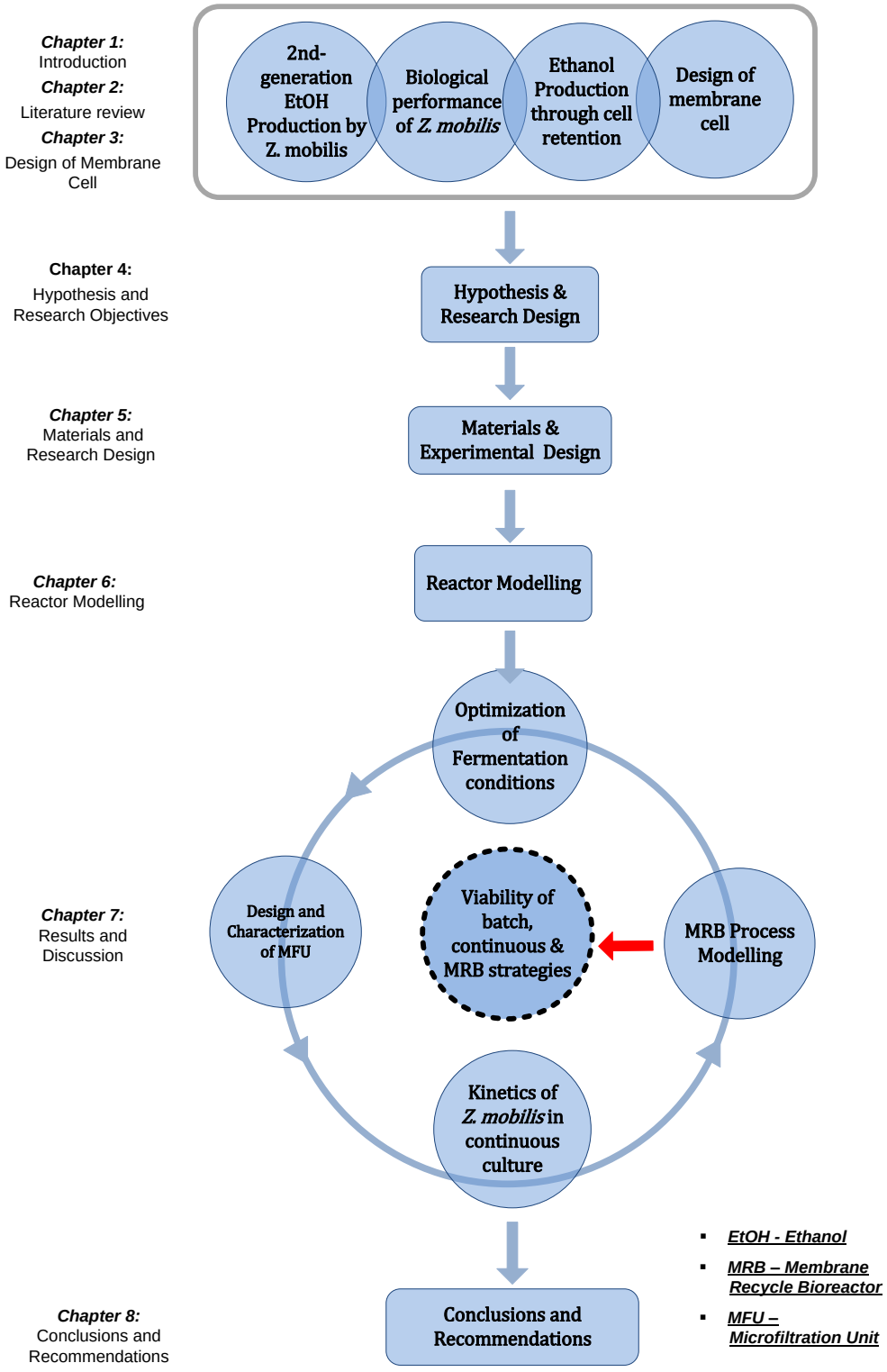


***Figure 1:*** *A layout of the thesis contents*

# CHAPTER 2

# ETHANOL PRODUCTION BY *Z. MOBILIS*

*Early bioethanol production studies have been performed in traditional batch reactors with yeast as the biocatalyst. The bacterium Zymomonas mobilis is recognized to be one of the fastest-acting ethanologen from glucose. This section reviews the potential of Z. mobilis for hexose and pentose fermentation and the factors that impact its kinetic performance. Moreover, physiological and bioprocessing approaches in view of improving the productivity of ethanol fermentation by this biocatalyst are reviewed.*

## 2.1 LIGNOCELLULOSIC BIOMASS

### 2.1.1 SECOND-GENERATION ETHANOL PRODUCTION

First-generation ethanol can be produced from many renewable sources of feedstock; typically starch and sugar crops such as sugar cane, wheat, and beet. However, first-generation biofuels tend to compete with the food supply chain whereby increased ethanol production/demand from food sources such as corn could result in higher corn prices and subsequently negatively impact the food industry (Refaat, 2012; Menon and Rao, 2012).The obstacles incurred in ethanol production from 'food' feedstock has lent toward the second-generation ethanol production through the biotransformation of lignocellulosic (LC) materials. LC materials potentially avoid direct competition for crops in the food supply chain through the use of crop and wood wastes as feedstock. Owing to their vast availability and low cost, LC biomass has been touted as a promising ethanol production feedstock (Stanley and Hahn-Hägerdal, 2010; Olsson and Hahn-Hägerdal, 1996; Lawford, 1988; Refaat, 2012; Zacchi, 2006; Zacchi *et al.*, 2007).

The most prominent lignocellulosic materials considered for ethanol production are hardwood, softwood, forestry residues, agricultural residues and municipal solid waste.

*Table 1* presents a sample of the composition of various lignocellulosic materials obtained from the four afore-mentioned feedstock sources. In general, the cellulose-hemicellulose (and subsequently the hexose-pentose sugar) distribution is dependent on the raw material. For example, the hemicellulose fraction for hardwoods and agricultural waste richer in pentose sugars compared to softwoods (Hahn-Hägerdal *et al.,* 2007).

***Table 1:*** *Composition of Different Lignocellulosic Materials*

| *Category* | *LC Material* | *Cellulose (%)[a]* | *Lignin (%) [a]* | *Hemi-cellulose (%)[†]* | *Ref.* |
|---|---|---|---|---|---|
| ***Agricultural Waste*** | Sorghum Straw | 32-35 | 15-21 | 24-27 | Vázquez *et al.,* 2007 |
| | Corn Stover | 35.1-39.5 | 11.0-19.1 | 20.7-24.6 | Menon & Rao, 2012 |
| | Sugarcane bagasse | 25-45 | 15-25 | 28-32 | Menon & Rao, 2012 |
| | Corn cob | 32.3-45.6 | 6.7-13.9 | 39.8 | McKendry, 2002 |
| ***Softwood*** | Spruce | 43 | 29 | 26 | Hahn-Hägerdal 1996 |
| | Softwood Stem | 45-50 | 18-25 | 24-40 | Howard *et al.,* 2003 |
| | Pine | 42-49 | 23-29 | 13-25 | Hahn-Hägerdal 1996 |
| ***Hardwood*** | Willow | 37 | 21 | 23 | Hahn-Hägerdal 1996 |
| | Hardwood Stems | 40-55 | 18-25 | 24-40 | Howard *et al.,* 2003 |
| | Aspen | 51 | 16 | 29 | Hahn Hägerdal 1996 |
| ***Forestry Residues*** | Saw Dust | 45-51 | 29 | 11-18 | Menon & Rao, 2012 |
| ***Municipal Solid Waste*** | Paper-Based | 43 | 6 | 13 | Hahn Hägerdal 1996 |
| | Processed | 47 | 12 | 25 | Hahn Hägerdal 1996 |
| | Newspaper | 40-55 | 18-30 | 34-39 | Howard *et al.,* 2003 |

† *% of total dry material. Ash and extractives are not included*

### 2.1.2 STRUCTURE OF LIGNOCELLULOSE

Lignocellulosic (LC) materials generally consist of 33-51% cellulose, 19-34% hemi-cellulose, 21-32% lignin with the balance being other inaccessible components (Lui, 2010).

Celluloses are the most abundant polysaccharide in biomass available in the biosphere. Celluloses are a linear syndiotactic (alternating spatial arrangement of the side chain) homopolymer consisting of many β-D-glucose monomer units linked together by β-(1 →4)-glycosidic bonds (Menon and Rao 2012; Hahn-Hägerdal *et al.,* 2007; Zacchi *et al.,* 2006). The nature of the β-(1 →4) bonds result in linear chains of glucose molecules. Intermolecular and intramolecular hydrogen bonds involving the hydroxyl groups and hydrogen atoms of adjacent glucose units enables cellulose to exist as crystalline fibres with irregular amorphous regions (Refaat, 2010). Its crystalline, rigid structure naturally resists degradation and therefore requires harsh treatment conditions or enzymatic action to break the material down to fermentable monomer sugars (Olsson and Hahn-Hägerdal, 1996; Liu, 2010). Consequently, ethanol production from LC biomass is more complex and expensive relative to starchy materials such as sugarcane that are associated with the food supply chain (Zacchi *et al.,* 2007).

Hemi-celluloses are polysaccharide polymers that are interconnected with the secondary cell wall of woody biomass by covalent bonds and weak secondary forces (Postma, 2012). They are typically composed of linear and branched hetero-polymers of β-D-xylose, α-L-arabinose, β-D-mannose, β-D-glucose, β-D-galactose and D-glucuronic acid. The major hemicellulose, arabinoxylan, consists of a xylan backbone made up of β-(1 →4) bonds of D-xylose monomer units with frequent arabinose side chains and is structurally similar to cellulose. However, the presence of the arabinose side chains

minimizes the presence of hydrogen bonds and as a result, the arabinoxylan fraction of hemicellulose is low in crystallinity. Similarly, the minor hemicellulose, glucomannan (which is a co-polymeric chain of glucose and mannose), is also low in crystallinity. As a result of their low crystallinity, hemi-celluloses are easier to hydrolyse (relative to celluloses) into the hexose and pentose monomeric sugar components (Zacchi *et al.,* 2006; Olsson and Hahn-Hägerdal, 1996; Liu 2010; Ackerson *et al.,* 1991).

Lignin is a heterogeneous polymer of substituted aromatic building blocks which typically constitute 21-32% of lignocellulosic biomass (Hahn-Hägerdal & Stanley, 2010; Olsson & Hahn-Hagerdal, 1996). Lignin is formed through the irreversible removal of water from sugars therefore creating highly resistant aromatic rings. These aromatic rings enable lignin to resist many microbial attacks, especially in anaerobic systems (McCrady, 1991). In addition to the variance in the hexose-to-pentose ratio with the type of lignocellulosic feedstock, the fermentable hexose and pentose monosaccharide ratio is highly dependent on the effectiveness of the lignocellulose pre-treatment method. As a result, second generation ethanol production process designs are typically required to be flexible with regards to the LC feedstock.

### 2.1.3 LIGNOCELLULOSE-TO-ETHANOL PROCESS DESIGN TRENDS

Of the many processing concepts for the conversion of lignocellulosic biomass to ethanol, the common thread includes a sequence of processing steps including biomass pre-treatment, cellulose enzymatic/acid hydrolysis, hydrolyzate detoxification and fermentation, distillation and effluent treatment (*Figure 2*). Whilst many processing flowsheets exist, a brief overview is presented here. Reviews by Cardona and Sanchez (2007); Rehaat 2010; Menon *et al.,* 2012; and Achyuthan *et al.,* 2010 can be studied for more detailed analyses on the advancements of these flowsheets.

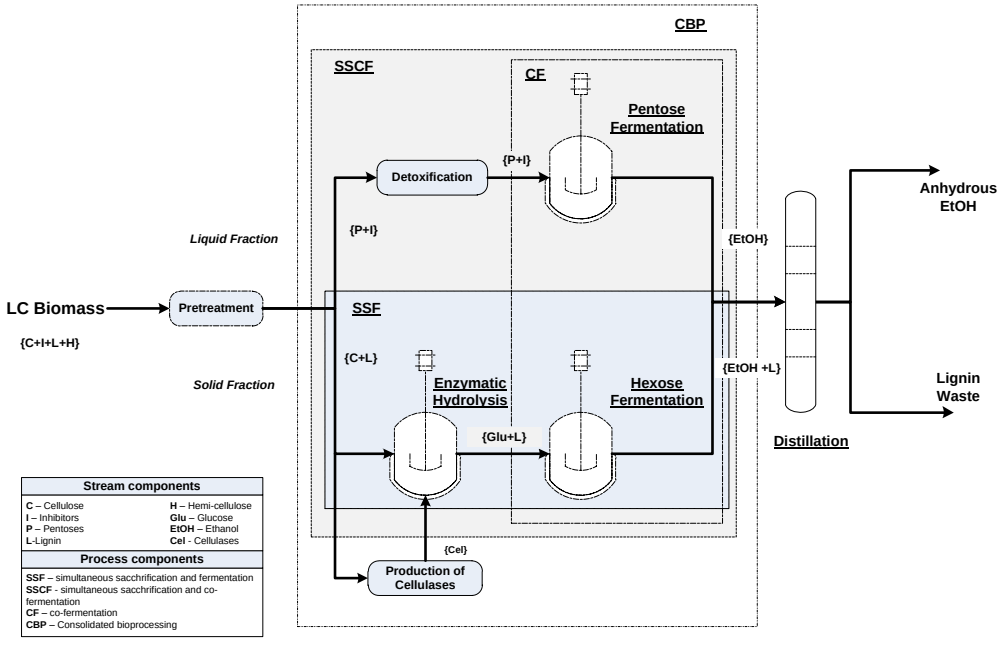


***Figure 2:*** *A general block diagram of process design configurations for ethanol production from LC biomass [Redrawn from (Cardona and Sanchez, 2007)]*

The LC-to-ethanol process is initiated by a biomass pre-treatment stage. The LC material pre-treated such that the hemi-cellulose fraction is solubilized into monomeric and oligomeric sugars and to reduce cellulose crystallinity (Hahn-Hägerdal *et al.,* 2007; Cardona and Sanchez 2007). The resultant stream consists of solid and liquid fractions that undergo hydrolysis (sacchrification) and hemi-cellulose hydrolyzate detoxification respectively. The solid fraction consists of cellulose in a form accessible to enzymes or acids (for hydrolysis) and insoluble lignin. Once cellulosic hydrolysis is completed, the cellulose hydrolyzate (comprising primarily of the monomeric sugar D-glucose and lignin) is converted into ethanol through fermentation (Zacchi *et al.,* 2007). The detoxified liquid fraction consisting pentoses and hemi-cellulose hydrolyzate inhibitors undergoes fermentation in an independent unit via a pentose-fermenting ethanologic biocatalyst (Inui *et al.,* 2010; Cardona and Sanchez, 2007). This process represents one of the most extensively tested configurations called Separate Hydrolysis and Fermentation (SHF).

The combination of the enzymatic hydrolysis and glucose fermentation has yielded a key simultaneous saccharification and fermentation (SSF) process within which glucose is rapidly converted into ethanol as soon as it is formed through hydrolysis in the same fermenter. This configuration minimizes glucose accumulation within the fermentation culture broth (Zacchi 2006; Zacchi *et al.,* 2007). Hydrolysis enzymes have been shown to be more sensitive to the sugar concentration relative to the ethanol concentration and therefore, the integration of these two steps would facilitate higher rates, yields and ethanol concentration compared to SHF (Aden *et al.,* 2010). Furthermore, since a single vessel would be required, SSF processes are easier to operate, require lower capital investments and the presence of higher ethanol concentrations reduces the risk of culture contamination (Wyman *et al.,* 1992). In contrast, the presence of lignin in SSF strategies makes the retention of the hydrolysis enzymes and ethanologic biocatalyst difficult (Zacchi *et al.,* 2007). In addition, since the optimum operating temperature and pH differ for the hydrolysis enzymes to that of the ethanologic biocatalyst, the conditions for SSF cannot be optimal for both the enzymes and the ethanologic biocatalyst (Cardona and Sánchez, 2007; Zacchi *et al.,* 2007; Hahn-Hägerdal *et al.,* 2007; Ezeji & Li, 2010).

Further configurations include the simultaneous saccharification and co-fermentation (SSCF) process strategy whereby the pentose fermentation, hexose fermentation and enzymatic hydrolysis are integrated into a single step. This strategy has been shown to be effective for conversion of xylose-rich LC materials to ethanol (Menon and Rao, 2012). Whilst the same advantages and disadvantages of the SSF process apply for SSCF, further drawbacks of the configuration include high by-product formation, poor hydrolysis enzyme stability, and conflicting optimum temperature and pH for the glucose and xylose fermenting organisms and the hydrolysis enzymes (Cardona and Sánchez, 2007). Lastly, consolidated bioprocessing (CBP) is a combination of the biological steps required for LC biomass to ethanol production into a single reactor. The distinction of CBP to the other strategies lies in that only a single microbial community is required for cellulose production, the hydrolysis of the polysaccharides present in pre-treated biomass, and the co-fermentation of hexose and pentose

sugars in a single unit. As a result, CBP facilitates potentially lower capital costs, costs for utilities associated with cellulose production and higher hydrolysis rates (Menon and Rao, 2012; Inui *et al.,* 2010). However, no single natural microorganism possesses all the required features for CBP and therefore research directed towards the integration and genetic engineering of features from several microorganisms into a single biocatalyst remains a strong area of interest.

In view of the LC biomass-to-ethanol configurations, literature suggests that the factors that have the greatest influence on the price of LC ethanol are: biomass transportation, process water, biomass pre-treatment, inhibitor tolerance by the biocatalysts, ethanol yield and the ethanol productivity (Hahn-Hägerdal, 2007). Based on cost analyses on the ethanolic fermentation of LC hydrolyzates, it is predicted that raw material costs, the effective conversion of all sugars to ethanol and the concentration of ethanol prior to distillation constitutes more than a third of the total production costs (Zacchi *et al.,* 2007; Galbe and Zacchi, 2002; Zacchi *et al.,* 2003). Zacchi and Axelsson (1989) reported that distillation only becomes feasible at ethanol concentrations above $40gL^{-1}$ (or 4wt%) (Zacchi and Axelsson, 1989).

Therefore, for ethanol production from the biotransformation of lignocellulosic biomass to be considered as an efficient techno-economic process, the complete fermentation of the sugars present in hydrolyzates becomes a vital objective. To this end, the evaluation of a desirable LC hydrolyzate fermenting biocatalyst must be reviewed in conjunction with ethanol yield (with minimal metabolic by-product formation) based on the total amount of sugars (hexoses and pentoses) in hydrolyzates.

## 2.2 ETHANOL PRODUCING BIOCATALYSTS

One of the major technical obstacles to the commercialization of the lignocellulose-to-ethanol bioprocess is the development of an efficient ideal biocatalyst (Bothast *et al.,* 1999). Since the feedstock can represent a significant portion of the process costs, an economical process would depend on the rapid and efficient conversion of both the fermentable hexose and the pentose fractions of LC biomass to ethanol. Therefore, the selection of the best biocatalyst for the fermentation process would contribute positively towards alleviating the techno-economic challenges facing the probable commercialization of this process (Hahn-Hägerdal & Stanley, 2010).

### 2.2.1 DESIRED BIOCATALYSTS FOR BIOMASS TO ETHANOL

Prior to exploring the various biocatalysts that could be considered for lignocellulose biomass conversion, it is important to realise the fundamental properties an ideal LC hydrolyzate fermenting biocatalyst should possess.

- ***Efficiently Ferment $C_5$ and $C_6$ sugars:*** The selected biocatalyst should be able to efficiently ferment both the pentose and hexose sugars LC hydrolyzates with high product selectivity and specific productivities. (Burton, 2001).

- ***Good Stability:*** The biocatalyst activity should be stable at the process operating conditions. Therefore, small fluctuations of the process operating conditions should not significantly alter the performance of the biocatalyst. In addition to stability, the biocatalyst should attain favourable functional stability to ensure long-term continuous operation without being replaced (Du Preez, 2008).

- ***High Tolerance of Ethanol and High Sugar Uptake Capability:*** The biocatalyst should exhibit high levels of tolerance towards the product, i.e. ethanol. The higher the tolerance of ethanol, the higher the potential for high volumetric productivities to be achieved from the fermentation process without decline in the fermentation performance. Furthermore, the biocatalyst should be capable of fermenting high concentrations of sugar without being inhibited by the sugar concentration.

- ***Resistant to hydrolyzate inhibitors:*** Pre-treatment by-products such as acetate, HMF, furfural, and other weak acids tend to inhibit/hinder the activity of biocatalysts and subsequently lead to lower ethanol yields and specific productivities. The ideal biocatalyst ought to be impervious to hydrolyzate inhibitors and continue converting hexoses and pentoses in the presence of these inhibitors without a significant decline in ethanol yield and productivity.

- ***Robust Grower:*** The biocatalyst is required to be a robust grower which requires simple, inexpensive medium for growth. Moreover, microbial growth in fermentation conditions that retard contaminants is desirable (acidic pH or higher temperatures). Even though the latter is not always possible, microorganisms that are flexible to growth conditions are always favourable (Shuler and Kargi, 2008).

- ***GRAS Organism:*** The last property requires the biocatalyst to be generally regarded as safe (GRAS) for use in industrial processes. In light of minimizing biological safety protocols in the work-place, GRAS organisms are typically favoured in industrial bioprocesses.

These fundamental properties are not concrete for all LC fermentation processes. However, they do form a basis upon which a suitable fermentation biocatalyst can be selected from a wide range of ethanologic microbes. Nonetheless, more microbe specific factors must to be investigated prior to selecting the best biocatalyst for a particular process configuration.

### 2.2.2 Wild-Type Zymomonas Mobilis

#### 2.2.2.1 Zymomonas Mobilis

Conventional ethanol production from starch-based raw materials has been traditionally performed in batch fermentation systems with yeast strains (such as *Sacchromyces cerevisiae*) due to their industrial reputation of being an efficient ethanol producers in the wine, brewing and distilled alcohol industries (Mohagheghi *et al.,* 2002; Liu, 2010).

An alternative biological approach to improving the LC biomass-to-ethanol productivity is to replace the traditional biocatalyst (i.e. yeast) with a more efficient and productive microbe (Gunasekaran and Chandra, 1999; Lawford, 1988). *Z. mobilis* has demonstrated superior ethanol production kinetics over *Saccharomyces* sp., suggesting significant promise of this organism as a vehicle for renewable energy production (Rogers *et al.,* 1979; Swings and De Ley, 1977; Zhang *et al.* 1995a). The comparative advantages of *Z .mobilis* relative to *S. cerevisiae* on the batch fermentation of a glucose substrate is summarised below. Publications by Panesar *et al.,* (2006), Senthilkumar and Gunasekaran, (2005), Deanda *et al.,* (1996); Zhang *et al.,* (1995b), Chander *et al.,* (2011), Bothast *et al.,* (1999) and Karsch *et al.,* 1983 can be consulted in support of the advantages listed below.

i. *Z. mobilis* has higher sugar uptake and ethanol yield capabilities (5-10% more ethanol produced based on the amount of sugar consumed) relative to *Sacchromyces* sp., (Skotnicki *et al.,* 1981)
ii. *Z. mobilis* achieves up to 2.5 fold higher specific ethanol productivity relative to traditional yeasts, (Dien *et al.,* 2003)
iii. *Z. mobilis* has lower biomass production requirements. *Z. mobilis* ferments glucose via the Entner-Douroroff (ED) pathway, therefore produces only 1 mol ATP per mol of glucose. Yeasts ferment glucose via the Embden-Meyerhoff-Parnas (EMP) pathway and produce 2 mol of ATP per mol glucose (Zhang *et al.,* 1995a). Hence, for glucose conversion to ethanol by *Z. mobilis*, more of the metabolized carbon is available for ethanol production rather than biomass formation (see *Figure 3* for the ED pathway and Appendix A for the EMP pathway for *Z. mobilis* and *S. cerevisiae* for glucose metabolism respectively).
iv. *Z. mobilis* is an anaerobic ethanologic microorganism. Therefore, it does not require the controlled addition of oxygen for growth during fermentation,
v. Since *Z. mobilis* is a prokaryote and yeasts are eukaryotes, *Z. mobilis* is more amendable to genetic manipulations (Liu, 2010).

Considering ethanol tolerance of the two biocatalysts, literature survey into the ethanol tolerance of S. *cerevisiae* relative to *Z. mobilis* reveals contradictory results. Whilst some studies have reported that *S. cerevisiae* has a higher tolerance to ethanol relative to *Z. mobilis*, *E. coli*, *K. oxytoca* (Hahn-Hägerdal *et al.,* 2007); opposing results indicating that ethanol tolerance by wild-type *Z. mobilis* is in fact higher than wild-type strains of *S. cerevisiae* have also been published (Rogers *et al.,* 1980, Gunasekaran *et al.,* 1986; Swings and De Lay, 1977). Rogers *et al.,* (1981) investigated and compared the fermentation kinetics *of Z. mobilis, S. cerevisiae* and *S. carlsbergensis* at high ethanol concentrations to eliminate discrepancy between the published results. At high ethanol concentrations (up to 12% m/v), *Z. mobilis* achieved higher ethanol yield and a faster specific rate of ethanol production relative to the two wild-type *Sacchromyces* strains.

However, despite the potential advantages of *Z. mobilis*, it does possess some limitations compared to yeasts. Firstly, its substrate utilization range is constrained to glucose, sucrose and fructose whereas yeasts can typically ferment sugars such as galactose and mannose as well (Nellaiah *et al.,* 1988; Gunasekaran and Chandra, 1999). Moreover, considering hydrolyzate fermentation, *Z. mobilis* is less tolerant to hydrolyzate inhibitors such as acetate, HMF, and furfural relative to *S. cerevisiae*.

To this respect, over-liming (precipitating the inhibitors with the addition of $Ca(OH)_2$) has been successfully proposed for hydrolyzate fermentation. Nonetheless, this process generates $Ca(SO4)_2$ which requires complex processing procedures to be removed from the system (Hahn-Hägerdal *et al.,* 2007, Lui, 2010).

Wild-type *Z. mobilis* metabolize glucose, fructose and sucrose through the ED pathway and is unable to utilize the EMP pathway as a result of the absence of 6-phosphofructokinase (which converts fructose-6-phosphate into fructose-1,6-bisphosphate). Despite the absence of this enzyme, it uses the ED pathway to produce the necessary building blocks for ethanol production at a lower ATP yield than the EMP pathway. To this end, glucose is metabolized via 2-keto-3-deoxy-6-phosphogluconate aldolase into pyruvate (*Figure 3*). Through the highly expressed pyruvate decarboxylase and ethanol dehydrogenase genes, the pyruvate is rapidly converted into ethanol. As a result of the low net ATP yield, *Z. mobilis* maintains a high glucose flux through the ED pathway (Lin and Tanaka, 2006; Lee *et al.,* 2010; Shuler and Kargi, 2008; Lui, 2010; Mohagheghi *et al.,* 1998). Lactate, acetate, and $CO_2$ are produced as metabolic by-products albeit at low concentrations (Rogers *et al.,* 1979).

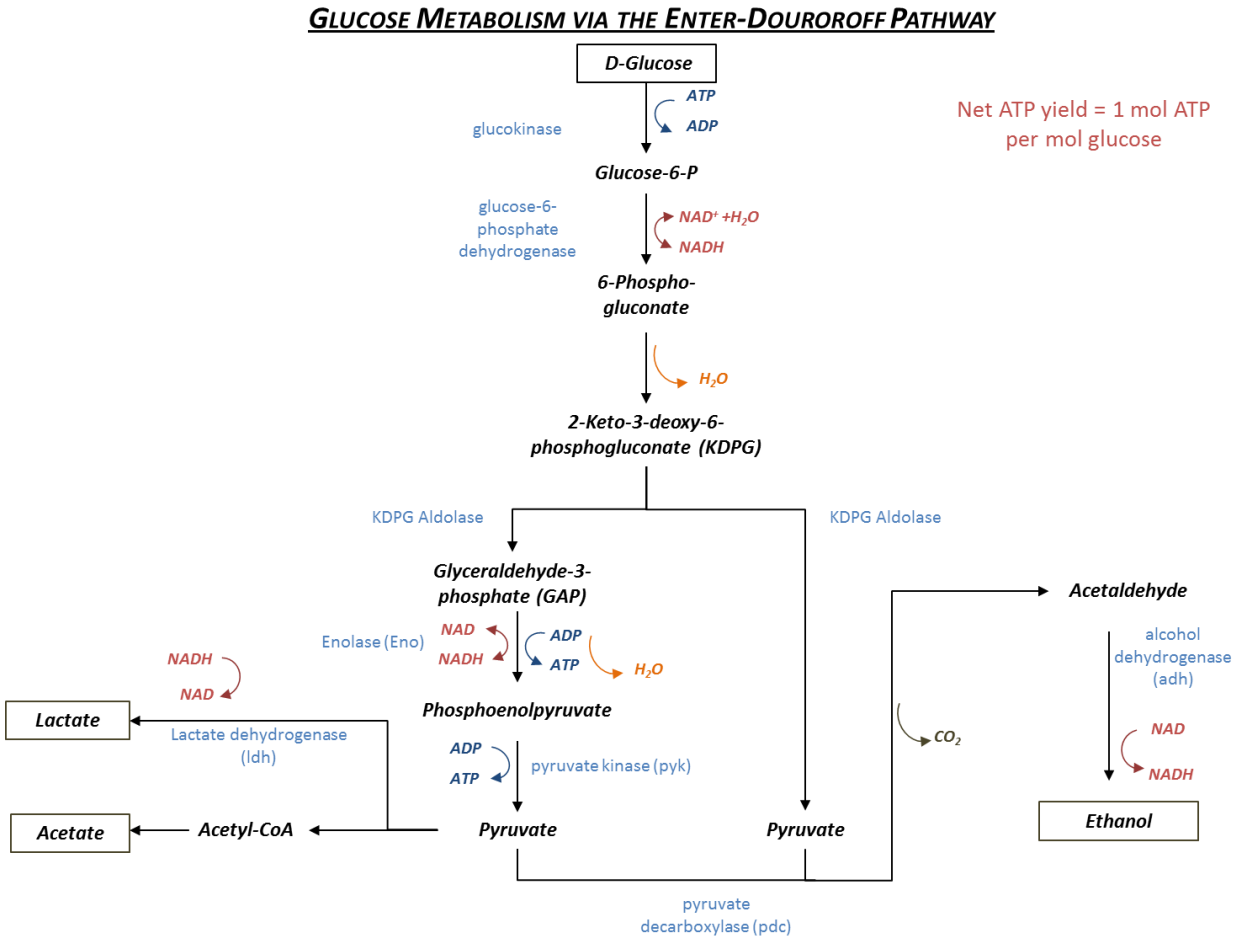


***Figure 3:*** *Glucose Metabolism via the Enter-Douroroff Pathway by wild-type Z. mobilis (redrawn from (Shuler and Kargi, 2008))*

Rogers *et al.,* (1979; 1980; 1981; 1983) have published a series of articles relating to the successful ethanol synthesis from glucose, fructose and sucrose with various strains *Z. mobilis*. Based on various criteria, they concluded that the best strain of *Z. mobilis* for glucose fermentation was *Z. mobilis* ZM4 (ATCC 31821). This strain achieved near theoretical ethanol yields (up to 98%) at low biomass accumulation and exhibited the highest ethanol tolerance and substrate uptake capabilities of the tested strains (Skotnicki *et al.,* 1981). These early studies further enhanced the reputation of *Z. mobilis* as a promising candidate for the fermentation of glucose to ethanol. Later, screening tests for the best wild-type strain of *Z. mobilis* for hydrolyzate fermentation validated that not only does *Z. mobilis* ZM4 out-performs the other strains, it also tolerates steam-pretreated Salix hydrolyzate with acetate concentration up to 10g.$L^{-1}$ (Olsson and Hahn-Hagerdal, 1996; Zhang *et al.,* 1995b).

Nevertheless, just like *S. cerevisiae*, this naturally occurring strain of *Z. mobilis* can metabolize only a narrow range of hexoses and lack the pentose metabolism pathways necessary to ferment xylose and arabinose commonly found in hemicelluloses (Zhang *et al.,*1995a; Liu, 2010). This attribute becomes a key limiting factor in their application as the desired biocatalyst for lignocellulosic biomass conversion.

#### 2.2.2.2 OTHER WILD TYPE ETHANOLOGIC MICROORGANISMS

Whilst *Z. mobilis* and *S. cerevisiae* cannot ferment pentoses, some wild-type bacterial and fungal species can ferment xylose under anaerobic and aerobic conditions respectively. Common pentose fermenting microbes include *Bacillus macerans, Klebsella pneumoniae, Clostridium acetobutylicum* and *Thermoanaerobacterium saccharolyticum*. However, many of these bacteria are susceptible to low ethanol tolerance and high by-product formation during the fermentation (Chander *et al.,* 2011). Several fungal species such as *Monilia* spp*., Neocallimastix* spp., have illustrated the ability to ferment cellulose/hemicelluloses substrates directly to ethanol and/or acetate in a single step. However, the commercial applicability of these fungi is impeded by their long fermentation periods, low ethanol productivities, high viscosity fermentation broths and the formation of by-products in high amounts (Chander *et al.,* 2011; Hahn-Hägerdal *et al.,* 2007).

Other naturally occurring yeasts such as *Pichia stipitis* and *Canadia shehatae* have also shown pentose fermenting capabilities. However, these pentose-fermenting yeasts have been reported to achieve low ethanol productivities and are not able to grow in the absence of oxygen. Moreover, these yeast species have been observed to be less tolerant of pH, ethanol and hydrolyzate inhibitors relative to *S. cerevisiae* (Chander *et al.,* 2011; Bothast *et al.,* 1999; Hahn-Hägerdal *et al.,* 2007).

### 2.2.3 GENETICALLY MODIFIED STRAINS

The limitations of wild-type strains for the fermentation of pentose sugars has resulted in an increase in impetus for the development of novel biocatalysts that can efficiently ferment mixed sugar substrates and tolerate hydrolyzate inhibitors (Bothast *et al.,* 1999). Genetic engineering

approaches such as recombinant DNA technology have been used to improve the pentose fermenting capabilities of many microbes. Two approaches have been commonly adopted for the genetic modification of these microbes. The first approach involves the genetic modification of microorganisms that can naturally produce ethanol (such as *Z. mobilis* and *S. cerevisiae*) by enhancing their genetic structure to enable them to metabolize multiple substrates. The second approach involves the genetic modification of microorganisms that can naturally ferment a wide range of substrates (such as *E. coli* and *K. oxytoca*) by enhancing their ethanol productivity (Bothast *et al.,* 1999; Olsson and Hahn-Hägerdal 1996; Hahn-Hägerdal *et al.,* 2007; Zhang *et al.,* 1995a; Deanda *et al.,* 1996; Mohagheghi *et al.,* 2002). The former of these approaches is briefly discussed for the genetic modification of *Z. mobilis*.

#### 2.2.3.1 GENETIC MODIFICATION OF Z. MOBILIS

The favourable fermentative characteristics of *Z. mobilis* have been attributed to its unique physiology. Metabolic engineering efforts for this microbe have focused on increasing its substrate utilization range whilst exploiting its naturally high ethanol productivity characteristics (Deanda *et al.,* 1996; Zhang *et al.,* 1995a).

Researchers at the NREL have successfully integrated xylose and arabinose utilization genes into the plasmid of *Z. mobilis*. Zhang *et al.,* (1995a) first developed the recombinant strain *Z. mobilis* CP4 (pZB5) by introducing and expressing the genes encoding xylose isomerase (xi), xylulokinase (xks), transaldolase (tal), and transketolase (tkt) from *E. coli* into the parent strain *Z. mobilis* CP4. The subsequent operon/shuttle vector (pZB5) containing the xylose-assimilation (xi, xks) and pentose-phosphate pathway genes (tal and tkt) was subsequently transferred into the plasmid of the host strain CP4. The resulting recombinant *Z. mobilis* CP4 (pZB5) was capable of growing on xylose as the sole carbon source and resulted in theoretical yields of approximately 86% (0.44g ethanol per g sugar consumed) (Zhang *et al.,* 1995a). *Figure 4* presents the glucose and xylose metabolism pathway for xylose-fermenting strains of *Z. mobilis*.

In an attempt to construct an improved xylose fermenting strain, the operon pZB5 was transferred into the ethanol-producing host strain *Z. mobilis* ZM4. The new recombinant strain ZM4 (pZB5) showed improved xylose and glucose fermentative performance and achieved a 90% theoretical yield (0.46g ethanol produced per g sugar consumed) (Rogers *et al.,* 1999; 2000; 2001; Zhang *et al.,* 1995b).

A strain that fermented arabinose was constructed using a similar strategy to the one used to engineer xylose metabolism in *Z. mobilis* CP4. Five genes encoding L-arabinose isomerase (araA), L-ribulokinase (araB), L-ribulose-5-phosphate-4-epimerase (araD), transaldolase (tal), and transketolase (tkt) from *E. coli* were transferred into *Z. mobilis* ATCC 39676 for arabinose utilization. The resultant transformed strain *Z. mobilis* 39676 (pZB206) grew and produced ethanol from L-arabinose as a sole carbon source at 98% of the theoretical ethanol yield (0.5 g ethanol per g sugar

consumed). However, the rate of arabinose utilization of this strain was found to be much lower relative to xylose and glucose utilization attained by the xylose-fermenting strains CP4 (PZB5) and ZM4 (pZB5) respectively (Deanda *et al.,* 1996).

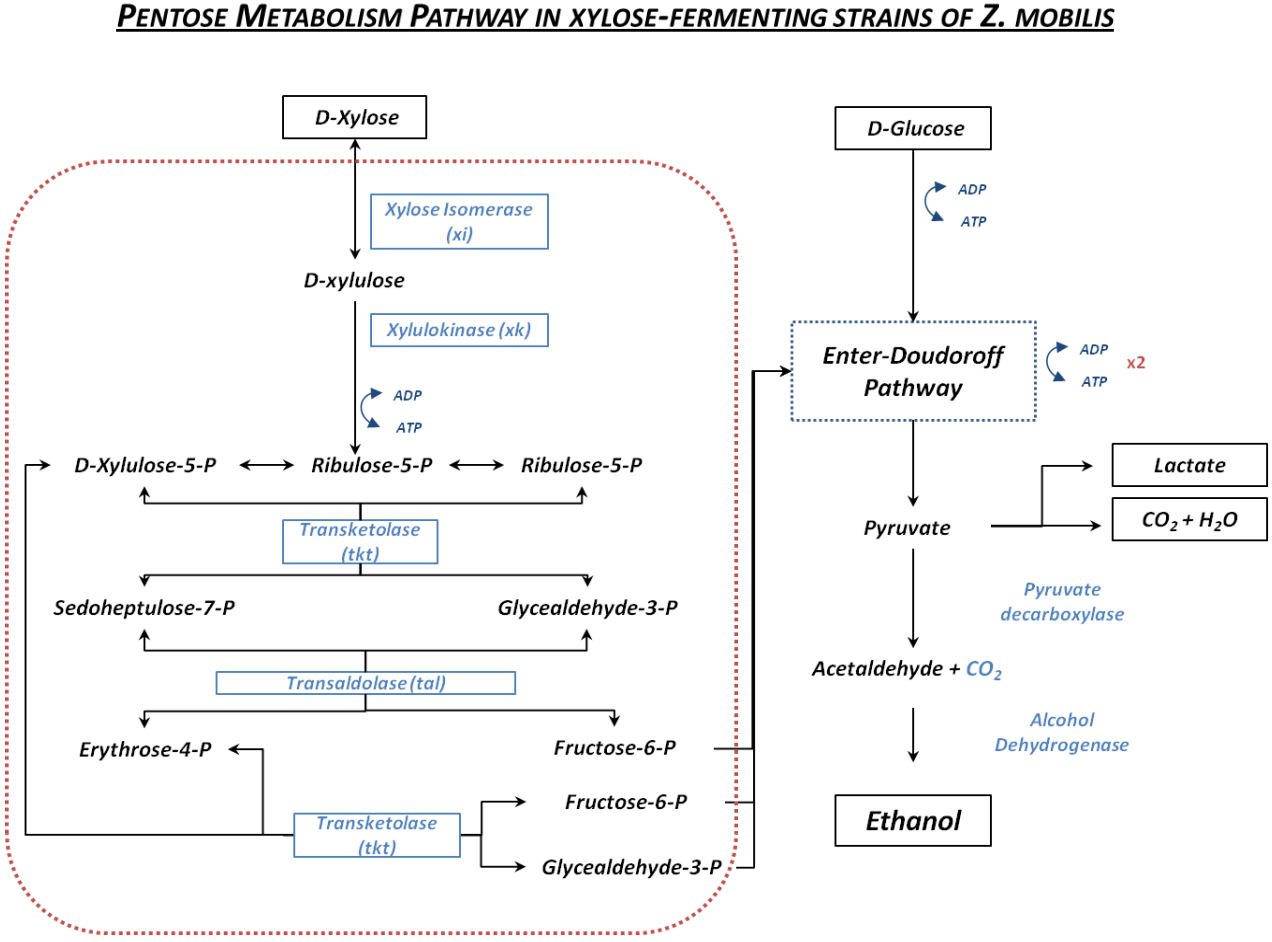


***Figure 4:*** *Schematic diagram of the metabolic pathway of recombinant strains Z. mobilis CP4 (pZB5), ZM4(pZB5) and 8b. The coloured boxes illustrate the encoded enzymes. [Redrawn from (M. Zhang 2003; Mohagheghi et al., 2002)]*

Subsequent work at NREL has yielded their latest (at the time of this study) strains *Z. mobilis* AX 101 and *Z. mobilis* 8b. The former of the two strains (AX 101) contains all seven xylose and arabinose metabolism genes i.e. xi, xks, araA, araB, araD, tal, and tkt. In addition to fermenting both sugars, this integrated strain has a stable plasmid (does not require an antibiotic for plasmid maintenance) and retains the ability to ferment both sugars after 160 generations, thereby exhibiting improved genetic stability (Mohagheghi *et al.,* 2002; Chander *et al.,* 2011; Dien *et al.,* 2003). *Z. mobilis* 8b is a chromosomal integrant of the xylose fermenting strain ZM4 (pZB5) with increased genetic stability and resistance towards the inhibitory compound acetate.

Even though high ethanol yields have been reported for the fermentation of a glucose-xylose-arabinose substrate using *Z. mobilis* AX 101, the major disadvantage of this biocatalyst was its sensitivity to the presence of acetate, which is a LC biomass pre-treatment as well as a metabolic by-product (Mohagheghi *et al.,* 2002). Its specific ethanol productivity decreased by 50% at acetate

concentrations greater than 2.5 $g.L^{-1}$ relative to the acetate free fermentation condition. To circumvent this problem, upstream acetate removal mechanisms such as "over-liming" (the addition of $CaCO_3$ to pre-treated hydrolyzate to remove aliphatic and aromatic acids and other aromatic compounds) have been successfully proposed (Mohagheghi *et al.,* 2006).

More recently, the same researches has developed acetate resistant and genetically stable strain, *Z. mobilis* 8b. This recombinant strain has demonstrated enhanced acetate tolerance (up to concentrations of 16 $g.L^{-1}$) without reduction in its activity, making *Z. mobilis* 8b one of the most effective biocatalysts for lignocellulose-to-ethanol conversion to date (Jeon *et al.,* 2002; Mohagheghi *et al.,* 2004).

#### 2.2.3.2 OTHER GENETICALLY MODIFIED ETHANOL PRODUCING STRAINS

The fermentation results for the various recombinant strains presented in literature cannot be accurately compared due to the different medium formulations, sugar mixtures, and inoculation protocols (Dien *et al.,* 2003; Jeffries and Jin 2004). Nonetheless, *Table 2* presents a literature summary of some promising ethanol producing microorganisms all performed in batch fermentation strategies.

***Table 2:*** *Comparative batch fermentations for promising fermentation biocatalyst*

| Strain | Host | Sugars | | | | EtOH Yield (%)[c] | EtOH Prod. ($g.L^{-1}.h^{-1}$)[d] | Reference |
|---|---|---|---|---|---|---|---|---|
| | | *Glu.* ($g.L^{-1}$) | *Xyl.* ($g.L^{-1}$) | *Ara.* ($g.L^{-1}$) | *Gal.* ($g.L^{-1}$) | | | |
| *E. coli* | KO11 | - | 90 | - | - | 89 | 0.85 | Ingram *et al.,* 1982 |
| | KO11 | 27 | 39 | 23 | 11 | 90 | 62 | Asghari *et al.,* 1996 |
| | KO11 | 70 | 30 | - | - | 85 | NA | Ingram *et al.,* 1988 |
| | FBR5 | - | 95 | - | - | 90 | 0.59 | Dien *et al.,* 2000 |
| | FBR5 | 30 | 30 | 15 | - | 90 | 0.92 | Dien *et al.,* 2000 |
| *S.cerevisiae* | 1400[a] | 31 | 15 | 10 | 2 | 90 | 0.92 | Krishnan *et al.,* 1999 |
| | 1400(pLNH33) | 52.8 | 56.3 | - | - | 78 | 1.22 | Krishnan *et al.,* 1999 |
| | TMB 3400 | - | 20 | - | - | 50 | NA | Stanley *et al.,* 2006 |
| | 424A (LHN-ST) | 70 | 30 | - | - | 82 | NA | Lau *et al.* 2010 |
| | 424A (LHN-ST) | - | 100 | - | - | 89.8 | NA | Lau *et al.,* 2010 |
| *Z. mobilis* | ZM4 (pZB5) | 65 | 65 | - | - | 90 | 1.29 | Rogers et al. 1999 |
| | AX 101 | 40 | 40 | 20 | - | 84 | NA | Mohagheghi *et al.,* 2002 |
| | AX 101 | 70 | 30 | - | - | 89 | NA | Mohagheghi *et al.,* 2002 |
| | 8b | - | 103 | - | - | 90 | 0.4 | Zhang, 2003 |
| | 8b | 35 | 35 | - | - | 99 | 1.4 | Zhang, 2003 |
| | 8b[b] | 16 | 69 | - | - | 83 | NA | Zhang, 2003 |

**a** *Arabinose not fermented to Ethanol*

**b** *experiments performed in mediums containing 16 g/l acetate*

**c** *% yield defined as follows: %Y = (actual of ethanol produced / theoretical amount of ethanol)*100*

**d** *Ethanol Productivity defined as follows: % P = maximum Ethanol concentration/ residence time*

Recombinant *E. coli* strains KO11 and FBR5 have been reported to achieve high ethanol productivities and convert a wide range of lignocellulosic monomer sugars including glucose and xylose (Dien *et al.,* 2000; Bothast *et al.,* 1999;Dien *et al.,* 2003; Ingram *et al.,* 1987; Ingram and Conway, 1988). However, these strains typically require nutrient rich growth media with large amounts of yeast extract (Chander *et al.,* 2011). Moreover, *E. coli* strains are not recognized as GRAS organisms and thus require biological safety protocols in the workplace (Dien *et al.,* 2000).

Various *S. cerevisiae* strains capable of fermenting xylose and glucose have been proposed in literature with *S. cerevisiae* TMB 3400 used in some industrial fermentations (Zacchi 2006; Zacchi *et al.,* 2007). The major advantage of *S. cerevisiae* over *E. coli* and *Z. mobilis* lies in its higher tolerance to inhibitors present in hydrolyzates and the lack of industrial-scale fermentation experience using either *Z. mobilis* or *E.coli*. Among other successfully genetically engineered xylose fermenting *Sacchromyces* strains are *S. cerevisiae* 1400-LNH-ST and *S. cerevisiae* 424A (LNH-ST). Krishnan *et al.,* (1999) studied the fermentation kinetics of recombinant *S. cerevisiae* 1400(pLNH33) which contains multiple copies of xylose metabolism genes. They found that this strain could attain high conversions (up to 78%) whilst simultaneously converting glucose/xylose sugar mixtures (Krishnan *et al.,* 1999). Zhang *et al.,* (2010) studied the co-fermentation of waste paper sludge to ethanol using the strains *Z. mobilis* 8b and *S. cerevisiae* RWB222. *Z. mobilis* 8b was reported to achieve a higher maximum ethanol yield (0.47g ethanol/g sugar consumed) relative to *S. cerevisiae* RWB222 (0.42g ethanol/g sugar consumed) at their best-studied temperatures of 30 ˚C and 37 ˚C respectively.

In spite of the advances in recombinant yeast strains encoded with xylose metabolism genes, the fermentation performance of the genetically modified yeast strains are limited by the formation of the by-product xylitol. The formation of xylitol is undesirable since it results in a corresponding reduction in the ethanol yield. Xylitol is formed when the cells are deficient in $NAD^+$, which is typically indicative of low or absence of oxygen supply or the absence of other electron acceptors (Stanley and Hahn-Hägerdal 2010; Liu 2010; Hahn-Hägerdal *et al.,* 2007). Moreover, these industrial S. cerevisiae strains still require hydrolyzate detoxification prior to fermentation, suggesting that the toxic nature of hydrolyzates is a significant challenge to the ethanol production process, irrespective of the biocatalyst selected.

The formation of xylitol from recombinant yeast strains was also observed in a study performed by Lau *et al.,* (2010) on the fermentation kinetics of *S. cerevisiae* 424A (LNH-ST), E. coli KO11 and Z. mobilis AX101 on corn steep liquor (CSL) media. In CSL media consisting of xylose and glucose sugars, S. cerevisiae obtained 98% sugar conversion at an maximal metabolic yield of 82% (0.42g ethanol/g sugar consumed) (Lau *et al.,* 2010). Nevertheless, the performance of this strain was setback by the formation of higher concentrations of the by-products xylitol and glycerol and lower ethanol yields relative to the recombinant *E. coli* and *Z. mobilis* strains KO11 and AX101 respectively.

Whilst this preferential glucose utilization has also been reported for recombinant strains of *Z. mobilis*, the xylose metabolization rate in *Z. mobilis* was about two fold higher relative to the metabolization in *S. cerevisiae* (Mohagheghi *et al.,* 2002; Zhang *et al.,* 1998).

Based on the properties identified for an ideal catalyst and the recombinant strains developed thus far, it is apparent that *Z. mobilis* strain 8b is the most promising recombinant strain for the fermentation of the hexose sugar glucose and the pentose sugars xylose. In view of its GRAS status, excellent activity and genetic stability towards pentose fermentation, this strain seems to be one of the most attractive biocatalysts for the co-fermentation of glucose-xylose substrates/hydrolyzates.

### 2.2.4 Physiological Approach: Kinetics of Z. mobilis Fermentation

Owing to the dependence of the biocatalyst performance on the process configuration and the type of LC feedstock, the familiarity of the kinetics of the biocatalyst becomes imperative for the design of efficient continuous fermenters (Lawford and Rousseau, 2002). During the catabolic metabolization of sugars by the fermentative microorganism, cell protein is continuously degraded and regenerated by the microorganism. Changes in the fermentation microenvironment over time can induce a reduction in the microbe activity by creating an imbalance in the protein degradation-regeneration process (Libicki *et al.,* 1985). In this section the ethanologic activity of *Z. mobilis* due to changes in the microenvironment were reviewed. The microbe activity was studied in response to changes in the fermentation temperature, pH, substrate concentration, ethanol concentration, dissolved oxygen concentration and the carbon dioxide partial pressure.

#### 2.2.4.1. Effect of Temperature

From a reaction kinetics perspective, the temperature is typically directly proportional to the kinetic energy and entropy of molecules in the fermenter. Therefore an increase in temperature is normally expected to increase the kinetic energy and the subsequent collisions between the molecules (substrate, products, growth nutrients) and the microorganisms (Lievenspiel, 1999; Du Preez, 2008). Due to an increase in these collisions, the rate of sugar metabolization (free of product inhibition) is therefore expected to increase with an increase in temperature. However, the fermentation kinetics of microorganisms are complex since there are a number of interactive factors contributing to the overall observed kinetics of the microbe. The rate of cell growth, ethanol production, sugar uptake, and product and substrate inhibition are all influenced by temperature (Huang and Chen, 1988).

##### 2.2.4.1.1. Wild-Type Strains of Z. mobilis

Whilst thorough research on the effect of the fermentation temperature on the cell viability, the rate of cell growth, rate of glucose consumption and the rate of ethanol production has been reported, the reported effects of temperature seem to be strain specific (King and Hossain, 1988; Huang and Chen, 1987; Rogers *et al.,* 1981; Swings and De Lay, 1977). In a review of the biology of *Z. mobilis* spp., Swings and De Lay (1977) reported that most strains of *Z. mobilis* do not grow at

temperatures greater than 40 °C. A further study of the effect of temperature on the kinetics of ethanol production by the wild-type strain *Z. mobilis* ZM4 demonstrated that at higher temperatures the cell viability, biomass yield, ethanol yield and the final ethanol concentration all decreased as the fermentation temperature was increased in the range 30-40 °C (*Figure 5*) (Rogers *et al.,* 1981).

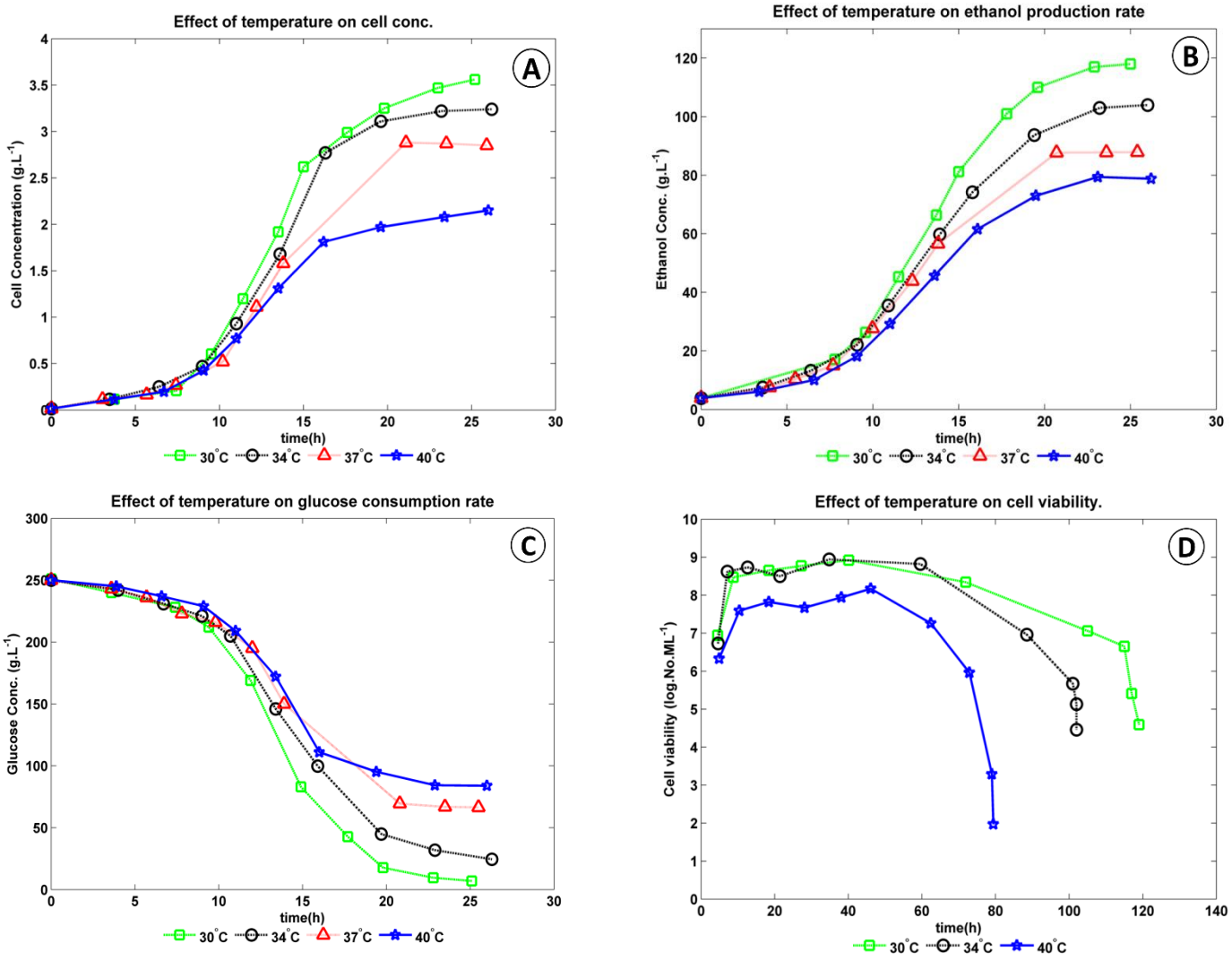


***Figure 5:*** *The effect of temperature on Z. mobilis ZM4 in 250g.L$^{-1}$ glucose medium:* ***(A)*** *cell concentration,* ***(B)*** *Ethanol concentration,* ***(C)*** *glucose consumption, (D) cell viability [Redrawn from (Rogers et al., 1981)]*

Although the maximum specific growth rate ($\mu_{max}$), the maximum specific rate of glucose consumption ($q_{s,max}$), and the maximum specific rate of ethanol production ($q_{p,max}$) were essentially constant within the studied temperature range, the biomass yield, ethanol yield and the final ethanol concentrations exhibited the greatest notable effects of temperature. The decrease in the biomass yield at higher temperatures was reported to indicate some degree of uncoupling of the catabolism from the anabolic reactions. Moreover, the production of metabolic by-products such as lactate, acetate and acetaldehyde were more pronounced at the higher temperatures (greater than 34 °C). To this end, the ethanol yield also declined as the fermentation temperature is increased.

Huang and Chen (1989) performed a series of batch fermentation experiments with wild-type *Z. mobilis* ATCC 29191 (ZM1) to determine the kinetic behaviour of the microbe with changes in the fermentation temperature. Maintaining the pH at a value to 5.0, with an initial sugar concentration in the range of 140-155 $g.L^{-1}$, they found that the maximum ethanol tolerance of the microbe decreases with an increase in temperature. The combined effect of ethanol inhibition and higher fermentation temperature on the decline of cell viability was attributed to the observed decline in ethanol tolerance at higher temperatures. Hence, for increasing the probability of attaining high ethanol yields and productivities by *Z. mobilis*, lower fermentation temperatures are recommended.

#### 2.2.4.1.2. RECOMBINANT STRAINS OF Z. MOBILIS

Mohagheghi *et al.,* (1998) studied the effect of temperature together with pH on the co-fermentation of a glucose/xylose/arabinose substrate by a co-culture of *Z. mobilis* ATCC 39676 (pZB4L) (glucose-xylose fermenting strain) and *Z. mobilis* ATCC 39676 (pZB206) (glucose-arabinose fermenting strain). A "black-box" approach was taken whereby the temperature and pH were set independently according to a statistical design and the significance of the temperature and pH towards the ethanol yield ($Y_{p/s}$), xylose conversion and arabinose conversion were determined statistically. The experimental results of the co-fermentation of $30gL^{-1}$ glucose, $30gL^{-1}$ xylose and $20gL^{-1}$ arabinose are revised in *Table 3*. Data was collected after a 72h fermentation period.

***Table 3:*** *Effect of Temperature and pH statistical design for glucose-xylose-arabinose fermentation by co-culture of 39676 (pZB4L) and 39676 (pZB206) [Redrawn from Mohagheghi et al., 1998]*

| Experimental Run No. | Temperature (ºC) | pH | $Y_{p/s}$ (% theoretical) | Xylose consumed (%) | Arabinose consumed (%) |
|---|---|---|---|---|---|
| **1** | 30 | 5 | 68.5 | 84.88 | 51.5 |
| **2** | 33.5 | 5 | 65.9 | 82.42 | 52.83 |
| **3** | 37 | 5 | 57.2 | 60.57 | 47.32 |
| **4** | 30 | 5.5 | 67.80 | 89.41 | 56.23 |
| **5** | 33.5 | 5.5 | 69.80 | 87.67 | 66.12 |
| **6** | 33.5 | 5.5 | 71.60 | 89.45 | 68.13 |
| **7** | 37 | 5.5 | 62.80 | 71.48 | 57.72 |
| **8** | 30 | 6 | 73.20 | 93.57 | 73.7 |
| **9** | 33.5 | 6 | 70.20 | 90.8 | 70.92 |
| **10** | 37 | 6 | 61.50 | 66.12 | 70.07 |

As demonstrated in *Table 3*, the highest $Y_{p/s}$ and xylose conversion were achieved at 30°C. In general, increasing the fermentation temperature had a negative effect on both the ethanol yield and amount of xylose consumed. Moreover, an increase in in temperature from 30-37°C resulted in a 10 and 20% drop in the $Y_{p/s}$ and xylose consumption respectively. A statistical analysis from the experimental data, confirmed that the $Y_{p/s}$ and xylose consumption were more sensitive to the fermentation temperature relative to the pH. The optimum fermentation temperature for glucose-xylose-arabinose co-fermentation was identified to be 31.5 °C.

Further work investigating the qualitative effect of temperature and pH on xylose and glucose batch fermentation for recombinant *Z. mobilis* strain ZM4 (pZB5) has been reported (Rogers and Joachimsthal, 2000). The kinetic data from their work is presented in *Table 4* below.

***Table 4:*** *Kinetics of the effect of temperature and pH on the fermentation of 25gL$^{-1}$ of Glucose and 25 gL$^{-1}$ of xylose [Redrawn from (Rogers and Joachimsthal, 2000)]*

| Kinetic Parameter | | pH = 4.5 T = 30 ˚C | pH = 4.5 T = 33 ˚C | pH = 4.5 T = 37 ˚C | pH = 5 T = 30 ˚C | pH = 5 T = 33 ˚C | pH = 5 T = 37 ˚C |
|---|---|---|---|---|---|---|---|
| *Glucose/ Xylose* | $\mu_{max}$ [$h^{-1}$] | 0.29 | 0.29 | 0.24 | 0.43 | 0.36 | 0.26 |
| | $q_{smax,\ glucose}$ [$g.g^{-1}.h^{-1}$] | 10.6 | 12 | 11.5 | 9.2 | 12.4 | 13 |
| | $q_{smax,xylose}$ [$g.g^{-1}.h^{-1}$] | 2.4 | 2.2 | 2.8 | 2.6 | 2.2 | 4 |
| | $q_{pmax}$ [$g.g^{-1}.h^{-1}$] | 5.3 | 6.1 | 3.9 | 4.7 | 6.1 | 6.8 |
| *Overall* | $Y_{p/s}$ | 0.47 | 0.48 | 0.33 | 0.47 | 0.45 | 0.45 |
| | $Y_{x/s}$ | 0.016 | 0.015 | 0.011 | 0.024 | 0.018 | 0.012 |

| | |
|---|---|
| $\mu_{max}$ | the maximum specific growth rate |
| $q_{smax,\ glucose}$ | the maximum specific glucose uptake rate |
| $q_{smax,xylose}$ | the maximum specific xylose uptake rate |
| $q_{pmax}$ | the maximum specific ethanol production rate |
| $Y_{p/s}$ | the overall yield of product (ethanol) based on the amount of substrate (xylose/glucose) consumed |
| $Y_{x/s}$ | the overall biomass yield based on the amount of substrate (xylose/glucose) consumed |

At temperatures greater than 37˚C, a significant reduction in the overall specific growth rate was observed due to a reduction in the cell viability and the accumulation of xylitol phosphate, which is known to increase with an increase in temperature. In addition, the xylitol accumulating in the form of xylitol phosphate has been shown to have inhibitory effects on the performance of *Z. mobilis* (Slininger *et al.,* 1990; Feldmann *et al.,* 1992; Liu, 2010). This result indicated that increasing the fermentation temperature (greater than 30 ˚C) has the undesirable consequence of decreasing the $Y_{p/s}$, the xylose conversion and the overall ethanol productivity of the fermenter.

Due to the effect the temperature has on the growth, substrate consumption and product formation kinetics, it is evident that the optimum temperature for growth and product formation may be different (Shuler and Kargi, 2008). However, it is recommended that the temperature of both wild-type and recombinant *Z. mobilis* strains be limited to the range 30- 34˚C to optimize the growth kinetics and to suppress ethanol inhibition at higher temperatures. Nonetheless, based on the evidence presented in *Table 3* and *Table 4*, there is a indication that the pH may have some interactive effect with the fermentation temperature on the fermentation kinetics of *Z. mobilis*.

### 2.2.4.2. EFFECT OF PH ON THE FERMENTATION KINETICS OF Z. MOBILIS

In microbial kinetics, the hydrogen ion concentration (pH) affects the activity of enzymes and therefore the microbial growth and metabolization rates (Shuler and Kargi, 2008). Enzymes possess amino acid groups that may be either positively or negatively charged at any pH. Therefore, depending on the pH, a large or small portion of the enzymes present in the microorganism may be active (Du Preez, 2008). The pH also affects the shape and charge of the substrate present in the reaction medium. Therefore, the adsorption of the substrate into the microorganism may be

influenced by the pH (Groot *et al.,* 1983). Lastly, variation in the pH of anaerobic cultures affects the product synthesis profile, maintenance energy requirements and consequently the degree of energetic uncoupling (Lawford, 1988).

#### 2.2.4.2.1. WILD-TYPE STRAINS OF Z. MOBILIS

Most of *Z. mobilis* fermentations in literature are reported at a pH of 5 or 5.5, even though Swings and De Lay (1977) reported that the optimum growth pH for many *Z. mobilis* strains including ZM4 was in the range 5-7 (Swings and De Ley, 1977). King and Houssain (1982) studied the effect of pH on the wild-type strain *Z. mobilis* ZM1 in a complex medium consisting of 0.6% (m/v) yeast extract, 10% (m/v) glucose at a temperature of 37 ˚C (King and Hossain, 1982). They stated that the specific ethanol productivity ($q_p$), $\mu_{max}$, $Y_{p/s}$ and the overall cell yield ($Y_{xs}$) remained relatively constant over the pH range 5-7, but declined significantly at pH's greater than 7.5. Moreover, $\mu_{max}$ and $q_p$ reach a maximum at pH 7. To this end, an optimum fermentation pH of 7 was suggested.

However, these experiments were performed at the suboptimal temperature of 37 ˚C (section 2.2.4.1 for the effect of the fermentation temperature); hence, low specific maximal growth rates were attained (Figure 6).

Lawford (1988) investigated the effect of the pH, as an alternative to growth medium manipulation for inducing the uncoupling of the catabolic and anabolic mechanisms, on $\mu_{max}$ in batch cultures in complex media consisting of 0.3% (m/v) yeast extract, 15mM $NH_4Cl$, and 5% glucose at 30 ˚C. The results of this study are contrasted to the results obtained by King and Houssain (1982) in Figure 6 below. The optimum pH for which the bacterial growth rate was greatest was determined to be in the range 6-7 with an apparent optimum at pH 6.5.

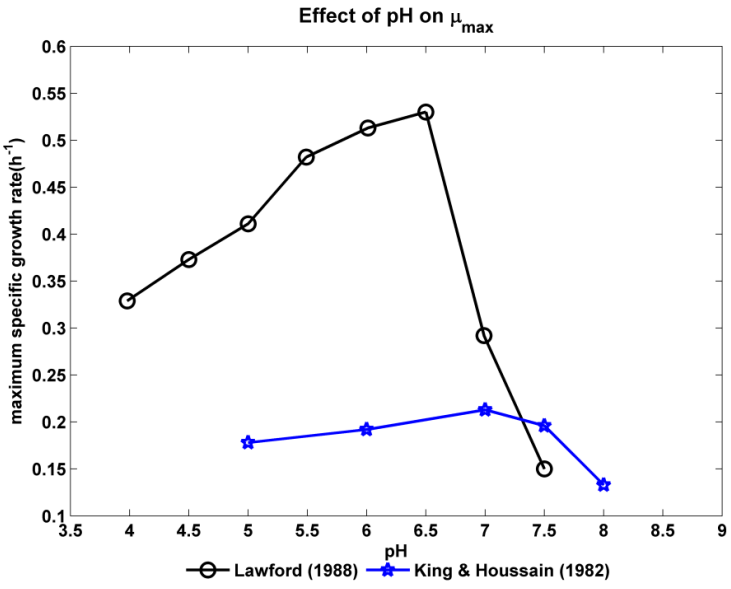


***Figure 6:*** *The effect of pH on the specific growth rate of Z. mobilis ATCC 29191 (at a fermentation temperature of 30 °C) and Z. mobilis ZM1 (at a fermentation temperature of 37 °C) [Redrawn from Lawford (1988) and King andHoussain (1982)]*

The difference in the results of these two studies can be attributed to one of two reasons. First, by comparing the variation in $\mu_{max}$ in both cases, it is apparent that at higher fermentation temperatures, the effect of increasing the fermentation pH becomes less significant (Mohagheghi *et al.,* 1998). Therefore, this suggests that either an interaction between the fermentation temperature and pH exists or the effect of the fermentation temperature is much greater to that of the pH. To this end, a statistical analysis would be sufficient to determine the significance of the temperature-pH interaction. Secondly, since two different strains were used, the reported data may suggest that no universal optimum fermentation pH for *Z. mobilis* exists. Consequently, the determination of the optimum fermentation pH for the wild-type strain used in this work (*Z. mobilis* ZM4) is a required.

#### 2.2.4.2.2. RECOMBINANT STRAINS OF Z. MOBILIS

Together with the effect of the fermentation temperature, the effect of the fermentation pH on the end of batch $Y_{p/s}$ and xylose conversion were presented in *Table 3*. Based on a statistical analysis, Mohagheghi *et al.,* (1998) found that at each of the investigated temperatures, the highest $Y_{p/s}$ and xylose conversions were obtained at pH 6.0. This indicated that both $Y_{p/s}$ and xylose conversion could be potentially improved by increasing the fermentation pH from 5-6. However, the experimental data gathered for the statistical analysis did not take into account the rate at which xylose was consumed and consequently the overall volumetric productivity of the fermentation. Hence, future work is recommended to incorporate the productivity as an additional statistical indicator of the effect of temperature or pH.

So, as mentioned in *section 2.2.4.1*, the effect high fermentation temperatures (greater than 34 ˚C) may potentially be more significant the effect of pH on the fermentation kinetics. As a result, it is imperative that an optimal combination of temperature and pH be established for glucose-xylose fermentations with the recombinant strain *Z. mobilis* 8b. Statistically derived optimal temperature and pH, with the quantification of the interactive effect of the temperature and pH for this organism have not been published in literature at the time of this study. Thus, determining whether temperature or pH is more significant towards microbial growth, rates of glucose and xylose consumption, or ethanol productivity is not possible from the available literature data. Nonetheless, based on literature findings, the optimal temperature and pH are expected to be within the ranges 30-34˚C and 5-7 respectively.

### 2.2.4.3. EFFECT OF SUBSTRATE CONCENTRATION

From a reaction kinetics viewpoint, increasing the substrate concentration should reduce the effective time required for the substrate molecules to collide with the microorganism. Hence, the rate of reaction (free of product inhibition) would be expected to increase with an increase in substrate concentration. At a specific high substrate concentration, the microorganism becomes saturated and the relationship of the specific growth rate to the substrate concentration follows saturation kinetics. To this end, the Monod model has been successfully used to predict the effect of

substrate limitation on growth patterns of many microorganisms (Lee and Rogers, 1983; Rogers et al., 2001; Shuler and Kargi, 2008).

Moreover, high substrate concentrations may cause inhibition of the microbial growth rate and the subsequent ethanol production rate. Substrate inhibition often occurs when the substrate binds to a second and non-active site on an enzyme and thereafter limits the activity of the enzyme (Shuler and Kargi, 2008). Consequently, if a single-substrate enzyme-catalyzed reaction is the rate-limiting step in the microbial growth pattern, then the inhibition of the enzyme by high substrate concentrations initiates inhibition of the microbial growth in the same pattern (Shuler & Kargi, 2008; Du Preez, 2008).

#### 2.2.4.3.1. WILD-TYPE STRAINS

Rogers *et al.,* (1979;1981) studied the batch and continuous kinetics of ethanol fermentations by *Z. mobilis* ZM4 at high initial glucose concentrations (100-300gl$^{-1}$)(P. . Rogers et al., 1981)(P. . Rogers et al., 1981)(P. . Rogers et al., 1981)(P. . Rogers et al., 1981)(P. . Rogers et al., 1981)(P. . Rogers et al., 1981)(P. . Rogers et al., 1981). *Figure 7* illustrates the effect of the initial substrate concentration on the maximum specific growth rate ($\mu_{max}$) of a batch culture in the exponential growth phase. A threshold glucose concentration of 100gL$^{-1}$ exists after which the specific growth rate reduces considerably. At concentrations lower than the threshold concentration, $\mu_{max}$ remains essentially constant at 0.5h$^{-1}$.

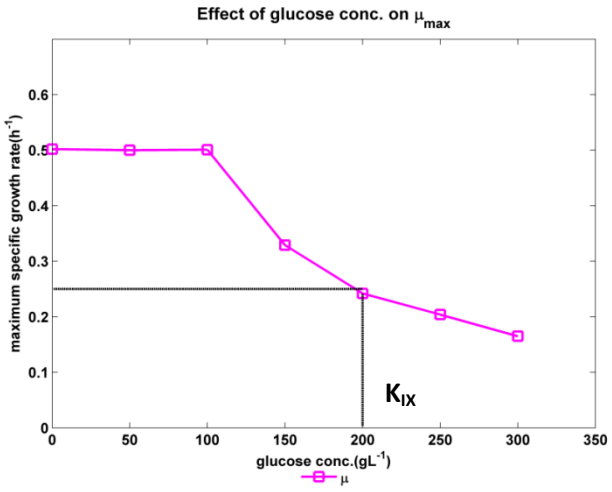


***Figure 7:*** *Effect of glucose concentration on the initial specific growth rate of Z. mobilis ZM4 (pH = 5; T = 30°C) [redrawn from Rogers and Lee, 1983]*

The following formulation was developed from this study for evaluating the effect of substrate inhibition of the growth kinetics of *Z. mobilis* by fitting a curve to experimentally determined data points:

$$G_x(s_i) = \left(\frac{K_{ix} - s_i}{(K_{ix} - s_i) + (s_1 - s_i)}\right) \qquad \textbf{(2.1)}$$

In equation (2.1), the extent of substrate inhibition on cell growth ($\mathbf{G_x(s_i)}$) is expressed as a non-linear function of the substrate concentration ($\mathbf{s_i}$) and the substrate inhibition constant for cell growth ($\mathbf{K_{ix}}$). In the case of *Z. mobilis* ZM4, the $K_{ix}$ has been reported to be 200g.L$^{-1}$.

#### 2.2.4.3.2. RECOMBINANT STRAINS

Rogers *et al.,* (1999) studied batch and continuous fermentation kinetics of the recombinant strain *Z. mobilis* ZM4 (pZb5) in various glucose-xylose mixed sugar concentrations. Holding the sugar ratio constant (at 1:1), they varied the total sugar concentration and evaluated the growth and fermentation kinetics of this recombinant strain.

At lower sugar concentrations (50/50 and 65/65 g.L$^{-1}$ xylose/glucose), they reported that the specific growth rate decreased slightly whilst the rates of sugar uptake and ethanol production remained relatively constant. However, at a higher substrate concentration of 75/75 g.L$^{-1}$ xylose/glucose, incomplete consumption of xylose was detected after 80h (although glucose was completely depleted after 35h). Moreover, the biomass yield from this high substrate concentration was less than half that obtained from the lower substrate levels with no growth detected after glucose was completely utilized (Rogers *et al.,* 1999).

In the development of a kinetic model for glucose-xylose fermentation by *Z. mobilis* ZM4 (pZb5), it was reported that the rate of growth and ethanol production would be significantly inhibited by glucose and xylose at concentrations greater than 200g.L$^{-1}$ and 600g.L$^{-1}$ respectively (Rogers *et al.,* 2001). Interestingly, the substrate inhibition constant for the parent strain ZM4 ($K_{IX}$ = 200gL$^{-1}$, *Figure 7*) is the same as this inhibitory glucose concentration for the recombinant strain. This result indicates that the encoding of the xylose assimilation genes has no evident effect on the substrate inhibition kinetics of the resultant recombinant strain.

### 2.2.4.4. EFFECT OF THE ETHANOL CONCENTRATION

The fermentation product, ethanol, generally has a toxic effect on microorganisms by either damaging the cell membrane or changing the membrane properties by retarding the membrane transport kinetics. In addition, ethanol has been shown to have a dehydrative effect on some intracellular enzymes such as alcohol dehydrogenase (*adh*) and pyruvate decarboxylase (*pdc*), therefore retarding the ethanol productivity of the microorganism (Huang and Chen, 1988). Even though *Z. mobilis* is a well-established ethanol tolerant microorganism, excessive ethanol concentrations can have inhibitory effects on both the growth and fermentation kinetics (Swings and De Lay, 1977).

#### 2.2.4.4.1. WILD-TYPE STRAINS

Lee and Rogers (1983) studied the batch fermentation kinetics of the ethanol production by the wild-type microorganism *Z. mobilis* ZM4. At various initial substrate concentrations, the effect of ethanol inhibition on the specific growth rate ($\mu$ or $r_x$), specific glucose uptake rate ($q_s$) and the

specific ethanol production rate ($q_p$) was determined. The relationships between these variables is summarised in *Figure 8*.

What is evident from Figure 8 is that there exists a threshold ethanol concentration after which linear ethanol inhibition occurs on $\mu_{max}$, $q_{smax}$, and $q_{pmax}$. For the $\mu_{max}$ the threshold ethanol concentration was 22 $g.L^{-1}$ and the maximum ethanol concentration above which no growth was possible was 86$g.L^{-1}$. Similarly, the threshold ethanol concentration and the maximum ethanol concentration for both $q_{pmax}$ and $q_{smax}$ was 55 $g.L^{-1}$ and 127$g.L^{-1}$ respectively.

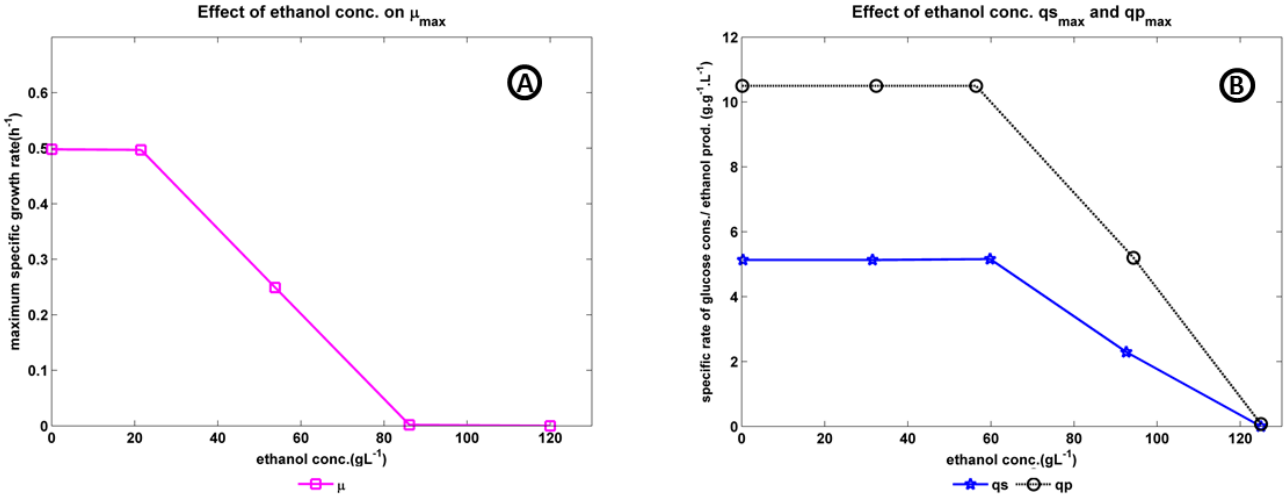


***Figure 8:*** *The effect of ethanol concentration on:* ***A*** *- the maximum specific growth rate ($\mu_{max}$ )of Z. mobilis ZM4 ;* ***B*** *– the maximum specific glucose uptake rate ($q_{smax}$) and the maximum specific ethanol production rate ($q_{pmax}$) [Adapted from Lee and Rogers, 1983]. Fermentation conditions: T = 30°C, pH = 5*

Based on the analysis of the effects of ethanol on cell growth and the specific ethanol production rate, the following piece-wise mathematical models were developed to model the contribution of non-competitive ethanol inhibition towards the specific growth rate and the specific ethanol production rate:

$$F_x(p) = \left(1 - \frac{p - p_{ix}}{p_{mx} - p_{ix},}\right) \qquad \textbf{(2.2)}$$

$$F_p(p) = \left(1 - \frac{p - p_{ip}}{p_{mp} - p_{ip},}\right) \qquad \textbf{(2.3)}$$

where $\mathbf{F_x(p)}$ denotes to the extent of ethanol inhibition on cell growth as a function of the threshold ethanol concentration for cell growth ($\mathbf{p_{ix}}$) and the maximum ethanol concentration for cell growth ($\mathbf{p_{mx}}$). Equation 2.3 describes the extent of ethanol inhibition on ethanol production ($\mathbf{F_p(p)}$) as a function of the ethanol concentration ($\mathbf{p}$), the threshold ethanol concentration for ethanol production ($\mathbf{p_{ip}}$) and the maximum ethanol concentration for ethanol production ($\mathbf{p_{mp}}$).

The piece-wise function however is only valid for the linear region (between the threshold and maximum tolerable ethanol concentrations). Therefore,

$$\frac{p - p_i}{p_{mx} - p_i} = 0 \quad for\ p \le p_i \qquad and \qquad \frac{p - p_i}{p_{mx} - p_i} = 1 \quad for\ p \ge p_m \qquad \textbf{(2.4)}$$

#### 2.2.4.4.2. RECOMBINANT STRAINS

In a model developed by Rogers *et al.,* (2001), the effect of ethanol on the recombinant strain *Z. mobilis* ZM4 (pZB5) was quantified experimentally and through non-linear regression analysis (Rogers *et al.,* 2001). The threshold and the maximum ethanol concentrations obtained for the specific growth rate on glucose and xylose were 28.6 $g.L^{-1}$ and 57.2 $g.L^{-1}$ (on glucose) and 26.6 $g.L^{-1}$ and 56.3 $g.L^{-1}$ (on xylose), respectively. Similarly the threshold and maximum ethanol concentrations for the specific ethanol production from glucose and xylose were 42.6$g.L^{-1}$ and 75.4$g.L^{-1}$ (on glucose) and 53.1$g.L^{-1}$ and 81.2$g.L^{-1}$ (on xylose) respectively. In general, cell growth was reported to be more sensitive to ethanol inhibition relative to the sugar uptake rate and the subsequent ethanol production rate (Rogers *et al.,* 1999; Rogers and Joachimsthal, 2000; Zhang *et al.,* 1995a).

Comparing these kinetic values to the threshold and maximum concentrations obtained from the wild-type strain *Z. mobilis* ZM4, it is apparent that the ethanol tolerance has somewhat decreased in this recombinant strain. Hence, the high expression of the xylose assimilation genes into the host strain (ZM4) has to some extent reduced the ethanol tolerance capabilities of the microorganism.

### 2.2.4.5. EFFECT OF THE DISSOLVED OXYGEN CONCENTRATION

*Z. mobilis* is facultative anaerobe that can catabolize glucose to ethanol anaerobically using the Enter-Douroroff (ED) pathway. Since *Z. mobilis* can grow under aerobic conditions, the fermentation performance of *Z. mobilis* at these conditions becomes an important aspect to the design of the fermentation vessel and the applied growth conditions. Ishikawa *et al.,* (1990) studied the batch kinetics of glucose fermentation under various oxygen supply concentrations. The mechanism proposed for the product formation shift due to the consumption of oxygen by *Z. mobilis* ATCC 29191 is illustrated in *Figure 9*.

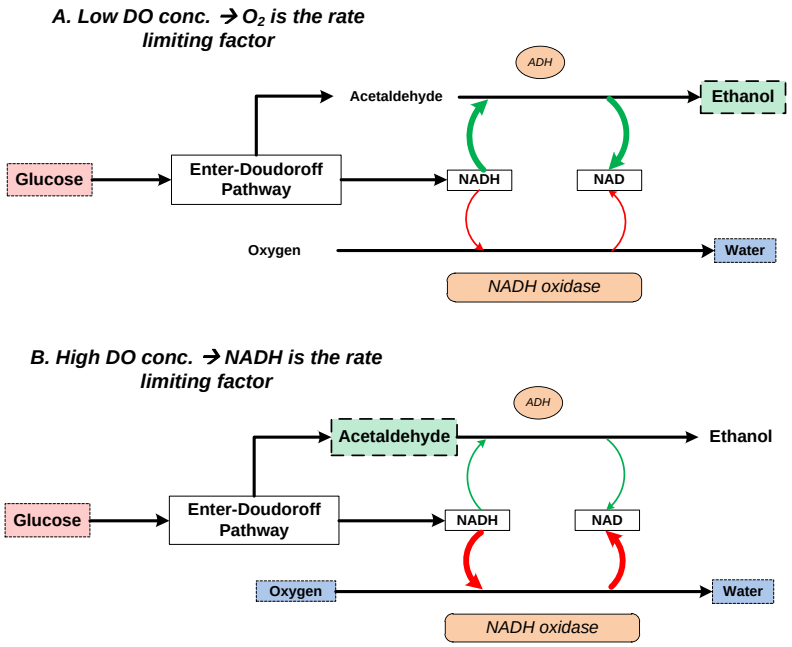


***Figure 9:*** *The mechanism of the product formation shift in Z. mobilis under aerobic conditions.* ***A*** *- At low dissolved oxygen (DO) concentrations (approximately 0.1 ppm).* ***B*** *- At high dissolved oxygen concentrations (approx. 3.5 ppm) [Redrawn from Ishikawa et al 1990]*

Whilst cell growth under conditions of oxygen supply remained unchanged, there was a significant difference in the relative amounts of acetaldehyde and ethanol formed when low and high oxygen gas flow rates were supplied to the fermentation broth (Ishikawa *et al.,* 1990). Bringer *et al.,* (1984) reported that there exists an enzyme in *Z. mobilis,* NADH oxidase, which catalyzes the oxidation of NADH in the presence of oxygen in a 2:1 molar ratio. In addition, the activity of this enzyme increases with an increase in the dissolved oxygen content. Therefore, through the utilization of NADH in the presence of oxygen, the reducing power of *Z. mobilis* is diverted from its metabolic functions towards oxygen removal. (Bringer *et al.,* 1984; Ishikawa *et al.,* 1990)

At low dissolved oxygen concentrations (close to zero), oxygen becomes the limiting factor to the NADH oxidation reaction (case *A* in *Figure 9*). Therefore, most of the NADH formed during the ED pathway is converted into ethanol by the reduction of acetaldehyde in the presence of the enzyme alcohol dehydrogenase (adh). As a result, minimal amounts of the intermediate remain in the final fermentation product. However, in the contrasting case of high dissolved oxygen concentrations (3.5 ppm, case B), the activity of the enzyme NADH oxidase increases and NADH becomes the limiting factor. Hence, most of the NADH formed from the ED pathway is diverted towards oxygen reduction and therefore acetaldehyde accumulates as the main product (Ishikawa *et al.,* 1990).

Nonetheless, at culture conditions with low oxygen supply (e.g. at conditions where the overall volumetric $O_2$ transfer coefficient ($kLa^0$) is below 11 $h^{-1}$), the growth activity, substrate uptake and ethanol production rates by *Z. mobilis* are in close proximity to fermentation under anaerobic conditions (Ishikawa *et al.,* 1990). Thus, as an aero-tolerant microorganism, there is no need for stringent anaerobic conditions. Yet, for optimal performance of *Z. mobilis*, fermentation must be performed under anaerobic culture conditions.

### 2.2.4.6. Effect of the Dissolved Carbon Dioxide Concentration

#### 2.2.4.6.1. Partial Pressure of $CO_2$

$CO_2$ is the inevitable by-product produced from the catabolic conversion of sugars such as glucose into ethanol. However, the literature based on the inhibition of the metabolically produced $CO_2$ on anaerobic growth and ethanol production capabilities of *Z. mobilis* are limited. Schreder *et al.,* (1934) performed preliminary studies on the inhibition kinetics of $CO_2$ on *Z. mobilis* and concluded that $CO_2$ inhibits the microbial growth of the *Z. mobilis* (Nipkow et al., 1985; Schreder et al., 1934).

Nipkow *et al.,* (1985) reviewed the effect of $CO_2$ on the growth of *Z. mobilis* ZM4 and ZM1 in a continuous culture (Nipkow *et al.,* 1985). They reported that the partial pressure of carbon dioxide in the reaction vessel can be controlled by $N_2$ gassing. $N_2$ gassing has the added potential for displacing dissolved $O_2$ whilst lowering $pCO_2$ as well. To nullify the effect of $N_2$ gassing on the displacement of the dissolved $O_2$ concentration, the redox potential of a strictly anaerobic continuous culture was compared to that of experiments performed under conditions where strict anaerobiosis was not

enforced. The subsequent redox potential experiments revealed that the changes in the continuous culture with changes in $N_2$ gassing were ascribed to $pCO_2$ and not the displacement of dissolved $O_2$.

Consequently, using this technique, the investigated partial pressure range was controlled at $pCO_2$ = 95 mbar to 1460 mbar. At a fixed dilution rate of $0.4h^{-1}$, they found that the reduction in $pCO_2$ from 1460mbar to 220mbar resulted in a 100 % increase in the steady-state biomass concentration in the fermentation broth (*Figure 10*). This is indicative of the inhibitive role that $pCO_2$ can play on the growth kinetics of *Z. mobilis*. At low dilution rates ($<0.3h^{-1}$), the reduction in $pCO_2$ resulted in an increase in both the volumetric substrate utilization ($q_s.x$) and the volumetric ethanol production rates ($q_p.x$).

To this end, minimizing the effect of $pCO_2$ at a fixed dilution rate would result in an increase in the steady state volumetric ethanol productivity (up to 50%).

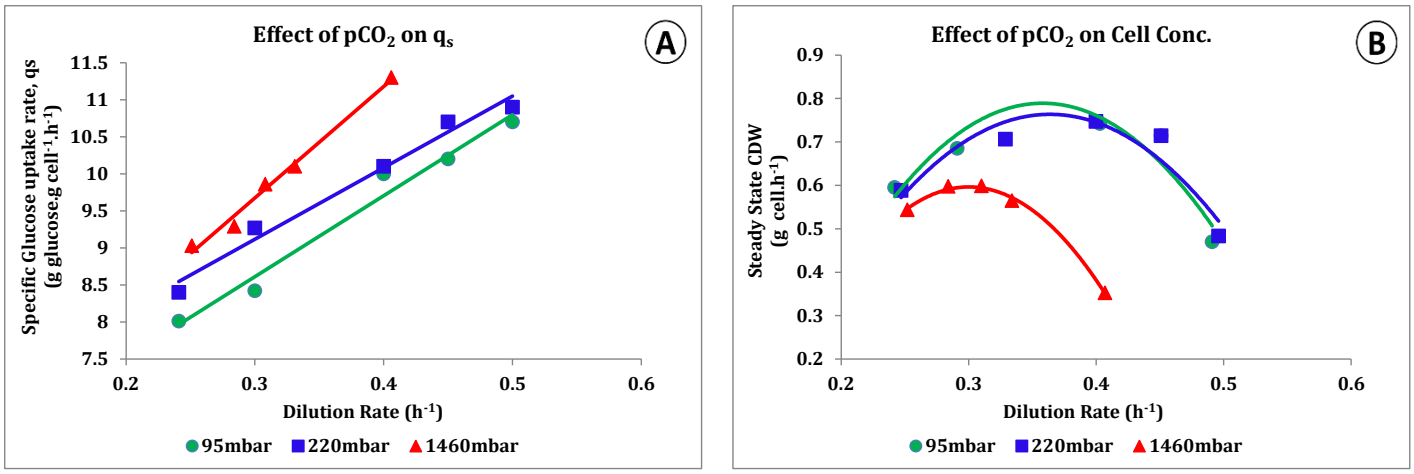


***Figure 10: A-*** *The effect of $pCO_2$ on the specific glucose consumption rate ($q_s$);* ***B-*** *the effect of $pCO_2$ on the steady state cell concentration.[Adapted from (Nipkow et al., 1985)]*

### 2.2.4.6.2. $CO_2$ EFFECT ON FERMENTATION pH

$CO_2$ can also inhibit the microbial growth, substrate consumption and product formation rates through its effect on the pH of the microenvironment. The solubility of $CO_2$ in water in the recommended optimum fermentation temperature range of 30-37 ˚C and at atmospheric pressure, is approximately 1.25-1 g $CO_2$ dissolved in 1kg of water (Anon, 2012). Even at this low pressure, it is evident that $CO_2$ is only slightly soluble in water. However, the presence of other compounds in the fermentation broth can severely alter the solubility of $CO_2$ in the solvent mixture. Solute species of $CO_2$ such as $HCO_3^-$, $H_2CO_3$, $CO_3^{2-}$ can influence the pH of the fermentation medium (Catapano *et al.,* 2009). Thus, increasing the $pCO_2$ in the fermentation broth would result in a subsequent decrease in pH. Therefore, in the design of fermentative systems, $CO_2$ removal and pH control become prerequisites for the best designs.

## 2.3. FERMENTATION STRATEGIES

Well established LC material fermentations have been traditionally performed in batch, fed-batch and continuous systems with the primary focus being on the conversion of sugars and starch materials into valuable products (Inui *et al.,* 2010). The selection of the most appropriate fermentation strategy depends largely on the kinetic properties and performance limitations of the fermentation microorganism and the process economics. Fermentations with cell-retention via cell recycle and/or cell immobilization have been touted as promising strategies for increasing the cell density in the fermenter, and subsequently leading to higher volumetric productivities (Olsson and Hahn-Hägerdal, 1996; Dhariwal, 2007; Mercier-bonin *et al..,* 2001).

### 2.3.1. BIOPROCESSING APPROACH: FREE-CELL FERMENTATION STRATEGIES

The previous section reviewed physiological approaches into improving the productivity of fermentation systems with *Z. mobilis*. The subsequent sections detail the advantages and limitations of cell retention systems within the ethanol production sphere.

#### 2.3.1.1. BATCH FERMENTATION

Traditional ethanol fermentations have been performed in batch fermenters, whereby the bioreactor is inoculated with the substrate-nutrient media and sub-cultured cells at initial conditions with the product extracted once all of the substrate or a limiting nutrient has been consumed. Batch bioreactors are typically characterized by operating conditions of high initial substrate concentrations and high product concentrations at the end of the fermentation (Roberts, 2009). As a result of transient conditions and elevated ethanol concentrations towards the end of fermentation, the rates of substrate uptake and ethanol production decline significantly towards the end of the batch fermentations (Inui *et al.,* 2010).

Some of the advantages of batch processes are realized in their ability to allow for: (i) low capital costs, (ii) ease of operation, (iii) reduced risk of contamination and (iv) low requirements for sterilization. However, drawbacks of batch fermentations have been characterized by low volumetric productivities, the existence of a lag phase at the start of new fermentations, and long downtimes during extraction of products and recharging of the substrate (Lin and Tanaka, 2006). As a result, the use of a series of batch fermenters to ensure a constant flow to product recovery has been proposed by many researchers in view of combating the low productivities from batch fermenters. However, this has the undesirable effect of adding to the initial capital expenses (Inui *et al.,* 2010; Liu 2010; Olsson and Hahn-Hägerdal, 1996).

### 2.3.1.2. CONTINUOUS FERMENTATION

In continuous fermentation processes, the substrate, growth medium and other nutrients are continuously fed into the reactor whilst the fermentation broth consisting of ethanol, residual sugars and active cells are continuously removed from the top of the bioreactor (Roberts 2009; Doran 1995; Shuler and Kargi, 2008). Due to the active biocatalysts already present in the bioreactor, potentially high rates of substrate consumption can be achieved whilst high concentrations of the product can be continuously produced. Moreover, continuous fermenters are typically operated such that the composition of the fermentation broth remains essentially constant and therefore allow for stable product quality to product recovery stages such as distillation (Inui *et al.,* 2010; Baily and Ollis, 1994).

For ethanol production, continuous culture fermentations are generally operated at low substrate concentrations, facilitating large amounts of ethanol to be produced during process operation (Rogers *et al.,* 1980). Subsequently, ethanol tolerance may limit the fermentation rate in continuous culture fermentations (Stanley and Hahn-Hägerdal, 2010). Continuous fermenters are easier to automate and generally require smaller reactor volumes relative to batch reactors due to shorter downtime periods (Inui *et al.,* 2010).

Despite numerous favourable advantages of continuous systems, they are particularly sensitive to the raw material quality since large feed/upstream process fluctuations would be difficult to attenuate and subsequently reach steady state conditions again. Moreover, at dilution rates necessary for the highest productivities, the residence time of the substrate and the active microorganisms decreases in an inverse relationship (Lievenspiel, 1999). As a result, cell washout is inflicted at dilution rates higher than the maximum microbial specific growth rate (Olsson and Hahn-Hägerdal, 1996; Lievenspiel, 1999; Inui *et al.,* 2010).Therefore, a frequent practical difficulty of continuous reactors is lower substrate conversions and ethanol product concentrations high dilution rates.

It has been reported that continuous operations tend to lead to mutations of the microorganisms due to long cultivation periods and are usually preferred for systems where the demand for a high volume product is necessary for the economic feasibility of the process. Nevertheless, the use of a mutation-stable microorganism can superimpose the possibility of mutation.

### 2.3.1.3. FED-BATCH FERMENTATION

Fed-batch fermentation strategies have found the most popularity in industrial starch-to-bioethanol plants, especially for SSF configurations (Rudolf *et al.,* 2005; Zacchi *et al.,* 2007). The fed-batch feeding is accomplished through continuous or sequential addition of substrate/nutrients to a batch culture to avoid or control substrate-associated inhibition (Ding & Tan, 2006). Under this fermentation strategy, the microorganism operates at low substrate concentrations with an increasing ethanol concentration during the fermentation process. The ability of maintaining low substrate concentrations through the intermittent addition of the substrate in fed-batch reactors

resolves the problem of substrate inhibition and catabolite repression which are in some cases prominent in batch and continuous systems (Shuler and Kargi 2008; Inui *et al.,* 2010; Liu, 2010; Olsson and Hahn-Hägerdal, 1996). The intermittent addition of the substrate improves the productivity of the fermentation by maintain low substrate concentrations (Shuler and Kargi, 2008). Additionally, fed-batch systems do not suffer from cell washout, which can become imminent in continuous culture fermentations. Concerning the fermentation of hydrolyzates from LC materials, cyclic/repeated fed-batch fermenters have been reported to facilitate in-situ detoxification of inhibitory hydrolyzate compounds by direct action from the fermenting biocatalysts (Lui, 2010).

On the other hand, similar to batch reactors, fed-batch culture systems typically necessitate stringent sterilization requirements and lengthy downtime periods are required to prepare the bioreactor for start-up conditions. Moreover, fed-batch systems typically require expensive and complex control systems that require highly qualified operators to conduct successful manufacturing operation. Nonetheless, fed-batch processes are favourable when continuous systems become impractical (such as high risk of culture mutation or contamination) and/or when the productivity of batch processes becomes too low.

#### 2.2.3.3 *FERMENTATION THROUGH BIOMASS RETENTION STRATEGIES*

Since ethanol is a high-volume-low value product, high volumetric productivities and yields are essential for the economic feasibility of the whole process. To this end, the cell concentration of ethanologic microbes in the fermentation broth becomes an important process variable given its relationship with $q_s$, $q_p$, $Y_{ps}$ and more importantly the volumetric productivity. The volumetric productivity is typically defined as:

$$VP = q_p * X \qquad \textbf{(2.5)}$$

where $\mathbf{q_p}$ is the specific rate of ethanol production (g EtOH .g $CDW^{-1}.h^{-1}$), **X** is the total active biomass concentration (g $CDW.L^{-1}$) and **VP** is the volumetric productivity (g $EtOH.L^{-1}.h^{-1}$). Therefore, high cell density cultures (HCDCs), providing that $q_p$ remains constant, have immense promise in improving volumetric productivity in many fermentation strategies (Dhariwal, 2007; Daubert *et al.,* 2003). HCDCs have been successfully used to improve the productivity of many fermentation systems (Mercier-bonin *et al.,* 2001; Groot *et al.,* 1993; Chaabane *et al.,* 2006; Roca and Olsson 2003; Persson *et al.,* 2001; Nishiwaki and Dunn 1999; Damiano *et al.,* 1985; Rogers *et al.,* 1981).

Although the productivity is proportional to the activity of the microbial cells in the fermentation broth ($q_p$), cell retention strategies can only be useful in continuous operation mode whereby the operating conditions are optimized so as to maintain high cell activity. Under these conditions, the productivity can be defined as follows:

$$VP = C_p * D \qquad \textbf{(2.6)}$$

In equation 2.6, the $\mathbf{C_p}$ is the ethanol concentration and **D** is the dilution rate ($h^{-1}$) (Doran, 1995; Shuler & Kargi, 2008; Daubert *et al.,* 2003). In general, as the dilution rate is increased, the cell activity increases due to the minimization of the effect of nutrient limitation that occurs at high cell concentrations (Doran, 1995). Moreover, at higher dilution rates the effect of maintenance energy becomes negligible relative to the rate of substrate metabolism. Hence, operating at higher dilution rates and product concentrations facilitates greater fermentation productivities (Daubert et al., 2003).

HCDC can be achieved by either (1) combining a continuous fermenter and a separator to facilitate separation of the biocatalyst from the liquid, or (2) by immobilizing the cells within a matrix inside the bioreactor. These two simple cases are illustrated in *Figure 11* below.

Whilst cell recycling has been successfully achieved using settlers for flocculating biocatalysts, centrifugation and hydrocyclones, the integration of a continuous bioreactor with cross-flow filtration unit has found greater success with respect to the cell concentration and volumetric productivity achieved (Chander et al., 2011; Daubert et al., 2003; Mercier-bonin et al., 2001).

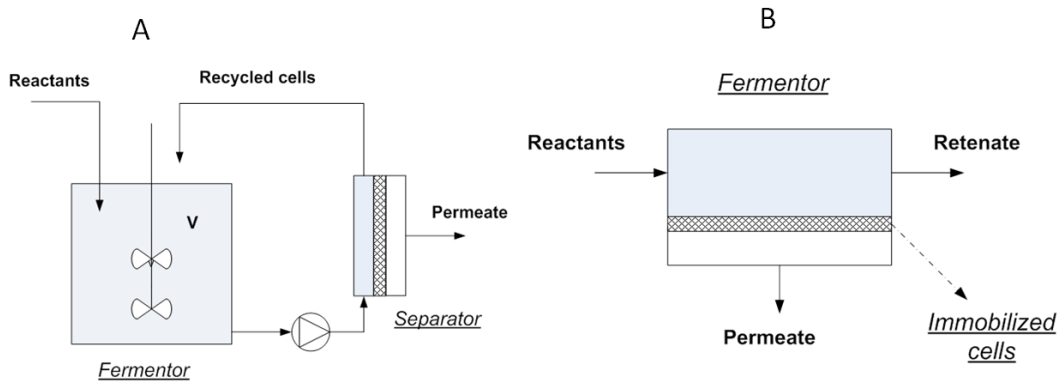


***Figure 11: A**- Fermentation Reactor Combined with a Membrane Cell Separation for cell Recycle ; **B** - Fermentation Reactor with Immobilized Cells and In-situ Product Removal [Redrawn* (Charcosset, 2006)*]*

### 2.3.2. Retention Through Cell Immobilization

Most cell immobilization systems are designed with the primary objectives of: (i) attaining high volumetric productivities, (ii) increasing the product concentration in the outlet stream and (iii) minimizing the substrate concentration in the outlet stream (Libicki *et al.,* 1985). The immobilization of cells is defined as the restriction of the mobility of the cells by confining them within a defined space (Shuler and Kargi 2008; Du Preez 2008; Charcosset 2006; Burton *et al.,* 1998). Immobilized cell cultures offer the following advantages over suspension (free-cell) cultures:

- Immobilization provides higher cell concentrations relative to suspension cultures (Shuler and Kargi, 2008).
- Immobilization of whole cell systems are not susceptible to cell washout inconveniences at higher dilution rates, hence combined with HCDCs per unit volume, they enhance the

probability of achieving high volumetric productivities relative to batch and continuous processes (Ezeji and Li, 2010; Inui et al., 2010; Shuler and Kargi, 2008).

- Immobilizing whole cells has also been reported to provide favourable micro-environmental conditions for the cells such as increased cell-cell contact, favourable pH and nutrient-product gradients. This improved microenvironment tends to result in a better performing biocatalyst (Shuler & Kargi, 2008; Scott, 1987; Zhu, 2007).
- Lastly, in some cases, immobilization provides genetic stability and offers protection towards shear damage for shear sensitive cells (Libicki *et al.,* 1985; Scott, 1987; Liu, 2010; Burton, 2001; Charcosset, 2006).

However, cell immobilization systems possess their own limitations in that they often lead to diffusional mass transfer limitations which can severely reduce the rate of product formation (Shuler and Kargi, 2008). As a result, the performance of these systems may be limited by the low rates of mass transfer between the immobilization matrix and the cell-free fermentation medium, and thus restricting $q_s$ and/or $q_p$ (Inui *et al.,* 2010). Hence, the productivity of these systems is sensitive to the mass transfer kinetics between the immobilization matrix and the fermentation media and the stability and activity of the biocatalysts at the operating conditions (Du Preez, 2008; Giorno and Drioli, 2000).

Additionally, the immobilization of growing cells can lead to production of gaseous by-products (such as $CO_2$ for anaerobic fermentations) that may have significant mechanical impact on the stability of the immobilization matrix.

On an industrial scale, whilst this technology has only been introduced about 35 years ago, major technical difficulties pertaining to rate-limiting aspects (i.e. mass transfer or kinetically limited), biocatalyst activity and stability, microbial contamination, and the requirement to operate at low substrate concentrations, have limited their success on biological systems such as LC-to-ethanol production (Charcosset, 2006). For detailed research on the use of immobilization technologies in ethanol production, reviews by Ezeji and Li (2010), Labecki *et al.,* (1985), Lui, (2010), Charcosset (2006), Giorno and Drioli, (2000) can be consulted.

### 2.3.3. Retention Through Cell Recycling

Cell recycling offers another alternative fermentation strategy for improving bioreactor productivity. Unlike immobilized cell continuous systems whereby the retained cells often lead to the formation of microbial biofilms or the disintegration of the immobilization matrix, recycled cells remain suspended in the fermentation broth and consequently minimize mass transfer limitations in anaerobic systems (Ezeji and Li, 2010).

Chander *et al.,* (2011) reported that increasing the cell density by cell recycling is best suited for increasing the volumetric productivity for processes involving slow growing microorganisms or for systems whereby low rates of product formation ($q_p$) limit the volumetric productivity of the

process. Moreover, in continuous operation, cell recycling facilitates higher substrate concentrations in the bioreactor feed due to the superior probability of substrate-cell contact. As a result, the continuous culture membrane recycle bioreactor (MRB) operational strategy facilitates the use of lesser amounts of nutrients, decreases cell mass synthesis, achieves higher dilution rates due to no expected cell washout, and increases ethanol yields (Chander *et al.,* 2011; Charcosset, 2006; Rogers *et al.,* 1980). Besides, MRB systems whereby a declining cell viability is significant, the addition of a cell bleed (<10% of the hydraulic dilution rate) has been reported to be sufficient for maintaining high cell viability within the fermenter (Ezeji and Li, 2010).

Even though MRBs have numerous advantages, they have also been associated with undesired operating conditions of high broth viscosities (due to cell proliferation), the evolution of high $pCO_2$ within the recirculation loop, high oxygen demand, declining cell viability, the accumulation of metabolic by-products to growth inhibitory levels, product degradation, and the decline in the permeate flux as the culture concentration increases (Gupta *et al.* 2002; Dhariwal, 2007). In the latter case, the hydraulic dilution rate capacity of the entire MRB system is dependent on the fouling rate of the membrane cell. Therefore, the upper limit of the operating culture concentration is limited by the filtration performance of the membrane or the effectiveness of the membrane anti-fouling techniques employed (Mercier-bonin *et al.,* 2001; Chander *et al.,* 2011; Escobar *et al.,* 2001).

Nonetheless, through careful design of the membrane cell and anti-fouling techniques, these systems have been successfully implemented in lab-scale and pilot plant glucose fermentation systems, albeit without loaded solids other than the biocatalysts (Rogers *et al.,* 1979; Escobar *et al.,* 2001; Groot *et al.,* 1993; Nishiwaki and Dunn, 1999; Chaabane *et al.,* 2006; Mercier-bonin *et al.,* 2001). Literature reported MRB systems will now be categorized with respect to ethanol production technologies within the hexose and pentose fermentation domains.

#### 2.2.3.1 *HEXOSE FERMENTATION*

Of the numerous continuous MRB fermentation systems proposed in literature, a sample of the most relevant in terms of the volumetric productivity are presented in *Table 5*. Lafforgue *et al.,* (1987; 1994) studied the continuous fermentation of a 150g.$L^{-1}$ glucose substrate with total cell recycle in a MRB. At pseudo-steady state, a high cell concentration of 330g.$L^{-1}$ was achieved at a dilution rate of 0.5$h^{-1}$ and product concentration of 65g.$L^{-1}$. The overall productivity of the system was 35g EtOH.$L^{-1}$.$h^{-1}$ and the cell viability remained greater than 75% without the addition of a cell bleed stream (Lafforgue *et al.,* 1994; Lafforgue *et al.,* 1987).

Rogers *et al.,* (1979) successfully performed the fermentation of glucose media with wild-type *Z. mobilis* ZM4 at concentrations 120-140 $g^{-1}$ in a MRB. In this study cell-liquid separation and cell recycling was facilitated by a cross-flow microfiltration module. The bioreactor was initially operated in fed-batch mode in order to increase the concentration of cells at start-up conditions. As a result, an initial cell concentration of 10-15 g.$L^{-1}$ was achieved in a 20L fermenter at start-up conditions. Based on this fermentation strategy, they obtained ethanol concentrations in the range 60-65 g.$L^{-1}$

with sustainable volumetric productivities in the range 120-200 g EtOH.$L^{-1}h^{-1}$ (*Table 5*). This was significantly higher than the productivity they previously reported from continuous culture (10-15 g EtOH $L^{-1}.h^{-1}$) (Rogers *et al.,* 1979).

***Table 5:*** *Comparison of ethanol production by continuous bioreactors integrated with membrane cell recycle modules*

| Biocatalyst | Feed Substrate conc. Glucose ($gL^{-1}$) | Xylose ($gL^{-1}$) | Lactose ($gL^{-1}$) | CDW. ($gL^{-1}$) | EtOH conc. ($gL^{-1}$) | VP (g EtOH.$L^{-1}.h^{-1}$) | Dil. Rate ($h^{-1}$) | $a_{s/v}$* ($m^{-1}$) | Reference |
|---|---|---|---|---|---|---|---|---|---|
| *S. cerevisiae* | 130 | - | - | 330 | 65 | **32.5** | 0.5 | n.a | (Lafforgue *et al.,* 1994) |
| *Baker's yeast* | 150 | - | - | 85 | 47 | **27.3** | 0.58 | 50 | (Melzoch et al., 1991) |
| *S. cerevisiae* | 100 | - | - | 56 | 47 | **19.3** | 0.41 | 44 | (Chang et al., 1993) |
| *K. fragilis* | - | - | 150 | 90 | 40 | **240** | 6 | 233 | (Cheryan and Mehaia, 1983) |
| *Z. mobilis ZM4* | 120-140 | - | - | 40-60 | 60-65 | **120-200** | 1-3 | n.a | (Rogers *et al.,* 1980) |
| *E. coli* | 140 | - | - | 170 | 65 | **85** | 1.31 | 60 | (Lee et al., 1989) |
| *S. cerevisiae* | 130 | - | - | 36.1 | 53.6 | **10.72** | 0.2 | n.a | (Damiano *et al.,* 1985) |
| *S. cerevisiae* | 210 | - | - | 60-100 | 100-115 | **11.5** | 0.1† | 1.33γ | (Escobar *et al.,* 2001) |
| *S. cerevisiae*‡ | 158 | - | - | 157 | 65 | **41** | 0.63 | 23 | (Chabaane *et al.,* 2006) |
| *S. cerevisiae*++ | 20 | 50 | - | 22 | 11.8 | **5.35** | 0.5 | 575 | (Roca and Olsson, 2003) |
| *Z. mobilis* Б | 40 | 40 | - | 11 | 41 | **6.15** | 0.15 | 70 | (Joachimsthal, and Rogers 2000) |

* effective membrane surface area/culture working volume
† dilution rate extrapolated from the residence time though the system
‡ 2-stage continuous bioreactor with cell-recycle. Second stage concentrations presented
γ Pilot plant with dual membrane cell system. Each membrane cell with effective area of $3.8m^2$
++ recombinant strain *S. cerevisiae* TMB 3001
Б Recombinant strain *Z. mobilis* (pZB5) whereby cell viability decreased significantly after 60 hours. No cell bleed was implemented

Similar volumetric productivities were obtained by Cheryan and Mehaia (1983) for the conversion of lactose (disaccharide sugar) to ethanol by *Kluyveromyces fragilis* in a MRB. In their work, an optimum productivity of 240g EtOH.$L^{-1}.h^{-1}$ was achieved at a relatively high dilution rate of 6 $h^{-1}$ (*Figure 12* in the following page). From an initial lactose concentration of $150gL^{-1}$, a cell concentration of $90gL^{-1}$ was attained in the bioreactor with the substrate conversion limited to 60%. The high dilution rates achieved during their study was primarily due to a relatively large ultrafiltration module relative to the working volume.

Indeed, by comparing the filtration surface area to the working volume in the fermenter ($a_{s/v}$ in *Table 5*), it is clear that the potential for improving the volumetric productivity increases as the membrane

surface area is increased. Large membrane surface areas facilitate greater volumetric flows from the membrane cell even at high cell densities and hence facilitate higher dilution rates (Belfort *et al.,* 1994).

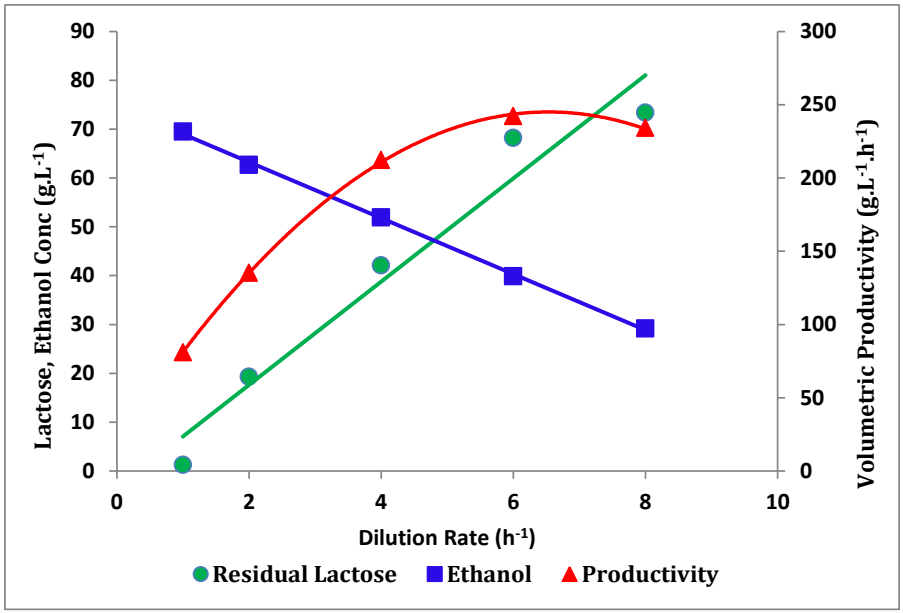


***Figure 12:*** *Continuous lactose fermentation in a MRB with cells of K. fragilis.* $X_o$ = $90gL^{-1}$, *Lactose in feed* ($S_f$) = $150g.L^{-1}$ *(Adapted from Cheryan and Mehaia 1983)*

Considering the applicability of the MRB to the glucose-xylose substrate ethanol production sphere, the addition of the microfiltration unit to a continuous culture bioprocess (without retention) must be justified by the ability of the MRB to operate at dilution rates/volumetric productivities that are not possible with traditional continuous culture.

However, the subsequent capital costs attached to the increase in the filtration area counteract the requirement of large dilution rates. Hence, depending on the process economics, a compromise between the desired process kinetics (productivity, residual substrate and product concentrations) and the capital costs exists. The selection of membrane cells and their subsequent surface areas will be discussed in *Chapter 3*.

### 2.2.3.2 *PENTOSE/ MIXED SUGAR FERMENTATION*

Whilst continuous MRBs for hexose fermentation have been shown to improve the volumetric productivity of the fermentation step, little research has been performed on pentose/ mixed sugar fermentations systems in continuous MRBs. With most pentose fermenting ethanologic microbes, the rate of substrate consumption, rate of ethanol production, and the specific growth rates of pentoses such as xylose and arabinose are much slower relative to that of glucose fermentation (*section 2.2.4*). As a result, an opportunity arises for increasing the productivity of pentose fermentation through continuous MRB fermentation strategy.

Roca and Olsson (2003) investigated the effect of total cell recycling for continuous ethanol production from xylose fermentation using the recombinant strain *S. cerevisiae* TMB 3001. At a fixed dilution rate of $0.5h^{-1}$, they reported an increase in the cell concentration from $2.2g.L^{-1}$ (without recycle) to $22g.L^{-1}$ (with recycle). Consequently, the ethanol productivity increased ten-fold from 0.5 to 5.4 g $EtOH.L^{-1}.h^{-1}$. Interestingly, the specific ethanol production rate ($q_p$) was not influenced by the recycled cells and thus the increase in the productivity was a direct result of the higher cell concentration (Roca & Olsson, 2003).

Rogers and Joachimsthal (2000) utilized a similar strategy to Rogers *et al.,* (1980) for the co-fermentation of glucose and xylose media in a MRB with total recycling of the recombinant strain *Z. mobilis* ZM4 (pZB5). At a working volume of 700mL and a glucose/xylose supply medium of composition 50/50 $g.L^{-1}$, a final biomass concentration of 11 $g.L^{-1}$ was obtained with an ethanol concentration and productivity of $50g.L^{-1}$ and 6.15 g $EtOH.L^{-1}h^{-1}$ respectively. However, the viability of the cells was reported to decrease significantly after 50h of operation with the negative effect of the sustained uncoupled mechanism (as seen by specific growth rates close to zero) identified as the major contributor to the reduction in cell viability (Rogers & Joachimsthal, 2000). However, Ezeji and Li (2010) suggested that recovery of cell viability could be achieved by adding a bleed to the recycle (Ezeji & Li, 2010). Therefore, as a modification to the process, the addition of a cell bleed becomes an essential component for sustaining long-life operation of the system.

Considering the fermentation of LC hydrolyzates, Jeffries and Sreenath (2000) reported that recycled *C. shehatae* adapted to hydrolyzate inhibitors present in wood hydrolyzate consisting of glucose and xylose as the fermentable sugars (Sreenath & Jeffreis, 2000). Similar traits were described by Purwadi *et al.,* (2007) whereby flocculating yeast was recycled (via a settler) into a continuous culture bioreactor with toxic dilute-acid hydrolyzate of spruce residues. By recycling the flocculating yeasts, the yeasts adapted to the toxic microenvironment and therefore reduced detoxification requirements (Purwadi *et al.,* 2007).

### 2.2.3.3 APPLICATION OF MRB TO CURRENT PROCESS DESIGNS

Although cell recycle systems are promising fermentation strategies, they are limited to systems whereby the separation of the cell culture from the fermentation liquid is possible. Hence, considering LC-to-ethanol production process flowsheets, MRBs are limited to systems where the lignin is removed prior to the fermentation stage. Two examples such processes are highlighted in flowsheets provided below:

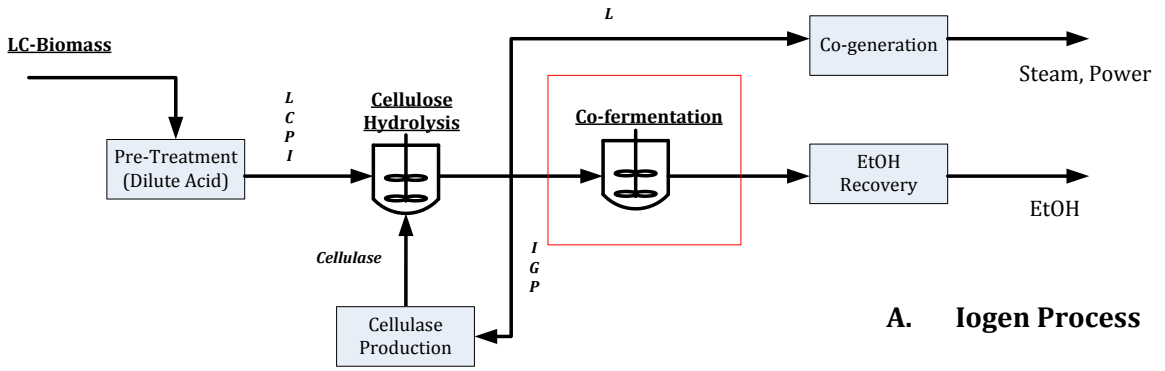


***Figure 13:*** *Iogen biomass to ethanol process proposal.* ***Notation:*** ***L****-Lignin,* ***C*** *– Cellulose,* ***P*** *– pentose,* ***I*** *– inhibitor [Redrawn from* (Lawford and Rousseau, 2003)*]*

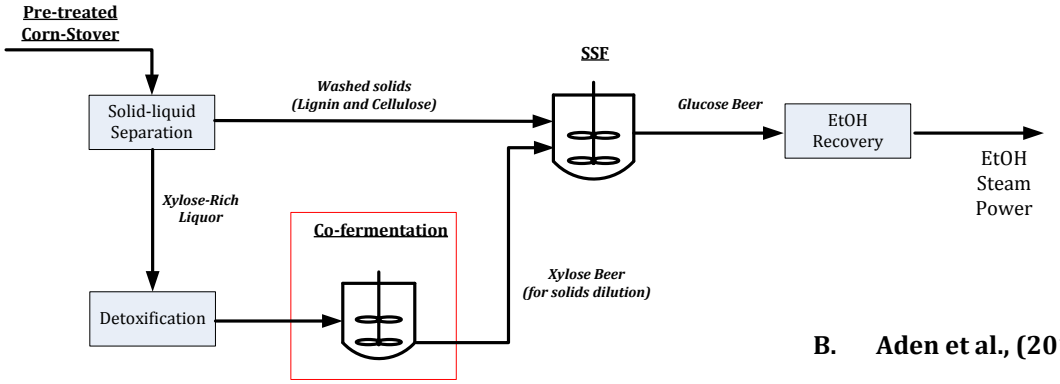


**Figure 14:** *Separate liquid solid and liquid processing with solids dilution with xylose beer [Redrawn from* (Aden et al., 2010)*]*

Iogen, a manufacturer of industrial cellulase and hemicellulose enzymes, have constructed a 40t/d biomass-to-ethanol pilot plant in view of integrating the enzyme and ethanol production facilities. Iogen process depicted in *Figure 14*, describes a proposed biomass to ethanol process characterized by the continuous co-fermentation of $C_6$ and $C_5$ sugars (from pre-treated and hydrolysed biomass) using recombinant *Z. mobilis* AX 101. The lignin fraction is separated from the hydrolyzate prior to fermentation and is used for steam and power generation (Lawford and Rousseau, 2003).

Aden *et al.,* (2010) performed an economic comparison of different fermentation process designs for the conversion of corn-stover to ethanol. The separate fermentation of the liquid and solid fractions

with recycling of the xylose beer to dilute the solids in SSF was found to give the lowest ethanol cost due to its higher final ethanol concentration after the fermentation step.

In summary MRB systems, provided that high dilution rates can be applied and inhibition conditions are avoided, facilitate high biomass concentrations, thereby decreasing substrate-cell contact time and subsequently improve the volumetric productivity of the unit. Considering pentose fermentation, MRBs appears to be a promising alternative fermentation strategy for improving the volumetric productivity of the ethanol production process. The following chapter continues with the literature survey but focuses on the challenges posed by the addition of a separation/retention unit to biologically active bioprocesses.

# CHAPTER 3

# MEMBRANE MODULE DESIGN

*The previous chapter highlighted the promise of MRBs in LC-to-ethanol fermentative systems. In addition to the fermentation conditions, the performance of a MRB fermentative system is highly dependent on the filtration performance of the membrane module at high cell densities. At these high densities, membrane fouling and subsequent anti-fouling techniques play a significant role in the efficiency of the MRB process configuration. Therefore, the coupling of a continuous fermenter with a cross-flow filtration membrane module on a laboratory and bench scale should be designed with future scale-up and operational techniques taken into consideration (Dhariwal, 2007).*

## 3.1 PARAMETERS AFFECTING MRB PROCESS DESIGN

The most significant parameters for the design of a MRB were highlighted in reviews by Carstensen *et al.,* (2012) and Catapano *et al.,* (2009) and are summarized in *Figure 15*. The identified factors by no means seclude the array of design parameters required for MBR designs but present basic ideas with this respect.

The design of an in-situ/ex-situ MRB is classified into six major categories: (1) the cell/biocatalyst characteristics, (2) process mode of operation, (3) the selection of the membrane geometry and module design, (4) definition of adequate anti-fouling measures, (5) the applicable sterilization techniques required to facilitate aseptic conditions and (6) scale-up capability. These categories have been identified as essential design areas which impact the viability and applicability of MRBs on a biotechnological scale. Whilst it is clear that these aspects overlap with each other, there is no single cultivation system that is suitable for all applications in the biotechnology sphere. Therefore, further discussion of these factors will be focussed on the proposed LC-ethanol production system.

In view of ethanol production with *Z. mobilis* as the biocatalyst, the characteristics of the biocatalyst and process modes of operation were detailed in sections 2.2 and 2.3 respectively. Considering an ex-situ MRB, the selection of a membrane type and material will be discussed with regard to the specific separation task. Furthermore, since membrane fouling is a major limitation for HCDCs, the enhancement of the filtration performance through the reduction of membrane fouling will be reviewed. Detailed discussion of sterilization techniques and scale-up opportunities go beyond the

scope of this work. The afore-mentioned reviews can be consulted for further details on the parameters affecting the sterilization and scale-up of the design of MRBs.

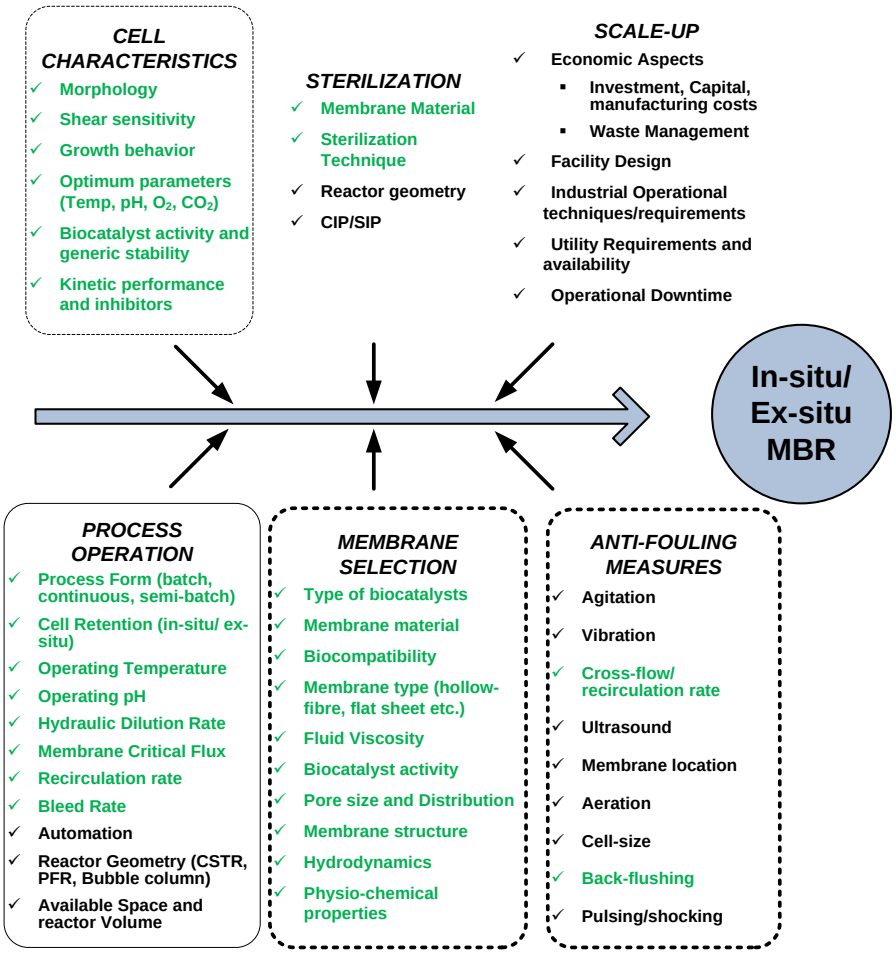


***Figure 15:*** *An overview of the factors influencing the design of MRBs (Adapted from Carstensen et al., (2012) and Catapano et al., 2009))*

## 3.2 MEMBRANE GEOMETRY AND MODULE SELECTION

### 3.2.1 MEMBRANE PORE SIZE

Microfiltration membranes typically characterized by the their ability to retain molecules of a specific molecular weight range (Du Preez, 2008). The molecular-weight cut-off (MWCO) defines the mean pore size of the selective/active layer, thereby defining the separation properties of the membrane. Wild-type *Z. mobilis* is a rod-shaped bacterium with an average length of 2-6µm and an average width of 1-1.4µm (1 µm = 10 000 kDA) (Swings and De Ley, 1977). The size of the permeable layer for bacteria retention is recommended to be at least three times smaller than the smallest dimension of the biocatalyst to prevent leakage of growing cells and to facilitate penetration of the reaction products (Libicki *et al.,* 1985).

In a review by Zhao *et al.,* (2000), it was reported that membrane fouling is more severe with increasing pore size, especially when the feed suspension consists predominantly of macromolecules (Zhao *et al.,* 2000). This stems from the fact that membrane fouling changes the effective membrane pore size and pore size distribution. As a result, the permeate flux, membrane selectivity and retention efficiency drop accordingly (Belfort *et al.,* 1994). Consequently, membranes with wide pore-size distribution have poor selectivity.

### 3.2.2 Selection of a Membrane Geometry

The most common membranes in bioprocessing are tubular and flat-sheet membranes. Flat sheet membrane cells are generally constructed in a 'plate-and-frame (PF)' or 'spirally-wound (SW)' f whilst tubular membranes are assembled with hollow-fiber (HF) membranes or capillary tubes (CT) in a multiple heat-exchanger configuration (Drioli and Giorno, 1999). Pearce *et al.,* (2011) defined that at ideal conditions, membranes should be configured such that they have:

- High membrane surface area to bulk volume ratio (packing density)
- High degree of turbulence for mass transfer promotion on the feed side
- Low energy requirements per unit product (filtrate) volume
- Low cost per unit membrane area
- Facilitate easy cleaning
- Design must permit modularization (scale-up)

In general, the minimization of the economic costs per unit membrane area is directly proportional to the desired permeate flow. However, some of the aforementioned factors are mutually exclusive. For example, increasing the degree of turbulence promotion requires higher energy requirements and is adversely affected by the packing density (Pearce *et al.,* 2011; Shirazi *et al.,* 2010). Moreover, the production of high membrane packing densities typically requires narrowing the pore channels (Zhao *et al.,* 2000).The subsequent narrowing the pore channels compromises the ease of membrane cleaning (Pearce *et al.*, 2011).

The characteristics of the four main membrane geometries are presented in *Table 6* below.

***Table 6:*** *Desired Membrane module characteristics [Adapted from Belfort et al., 1994; Pearce (2011)]*

| Membrane Geometry | Packing Density | Turbulence Promotion | Permeation Flux | Back-flushable? | Scale-up |
|---|---|---|---|---|---|
| *PF* | intermediate | intermediate | High | No[#] | difficult |
| *SW* | intermediate | low | intermediate | No | difficult |
| *CT* | intermediate-high | intermediate | High | Yes | easy |
| *HF* | very high | intermediate* | Low | Yes | easy |

*# - newer panels are back-flushable*
** - dependent on packing density*
PF - "plate and frame" flat sheet; SW - "spirally wound"; CT "capillary tube"; HF - "hollow fibre"

Cell culture media/suspensions typically consist of macromolecules and foulants that tend to form compressible cakes and subsequently deteriorate the filtration performance of the membrane cell. Principally, the filtration performance of microfiltration membranes for difficult suspensions such as cell culture requires very high cross-flow velocities (in the turbulent regime) to promote tangential momentum on the membrane surface (Belfort *et al.,* 1994; Shirazi *et al.,* 2010; Catapano *et al.,* 2009). Therefore, considering cell retention, capillary or hollow-fibre membranes have been favoured due to the following rationale:

- They are less expensive (per unit membrane area) relative to flat-sheet or spirally wound membranes (Du Preez, 2008)
- They have higher packing densities (Charcosset, 2006; Carstensen *et al.,* 2012)
- Higher potential for turbulence promotion which induces tangential flow along the membrane surface and limits fouling (Du Preez, 2008; Drioli and Giorno, 1999)
- They facilitate minimal cell loss during operation due to the nature of the support and permeable layer.
- Membrane flux can be recovered through back-flushing. Back-flushing reverses the driving force direction across the membrane, and subsequently removes solids and/or compressible cakes from the membrane pores
- The flow hydraulics can be controlled (Shuler and Kargi, 2008; Belfort *et al.,* 1994)
- They are easier to sterilize.

As a result, a tubular membrane has been selected as the preferred membrane geometry for this work. *Figure 16* presents a photomicrograph of a hollow-fiber membrane.

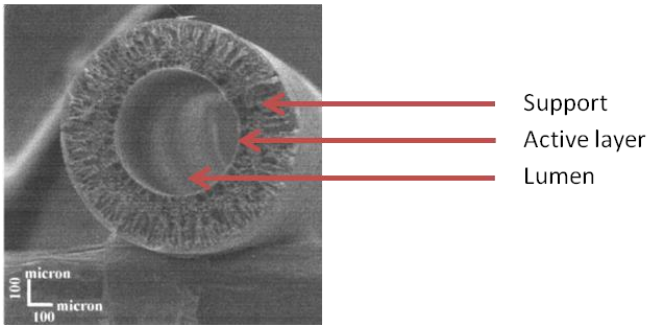


***Figure 16:*** *Photomicrograph of the cross section of a anisotropic ultrafiltration hollow fiber membrane with an active/permeable layer on the lumen side [Adapted from (Ferraz et al., 2001) with permission from Elsevier*]

### 3.2.3 MEMBRANE MATERIAL

Tubular membranes are usually fabricated to attain high surface porosity and narrow pore size distribution. However, the mechanical strength (structural integrity) of membranes is a significant characteristic considering long-term operation (Dhariwal, 2007; Persson *et al.,* 2001). Consequently, hollow-fiber and capillary membranes generally comprise a thin selective/permeable layer, which provides the required selectivity/retention efficiency, and a thick spongy/porous support that

provides the required mechanical stability (Pearce *et al.,* 2011). In addition to mechanical stability, the membrane material selection criteria should encompass the following aspects:

i. the suitability of the membrane towards the operating temperature and pH range (Pearce *et al., 2011)*,
ii. stability towards sterilization (e.g. autoclaving at 121 $^{o}$C, 2bar) (Belfort *et al.,* 1994; Du Preez, 2008; Persson *et al.,* 2001),
iii. the membrane material should be biocompatible (Carstensen *et al.,* 2012),
iv. physio-chemical properties (e.g. hydrophilicity and surface charge effects) should not contribute to membrane fouling (Zhao *et al.,* 2000; Pearce *et al.,* 2011),
v. the membrane permeability (Carstensen *et al.,* 2012)
vi. and the capital cost of the membrane (Carstensen *et al.,* 2012)

In reviews by Zhao *et al.,* (2000) and Belfort *et al.,* (1994), physiochemical interactions between the macromolecules, such as proteins and sugars, and the membrane material were reported to be significant factors in promoting or reducing membrane fouling. The physiochemical interactive mechanisms include electrostatic interaction, hydrophobic effects, charge transfer (e.g. hydrogen bonding) and/or a combination of these.

#### 3.2.3.1 *SURFACE CHARGE*

The surface charge on a membrane is greatly affected by the solution pH, ionic strength and the membrane material (Zhao *et al.,* 2000). Moreover, it has been shown that the permeate flux through the membrane can be promoted by operating at conditions whereby the membrane and the macrosolute are of similar charge (Nakao *et al.,* 1988). However, in biological systems, the filtration solution is fixed by the nutritional requirements of the biocatalysts and therefore maintaining similar surface charge between the macrosolute and the membrane without interfering with the activity of the biocatalyst is currently a challenging prospect.

#### 3.2.3.2 *HYDROPHILICITY/HYDROPHOBICITY*

The extent of membrane surface "wetting" is defined by another key surface property, i.e. the hydrophilicity. Hydrophilic membrane surfaces are easily wetted and therefore facilitate higher permeabilities compared to hydrophobic surfaces (Pearce *et al.,* 2011). Moreover, since hydrophobic interactions generally occur between macrosolutes, microbial cells, and the membrane material, membrane fouling is expected to be more severe in hydrophobic membrane surfaces relative to hydrophilic surfaces (Pearce *et al.,* 2011). As a result, hydrophilic surfaces are often referred to as low-fouling surfaces (Belfort *et al.,* 1994; Zhao *et al.,* 2000; Pearce *et al.,* 2011). However, the hydrophilic nature of the membrane surface can be potentially offset by the effects of concentration polarization and/or reversible membrane fouling (Le Clech *et al.,* 2003; Pearce *et al.,* 2011; Zhao *et al.,* 2000).

#### 3.2.3.3 *POLYMERIC AND CERAMIC MEMBRANES*

Classic biotechnological membrane materials include polymeric and ceramic membranes due to their chemical and heat stability (Giorno and Drioli, 2000). Commercial ultrafiltration/microfiltration polymeric membranes such as polyethersulfone (PES), polysulfone (PS) and polytetrafluorethylene (PTFE) have been used extensively in bioprocesses owing to their high thermal and chemical stability, their wide hydrophobic/hydrophilic range, and their relatively low-cost. However, sterilization of polymeric membranes by autoclaving tends to be problematic.

Ceramic membranes are advantageous for bioprocesses in view of their high resistance towards sterilization temperatures and pressures, resistance to harsh chemicals, and high mechanical strength. In addition, ceramic membranes generally have a well-distributed pore structure and exhibit a higher permeability relative to polymeric membranes (Giorno and Drioli, 2000; Strathmann *et al.,* 2000; Carstensen *et al.,* 2012; Du Preez, 2008; Dhariwal, 2007). The short-coming of ceramic membranes is their relatively high initial capital cost. Nonetheless, a ceramic membrane material shall be adopted in this research in view of their potential for higher permeate flux, higher mechanical strength, longer production runs between cleaning, and shorter cleaning times.

## 3.3 MEMBRANE FOULING

Membrane fouling mechanisms such as pore plugging and cake layer formation by the microorganisms are almost inevitable for pressure-driven membrane processes and can be considered a significant intrinsic phenomena (Drioli and Giorno, 1999; Giorno and Drioli, 2000; Steynberg, 2012; Pearce *et al.,* 2011). The fouling behaviour is influenced by a many factors such as the operating hydrodynamic conditions, suspension chemical characteristics, membrane surface charge, hydrophobicity, molecular size and the membrane material. In general the consequence of membrane fouling is a decline in the permeate flux, high energy requirements to maintain a constant flux, and frequent membrane cleaning (Belhocine *et al.,* 2000; Saroj *et al.,* 2008; Dhariwal 2007; Carstensen *et al.,* 2012).

### 3.3.1 *CROSS-FLOW AND DEAD-END FILTRATION*

Classical pressure-driven membrane processes can typically be operated in one of two modes, i.e. cross-flow filtration or dead-end filtration (*Figure 17*). Dead-end (DE) filtration, whereby the fluid motion is perpendicular to the membrane surface and is characterised by the absence of a retenate stream, usually forms a concentrated cake layer due to the accumulation of retained particles on the membrane surface. In this case, the resistance to the permeability of the membrane is proportional to the thickness of the concentrated cake layer (Belfort *et al.,* 1994; Charcosset, 2006; Carstensen *et al.,* 2012; Pearce *et al.,* 2011; Drioli *et al.,* 2010).

The cross-flow (CF) filtration mode is often favoured in most MRBs since the feed suspension (upstream of membrane) flows parallel to the membrane surface and permeates through the perm-selective membrane due to a pressure difference induced by a trans-membrane pressure (TMP) (Du Preez, 2008). As a result of tangential flow at the membrane surface, the probability of cake layer formation is reduced and this subsequently extends the operational time. In CF filtration mode, pseudo-steady state is achieved when the adhesive forces binding the cake layer are balanced by the tangential forces induced by the parallel velocity (Belfort *et al.,* 1994; Pearce *et al.,* 2011). Due to the favourable characteristics of the cross-flow configuration, a cross flow substrate feed was adopted for the MBR design in this work.

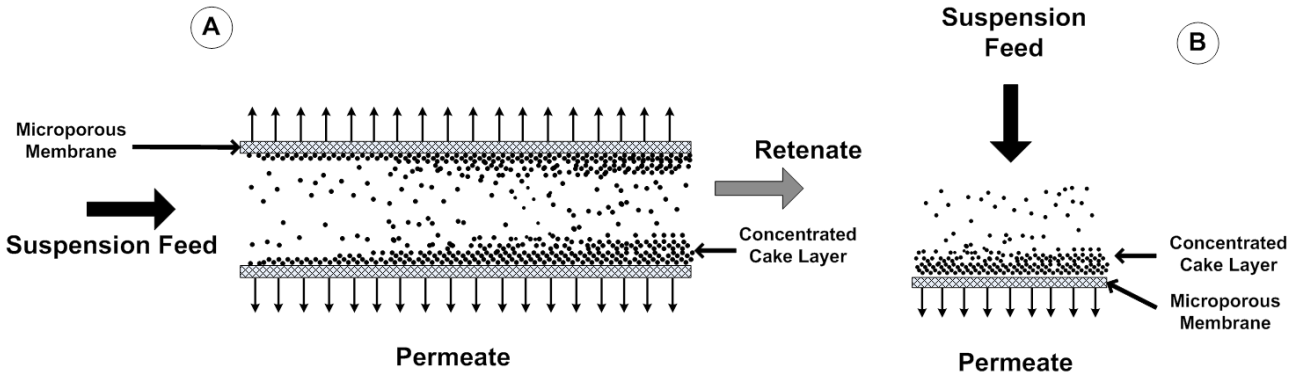


***Figure 17:*** *Filtration Principles in Membrane Processes; A - Cross-flow filtration Dead-end filtration; B - Dead-end filtration [Redrawn from* (Pearce et al., 2011)*]*

### 3.3.2 CONCENTRATION POLARIZATION

According to Belfort *et al.,* (1994) "concentration polarization (CP) is the reversible accumulation of dissolved or suspended solute in the solution phase near the membrane-solution interface due to a balance between the convective drag toward and through the membrane (permeate flux) and the back-transport flux away from the membrane". This phenomenon is illustrated in *Figure 18*.

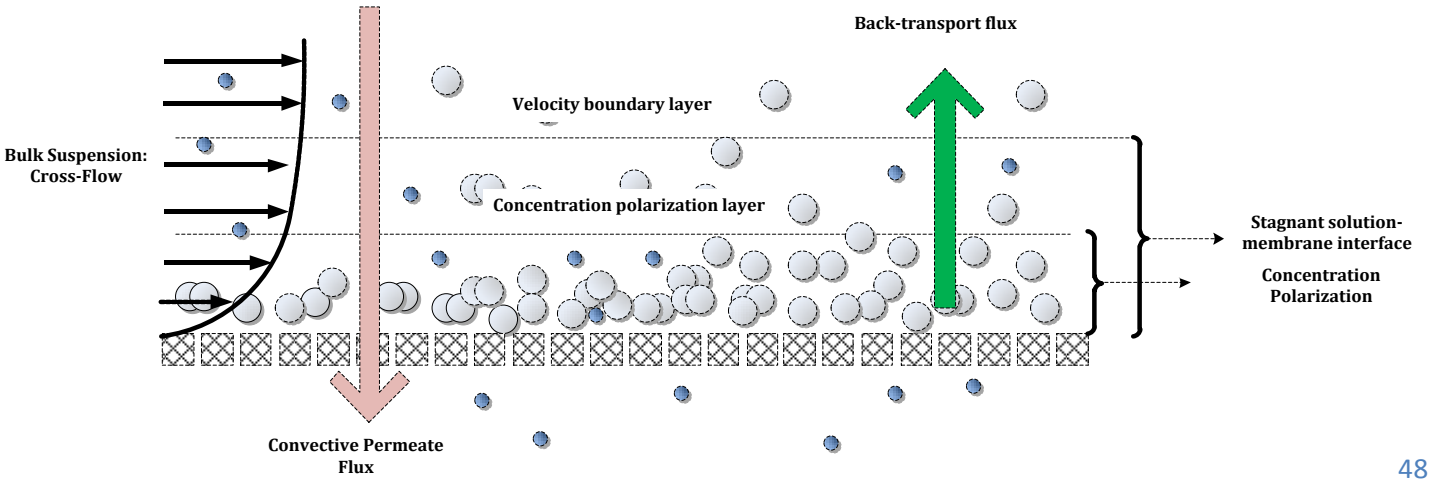


***Figure 18:*** *Concentration polarization mechanism [Redrawn from* (Pearce *et al.,* 2011)*]*

During cross-flow microfiltration, the velocity near the membrane surface is assumed to be laminar. Moreover, the velocity at the membrane surface is assumed to be zero due to wall friction effects. As a result, a velocity boundary layer is formed in a region near the membrane surface. Subsequent to the rejection of solutes at the membrane surface, a concentration boundary layer develops within the velocity boundary layer with concentrations higher than those in the bulk suspension.

At the velocity boundary layer interface, the concentration of the solute is greater than that in the bulk suspension feed. Hence, due to a solute concentration gradient between the interface and the bulk suspension, back-diffusion of the solute into the bulk suspension is induced. This phenomenon occurs until the convective flow is balanced by back-diffusion (Pearce *et al.,* 2011).

The presence of CP usually results in a reduction in the permeate flux by increasing the osmotic pressure upstream of the membrane (Belfort *et al.* 1994; Steynberg, 2012). Consequently, the presence of the osmotic pressure (acting in the opposite direction of the TMP), decreases the effective TMP driving force.

The effects of CP become more significant in micro-filtration systems with colloids (cells in biological systems) which permit low back-diffusion coefficients. In such systems, the probability for cell deposition onto and into the membrane pores at higher permeation fluxes is much higher relative to the back-transport mechanisms (Belfort *et al.,* 1994). Therefore, for minimizing CP, factors which enhance back-diffusion such as increased cross-flow velocity (decreasing the thickness of the stagnant film) and higher temperature operation are essential. On the other hand, higher TMPs or permeate fluxes increase convection through the membrane and subsequently increases CP (Shirazi *et al.,* 2010).

### 3.3.3 Physical Mechanism for Flux Decline

The accumulation of suspension particles/materials at the membrane surface and/or their adsorption into the membrane pores, which result in the reduction of the permeate flux, is termed membrane fouling. Following this definition of membrane fouling, the CP phenomena is not considered as fouling, even though it too contributes to the decline in the permeate flux (Shiraiz *et al.,* 2010). Once, the filtration process has ceased, the velocity boundary layer and the CP phenomenon vanish too. Nonetheless, Belfort *et al.,* (1994) described the physical fouling process as a multi-phase mechanism that includes: macromolecular adsorption (phase I), particle deposition (phase II), multiple sub-layer development (phase III), sub-layer compaction/ compression (phase IV), and sub-layer binding (phase V). The schematic of this multi-phase mechanism is presented in *Figure 19*.

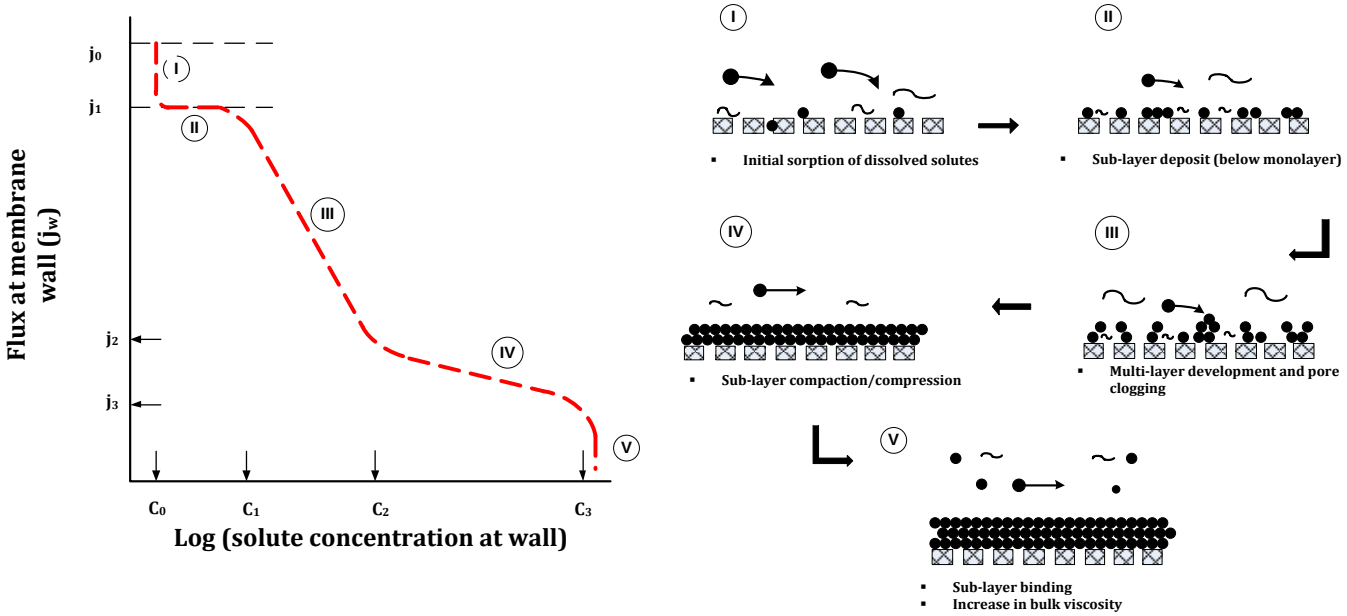


***Figure 19:*** *Phases of physical fouling phenomena [Redrawn from (Belfort et al., 1994)]*

### 3.3.3.1 *PHASE I: RAPID ADSORPTION OF MACROMOLECULES*

The initial phase is characterised by the adsorption of dissolved macromolecules, which are present in the culture medium (e.g. polysaccharides, protein), into the membrane pores and/or surface. As a result, the permeate flux declines at a rapid rate due to fast adsorption kinetics and high macromolecule-membrane binding constants. The flux decline continues until all the adsorption sites are unavailable, at which point pseudo-steady state is achieved.

### 3.3.3.2 *PHASE II: SUB-LAYER DEVELOPMENT*

Suspended cells (fed into a pressure-driven membrane) begin to deposit onto the membrane surface without forming a uniform monolayer. Due to significant portions of the membrane surface being cell-free, the initial deposition of the cells onto the membrane surface has negligible effect on the permeate flux. However, as monolayer coverage is approached, the flux begins to decline and the mechanism shifts towards phase III.

### 3.3.3.3 *PHASE III: MULTI SUB-LAYER DEVELOPMENT*

The third phase is characterised by a sharp but constant decline in the permeate flux. During this phase, the flux decline or rate of solids deposition onto the membrane remains relatively constant and at a maximum (indicated by constant negative slope in *Figure 19*). As the cell deposit monolayer begins to develop into multiple sub-layers, it affects both the cross-flow velocity and the flux rate at the membrane wall. Operating at a constant volumetric flowrate, sub-layer development decreases the cross-sectional area and subsequently increases the wall shear rate. The increasing wall shear rate favours the back-diffusion of the cells back into the cell suspension. However, at the same conditions, multiple sub-layer development increases the axial TMP. The additional TMP

subsequently increases the driving force for permeation velocity but also compresses the cell sub-layers which decrease the effective surface porosity and the permeation velocity. Therefore depending on the magnitude of the TMP increase, an increase or decrease in the overall permeation velocity can be expected.

#### 3.3.3.4 *PHASE IV: SUB-LAYER COMPACTION/COMPRESSION*

Once the rate of sub-layer development has stabilized, the permeation rate decreases slowly. Throughout this phase, the rate of mass transport is predominantly influenced by the densification/cell layer arrangement within the sub-layers.

#### 3.3.3.5 *PHASE V: SUB-LAYER BINDING*

When the cell concentration in the feed solution approaches that of the multiple sub-layers on the membrane surface, a sharp decrease in the permeate velocity is expected due to difficulty in the permeation of the very viscous solution.

### *3.3.4 BIO-FOULING*

#### 3.3.4.1 *EXTRACELLULAR POLYSACCHARIDES (EPS)*

Other than particulate fouling, other membrane fouling mechanisms such as biofouling exist for microbial systems. Many microorganisms produce extracellular polysaccharides (EPS), some of which can be sources of diffusive resistances (Libicki *et al.,* 1985). EPSs are a complex mixture of proteins, carbohydrates, DNA lipids, and humic substances that surround the cells and form a matrix of microbial flocs under specific operational conditions. These EPSs tend to increase the viscosity of the fouling sub-layers and therefore increase the filtration resistance across the membrane (Dhariwal, 2007).

*Z. mobilis* has been reported to produce the extracellular substance levansucrase under certain conditions of sucrose fermentation. Nonetheless, there is no mention in literature of the formation of this EPS for glucose or xylose fermentations.

#### 3.3.4.2 *SURFACE-GROWTH*

Due to CP, the concentration of the dissolved nutrients at the membrane surface facilitates ideal growth conditions. Consequently, cells deposited onto the membrane surface through either physical fouling or CP may grow at the surface and form a gel-like layer or biofilm (Steynberg, 2012). The formation of this gel-layer/bio-film is undesired since the effect of the wall shear forces induced at high cross-flow velocities is minimized by the increased binding of the “immobilized” culture.

### 3.3.5 MEMBRANE RESISTANCE

Several models have been developed to describe the degree of flux decline, most of which are solution and equipment related (Van den Berg and Smolders, 1990). In general, the observed flux decline has been explained by a decreasing driving force and/or an increased resistance on the membrane surface due to membrane fouling. The primary resistances that account for decreasing the permeate flux are, membrane resistance ($R_m$), CP resistance ($R_{cp}$), Cake resistance ($R_c$), pore-blocking resistance ($R_p$) and macrosolute adsorption resistance ($R_{ads}$). A schematic of the aforementioned resistances for porous membranes is presented in *Figure 20*.

Mathematically, the flux for constant pressure driven processes can be described by Darcy's Law as follows:

$$J = \frac{dV}{A_{mem} * dt} = \frac{\Delta P}{\eta_0 * (R_{cp} + R_c + R_m + R_p + R_{ads})} \qquad \textbf{(3.1)}$$

In Equation 3.1, $\boldsymbol{\eta_0}$ represents the fluid viscosity, $\Delta$**P** is the transmembrane pressure (kPa), **V** is the volume of permeate recovered (L), $\mathbf{A_{mem}}$ is the membrane surface area ($m^2$), and **J** is the permeate flux rate ($L.m^{-2}.h^{-1}$) Membrane resistance is triggered by the membrane itself and is dependent on the membrane thickness, tortuosity, porosity, surface chemistry and pore size distribution (Shiraz *et al.,* 2010). Pore-blocking and adsorption of the solute onto the walls of the both result in a decline in the membrane permeability. These two resistances are explained by Phase I in the physical fouling mechanism (*section 3.3.3.1*). CP is characterized by the accumulation of the solute at the membrane surface-bulk flow interface such that the concentration at this interface becomes so high that it forms an additional resistance layer.

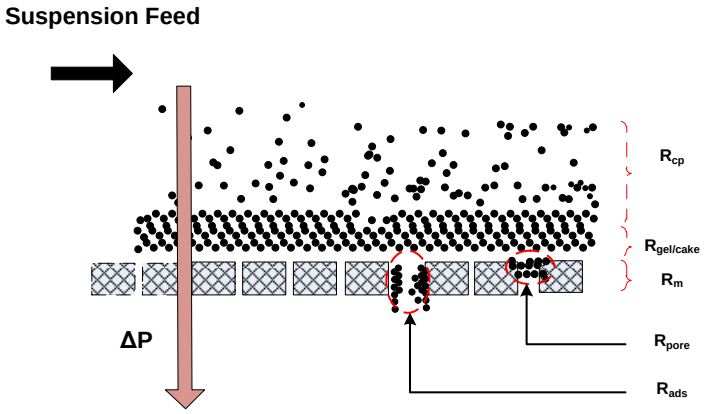


***Figure 20:*** *Overview of the major resistances contributing to the permeate flux decline of a porous membrane during filtration [Redrawn from (van den Berg and Smolders, 1990)]*

In cases whereby the suspension feed consists primarily of particles that are too large to inflict pore resistance, a surface filtration mechanism of sieving occurs (Belfort *et al.,* 1994). Hence, the accumulation of these particles results in a growing cake layer and subsequently an increasing resistance to filtration. This filtration resistance is linked to Phase's III and IV of the fouling mechanism. Moreover, mathematical modelling of the resistance of the filtration cell cultures, which are highly compressible, becomes challenging.

### 3.3.6 TUBULAR MEMBRANE FLOW CONFIGURATION

The performance of tubular membranes is determined to a large extent by the transport rate of key nutrients and/or and products through the membrane. Therefore, a large diffusional resistance provided by the membrane would severely limit the performance of the membrane (Paterson *et al.,* 1988; Kelsey *et al.,* 1990).

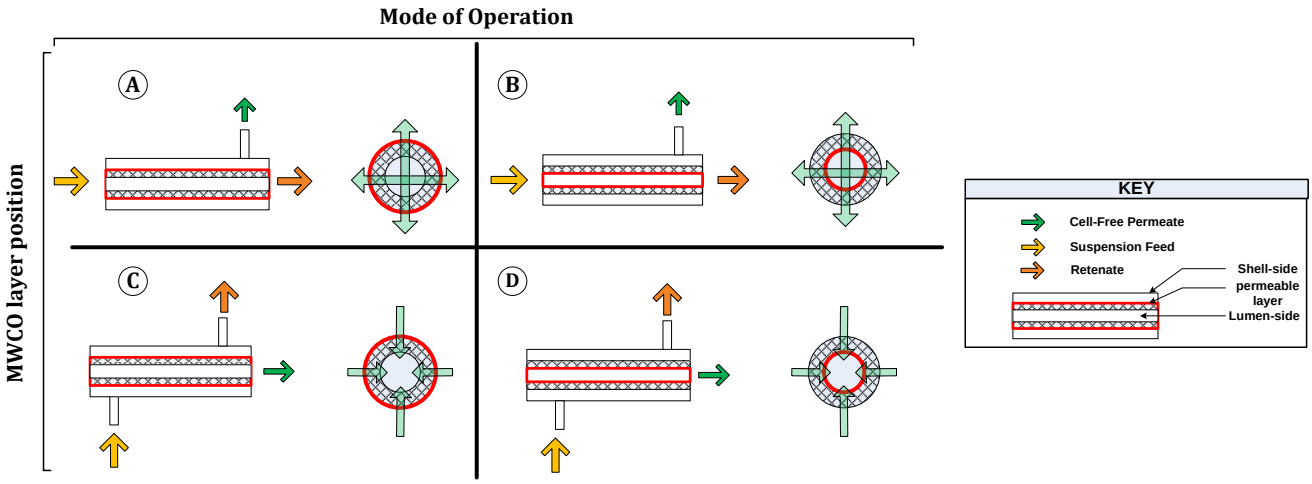


***Figure 21:*** *Various Mode-of-Operation and position of permeable layer.* ***A*** *- permeable layer outside, "Lumen-to-Shell" flow direction;* ***B*** *– permeable layer inside, "Lumen-to-Shell" flow direction;* ***C*** *– permeable layer outside, "Shell-to-Lumen" flow direction;* ***D*** *- permeable layer inside, "Shell-to-Lumen" flow direction*

The mode-of-operation, typically expressed in terms of the direction of flow, is determined by the desired flow mechanism driven by the TMP (*Figure 21*). The TMP can be created either by applying a vacuum on the permeate side in a "lumen-to-shell" configuration (A and B) or by increasing the pressure on the shell side in a "shell-to-lumen" configuration (C and D). Moreover, the permeable layer can be positioned either on the inside (lumen-side) or outside (shell-side) of the tubular membrane.

The position of the permeable layer is known to affect the rate of membrane fouling and the subsequent ease of flux recovery from the membrane cell (Carstensen *et al.,* 2012, Belfort *et al.,* 1994). Considering biological MRBs used exclusively for cell retention purposes, hardly any information pertaining to the effect of the MWCO position was found in literature. However, considering the fouling mechanism presented in *section 3.3.3* and minimizing flux decline as a function of membrane fouling and concentration polarization, only the configurations with the cut-off layer on the tangential cross-flow side were considered (case B and C). The use of surface hydrodynamics (such as operating at high cross-flow velocities) is only effective for in minimizing external membrane fouling (by arresting cake layer thickness) and concentration polarization (promoting back-diffusion) (Mercier-bonin *et al.,* 2001). In the operational strategies A and D, surface hydrodynamics would have minimal effect in minimizing internal fouling through pore-plugging and solute adsorption. As a result, flux recovery would be more difficult to perform.

### 3.3.6.1 *LUMEN-TO-SHELL (CONTINUOUS OPEN LUMEN)*

The lumen-to-shell (L-S) configuration is based on the concept of feeding the reactor effluent (cell suspension, unconverted substrate, products) in the lumen side and extracting the cell-free product out the shell side of the membrane (*Figure 22*). Following from the previous section, the permeable layer is generally on the lumen side. This operational strategy is driven by the differential pressure across the membrane to facilitate cell-liquid separation (Paterson *et al.,* 1988).

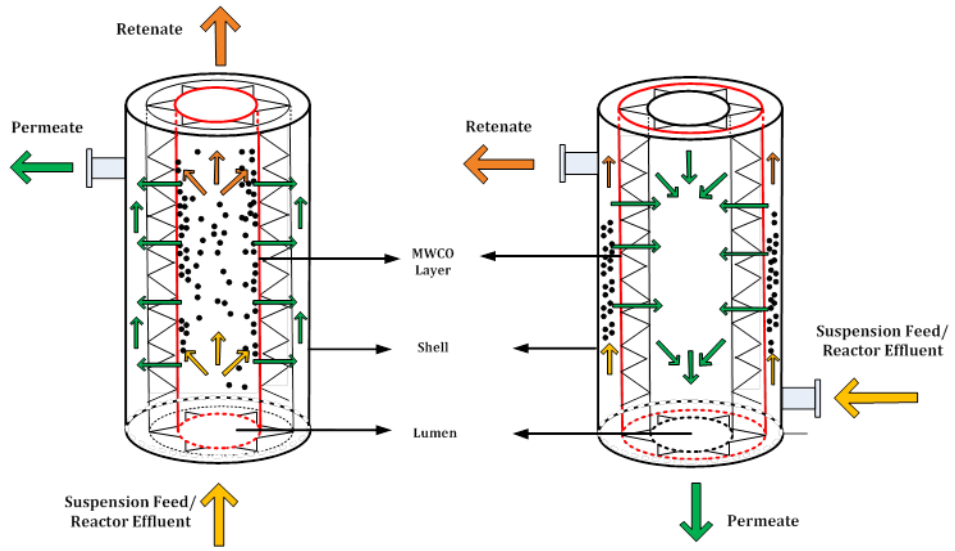


***Figure 22:*** *A single channel tubular membrane encased in a pressure vessel (shell). Configuration A: Lumen-to-Shell (left); Configuration. B – Shell-to-Lumen (right)*

The desirability of this configuration is manifested in the ability to (1) control the surface hydrodynamics by selecting the lumen-side diameter and (2) the ease of scale-up by selecting tubular membranes with multiple flow channels. For example, single channel hollow-fiber membranes can be replaced with a multiple channel membrane with a higher overall surface area. The increased surface area facilitates higher permeate flux rates. In addition, the exponential increase in the surface shear rate with the reduction in the pore channel diameter makes this configuration favourable for minimizing the thickness of the cake layer formed through particulate accumulation at the membrane surface.

However, depending on the concentration and particle size of the biocatalyst to be filtered, risk of channel blocking defines the lower limit of the size of the tubular diameter.

### 3.3.6.2 *SHELL-TO-LUMEN (CONTINUOUS OPEN SHELL)*

The shell-to-lumen (S-L) configuration, the membrane cell resembles a shell-and –tube heat exchanger whereby the bioreactor effluent is recycles through the shell side and the permeate is collected from the lumen. For a single channel membrane (of same diameter as the L-S configuration), this configuration presents a filtration higher surface area and theoretically can

permit higher permeate fluxes. Provided that the surface hydrodynamics of the L-S configuration can be met, the effect of the permeate flux decline due to the development of a filtration cake resistance is less severe. This is due to the smaller effect the radius of curvature has on increasing the cake resistance (as the cake thickness increases in the radial direction) in the S-L configuration relative to the L-S configuration (Belfort *et. al,* 1994).

However, increasing the membrane surface area is only possible through increasing the number of membranes in the module. Moreover, increasing the cross-flow velocity is only possible through varying the interstitial distance (distance between the tubular membrane elements) or increasing the upstream pump's volumetric flow. In the latter case, this would increase the energy requirements of the process (Pearce *et al.,* 2011).

### 3.3.7 ANTI-FOULING MEASURES

Due to membrane fouling, the observed flux decline can be classified as either reversible or irreversible, depending on the anti-fouling protocol and the available cleaning technology (Shiraiz *et al.,* 2010). Reversible fouling can be described as the portion that can be recovered by physical cleaning techniques such as backwashing/back-flushing. Back-flushing reverses the flow direction in order to remove solid particulate deposited on the membrane surface and is generally a more rapid flux recovery method relative to chemical cleaning (Pearce *et al.,* 2011; Carstensen *et al.,* 2012). Flux decline attributed to irreversible fouling cannot be recovered by physical cleaning methods and either requires chemical cleaning or replacement of the membrane. The effect of reversible and irreversible fouling on the permeate flux is illustrated in *Figure 23*.

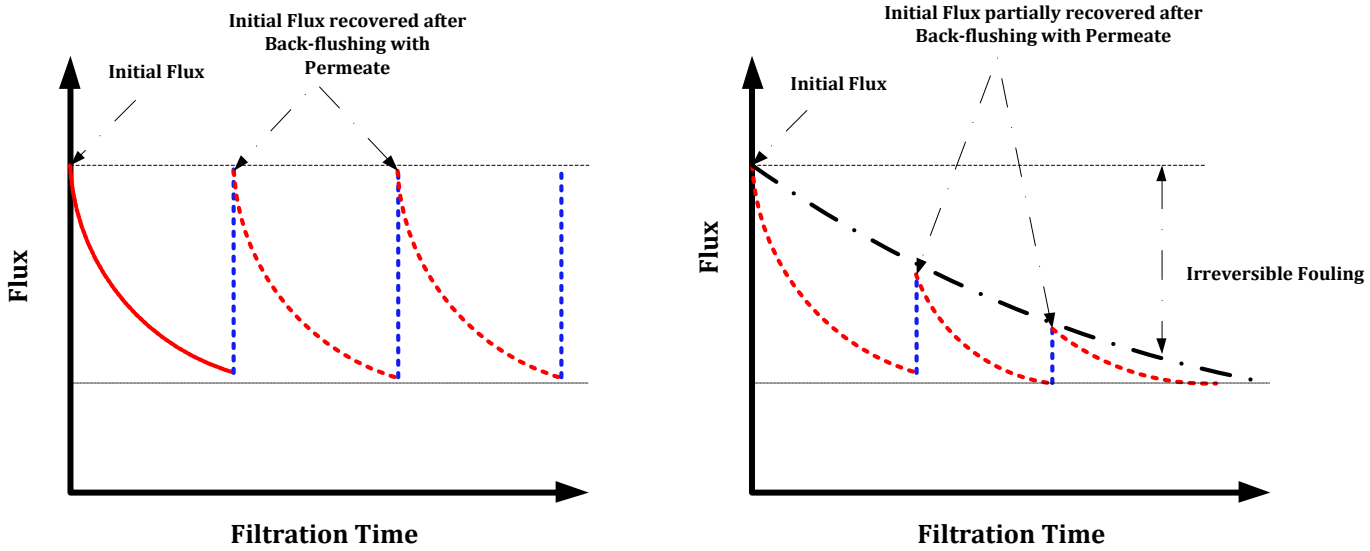


***Figure 23:*** *The schematic representation flux recovery through back-flushing for porous membranes.* ***A****- reversible fouling,* ***B****- irreversible fouling [Adapted from (Shiraiz et al., 2010)]*

Literature recommendations for controlling membrane fouling include (Dhariwal 2007; Carstensen *et al.,* 2012; Belfort *et al.,* 1994; Shiraiz *et al.,* 2010):

- High axial flowrates with lower TMPs to promote the membrane surface shear rate and minimize CP
- Operating at constant flux rather than constant TMP (below the critical flux),
- Optimizing the module configuration and orientation,
- Periodic backwashing/back-flushing with the permeate or fresh substrate,
- Ultrasound treatment of membrane cell during/after operation,
- Modifying the solution chemistry, e.g. ionic composition in the solution to improve the membrane surface charge characteristics ,
- Increasing the suspended particle size of the filter solution. Large particles are more easily swept away by the axial velocity,
- Selecting hydrophilic membrane (*section 3.2.3.2*)
- Operating at higher surface and bulk temperatures to decrease the bulk solution viscosity and subsequently increase permeate flux.
- Membrane Vibration

While there are many established anti-fouling protocols for minimizing membrane fouling, only those that minimize process operation costs are considered for low-value high-volume products such as ethanol. Hence, physical cleaning through back flushing and improving the operation hydrodynamics (TMP and cross-flow velocity) were the favourable anti-fouling measures selected in this work due to their ease of operation in addition to their low operational costs.

### 3.3.8 CRITICAL FLUX

The critical flux concept was first introduced by Fields *et al.,* (1995) who stated that: "Considering MF/UF processes, at start-up conditions there exists a critical permeate flux at start-up below which a decline of flux with time does not occur; above it, fouling is observed". As a result, it was hypothesized that operating below the critical flux (sub-critical flux) would permit long term operation without significant particulate accumulation at the membrane surface (Bacchin et al., 2006). To this end, the critical flux concept has two distinct forms, i.e. a strong form and a weak form. The following equations were used to explain the sub-critical flux region for the two critical flux forms:

***Strong Form:*** $J_{c_s} = \frac{\Delta P}{\eta_0 (R_m)}$ **for $J<J_{c_s}$** **(3.2a)**

***Weak Form:*** $J_{c_w} = \frac{\Delta P}{\eta_0 (R_m + R_{ads})}$ **for $J<J_{c_w}$** **(3.2b)**

In equations 3.2a and 3.2b, $J_{cs}$ relates to the strong form critical flux and $J_{cw}$ defines the weak form of the critical flux. Considering the strong form, the sub-critical flux membrane operation of a suspension has the same permeability as pure water and the permeate flux increases linearly with an increase in the TMP. However, the flux corresponding to the point of where the TMP-flux curve starts to deviate from linearity is the defined as the critical flux. This flux definition distinguishes between no fouling conditions relative to those where additional resistances (other than $R_m$) occur.

However, as with most suspensions, clean water fluxes are rarely achieved due to irreversible adsorption of some macrosolutes present in the suspension. Therefore, the weak form takes into account the change in the membrane permeability due to internal fouling through macrosolute adsorption. As a result, the sub-critical flux hydraulic resistance is defined as the sum of the membrane resistance and the resistance due to macrosolute adsorption (Bacchin et al., 2006; Beier, 2008; Hamann, 2010; Pearce et al., 2011). Graphical representation of both forms of the critical flux are presented in *Figure 24.*

The critical flux can be obtained through a graphical experimental approach whereby the steady-state permeate flux of a solution is plotted against the operational TMP. This method measures the change in permeability of the bulk flowing fluid within the membrane with changes in the TMP. Theoretically, a linear relationship between the TMP and the permeate flux at fluxes below the critical flux should exist. The point of departure from this linear relationship defines the membrane critical flux and the TMP whereby irreversible membrane fouling commences.

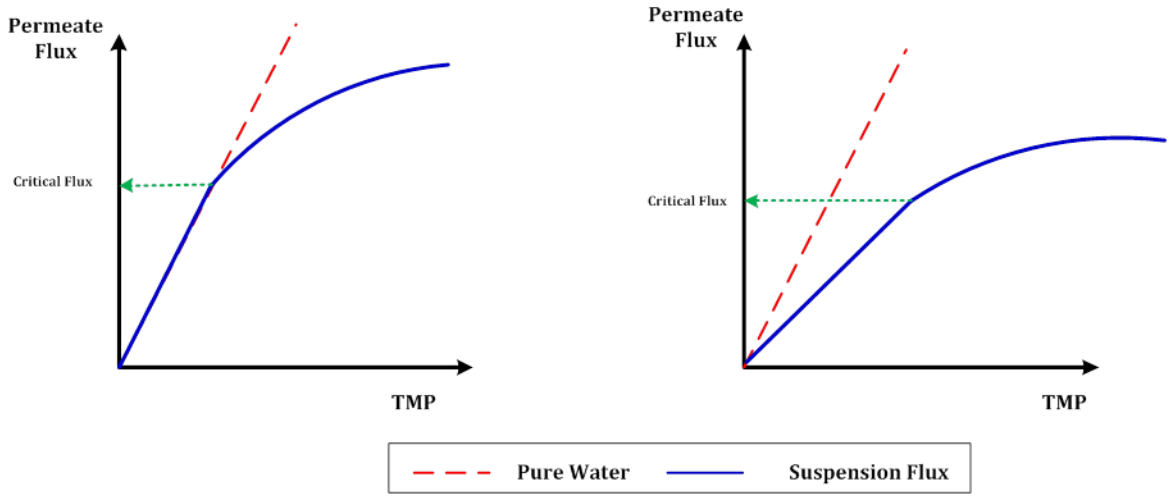


***Figure 24:*** *Determination of the critical flux: strong form (left); weak form (right) [Redrawn from (Bacchin et al., 2006)]*

## 3.4 CONCLUDING REMARKS FROM LITERATURE

Second-generation bioethanol production from the low-cost, vastly available and renewable energy-source, lignocellulose, is an attractive process. Literature highlights process water usage, biocatalyst inhibitor tolerance, ethanol yield and ethanol productivity as the factors which have a significant impact on the lignocellulosic ethanol processing cost. However, the effective conversion of all sugars (pentose and hexose) to ethanol and the ethanol concentration from the fermentation step to distillation impact the lignocellulosic ethanol production cost more than any other factors.

To this end, the efficient conversion of mixed sugar hydrolyzate is an essential factor towards alleviating the techno-economic challenges encountered in LC-to-ethanol production process. Considering its GRAS status, superior kinetics, and yield characteristics; *Z. mobilis* remains one of the most efficient LC-to-ethanol fermentative biocatalysts. Moreover, the acetate tolerant-xylose fermenting recombinant strain *Z. mobilis* 8b, has been reported to exhibit high ethanol yields from xylose-based substrates, albeit at rates much slower compared to glucose based substrates.

Critical literature analysis revealed that the fermentation temperature, pH, initial substrate concentration, and the ethanol concentration were all significant factors towards the fermentative performance of both wild-type and recombinant *Z. mobilis*. Moreover, this biocatalyst is an aero-tolerant microorganism and therefore does not require operational strategies with stringent oxygen supply or removal. Yet, no statistically optimized fermentation conditions for improving the kinetic performance of the wild-type strain *Z. mobilis* ZM4 and the recombinant strain *Z. mobilis* 8b were found in literature. In addition, whilst the sugar content extracted from the hemi-cellulose fraction of LC consists of both glucose and xylose in significant quantities, quantitative analysis of the effect of the presence of glucose on xylose fermentation by *Z. mobilis* 8b has been sparsely reported.

Cell retention strategies provide alternative fermentative strategies for improving the volumetric productivity and ethanol yield and subsequently the economic feasibility of the process. MRBs are best suited for increasing the volumetric productivity for processes involving slow growing microorganisms or for systems whereby $q_p$ limits the volumetric productivity of the process. Whilst the use MRBs for glucose fermentation has been studied extensively, no work has been reported for improving pentose fermentation by recombinant *Z. mobilis* 8b.

Although improving the volumetric productivity for pentose fermentation through a membrane based cell retention strategy is a promising process, membrane fouling bottlenecks the viability of the process. The design of an effective membrane cell is characterized by optimizing the operating surface hydrodynamics and TMP driving force in the presence of the cell culture at the expected concentration range. Moreover, the selection of a suitable membrane material, geometry and mode-of-operation are significant factors in facilitating effective chemical and physical cleaning.

# CHAPTER 4

# HYPOTHESIS AND RESEARCH OBJECTIVES

*Based on the literature survey, the optimization of the fermentation conditions, the design of an effective membrane module, the quantification of the kinetics of Z. mobilis in continuous culture and the modelling of the proposed MRB system define the backbone of this work. As a result, the discussion of this project will be subdivided into the four aforementioned main segments. This section highlights the hypotheses related to the four main sections with subsequent key questions and project objectives. These fundamental objectives define the approach to be undertaken to prove or reject the proposed hypothesis.*

The key project aims and the project scope have been highlighted in Chapter 1 (section *1.5 Research Scope*). Nonetheless, the fundamental project objectives are restated in greater detail below with respect to specific project hypotheses.

## 4.1. Optimization of Free-cell Fermentation Conditions

Temperature and pH are known to have significant impact on both the growth and fermentation kinetics of *Z. mobilis*. Whilst some studies have investigated the effect of temperature and pH on glucose-xylose substrate fermentation kinetics independently, there is no sufficient quantitative data in literature describing the statistical interaction of temperature and pH for strains *Z. mobilis* ZM4 and *Z. mobilis* 8b.

### 4.1.1 Hypothesis 1-A

***"There exists an optimal combination of temperature and pH that results in an optimum volumetric productivity and ethanol yield from the fermentation of glucose-xylose substrates."***

#### 4.1.1.1 Key questions pertaining to hypothesis 1-A

***A.*** How are the free cell kinetics affected by the interactive effect of temperature and pH?

***B.*** Is the fermentation temperature, pH and/or their interactive effect statistically significant towards the volumetric productivity and ethanol yield from glucose only and mixed-sugar substrates?

#### 4.1.1.2 FUNDAMENTAL OBJECTIVES

- A critical analysis of the free cell kinetics for both the wild-type and recombinant biocatalysts. The fermentation temperature and pH will be optimized by means of a statistical analysis, with the overall cell yield, product yield and the productivity being the response variables.

### 4.1.2 HYPOTHESIS 1-B

***"Moreover, the presence of glucose in a glucose-xylose substrate improves the overall rate of xylose ($Q_{s\_xylose}$) fermentation but has no significant effect on the specific rate of xylose consumption ($q_{s\_xylose}$)"***

#### 4.1.2.1 KEY QUESTIONS PERTAINING TO HYPOTHESIS 1

***A.*** Since the glucose-xylose composition of hydrolyzates is dependent on the feedstock material and pre-treatment method, what is the effect of glucose on xylose fermentation?

#### 4.1.2.2 FUNDAMENTAL OBJECTIVES

- The effects of the substrate composition will be quantified in view of improving the overall rate of xylose fermentation. The fermentation kinetics obtained during these experiments shall be used as a basis for the design of the MRB cell retention system.

## 4.2. CHARACTERIZATION OF MEMBRANE MODULE

In the optimization of the permeate flux rate, the primary process operating parameters that affect the flux are the TMP, shear rate/ cross flow velocity, membrane pore size, membrane geometry and area, cell concentration to the membrane and the process temperature. Therefore, since the system hydraulic dilution rate is dependent on the permeate flux, optimal flux conditions are desired.

### 4.2.1 HYPOTHESIS 2

***"Within the expected cell concentration range, an optimal combination of the membrane cross-flow velocity and TMP, which maximise the possible flux, exist"***



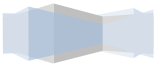

### 4.2.2 KEY QUESTIONS PERTAINING TO HYPOTHESIS 2

***A.*** How is the membrane critical flux impacted by the hydrodynamic conditions?

***B.*** How does the membrane water permeability compare to the filtration cell-free process media?

***C.*** Is the change in media viscosity significant for the membrane permeability?

***D.*** Is membrane back-flushing an effective anti-fouling technique?

***E.*** Are the operating TMP, cross-flow velocity and cell concentration statistically significant towards the observed permeate flux?

### 4.2.3 FUNDAMENTAL OBJECTIVES

- The determination of the membrane critical flux for operations with cell free water and process media as the working fluids.
- The characterization of the effect of process parameters (such as the substrate concentration, trans-membrane pressure, the CF velocity, flow-direction, and the membrane configuration) on the flux through the microfiltration unit. Moreover, the effectiveness of a hydrodynamic approach or periodic back-flushing as fouling control techniques will be evaluated.
- The statistical evaluation of the combination of the TMP and CF velocity that yields the best permeate flux at various cell concentrations.

## 4.3. QUANTIFICATION OF KINETICS OF *Z. MOBILIS* IN CONTINUOUS CULTURE

Literature reports that continuous culture with cell retention through cross-flow membrane (MBR) has the potential for improving the process volumetric productivity relative to continuous culture (without cell retention). Moreover, this process has more appeal for pentose fermentation which is characterised by low specific rates of xylose consumption ($q_{s\_xylose}$).

### 4.3.1 HYPOTHESIS 3:

***"For glucose- xylose substrate fermentation, the volumetric productivity of recycled cells of Z. mobilis 8b will be higher relative to batch and continuous culture (without cell retention) fermenters"***



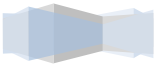

### 4.3.2 KEY QUESTIONS PERTAINING TO HYPOTHESIS 3:

***A.*** How do the fermentation kinetics of the MRB (closed-type continuous culture) compare to those in batch and open-type continuous culture (without cell retention) at the optimized fermentation conditions?

***B.*** What is the effect of the substrate ratio on the volumetric productivity of the MRB?

***C.*** Is membrane fouling a significant parameter towards the viability of this process?

***D.*** Considering the application of the MRB technology in LC-to-ethanol process designs (or configurations), what are its limitations and potential advantages?

### 4.3.3 FUNDAMENTAL OBJECTIVES

- Design an experimental MRB system with effective retention of the fermentation biocatalyst.
- The quantification of the fermentation kinetics of the developed MRB system
    - The evaluation of the effect of cell retention relative to a continuously operating process (without cell retention) at the same hydraulic dilution rate and substrate concentration.
    - The fermentation of glucose and xylose substrates, with glucose-xylose ratios resembling the hydrolyzates reported for the Iogen and the Aden *et al.,* 2010 processes.
    - Ensuring that the target ethanol concentration from the MRB and continuous culture (without cell retention) is greater than 4% (wt).
- The evaluation of cell immobilization as an alternative form of cell retention by immobilizing the microbial cells within the pores of the semi-permeable tubular membrane.

## 4.4. PROCESS MODELING

Kinetic models constructed from first principles are significant in view of their ability to predict the system behaviour as a function of the characteristic properties of the system. Therefore, with the aid of these models, system response to changes in the characteristic properties of the system (e.g. dilution rate, feed substrate concentration etc.) can be predicted without evaluating for the system response experimentally (Wimpenny, 1997).

### 4.4.1 HYPOTHESIS 4:

***"A mathematical kinetic model developed from first principles accurately predicts batch and cell recycled fermentation kinetics"***

### 4.4.2 KEY QUESTIONS PERTAINING TO HYPOTHESIS 4:

***A.*** How does the kinetic model predict batch or free-cell fermentation systems?

***B.*** What is the extent of reaction in the membrane cell (as a result of immobilized cells)?

***C.*** What are the limitations of the proposed model?

***D.*** What system response variables will be predicted by the model?

***E.*** How will the model be validated?

### 4.4.3 FUNDAMENTAL OBJECTIVES

- A mathematical model shall be developed from first principles to predict the performance of the proposed system. The mathematical model shall be compared and validated with experimentally obtained. A statistical analysis shall also be performed in the validation of the kinetic model.

The reconciliation of the research objectives based on the key questions and fundamental project objectives was performed at the end of this study. The subsequent discussion as to whether these objectives have been met will be addressed in the subsequent chapters of this work.



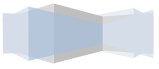

# CHAPTER 5

# MATERIALS AND EXPERIMENTAL DESIGN

*This section summarizes the methodology and experimental design for evaluating the biological performance of Z. mobilis in batch, continuous culture and MRB fermentation strategies. The experimental approach undertaken in this work has been subdivided into three sections: (1) a materials and analyses methods section for the description of the materials used, inoculum preparation, analysis techniques (2) a description of the experimental apparatus used and the operational methodology applied, and (3) an experimental design section based on the four segments presented in the previous chapter.*

## 5.1 MATERIALS AND ANALYSES METHODS

A list of all the chemicals used in this work is presented in Appendix B.

### 5.1.1 MICROORGANISM AND CULTURE MAINTENANCE

The wild-type strain *Z. mobilis* ZM4 and the xylose fermenting recombinant strain *Z. mobilis* 8b were used in this work. Ethanol fermentations from glucose substrate were performed with *Z. mobilis* ZM4. This microorganism was obtained from the American Type Culture collection (ATCC) with the item number ATCC 31821 (ZM4). Mixed sugar (i.e. glucose-xylose or G:X) fermentations were performed with the recombinant strain *Z. mobilis* 8b. This patented microorganism was obtained from the ATCC with the item number ATCC-PTA-6976 (Zhang *et al.,* 2007).

For long-term storage, stock cultures of the wild-type and recombinant strains were stored in cryovials containing 50 $g.L^{-1}$ fermentable sugar, 5 $g.L^{-1}$ yeast extract and 20% (v/v) glycerol. The fermentable sugar content was 50 $g.L^{-1}$ glucose for the wild-type strain and 25 $g.L^{-1}$: 25 $gL^{-1}$ G:X for the recombinant strain. The cryovials were refrigerated at -20 ˚C.

For experimental use, both strains were maintained on rich agar slants consisting of 50 $g.L^{-1}$ fermentable sugar (25:25 G:X for stain 8b), 5$gL^{-1}$ yeast extract and 20$gL^{-1}$ agar. The nutrient rich agar slants were prepared by aseptically transferring one loopful of the frozen culture into 20mL nutrient broth in a 100mL shake flask. The culture was thereafter incubated in an orbital shaker (Labcon) incubator at 200rpm and 30 ˚C for 16 hours. A loopful of the resultant culture was spread onto the surface of the rich nutrient agar slant. Colonies were gown on the nutrient rich slants for 24 hours at 30 ˚C. The slants were kept under refrigeration at -4 ˚C for a maximum period of 2 months.

### 5.1.2 CULTURE MEDIA

The inoculum development protocol adopted for the preparation of a seed culture of *Z. mobilis* for the production of ethanol was divided into two growth stages, a pre-inoculum stage (1st stage) and a inoculum or seed stage (2nd stage). The classical two-stage inoculum protocol was necessary to warrant consistent seed culture and for minimizing the length of the lag phase expected for the fermentation experimental work (Mohagheghi *et al.,* 2004).

***Table 7:*** *The composition of the culture media used for Z. mobilis ZM4 and Z. mobilis 8b during the investigation of the free cell fermentation kinetics of this bacterium*

| Media Composition | | | | | | |
|---|---|---|---|---|---|---|
| | ***Pre-Inoculum*** | | ***Seed/Inoculum*** | | ***Fermentation Media*** | |
| *Strain* | ZM4 | 8b | ZM4 | 8b | ZM4 | 8b |
| *Glucose ($gL^{-1}$)* | 50 | 75 | x[a] | x[a] | x[a] | x[a] |
| *Xylose ($gL^{-1}$)* | - | 25 | - | y[b] | - | y[b] |
| *Sorbitol ($gL^{-1}$)* | - | - | 1 | 1 | - | - |
| *YE ($gL^{-1}$)* | 10 | 10 | 10 | 10 | 10 | 10 |
| *$KH_2PO_4$ ($gL^{-1}$)* | 2 | 2 | 10.99[c] | 10.99[c] | 10.99[c,d] | 10.99[c,d] |
| *$K_2HPO_4$ ($gL^{-1}$)* | - | - | 3.33[c] | 3.33[c] | 3.33[c,d] | 3.33[c,d] |
| *$(NH_4)_2SO_4$ ($gL^{-1}$)* | 1 | - | 1 | 1 | 1 | 1 |
| *$MgSO_4.7H_2O$ ($gL^{-1}$)* | 0.5 | - | 0.5 | 0.5 | 0.5 | 0.5 |
| *Water Source* | De-ionised | De-ionised | De-ionised | De-ionised | De-ionised | De-ionised |
| *Buffer Cap[d]* | - | - | 100mM | 100mM | 100mM | 100mM |
| *$pH_0$* | 6 | 6 | 6 | 6 | 6 | 6 |
| *Temp* | 30 | 30 | 30 | | 30 | 30 |

***a*** *– The glucose concentration required/investigated depending on the experiment*
***b****- The xylose concentration required/investigated depending on the experiment*
***c****- Phosphate buffer concentrations in the buffer capacity range of 0-200mM were investigated. As an illustration, a 100mM buffer capacity is listed above.*
***d****- As required by the experiment. Only necessary for shake-flask experimental work*

Pre-inoculum media for *Z. mobilis* 8b consisted of 100g.$L^{-1}$ fermentable sugar (75:25 G:X), 10g.$L^{-1}$ yeast extract and 2g.$L^{-1}$ $KH_2PO_4$. The pre-inoculum stage has the primary target of building-up cell mass from the refrigerated slants and has been reported to be mainly controlled by the carbon and yeast extract sources for *Z. mobilis* (Sreekumar et al., 1999).

The media selected for the inoculum stage resembled the media composition of the fermentation media to minimize the adaptation period (or lag phase) of the fermentation inoculum. For both microbes, the inoculum was supplemented with 1 g.$L^{-1}$ $(NH_4)_2SO_4$, 0.5 g.$L^{-1}$ $(MgSO_4).7H_2O$ and 1 g.$L^{-1}$ sorbitol. The latter component was added to modify the osmotic strength of the growth medium without the addition of toxic compounds (Helle and Duff, 2004).

The media was prepared by dissolving the sugars in de-ionized water and autoclaving (at 121 °C, 1bar(g)) the sugar solution separately from the minerals and yeast extract. The subsequent sugar and mineral solutions were mixed aseptically once they had cooled down to room temperature.

Excessive changes into the hydrogen ion concentration (pH) in the medium were prevented by the addition of a phosphate buffer. As an illustration, the inoculum or the fermentation media was supplemented with 10.99 $g.L^{-1}$ $KH_2PO_4$ and 3.34 $g.L^{-1}$ $K_2HPO_4$ for a buffer capacity of 100mM and the maintenance of a fermentation pH at 6. The effect of the addition of the buffer to the medium will be discussed in Chapter 7.

### 5.1.3 PREPARATION OF INOCULUM

The two-stage inoculum preparation protocol was performed under strict aseptic conditions in a laminar flow cabinet (Labcon). All inocula were prepared at a fermentation temperature of 30 $^{o}$C. Pre-inoculum cultures were initiated by transferring a single colony of *Z. mobilis* ZM4 or 8b from the stock slant into 50mL of sterile pre-inoculum media in a non-absorbent cotton wool plugged 100mL Erlenmeyer flask. This flask was incubated at the fermentation temperature at 200rpm for 14-16 hours.

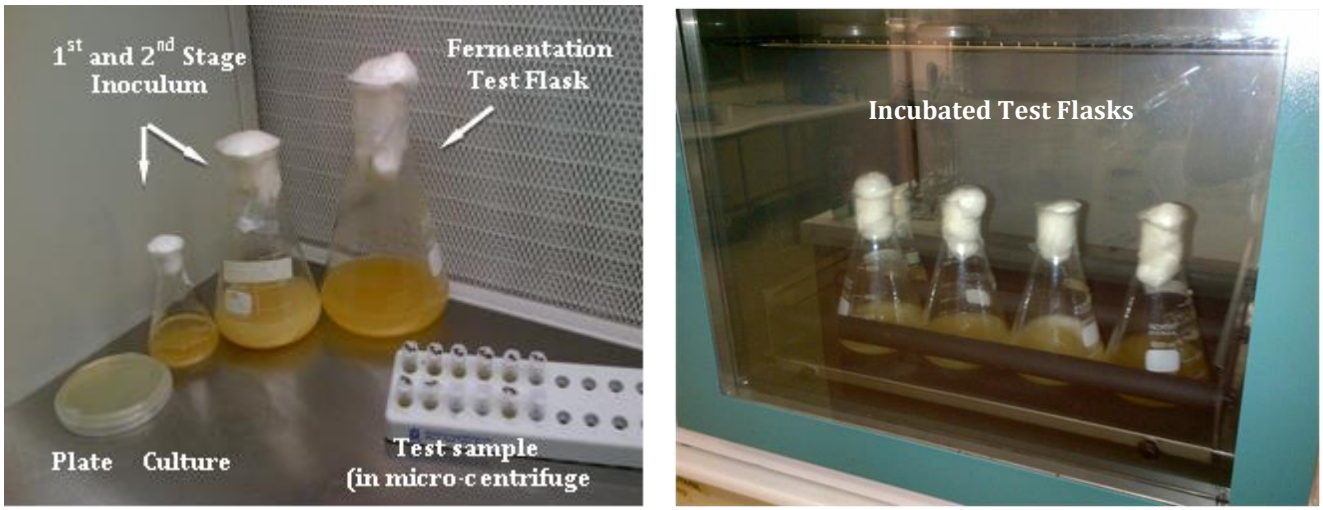


***Figure 25:*** *Inoculum Preparation apparatus (left); incubated experimental test flasks (right)*

The second inoculum was initiated by aseptically transferring 20mL of the pre-inoculum culture into a 180mL of sterile inoculum media in a 500mL flask using a 10ml air displacement pipette (Eppendorf). This inoculum flask was incubated for 4-6 hours at the relevant fermentation temperature and rotational speed of 200rpm. Prior to the inoculation of the main fermentation flask/bioreactor, the OD of the resultant seed culture measured ($OD_{660}$ approximately 1.5-2). The subsequent sub-cultured seed was aseptically inoculated into the main fermentation Erlenmeyer flask/bioreactor at 10% (v/v) to achieve an initial OD of 0.1-0.5 (32.6 $mg.L^{-1}$ –163 $mg.L^{-1}$).

## 5.1.4 Analytical Techniques

### 5.1.4.1 Cell Mass Concentration

Cell growth for all the experimental work was determined turbidometrically using a Spectrophotometer (Varian UV-Vis Superscan 3) at a length of 660nm (1-cm light path). A calibration curve plotting the cell dry weight (CDW) as a function of the optical density (OD) was constructed and used to convert the OD obtained from the experimental test flask/ bioreactor fermentation experiments to CDW equivalents.

#### 5.1.4.1.1 Absorbance/ Optical Density measurements

For optical density measurements of *Z. mobilis*, 1mL samples from the experimental test flask were aseptically removed and transferred into a micro-centrifuge tube (Eppendorf) using a sterile air-displacement pipette (Eppendorf). The cell-containing micro-centrifuge sample was centrifuged (Minispin Plus, Eppendorf) at 10 000rpm for 5 minutes. Thereafter, the substrate-product containing supernatant was removed and prepared for HPLC analyses (*section 5.1.4.2*) and the cell pellet was re-suspended in a 0.85% (m/v) NaCl solution (physiological saline).

The absorbance of the re-suspended cell pellet was measured using the spectrophotometer at a 660nm wavelength. The linear region of absorbance versus cell concentration was determined to be in the range 0.05-0.9. A blank cuvet filled with saline was used to establish absorbance reading of zero at 660nm.

#### 5.1.4.1.2 Cell Dry Weight (CDW)

Due to the quantification of the cell density by measuring the absorbance of the culture broth being an indirect method, CDW equivalents were determined to determine a relationship between the CDW and the measured absorbance. Prior to the measurement of the CDW, unused 0.2µm pore sized filter paper disks (Anatech) were vacuum dried in a vacuum oven (Shell lab) at 60 ˚C overnight. The dried filter disks were thereafter cooled and stored at ambient conditions in a desiccant to prevent atmospheric water from absorbing onto the filter paper. After cooling, the dried and cooled filter disks were weighed (Ohaus adventurer).

For CDW measurements, 10-30mL samples were aseptically removed from the fermentation broth/test flask and transferred into 50mL falcon tubes (Eppendorf). The subsequent 10-30mL sample was filtered using a Buchner vacuum filter (Millipore). The wetted filter paper containing the cells was washed three times using distilled water and thereafter vacuum dried in the vacuum oven at 60 ˚C for 24 hours. After the drying period, the filter paper with the dried cells was cooled in a desiccant at ambient conditions. Once cooled, the cell-holding filter paper was weighed as before. The difference in weight between the unused filter paper and the cell-holding filter paper was attributed to the cell dry weight of the cells.

The relationship between the broth OD and the CDW is presented in *Figure 26*.

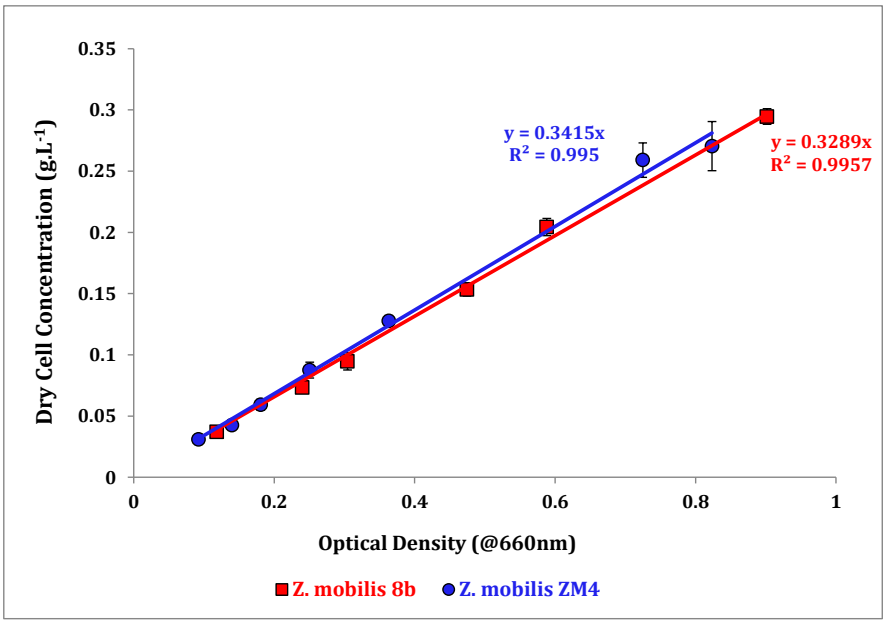


***Figure 26:*** *The OD vs. CDW calibration curves for Z. mobilis ZM4 and 8b strains*

Samples which exhibited ODs outside of this linear range were diluted with physiological saline. As a result, the following formula was used to calculate the CDW from the fermentation broth:

$$C_{CDW} = D * Slope * OD_{660nm} \qquad \textbf{(5.1)}$$

where $\mathbf{C_{CDW}}$ is the cell dry weight concentration ($g.L^{-1}$), **D** is the dilution factor, **Slope** is the calibration gradient for the respective strain analysed for ($g.L\text{-}1.AU^{-1}$), and $OD_{660nm}$ is the optical density obtained from the spectrophotometer ($AU^{-1}$).

### 5.1.4.2 SUGAR AND ETHANOL CONCENTRATIONS

Glucose, xylose and ethanol concentrations were determined from sample supernatants using high performance liquid chromatography (HPLC) with an Aminex HPX-87H column (Bio-Rad, Hercules, CA) with 5mM $H_2SO_4$ as the mobile phase. Detailed HPLC sample analysis specifications are given in the table below:

***Table 8:*** *HPLC Specifications for Xylose, Glucose and Ethanol concentration measurements*

| HPLC Specifications | |
|---|---|
| ***Column*** | Aminex HPX-87H column (Bio-Rad, Hercules, CA) connected to All-Guard Cartridge System (Grace Davison Discovery Sciences, Deerfield, IL, USA) |
| ***Mobile phase*** | 5mM $H_2SO_4$ |
| ***Injection Volume*** | 30 µL |
| ***Flow rate*** | 0.6 mL/min |
| ***Detector*** | Refractive Index |
| ***Detector Temp.*** | 65 ˚C |

Calibration curves were established for glucose, xylose, ethanol, acetic acid, glycerol and formic acid to obtain a linear relationship between the integrated peak area and the component concentration. Quality control samples containing known concentrations of all the pure components expected in the sample were run periodically to verify the accuracy of the calibration curves. Typical sugar calibration curve and a sugar analysis chromatograph are presented in *Figure 27* and *Figure 28* respectively.

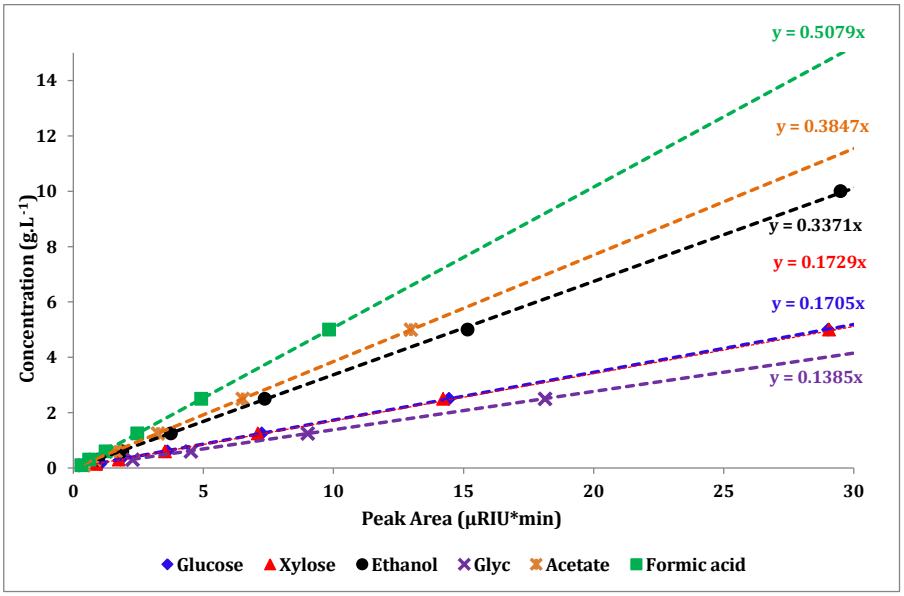


***Figure 27:*** *Calibration curves for sugar, ethanol, glycerol, acetic acid and formic acid analysis*

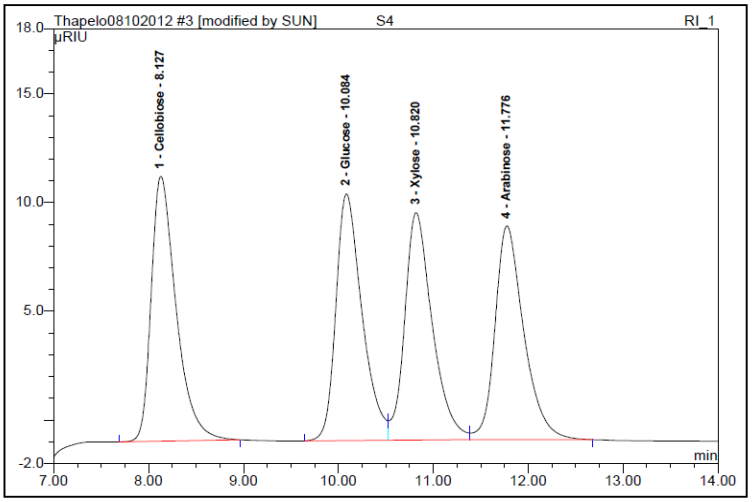


***Figure 28:*** *A typical HPLC chromatogram for sugar analysis*

### 5.1.4.3 *HPLC SAMPLE PREPARATION*

A standard sample preparation method was employed for HPLC analyses. First, the desired volume of the supernatant from the centrifuged fermentation culture was removed and diluted into a 2mL micro-centrifuge tube with distilled water ($dH_2O$) to meet the HPLC detection range. Whilst the volume of the supernatant removed for analysis is dependent on the experimental conditions, the

total volume of the diluted supernatant was 1.8mL (e.g. for sugar/ethanol concentrations below 50g.L$^{-1}$, 1.3mL $dH_2O$ is added to 0.5mL supernatant).

Next, 109.8µL, 35% (v/v) Perchloric acid (PCA) was pipetted into the dilute supernatant in the micro-centrifuge tube and refrigerated at 4 °C for 1 hour (can be refrigerated at 4 °C for a maximum period of two weeks). After cooling, 99.2µL of 7N KOH solution was added to the micro-centrifuge tube to precipitate the added PCA and to remove any salts that were present in the supernatant. Precipitation was allowed to commence overnight in the refrigerator (at 4 °C).

After precipitation had been complete, the micro-centrifuge tube was centrifuged at 14 000 rpm for 5 minutes. The supernatant was filtered using 5mL disposable syringes attached to 0.22µm syringe filters (Anatech) into a 2mL HPLC vial. The vial was marked with a permanent marker and transferred into the HPLC for analysis.

The actual sugar or product concentration present in the fermentation broth ($C_i$) was calculated as follows:

$$C_i = Area_{component_i} * Slope_{calibration} * D_{supernatant} \quad \textbf{(5.2)}$$

where $\textbf{Area}_{\textbf{component}_i}$ is the HPLC integrated area of component i, $\textbf{slope}_{\textbf{calibration}}$ is the slope of the calibration curve of component i, and $\textbf{D}_{\textbf{supernatant}}$ is the dilution factor of the supernatant with $dH_2O$.

Assuming volume contraction or expansion are negligible, simple dilution was used to obtain the required 35% (v/v) PCA using the following expression:

$$V_{PCA} = \frac{35\% * V_{total}}{60\%} \quad \textbf{(5.3)}$$

where $\textbf{V}_{\textbf{PCA}}$ is the volume of 60% (v/v) PCA required to achieve 35% (v/v) in the diluted solution, and $\textbf{V}_{\textbf{total}}$ is the total volume of the diluted sample. For example, for the preparation of 100mL of 35% (v/v) PCA, 30mL of MilliQ water was pipetted into clean 200mL Schott bottle and followed by the addition of 58.33mL 60% (v/v) PCA (obtained from equation 4.3). Thereafter, MilliQ water was added to bring the final volume of the mixture to 100mL.

#### 5.1.4.3 VISCOSITY MEASUREMENTS

The viscosity of the fermentation media solution at various sugar concentrations (50gL$^{-1}$, 75gL$^{-1}$, 100gL$^{-1}$, 150gL$^{-1}$ glucose) was measured using a rotating rheometer (Anton Paar MCR 501) fitted with a 50mm 2° steel cone-plate geometry. All samples were measured at a shear rate ($d\gamma/dt$) of 0.01 (s$^{-1}$) and a temperature of 30 °C. Samples were readied for analysis by following the procedure highlighted in section 5.1.2 and stored in 50mL Falcon tubes in the refrigerator at 4 °C.

#### 5.1.4.4 PARTICLE SIZE DISTRIBUTION

*Z. mobilis* are rod-shaped bacteria with an approximated width of 1-1.4µm and length of 2-6µm. However, elongated cells with lengths up to 13µm have been reported for cells obtained from continuous culture in ethanol inhibiting conditions (Vaija *et al.,* 1995). In order to ensure a highly selective membrane was used for cell retention, the cell size distribution was analysed using a Saturn Digitizer 5200 V1.10 analyser (Micrometrics Instrument Company). The refractive index (RI) of the cells was approximated as 1.378 and the RI of water was 1.331. Cells were removed from a continuous culture (at D = $0.1h^{-1}$) and re-suspended in a 0.0055% (v/v) tetra sodium pyrophosphate solution. Pure Nitrogen gas (>99.5%) and compressed air were used the nitrogen and oxygen sources respectively.

#### 5.1.4.5 SCANNING ELECTRON MICROSCOPE (SEM) IMAGING

Ceramic membranes are typically composite materials consisting of a macroporous support and a microporous permeable layer. The structure of the selected tubular membranes was identified using a Zeiss Leo 1430VP Scanning Electron Microscope. Prior to scanning, the membrane samples were mounted on aluminium stubs and coated with a thin gold film to prevent thermal damage and surface charging. The apparatus was operated at a tilt angle of $0^{o}$, accelerating voltage of 20keV, aperture size of 30µm and a working distance of 17mm.

## 5.2 EXPERIMENTAL APPARATUS AND METHODOLOGY

### 5.2.1 SHAKE FLASK EXPERIMENTS

All experimental work relating to the free-cell optimization of the fermentation conditions were conducted in narrow headed 1000mL Erlenmeyer flasks fitted with non-absorbent cotton wool plugs. The working volume was limited to 300mL and less than 10% of the initial working volume was removed during sampling. The inoculum preparation methodology was described in *section 5.1.3*. Conditions of constant temperature and agitation were ensured by incubating the fermentations flasks at the desired temperature and agitation speed.

### 5.2.2 BIOREACTOR EXPERIMENTS

Shake flask validation, batch and continuous culture experiments were performed in a custom build instrumented 1.5L bench-top fermenter with minimum and maximum working volumes of 500mL and 1000mL used. An ISO schematic of the bench-top fermenter used in this work is shown in *Figure 29*. The bench-top fermenter was designed exclusively for anaerobic fermentation.

The bench-top bioreactor consists of three stainless steel (SS) 316 flanges for vessel stability and housing reactor ports. The top layer flange consists of six SS 316 pipes (OD = 3mm) (part 8), one SS 316 pH dosing pipe (OD = 1.5 mm) (part 10), a hollow temperature sensor slot for housing a PT100

thermocouple (part 7), a pH probe (Mettler Toledo) (part 12), and six SS 304 sealing nuts (part 9) to bind the top layer and glass holding flanges. SS 316 baffles were included in the design to improve the mixing inside the glass vessel. The reaction vessel was a jacketed glass section designed and made by GlassChem (Stellenbosch). All the stainless steel parts were supplied by Fabrinox (Paarl).

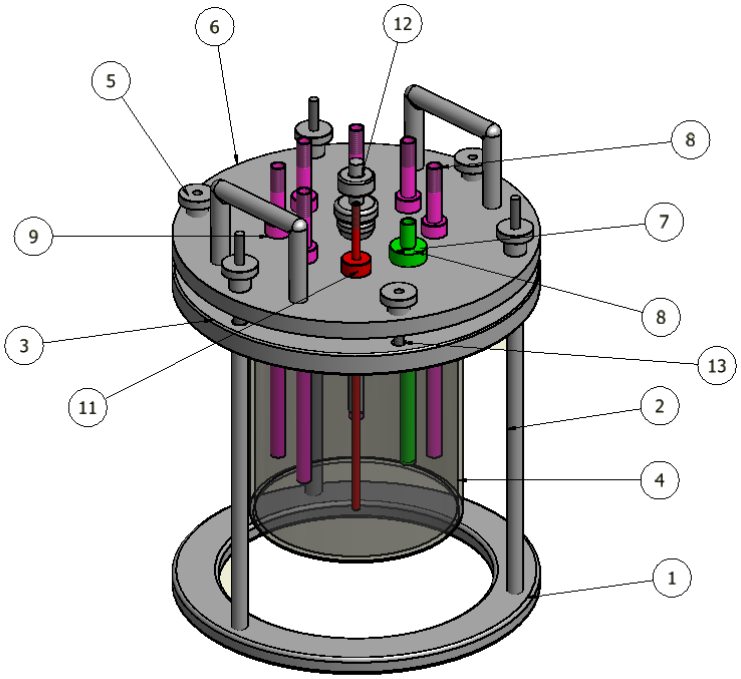


| PARTS LIST | | |
|---|---|---|
| ITEM | QTY | PART |
| 1 | 1 | S.S 316 bottom section holder flange |
| 2 | 3 | S.S 304 Screw |
| 3 | 1 | S.S 316 Glass section holder flange |
| 4 | 1 | Jacketed glass vessel |
| 5 | 6 | S.S 304 Top Layer sealing nut |
| 6 | 1 | S.S 316 Top Layer flange |
| 7 | 1 | Temperature sensor slot |
| 8 | 6 | S.S 316 reactor ports |
| 9 | 6 | S.S 304 reactor port nut |
| 10 | 1 | small pH dosage port |
| 11 | 1 | pH dosage port seal |
| 12 | 1 | pH Probe |
| 13 | 3 | Top Layer sealing bolts |

***Figure 29:*** *ISO schematic of the 1.5L bench-top fermenter designed and used in this work.*

#### 5.2.2.1 *BATCH OPERATION*

The temperature was controlled at the desired setting by circulating water from an external water bath (controlled at a fixed temperature) around the glass jacket. The temperature inside the culture broth was confirmed by inspecting the temperature reading indicated by the PT100 thermocouple on the pH controller. The thermocouple was inserted into the hollow-tube port filled with 80% (v/v) glycerol.

The pH was controlled by the addition 4M $KOH_{(aq)}$ using an automated peristaltic pump (Watson Marlow) connected to a pH controller unit (Alpha pH 1901). A PID pH controller operating with feedback control mechanism was used to maintain the culture pH at the desired set-point. When the culture pH exceeded the set-point value (plus hysteresis loop), the peristaltic pump was automatically switched off.

The physical set-up of the bioreactor also included a 0.22µm air-filter (Acro) which was connected to a vapour condenser. The air-filters provided pressure-release (mostly $CO_2$) from the fermenting culture with the condenser ensuring that no liquid vapour condensed on the air filters, thereby minimizing liquid loss from the culture. Water chilled in ice was used as the cooling medium for the vapour condenser. Agitation was provided by a magnetic stirrer plate. Due to the narrow diameter

of the glass vessel, sufficient mixing was using the stirrer was achieved. Prior to beginning any experimental work, the temperature and pH probes are adequately calibrated using reference standards and the fermenter was autoclaved at 121 °C and a pressure of 1 bar(g).

#### 5.2.2.2 *CONTINUOUS OPERATION (WITHOUT CELL RETENTION)*

Continuous culture experiments were performed using the same bench-top fermenter and equipment as batch culture experiments. Two peristaltic pumps (Vera Plus) were used for substrate feed to and culture extraction from the fermenter respectively. A schematic diagram and a photo of the experimental set-up are presented in *Figure 30* and *Figure 31* respectively.

The continuous culture experiments were executed by following a consistent routine. First, fresh culture media and inoculum were prepared (as per *sections 5.1.2* and *5.1.3*) in 10L Schott bottles (item 1 in *Figure 31*) and 1000mL Erlenmeyer flasks respectively. The sugar composition of the fresh media was dependent on the experimental conditions. The bench-top fermenter, the fresh media solutions, and the reactor effluent vessel (10L Schott bottle, item 7) were all autoclaved separately and combined aseptically in the laminar flow cabinet. The fermenter was filled with 700mL de-ionized water prior to sterilization.

After aseptically combining the system components, the contents of the fermenter were pumped out to the reactor effluent vessel and replaced with 900mL culture media from the fresh substrate reservoir. Thereafter, the fermenter was inoculated via the inoculation port with 10% (v/v) inoculum (100mL). At start-up conditions, the system was operated in batch culture mode. Batch operation was allowed to commence until the culture reached mid-exponential phase, at which point, continuous operation was initiated by switching on the fermenter feed and effluent pumps and setting them at equal flow speeds. Feed and effluent valves were used to account for slight flow differences between the two pumps until the working volume inside the fermenter stabilized and remained constant at 1000mL. Steady-state conditions were assumed after approximately four-to-six working volume changes.

The dilution rate was calculated as follows:

$$D = \frac{F_{in}}{V_{working}} \qquad \textbf{(5.4)}$$

where **D** is the dilution rate ($h^{-1}$), $\mathbf{F_{in}}$ is the feed flow rate to the fermenter ($L.h^{-1}$), $\mathbf{V_{working}}$ is the constant working volume in the fermenter (L).

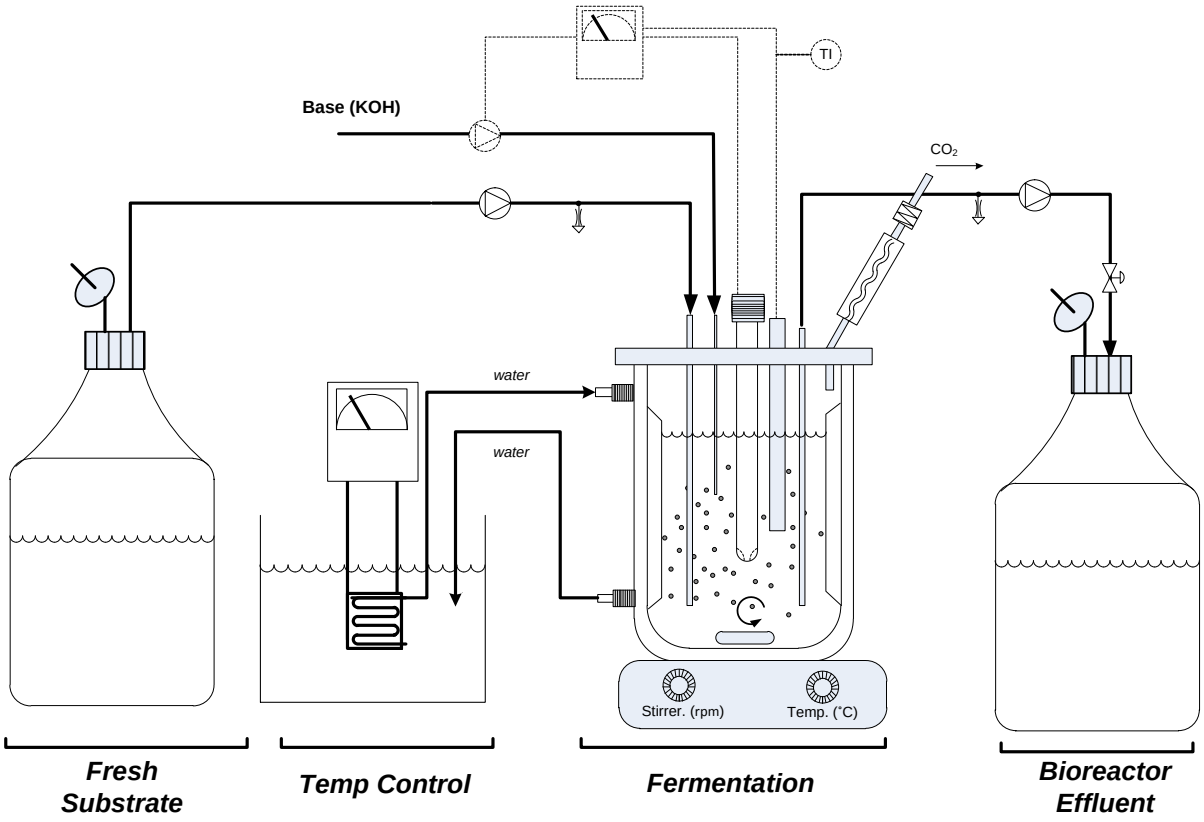


***Figure 30:*** *Block flow diagram of continuous culture experiments*

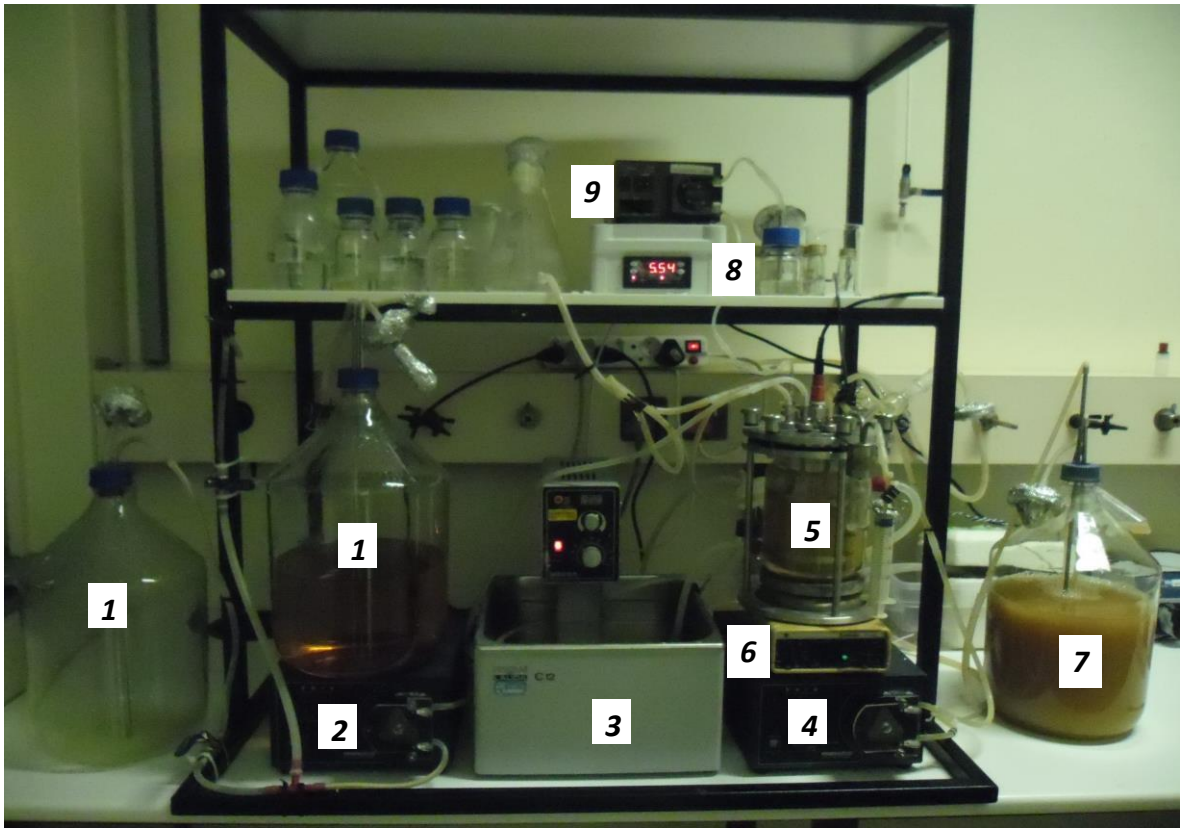


***Figure 31:*** *Picture of the experimental set-up used for continuous culture studies.* ***(1)*** *– Fresh Substrate reservoir,* ***(2)*** *–Feed Pump,* ***(3)*** *–Temp controlled water bath,* ***(4)*** *–Effluent Pump,* ***(5)*** *– Bench-top fermenter,* ***(6)*** *– magnetic stirrer,* ***(7)*** *– bioreactor effluent,* ***(8)*** *– pH controller,* ***(9)*** *– automated pH dosing pump*

### 5.2.3 MEMBRANE RECYCLE BIOREACTOR OPERATION

#### 5.2.3.1 MICROFILTRATION UNIT

Microfiltration was performed using a composite ceramic, mono-channel tubular membrane with an inner diameter of 6mm, an $\alpha$-$Al_2O_3$ macroporous support matrix thickness of 2mm, and a thin permeable layer with mean pore size of 0.2 µm (*Atech Innovations GmbH*, Germany). The mean pore size of the macroporous support matrix was 6-8 µm. Two membranes were used in this work, differentiated only by the position of the permeable layer (*Figure 32*). Membrane A, equipped with a permeable layer on the inside (lumen-side) had a permeation surface area of $0.0014m^2$, whilst Membrane B (permeable layer on the outside (shell-side)) had a permeation surface area of $0.0024m^2$. Both membranes have an average porosity of 0.3 and are 250mm in length.

A borosilicate glass (GlassChem) microfiltration unit (MFU) was designed to accommodate a single tubular membrane. The glass microfiltration unit allowed for either lumen-to-shell or shell-to-lumen flow configurations. To ensure effective sealing was achieved, silicon seals were used to connect the membranes to the SS (316) housing ports (*Figure 33*). The entire unit was autoclavable.

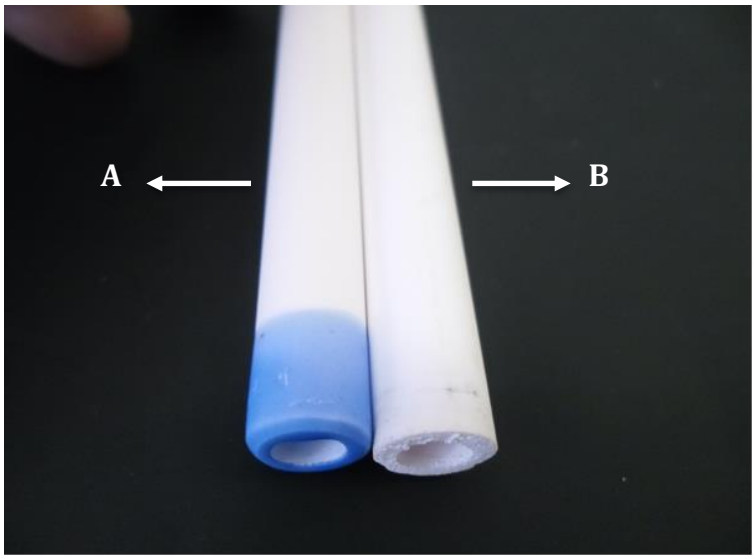


***Figure 32:*** *$Al_2O_3$ tubular membranes with 0.2µm MWCO.* ***A*** *- permeable layer on lumen side,* ***B*** *– permeable layer on Shell side* (*atech innovations GmbH*, Germany)

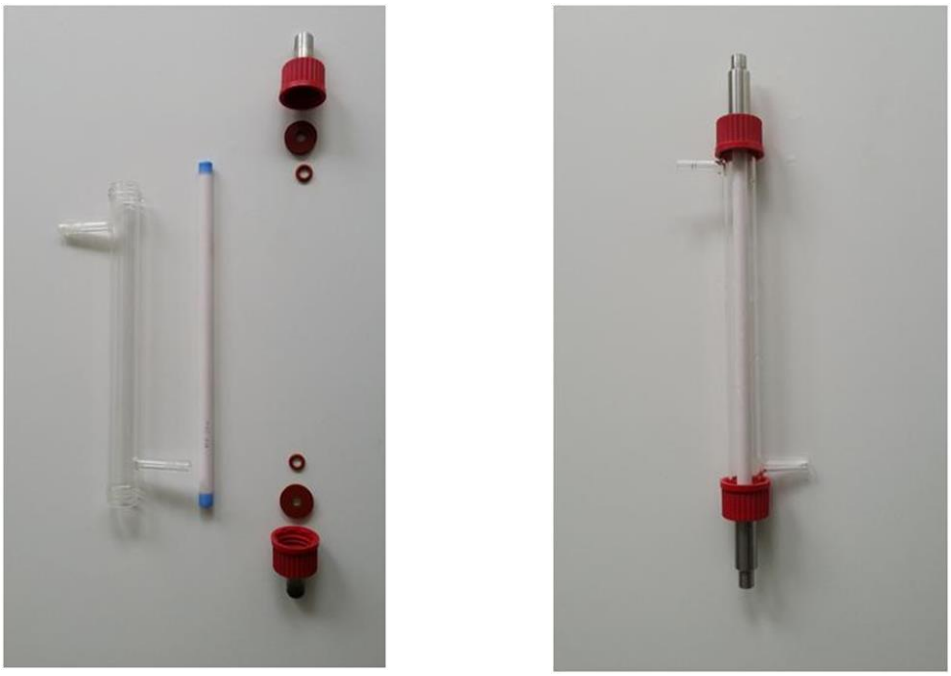

***Figure 33:*** *Parts used to construct the MFU (left), assembled MFU (right)*

#### 5.2.3.2 *INTEGRATED MRB FERMENTATION UNIT*

A schematic of the MRB experimental system is presented in *Figure 34*. A detailed process flow diagram of the experimental system is presented in *Figure 35*. The MRB experimental set-up is a modification the continuous culture set-up. The bioreactor effluent vessel (Item 7 in *Figure 31*) is replaced by a microfiltration section that consists of a MFU, cell recycle stream, cell bleed stream, permeate stream and a back-flush/back-washing stream. Images of the experimental set up can be viewed in Appendix B.3.

***Figure 34:*** *Photo of the experimental set-up of the MRB system*

Cell recycle and membrane back-flushing were executed using variable speed peristaltic pumps (Vera Plus and Welch 3100C-02, respectively). The MRB connectors and sampling ports are constructed from borosilicate glass (GlassChem). Autoclavable SS pressure gauges (SpiraxSarco) with a pressure range of 0-250 kPa were used to profile the TMP through the membrane. The cell bleed was controlled by manual manipulation of the process diaphragm valves (Jachris).

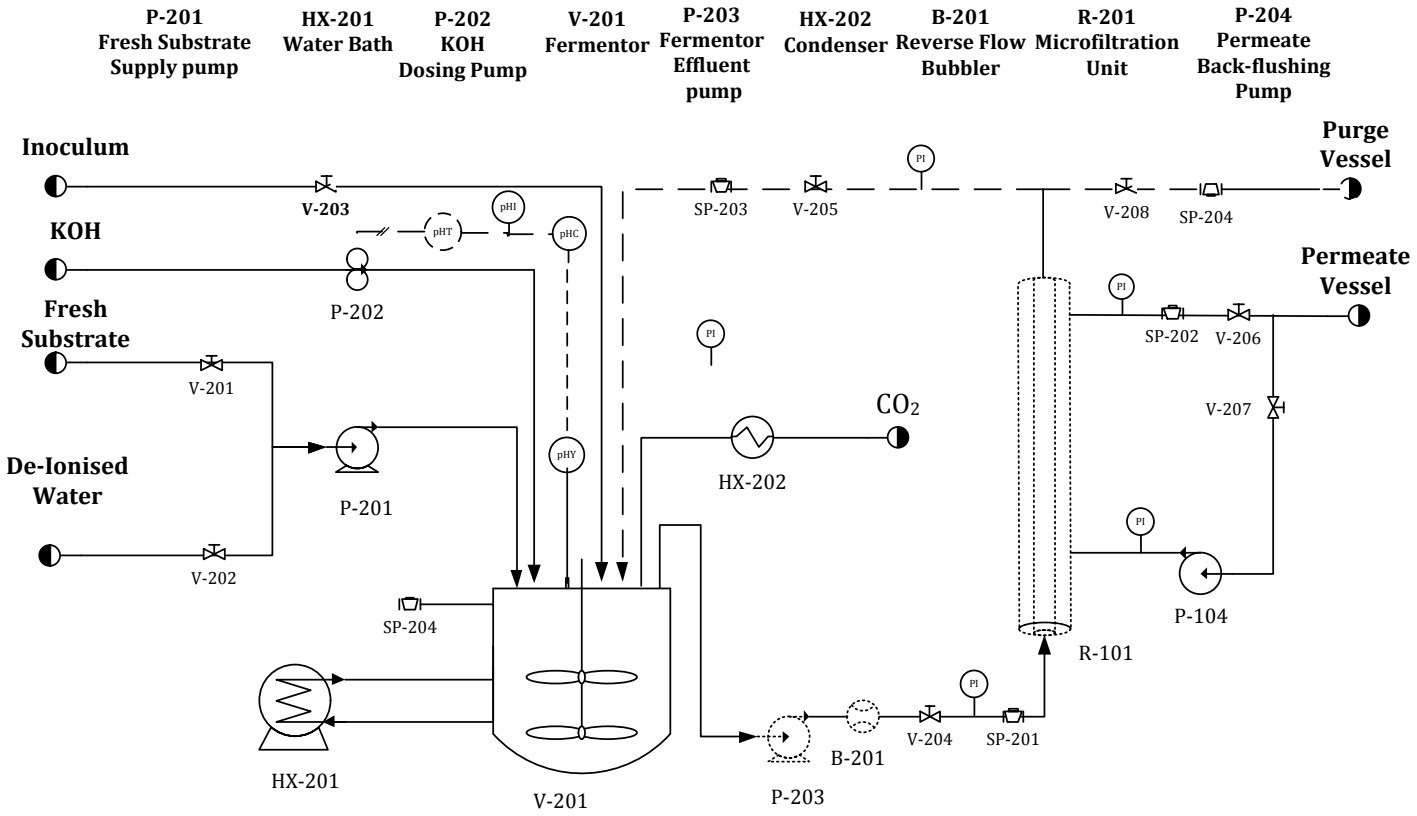


***Figure 35:*** *Process Flow Diagram of the MRB experimental set-up*

#### 5.2.3.2.1 START-UP AND OPERATION

Prior to start-up, the same media preparation, inoculum preparation, system sterilization protocol as continuous culture experiments was adopted for MRB experiments.

At start-up conditions, the fermenter was inoculated with 10% (v/v) inoculum and operated in batch mode until the culture was in mid-exponential phase. During batch culture, all the process valves in the cell recycle section were all maintained in a closed position. Once exponential phase had been reached, the recycle process valves (v-204 and v-205) were fully opened and fermenter effluent pump (P-203) was switched on at the desired pump speed to initiate recycling of the fermentation culture through the MFU. In this mode, the TMP (driving force through the membrane) was maintained at zero for one hour.

Once a stable flow through the membrane had been established, retenate diaphragm valve (v-205) was manually manipulated so as to induce back-pressure in the retenate side of the MFU. The

pressure at the feed and retenate side of the membrane was indicated by low pressure range SS needle pressure gauges. Noise in the pressure gauge readings due to the oscillatory flow from the peristaltic pump was attenuated by filling all the gauges with glycerine and including a reverse flow bubbler (B-201) (GlassChem) in the recycle stream. The retenate valve was manipulated until the desired TMP was achieved. When the desired TMP had stabilized, the TMP and the initial flux through the membrane were recorded.

The TMP was calculated as follows:

$$TMP\ (kPa) = \frac{(P_{feed} - P_{permeate}) + (P_{retenate} - P_{permeate})}{2} \qquad \textbf{(5.5)}$$

where $\mathbf{P_{feed}}$ is the MFU feed pressure (kPa), $\mathbf{P_{permeate}}$ is the pressure at the permeate stream (kPa), and $\mathbf{P_{retenate}}$ is the MFU retenate pressure (kPa).

Once the MFU was in operation, the procedure highlighted in the schematic below was followed to establish continuous operation and a constant fermenter volume.

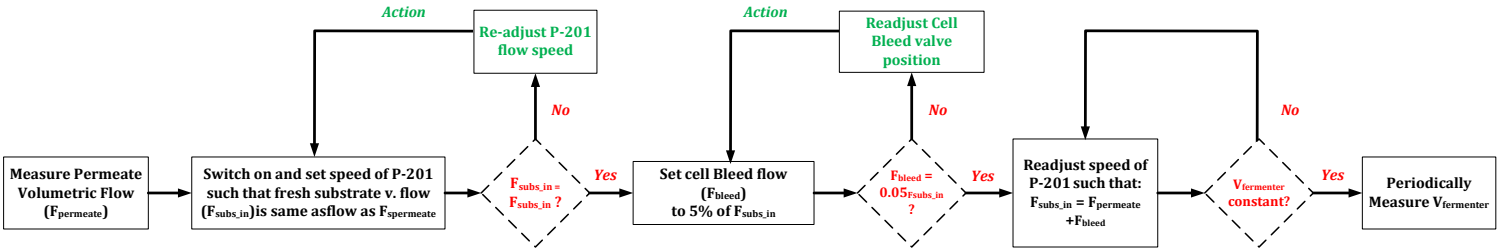


***Figure 36:*** *Flow diagram for establishing a constant fermenter volume during MBR experimental operation*

The volumetric flow through the MFU was obtained by taking frequent volume versus time measurements from sampling port (SP-205) in the permeate stream. The flux through the membrane was calculated as follows:

$$J = \frac{Q_{permeate}}{A_{membrane}} = \frac{V_{permeate}}{A_{membrane} * t} \qquad \textbf{(5.6)}$$

where **J** is the permeate flux rate ($L.m^{-2}.h^{-1}$), $\mathbf{Q_{permeate}}$ is the volumetric flow in the permeate stream ($L.h^{-1}$), $\mathbf{A_{membrane}}$ is the membrane surface area on the MWCO side ($m^2$), $\mathbf{V_{permeate}}$ is the volume of permeate collected (L) and **t** is the time required to collect the permeate volume (h).

Fresh media was added to the fermenter by switching on the fresh substrate supply pump (P-201) and setting the pump speed such that its volumetric flow was equal to that of the permeate stream so as to maintain a constant fermenter volume. A calibration curve of the volumetric flow from the supply pump as a function of the pump speed is presented in Appendix B.

After configuring the fresh substrate volumetric flow ($F_{sub\_in}$), the cell bleed stream was activated by opening ball valve (v-208) such that the cell bleed rate was 5% of $F_{sub\_in}$ (or $F_{permeate}$). Once a the cell

bleed rate has been established, the fresh substrate feed pump speed was re-adjusted such that the volumetric flow into the fermenter was equated to that of the sum of the volumetric flows of permeate and cell bleed streams.

Owing to the rapid decline of the permeate flux (and subsequently the volumetric flow from the MFU) due to membrane fouling at initial conditions, the $F_{permeate}$ and $V_{fermenter}$ were continuously monitored. The aforementioned process was repeated to attenuate the flow deviation caused by permeate flux change.

Pseudo steady-state permeate flux conditions were assumed when the change in $F_{permeate}$ was less than 5% within a 6 hour period. Under these conditions, the volumetric flow from the substrate supply pump was maintained constant.

In all the MRB experiments in this work, the pseudo steady-state fermenter volume was maintained at 500mL. For kinetic performance evaluation, periodic sampling was performed on sampling port (SP-204) on the fermenter.

#### 5.2.3.2.2 MEMBRANE CLEANING

Irreversible fouling constituents such as adsorbed organic materials and cell debris attached to the membrane surface/pores were cleaned by using a combination of hot caustic soda, Perchloric acid, and membrane back flushing. Upon the completion of each experiment, the membrane was stored in 0.0035 % (m/v) sodium hypochlorite to preserving the membrane until the next experiments were ready to be performed. However, prior to its next usage, the MFU was cleaned using the following proposed procedure (Du Preez, 2008; Belfort *et al.,* 1994):

***Caustic Wash:*** A 2% (w/v) NaOH solution (caustic soda) at 70 $^{o}$C was circulated through the MFU for two hours. The MFU was held at a TMP of 50kPa. Moreover, the MFU was back-flushed periodically at a TMP of 100kPa every 30 minutes using the permeated caustic. After the two-hour period, the caustic solution was purged into a purge vessel.

***Rinsing:*** After the caustic wash step, deionised water (8-10L) was re-circulated throughout the system until the pH in the fermenter was to pH 7. The water was maintained as 50 $^{o}$C. The diluted caustic in the permeate vessel was disposed.

***Acid Wash:*** Dilute Perchloric acid (1mL of 35% PCA per litre $dH_2O$) was thereafter circulated through the MFU for one hour at 70 $^{o}$C at a TMP of 50kPa. The permeated acid solution was periodically back-flushed at a TMP of 100kPa every 15min.

***Rinsing:*** The same rinsing procedure as above was followed in rinsing the MFU.

### 5.2.4 IMMOBILIZED CELL BIOREACTOR

One experiment was conducted on an immobilized cell bioreactor whereby the biocatalytic cells were immobilized within the macroporous support matrix of the composite/asymmetric membrane. This experiment was performed to ascertain that using an immobilized cell bioreactor as an alternative fermentation strategy was not a viable option. The immobilization technique was adopted from Giorno et al., (2000) for the immobilization of fumarase in the pores of an asymmetric polysulfone capillary membrane. However, in this work, the immobilized cell bioreactor was operated in a lumen-to-shell configuration. As a result, an asymmetric membrane with the permeable membrane (0.2µm) on the outside (or shell side) was used with a macroporous support matrix (6-8 µm) on the lumen side to facilitate the entrance of the immobilized cells into the pores of the membrane (mode A in *Figure 21*). The same process flow highlighted in *Figure 35* will be used to describe the immobilization procedure.

The inoculum development protocol previously described in section 5.1.3 was used to prepare a culture of cells in their exponential growth phase. The inoculum was grown in the fermenter (V-201) until the initial inoculum concentration was approximately 3 $g.L^{-1}$. The initial mass of the inoculum was calculated as the product of the inoculum volume and the inoculum concentration ($C_{inoculum}$ x $V_{inociulum}$). Once the inoculum reached the desired concentration, recirculation valves (v-204) and (v-205) were open, the fermenter effluent pump (P-203) was switched on and thus facilitating the removal of the inoculum from the fermenter towards the MFU and back into the fermenter.

Once stable inoculum recirculation was achieved, the MFU was operated at mild conditions (TMP of 50kPa with a cross-flow velocity of $0.233m.s^{-1}$). Operation at this pressure allowed the biocatalytic cells to gently force the cells through the membrane macroporous support matrix with the permeable layer preventing the cells from leaking into the permeate (shell-side). The circulation and immobilization procedure was allowed to commence for a period of four hours. After this immobilization period, the fermenter was drained by closing the valve (v-205) and opening the purge/bleed valve (v-208). Once the fermenter and the pump lines were drained, the whole system was washed with approximately 20 L of distilled water to remove all the microbial cells that did not enter the pores of the membrane. The cell concentration and total volume of the wash and permeate streams were recorded and used in the calculation of the total mass of cells immobilized within the pores.

The amount of cells immobilized within the semi-permeable membrane at initial conditions was calculated by means of a mass balance around the entire system (*Figure 74*):

$$m_{immobilized} = m_{inoculum} - m_{bleed} + m_{permeate} \qquad \textbf{(5.7)}$$

Where $m_{immobilized}$ denotes the mass of cells immobilized, $m_{inoculum}$ denotes the mass of cells in the initial inoculum, $m_{bleed}$ denotes the amount of cells in the wash stream and $m_{permeate}$ denotes the amount of cells in the permeate stream.

# 5.3 EXPERIMENTAL DESIGN

## 5.3.1 OPTIMIZATION OF THE FERMENTATION CONDITIONS

### 5.3.1.1 DETERMINATION OF THE OPTIMUM TEMPERATURE AND PH

Considering the fermentation temperature and pH, literature review suggested that either the effect of the fermentation temperature is much greater than that of the pH or the temperature-pH interaction is significant. To this end, a statistical approach was undertaken to ascertain the effect of the fermentation temperature and pH on the fermentation kinetics from a glucose substrate (by *Z. mobilis* ZM4) and a glucose-xylose substrate (by *Z. mobilis* 8b)

Two $3^2$ full factorial statistical designs were proposed with the aim being to investigate the possible occurrence of an optimal temperature and pH combination for single substrate (glucose) and mixed substrate (glucose-xylose) fermentation. A schematic and tables of the statistical designs are presented *Figure* 37, *Table 9*, and

*Table 10* respectively. This statistical approach investigated the effect varying these two process variables on three response variables, i.e. the ethanol yield ($Y_{p/s}$), volumetric productivity (VP), and the overall rate of xylose consumption ($Q_{s\_x}$). The temperature and initial pH ranges were selected based on literature survey on the range whereby the optimum conditions are expected.

***Figure 37:*** *A schematic of the statistical design for optimizing the fermentation temperature and pH*

A second-degree polynomial regression model was used to predict each response variable ($Y_{ps,}$ VP, $Q_{s_{xylose}}$) as a function of the input variables ($x_1$, $x_2$). The second-degree polynomial was fitted to the experimental responses obtained at the various input variable combinations ($x_1$, $x_2$), as proposed by the full factorial design. The second degree polynomial regression model was expressed as follows:

$$Y_i = \beta_0 + \sum_{i=1}^{2} \beta_i x_i + \sum_{i=1}^{2} \beta_{ii} x^2{}_{ii} + \sum_{i=1}^{2} \beta_{ij} x_i x_j + \varepsilon \quad \textbf{(5.7)}$$

where $\beta_0$ represents the intercept, $\beta_i$ represents the linear effect coefficient for temperature ($x_1$) and $pH_0$ ($x_2$), $\beta_{ii}$ represents the quadratic effect coefficient for $x^2_{11}$ and $x^2_{22}$ and $\beta_{ij}$ represents the interaction effect coefficient for $x_1x_2$. The experimental or random error was represented by $\varepsilon$.

The complete second degree polynomial regression model was refined using backward elimination. Backward elimination involves the removal of model parameters that are associated with regression coefficients that are deemed insignificant by an analysis of variance (as indicated by $p>0.05$ for a 95% confidence interval). However, backward elimination was conducted in such a way that the integrity of the model hierarchy was retained. All statistical analyses were performed in Statistica (software, version 12).

For statistical inference of the ANOVA analysis, the residuals were assumed to be homogeneous and originate from a normal distribution. These assumptions were later validated and presented in Appendix C.

In optimizing the fermentation temperature and initial pH for a mixed sugar substrate, a glucose-to-xylose ratio resembling that of dilute acid pretreated corn-stover liquor (xylose-rich hydrolyzate) was selected (Aden *et al.,* 2010). However, to eliminate effects of ethanol and substrate inhibition on the metabolization of xylose, the total initial sugar concentration was limited to 50g.$L^{-1}$.

***Table 9:*** *$3^2$ factorial design for obtaining the optimum operational temperature and pH for glucose fermentation by Z. mobilis ZM4. All the experimental runs were performed at 50g.$L^{-1}$ glucose, agitation speed of 150rpm, $KH_2PO4$-$K_2HPO_4$ buffer conc. = 100mM*

| **GLUCOSE FERMENTATION: $3^2$ FULL FACTORIAL DESIGN** | | | | |
|---|---|---|---|---|
| **Experiment No.** | ***Process Variable*** | | ***Response Variable*** | |
| | ***Temperature (°C)*** | ***$pH_0$*** | ***% Theoretical Ethanol Yield*** | ***Volumetric Productivity (g EtOH.$L^{-1}$.$h^{-1}$)*** |
| **1** | 40 | 8 | $R_{1\_1}$ | $R_{2\_1}$ |
| **2** | 35 | 8 | $R_{1\_2}$ | $R_{2\_2}$ |
| **3** | 30 | 8 | $R_{1\_3}$ | $R_{2\_3}$ |
| **4** | 40 | 6 | $R_{1\_4}$ | $R_{2\_4}$ |
| **5** | 40 | 7 | $R_{1\_5}$ | $R_{2\_5}$ |
| **6** | 35 | 6 | $R_{1\_6}$ | $R_{2\_6}$ |
| **7** | 30 | 7 | $R_{1\_7}$ | $R_{2\_7}$ |
| **8** | 35 | 7 | $R_{1\_8}$ | $R_{2\_8}$ |
| **9** | 35 | 7 | $R_{1\_9}$ | $R_{2\_9}$ |
| **10** | 35 | 7 | $R_{1\_10}$ | $R_{2\_10}$ |
| **11** | 30 | 6 | $R_{1\_11}$ | $R_{2\_11}$ |

***Table 10:*** *$3^2$ factorial design for obtaining the optimum operational temperature and pH for glucose:xylose fermentation by Z. mobilis 8b. All the experimental runs were performed at 13:37 g.L$^{-1}$ glucose:xylose substrate conc., agitation speed of 150rpm, $KH_2PO_4$-$K_2HPO_4$ buffer conc. = 100mM*

| GLUCOSE - XYLOSE FERMENTATION: $3^2$ FULL FACTORIAL DESIGN | | | | | |
|---|---|---|---|---|---|
| **Experiment No.** | ***Process Variable*** | | ***Response Variable*** | | |
| | ***Temperature (°C)*** | ***$pH_0$*** | ***$Q_{s\_x}$ (g xylose cons.L$^{-1}$.h$^{-1}$)*** | ***% Theoretical Ethanol Yield*** | ***Volumetric Productivity (g EtOH.L$^{-1}$.h$^{-1}$)*** |
| **1** | 37 | 8 | $R_{1\_1}$ | $R_{2\_1}$ | $R_{3\_1}$ |
| **2** | 33.5 | 8 | $R_{1\_2}$ | $R_{2\_2}$ | $R_{3\_2}$ |
| **3** | 30 | 8 | $R_{1\_3}$ | $R_{2\_3}$ | $R_{3\_3}$ |
| **4** | 37 | 6 | $R_{1\_4}$ | $R_{2\_4}$ | $R_{3\_4}$ |
| **5** | 37 | 7 | $R_{1\_5}$ | $R_{2\_5}$ | $R_{3\_5}$ |
| **6** | 35 | 6 | $R_{1\_6}$ | $R_{2\_6}$ | $R_{3\_6}$ |
| **7** | 30 | 7 | $R_{1\_7}$ | $R_{2\_7}$ | $R_{3\_7}$ |
| **8** | 33.5 | 7 | $R_{1\_8}$ | $R_{2\_8}$ | $R_{3\_8}$ |
| **9** | 33.5 | 7 | $R_{1\_9}$ | $R_{2\_9}$ | $R_{3\_9}$ |
| **10** | 33.5 | 7 | $R_{1\_10}$ | $R_{2\_10}$ | $R_{3\_10}$ |
| **11** | 30 | 6 | $R_{1\_11}$ | $R_{2\_11}$ | $R_{3\_11}$ |

#### 5.3.1.2 EFFECT OF SUBSTRATE COMPOSITION ON DUAL-SUBSTRATE FERMENTATION

A literature survey indicated that the sugar composition of LC biomass and the subsequently pre-treated liquor (liquid fraction in *Figure 2*) generally consists of both glucose and xylose as the major monomeric sugar constituents. Moreover, although pre-treated liquor consists of a greater concentration of xylose, there is an area of uncertainty pertaining to the effect of the presence of glucose on the overall rate of xylose consumption. *Table 11* presents the experimental conditions selected for the investigation of the effect of glucose on xylose fermentation. The experimental conditions were maintained at the optimal fermentation temperature and initial pH from the previous section. The effect of the initial sugar composition was quantified based on the overall rate of xylose consumption and the ethanol yield.

***Table 11:*** *Experimental Conditions for Determining the Effect of Sugar Composition on the Ethanol Production Rate*

| QUANTIFICATION OF THE EFFECT OF SUGAR COMPOSITION | | | | |
|---|---|---|---|---|
| ***Sugar*** | ***Experiment 1*** | ***Experiment 2*** | ***Experiment 3*** | ***Experiment 4*** |
| *Glucose [g.L$^{-1}$]* | 0 | 13 | 37 | 50 |
| *Xylose [g.L$^{-1}$]* | 50 | 37 | 13 | 0 |

### 5.3.2 CHARACTERIZATION OF THE MICROFILTRATION UNIT

The permeate flux of MRB processes is generally optimized in view of minimizing membrane area and/or cycle time requirements (Russotti and Goklen, 2001).The main operating parameters that must be characterized for flux optimization purposes include the hydrodynamic conditions (TMP and the shear rate/cross-flow velocity) and the feed solution properties (the fluid viscosity and the cell concentration). As described in the physical fouling mechanism, the effects of these parameters are not mutually exclusive. Therefore, the application of cross-flow MFU for cell recovery requires extensive knowledge of how the process parameters contribute to the declining permeate flux rate.

### 5.3.2.1 DETERMINATION OF THE MEMBRANE CRITICAL FLUX

The initial filtration performance of the MFU was characterized by measuring the permeability of de-ionised water as a function of the TMP and the cross-flow velocity. The TMP and cross-flow velocity ranges were limited by the experimental equipment to 0-150 kPa and 0.09-0.4328 $m.s^{-1}$ respectively. The flux of water was used as a basis for the quantification of the extent of irreversible membrane fouling after an experiment had been completed and the membrane had been chemically and physically cleaned.

Considering the flux of water to be that of pure fluid, the effect of the process media substrate composition on the permeate flux was investigated. Sugar molecules in a water based medium not only increase the fluid viscosity but also act as macrosolutes which have the tendency to adsorb onto the membrane pores (mainly within the membrane structure) and subsequently provide additional resistance to the flux (Belfort *et al.,* 1994). Therefore, the effect of the substrate concentration on the observed critical flux relative to water was quantified using the technique described in *section 3.3.8*.

The procedure for evaluating water permeability and the critical flux was:

- To measure the permeate flux as a function of time at various TMPs and the pseudo steady state flux values were plotted as a function of the TMP.
- The permeability was ascribed to the slope of the linear region from this plot
- Depending on the process media slope relative to pure water, the critical flux (weak or strong form) was ascribed to the point of departure from linearity

The experimental conditions for determining the critical flux are presented in *Table 12*. All of these experiments were performed at a constant and fixed cross-flow velocity.

***Table 12:*** *Experimental conditions for quantifying the effect of the substrate concentration on the critical flux. Cross-flow velocity maintained at 0.2 $m.s^{-1}$, Temperature = 30 $^{o}C$, media pH = 5.5.*

| QUANTIFICATION OF THE SUBSTRATE COMPOSITION ON CRITICAL FLUX | | | | |
|---|---|---|---|---|
| ***Sugar*** | ***Experiment 1*** | ***Experiment 2*** | ***Experiment 3*** | ***Experiment 4*** |
| *Glucose [$g.L^{-1}$]* | 0 | 50 | 100 | 150 |
| *TMP range (kPa)* | 0-150 | 0-150 | 0-150 | 0-150 |

### 5.3.2.2 QUANTIFICATION OF THE EFFECT OF THE HYDRODYNAMIC CONDITIONS ON MEMBRANE PERMEABILITY

In an attempt to isolate the effect of the shear rate/cross-flow velocity (CFV) on the critical flux from the effect of the substrate concentration, the CFV was varied within the experimentally limited range of 0.09–0.4328$m.s^{-1}$ for the filtration of cell-free fermentation media (maintained constant at 100$g.L^{-1}$ glucose). The experimental conditions are presented in *Table 13*.

***Table 13:*** *Experimental conditions for quantifying the effect of the cross-flow velocity on the critical flux. Substrate conc. maintained at 100 g.L$^{-1}$, Temperature = 30 °C, media pH = 5.5.*

| QUANTIFICATION OF THE CROSS-FLOW VELOCITY ON CRITICAL FLUX | | | | |
|---|---|---|---|---|
| ***Sugar*** | ***Experiment 1*** | ***Experiment 2*** | ***Experiment 3*** | ***Experiment 4*** |
| *Glucose [g.L$^{-1}$]* | 100 | 100 | 100 | 100 |
| *CFV (m.s-1)* | 0.0932 | 0.198 | 0.3202 | 0.4328 |

### 5.3.2.3 STATISTICAL OPTIMIZATION OF THE PERMEATE FLUX

In the examination of the effect of the substrate concentration and the CFV on the permeate flux, it is important for the flux to be studied over the course of the cell concentration range expected during the cell recycling experimental work. However, the mathematical modelling of the relationships between the hydrodynamics, suspension properties and the permeate flux through mass transfer kinetic models is extremely complex (van den Berg and Smolders, 1990).

As a result of the complex mass transfer modelling, a statistical approach was undertaken to determine the effect of the hydrodynamic conditions and the solution feed properties, with the main objective being to determine the properties that have statistical significance towards the permeate flux. A Response Surface Methodology (RSM) technique was adapted to allow for the fitting of a quadratic regression model to the experimental data and interpreting the fitted model through surface plots and ANOVA analyses (Donkoh *et al.,* 2012). A face-centred Central Composite Design (CCD) was used to fit a second order regression model to the experimental data. The main objective of the CCD was to attain an empirical model that could predict the pseudo-steady state permeate flux through the membrane as a function of the TMP, cell concentration and the cross-flow velocity. The cross-flow velocity, TMP and the cell concentration were selected as the process variable and the permeate flux as the response variable. The following second order non-liner regression model was used to evaluate for the pseudo-steady state permeate flux as a function of the TMP, CFV and cell concentration:

$$Y_i = \beta_0 + \sum_{i=1}^{3} \beta_i x_i + \sum_{i=1}^{3} \beta_{ii} x^2{}_{ii} + \sum_{i=1}^{3} \beta_{ij} x_i x_j + \varepsilon \qquad \textbf{(5.6)}$$

In equation 5.6, $Y_i$ denotes the response factor (pseudo-steady state permeate flux); $x_i$, denote the process variables (TMP ($x_1$), CFV($x_2$), and cell conc. ($x_3$) respectively). $\beta_0$ denotes the model intercept, and $\beta_i$, denotes the model coefficients for the linear effect of the process variables $x_1$, $x_2$, and $x_3$ respectively. $\beta_{ij,}$ denote the model coefficients for the interaction effect of the process variables $x_1x_2$, $x_1x_2$ , and $x_2x_3$ respectively. Lastly, $\beta_{ii,}$ denotes the model coefficients for single factor quadratic effect of the process variables for $x_1^2$, $x_2^2$, and $x_3^2$ respectively. The experimental random error was represented by ε.

To ensure that the CCD statistical design was rotatable, the axial spacing (alpha, α) of the face-centred star points was set as $(2^k)^{0.25}$ units, where k is the number of process variables used. Lawson and Erjavec (2001) defined rotatability as "the implication that the accuracy of the regression model

prediction is dependent on the distance the point is from the origin, and not the direction of that point". Hence, for three factors the axial spacing was selected as 1.682 (Lawson and Erjavec, 2001). For CCDs, the factorial points (corner points) determine the main and interaction effects of the regression model. The axial points (star points) and centre points allow for the determination of the quadratic terms and adequacy of the regression model respectively (Donkoh *et al.,* 2012). In this work, two additional centre point runs were added to the CCD to increase the statistical inference of the quadratic model. A schematic and table of the CCD design is presented in *Figure 38* and *Table 14* respectively.

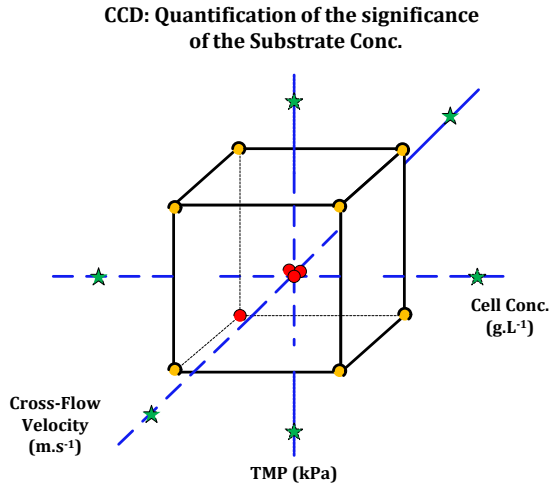


***Figure 38:*** *Central Composite Designs for the statistical quantification of the effect of the hydrodynamic conditions and the suspension solution properties on the permeate flux.*

***Table 14:*** *Central Composite Design for the quantification of the effect of the hydrodynamic conditions and the cell concentration on the permeate flux.*

| Experiment No. | *Process Variable* | | | *Response Variable* |
|---|---|---|---|---|
| | *CFV ($m.s^{-1}$)* | *Cell Conc. ($g.L^{-1}$)* | *TMP (kPa)* | *Permeate Flux ($L.m^{-2}.h^{-1}$)* |
| **1** | 0.1413 | 1.5 | 30 | $R_{1\_1}$ |
| **2** | 0.2547 | 1.5 | 30 | $R_{1\_2}$ |
| **3** | 0.1413 | 1.5 | 90 | $R_{1\_3}$ |
| **4** | 0.2547 | 1.5 | 90 | $R_{1\_4}$ |
| **5** | 0.1413 | 5.5 | 30 | $R_{1\_5}$ |
| **6** | 0.2547 | 5.5 | 30 | $R_{1\_6}$ |
| **7** | 0.1413 | 5.5 | 90 | $R_{1\_7}$ |
| **8** | 0.2547 | 5.5 | 90 | $R_{1\_8}$ |
| **9** | 0.1980 | 0.136 | 60 | $R_{1\_9}$ |
| **10** | 0.1980 | 6.863 | 60 | $R_{1\_10}$ |
| **11** | 0.1980 | 3.5 | 9.546 | $R_{1\_11}$ |
| **12** | 0.1980 | 3.5 | 110.454 | $R_{1\_12}$ |
| **13** | 0.1025 | 3.5 | 60 | $R_{1\_13}$ |
| **14** | 0.2934 | 3.5 | 60 | $R_{1\_14}$ |
| **15 (C)** | 0.1980 | 3.5 | 60 | $R_{1\_15}$ |
| **16 (C)** | 0.1980 | 3.5 | 60 | $R_{1\_16}$ |
| **17 (C)** | 0.1980 | 3.5 | 60 | $R_{1\_17}$ |
| **18 (C)** | 19.90 | 3.5 | 60 | $R_{1\_18}$ |

The experimental design presented *Table 14* constituted 18 runs. In the development of the empirical model, the residuals were assumed to be homogenous and originate from a normal distribution. All the statistical calculations were performed in Statistica™ (Hill and Lewicki, 2007).

### 5.3.3 QUANTIFICATION OF THE KINETICS OF Z. MOBILIS IN CONTINUOUS CULTURE

The kinetic performance of *Z. mobilis* in continuous culture was investigated by comparing the continuous culture (without cell retention) to continuous culture with cell retention fermentation strategies, both performed at the same experimental conditions. Continuous culture with cell retention was evaluated using two fermentation strategies, i.e. cell immobilization and cell retention via an external cross-flow microfiltration membrane. The comparative performance of the three fermentation strategies was quantified terms of the overall volumetric productivity, the ethanol yield (as a percentage of the theoretical yield) and the final ethanol concentration. All the experiments in this section were performed at the optimum fermentation and pH conditions.The experimental design for this section is presented in *Table 15*. The fermentation performance of the MRB was compared to batch and continuous culture (without retention) fermentation strategies operating at the same initial conditions of substrate composition, fermentation temperature and pH (Experiments 2, 5, 7). A preliminary glucose-to-xylose ratio of 1:1 was used in comparing the performance of the three process configurations.

***Table 15:*** *The experimental conditions tested for the comparative quantification of the kinetics of Z. mobilis in continuous culture*

| QUANTIFICATION OF THE MBR FERMENTATION KINETICS | | | | |
|---|---|---|---|---|
| **Experiment No.** | ***Configuration*** | ***Sub. Concentration (g.L$^{-1}$)*** | | ***M. organism*** |
| | | ***Glucose*** | ***Xylose*** | |
| **1** | Continuous‡ | 100 | - | ZM4 |
| **2** | Continuous | 50 | 50 | 8b |
| **3** | Immobilized Cell†† | 50 | 0 | ZM4 |
| **4** | MRB | 50 | 50 | 8b |
| **5** | MRB‡‡ | 75 | 25 | 8b |
| **6** | MRB‡‡‡ | 25 | 75 | 8b |

† Batch experiments performed in the custom build 1.5L fermenter with temperature and pH control

‡ Continuous experiment performed in the dilution range 0.05-0.4. Steady-state assumed after at least four working volume changes. No cell retention imposed

†† Immobilized cells operated in a lumen to shell configuration with membrane B (permeable layer on outside, *Figure 32*)

‡‡ Glucose-to-xylose ratio of conditioned liquor from the Iogen process design (Tolan, 2002; Lawford and Rousseu, 2003).

‡‡‡ Glucose-to-xylose ratio of dilute sulphuric acid pre-treated liquor from Corn Stover (Pioneer 34M95) (Aden *et al.,* 2010)

The effect of the substrate composition on the performance of the MRB was investigated for process designs whereby the fermentation step is performed in the absence of lignin (*section* 2.2.3.3). The total substrate concentration was maintained at 100g.L$^{-1}$ and the glucose-to-xylose ratio was varied. In experiment 5, the ratio of glucose to xylose (xylose rich substrate) was selected from dilute acid

pre-treated corn-stover liquor (Aden *et al.,* 2010). In experiment 6, the glucose –to-xylose ratio reported from the Iogen process design was used to evaluate for the co-fermentation of glucose rich system (Tolan, 2002; Lawford and Rousseau, 2003).

The kinetics of immobilized cells (an alternative form of cell retention) were quantified by immobilizing the cells within the macroporous support matrix of membrane B (permeable layer on the outside), operating in a lumen-to-shell flow configuration. For this experiment, the experimental set-up indicated in *Figure 35* was used. However, the MFU was used as a bioreactor and the 1.5 L bioreactor was used as an unused substrate recirculation vessel (RV). A low substrate loading of 50 $g.L^{-1}$ was used to quantify the extent of reaction of the substrate by the immobilized cells in the MFU.

# CHAPTER 6

## REACTOR MODELING

*In this section, a mathematical formulation predicting the performance of the MRB under various operating conditions is developed from first principles. The performance of the MRBwas simulated to predict the substrate, cell dry weight and ethanol concentration profiles as functions of time during the fermentation process.*

## 6.1. PROBLEM DEFINITION

A kinetic model built from first principles that can accurately predict the behaviour of the proposed membrane recycle bioreactor (MRB) system was desired. In this system, a dual substrate feed stream consisting of the glucose and xylose was converted into ethanol by *Z. mobilis* 8b, in a continuously operating MRB. The simulation model for the MRB is influenced by the following system parameters: the process configuration, the magnitude of the recirculation stream, the location/presence of a bleed stream, and the internal volume of the membrane section (Groot *et al.,* 1993). Depending on the system parameters, the simulation of the proposed MRB system can take one of the four cases presented below:

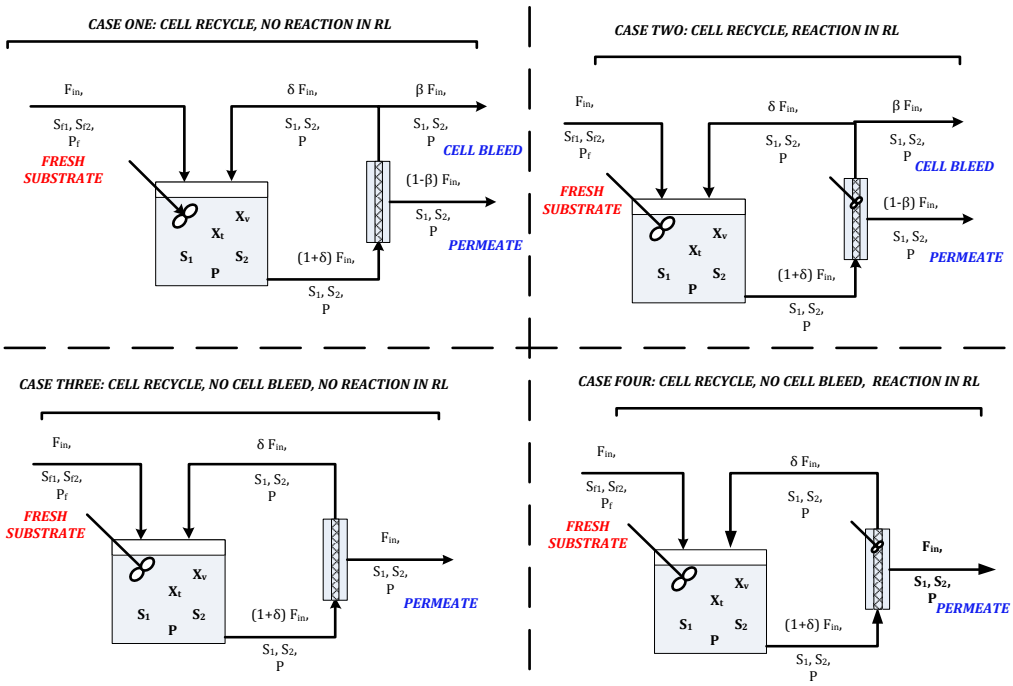


| Key | Description |
|---|---|
| $F_{in}$ | Volumetric flow in (L/h) |
| $S_{f1}$ | Glucose feed conc. (g/L) |
| $S_{f2}$ | Xylose feed conc. (g/L) |
| $P_f$ | Ethanol feed conc. (g/L) |
| $S_1$ | Glucose conc. (g/L) |
| $S_2$ | Xylose conc. (g/L) |
| $X_t$ | Total cell conc. (g/L) |
| $X_v$ | Viable cell conc. (g/L) |
| P | Ethanol conc. (g/L) |
| β | Cell bleed fraction (g/L) |
| δ | Cell recycle fraction (g/L) |

***Figure 39:*** *Schematic representation of the simulation cases for describing the current MRB.* ***RL*** *– Recirculation Loop*

Case one represents a system whereby the total liquid volume of the system (fermenter and membrane recirculation loop (RL)) can be assumed to be well mixed with negligible substrate conversion occurring in the RL. The latter assumption is based on a characteristic time concept presented by Sweere *et al.,* (1987). They stated that: "the characteristic time provides a tool for distinguishing between important and less important mechanisms. The characteristic time is low when the process is fast, and high when the process is slow. Hence, mechanisms with low characteristic times are negligible". In the current system, the fermentation broth is pumped at a relatively faster rate through the microfiltration unit (MFU) and the RL compared to the specific growth rate of the ethanologic microorganisms. Therefore, the characteristic time through the RL (residence time in the RL) is much smaller relative to the characteristic time for biocatalyst growth (defined as the inverse of the specific growth rate). Hence, the cell production in the RL can be assumed to be negligible (Groot *et al.,* 1993). The same analogy can be applied to the rates of substrate consumption and ethanol production.

Case two defines fermentative systems whereby the cells fouling the membrane significantly contribute to the overall rate of sugar-to-ethanol conversion. The growth of cake forming cells on the membrane surface creates additional resistance to the permeate flux through the MFU. The prediction of the characteristic time through the cake layer is complex and, therefore, alternative methods are required to estimate the relative rate of substrate conversion in the MFU. Case three and Case four describe systems where total cell retention is imposed. Ezeji and Li (2010) reported that the addition of a cell bleed stream to MRB processes is necessary for the recovery of cell viability within the fermenter and subsequently for sustaining long-life process operation. As a result, Case three and Case four are not applicable to the current system due to the presence of a cell bleed stream in the proposed MRB design.

Therefore, the simulation of the dual substrate conversion model was performed using case one as the base process design. However, to check for the extent of reaction in the MFU, cells were be immobilized inside the macroporous support matrix of the membrane and the substrate and ethanol concentrations were evaluated through the membrane-cell aggregate.

## 6.2 Model Assumptions and Simplifications

In assembling a mathematical model for representing the observed MRB fermentation kinetics, the following assumptions were made:

*I.* ***Fermenter is Well-Mixed***: The fermenter is agitated by a magnetic stirrer and the presence of baffles in the fermenter minimizes areas of dead volume the fermenter. The velocity of the fermentation broth entering the fermenter from the recirculation loop is typically pre-determined by the required hydrodynamic conditions in the MFU. The high inlet velocity typically induces turbulence in the fermenter and subsequently more intense mixing.

II. ***Non-steady state behaviour:*** Operating the MFU at constant TMP, membrane fouling is expected to initially induce a decline in the permeate flux with time until pseudo-steady state conditions are reached. Therefore, a non-steady state model type was assumed.

III. ***Sterile Fermenter Feed***: The substrate fed into the fermenter was sterilized prior to operation. Therefore the cell concentration in the feed was negligible.

IV. ***The Recirculation loop is Isothermal:*** Temperature changes of the fermentation culture through the RL (due to heat dissipated by the recirculation pump and heat exchange with the environment) are assumed to be negligible.

V. ***Negligible Amounts of By-Products are formed:*** *Z. mobilis* 8b has been shown to form a small percentage of by-products during xylose and glucose fermentation. However, for model simplification purposes, the formation of these products was considered to be negligible relative to the formation of ethanol.

VI. ***Rate expressions by Rogers et al., (1983; 2001) are applicable:*** Rogers *et al.,* (2001) developed a free-cell kinetic model for the simultaneous conversion of glucose and xylose into ethanol with *Z. mobilis* ZM4 (pZB5) as the biocatalyst. For simplification purposes, the same rate expressions used in their work were adapted for this work. (Rogers *et al.,* 1983; 2001).

VII. ***Ethanol inhibition is significant, substrate inhibition effects are negligible:*** The experimental work on the MRB was executed at conditions whereby substrate inhibition was negligible (initial substrate concentration was below the threshold concentration). However, theoretical ethanol concentrations up to 5% (w/v) are expected, and thus ethanol inhibition of the rates of cell mass production, substrate consumption and ethanol production is expected.

VIII. ***Maximum and threshold ethanol inhibitory concentrations provided in literature***: Due to the lack of kinetic data for *Z. mobilis* 8b, the maximum and threshold ethanol concentrations will be inferred from the kinetic data of its predecessor strain *Z. mobilis* ZM4 (pZM5). Literature suggests that maximum and threshold ethanol concentrations are dependent on the type of *Z. mobilis* strain. However, as a first approximation model, this assumption will be held.

IX. ***Permeate is cell-free:*** The MWCO of the MF membrane is approximately five times smaller than the smallest reported dimension of *Z. mobilis* and therefore for the purposes of simplifying the mass balances, the retention efficiency of the membrane was assumed to be 100%.

X. ***Intracellular glucose, xylose and ethanol concentrations are negligible:*** The substrate and product concentrations were based on the abiotic volume of the cell free liquid.

## 6.3. MODEL DEVELOPMENT

The mathematical model was developed from first principles through the quantification of mass balances around the entire system (control volume). Based on the model assumptions, a block flow diagram of the simplified process is presented below:

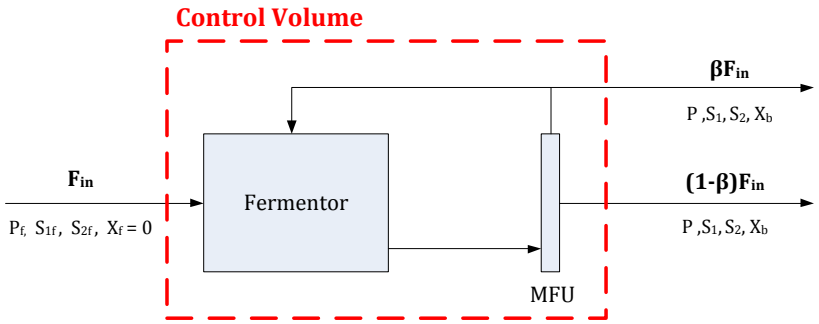


***Figure 40:*** *Block flow diagram of the simplified MRB process*

The final derived mathematical model should adequately predict the performance of the system with regards to the conversion of glucose ($S_1$) and xylose ($S_2$) to ethanol (P) at any instant during the fermentation step.

### 6.3.1 REACTION STOICHIOMETRY

Model construction is generally initiated by the definition of the stoichiometry of the reactions to be considered in the model. Considering ethanol production from glucose and xylose (through the ED pathway, *sections 2.2.2 and 2.2.3*), the overall stoichiometric reactions of these sugars are summarised by the reactions below:

$$ADP + Glucose = 2\,Ethanol + 2CO_2 + ATP \quad \textbf{(6.1)}$$

$$3ADP + 3Xylose = 5\,Ethanol + 5CO_2 + 3ATP \quad \textbf{(6.2)}$$

In the overall fermentation reaction of glucose, 1 mol of glucose is converted to 2 mol of ethanol (EtOH) and 2 mol of the metabolism by-product $CO_2$ (Neglecting the NAD(P)H balance) (Shuler & Kargi, 2008). The theoretical EtOH yield based on the stoichiometry is 2 mol EtOH produced per mol of glucose consumed (or 0.51g EtOH/g glucose). Similarly, for the overall xylose fermentation reaction, 3 mol of xylose are converted to 5 mol of EtOH and 5 mol of the metabolism by-product $CO_2$. In this case, the theoretical EtOH yield based on the stoichiometry is 1.67 mol EtOH produced per mol of xylose consumed (or 0.51g EtOH/g xylose) (Zhang *et al.,* 1995a; Nunez *et al.,* 1989).

### 6.3.2 MASS BALANCES

The general mass balance around the control volume for species *i* in a non-steady-state continuous reactor is defined as follows:

$$Accumulation_i = Inlet_i - Permeate_i - Bleed_i + Rate_i \quad \textbf{(6.3a)}$$

$$V_{tot}\frac{dC_i}{dt} = F_{in}C_{i_{in}} - (1-\beta)F_{in}C_{i_{permeate}} - \beta F_{in}C_{i_{bleed}} + rate_i V_{tot} \quad \textbf{(6.3b)}$$

$$\frac{dC_i}{dt} = D_H C_{i_{in}} - (1-\beta)D_H C_{i_{permeate}} - \beta D_H C_{i_{bleed}} + rate_i \quad \textbf{(6.3c)}$$

In equation 6.3, $\mathbf{V_{tot}}$ is the total reaction volume (the sum of the RL and fermenter volume) [L], $\mathbf{F_{in}}$ is the volumetric flow rate into the fermenter [L.h$^{-1}$], $\mathbf{C_i}$ is the concentration of species i [g.L$^{-1}$], $\mathbf{C_{ipermeate}}$ is the concentration of species i in the permeate [g.L$^{-1}$], $\mathbf{C_{ibleed}}$ is the concentration of species i in the bleed (same as permeate) [g.L$^{-1}$], $\boldsymbol{\beta}$ is the bleed rate, $D_H$ is the hydraulic dilution rate (Fin/Vtot) [h$^{-1}$] and $\mathbf{rate_i}$ is the kinetic rate of species i generation or consumption [g.L$^{-1}$.h$^{-1}$].

Simplifying the general mass balance for the cell mass (***x***), glucose (***S$_1$***), xylose (***S$_2$***) and ethanol (***P***), the following mass balance equations were derived for an unsteady-state MRB:

***Cell Mass:*** $$\frac{dx}{dt} = (r_x - \beta D_H)\cdot x \quad \textbf{(6.4)}$$

***Glucose:*** $$\frac{ds_1}{dt} = D_H(s_{f_1} - s_1) - r_{s_1}\cdot x \quad \textbf{(6.5)}$$

***Xylose:*** $$\frac{ds_2}{dt} = D_H(s_{f_2} - s_2) - r_{s_2}\cdot x \quad \textbf{(6.6)}$$

***Ethanol:*** $$\frac{dP}{dt} = D_H(P_f - P) + r_p \cdot x \quad \textbf{(6.7)}$$

### 6.3.3 RATE LAWS

Many kinetic models have been proposed in literature for the description of the fermentation kinetics of glucose-xylose substrates to ethanol. However considering Z. mobilis, the rate expressions derived by Roger *et al.,* (2001) were adapted. The rate expressions are briefly presented here, Rogers et al., (2001) may be consulted for more detailed information (Rogers *et al.,* 2001).

#### 6.3.3.1 MICROBIAL GROWTH RATE ($r_X$)

Zhang *et al.,* (1995a) reported that microbial growth by *Z. mobilis* on glucose and xylose occurs simultaneously. Assuming that both glucose and xylose compete for uptake through a common and unchanged transport system in *Z. mobilis*, the contribution of glucose and xylose to the microbial growth rate was described as follows:

***Glucose:*** $$r_{x_1} = \frac{\mu_{max_1}\cdot s_1}{K_{sx_1}+s_1}\cdot\left(1 - \frac{P - p_{ix_1}}{p_{mx_1} - p_{ix_1}}\right) \quad \textbf{(6.8a)}$$

***Xylose:*** $$r_{x_2} = \frac{\mu_{max_2}\cdot s_2}{K_{sx_2}+s_2}\cdot\left(1 - \frac{P - p_{ix_2}}{p_{mx_2} - p_{ix_2}}\right) \quad \textbf{(6.8b)}$$

***Overall:*** $$r_x = \{\alpha\cdot r_{x_1} + (1-\alpha)\cdot r_{x_2}\} - k_D \quad \textbf{(6.8c)}$$

Equations 6.8a and 6.8b are rate expressions for microbial growth on the individual sugars and comprise a Monod model term for describing substrate limited cell growth and an ethanol inhibition term. In combining the individual rate expressions for simultaneous glucose and xylose uptake a proportionality factor (α) that indicates the competition of the two sugars via an unchanged and constant sugar transport system was implemented (Rogers *et al.,* 2001).

#### 6.3.3.2 *SUBSTRATE CONSUMPTION ($r_{s_1}$ AND $r_{s_2}$)*

In defining the rate expressions for the consumption of glucose and xylose, the two rate equations were approached separately. However, the same proportionality constraint (as in the definition of the microbial growth rate) was employed to account for the presence of both sugars in the same system. The rates of glucose and xylose consumption are formulated in Equations 6.9 and 6.10 respectively.

***Glucose:***
$$r_{s_1} = \alpha \cdot \frac{q_{smax_1} \cdot s_1}{K_{ss_1} + s_1} \cdot \left(1 - \frac{P - p_{is_1}}{p_{ms_1} - p_{is_1}}\right) \quad \textbf{(6.9)}$$

***Xylose:***
$$r_{s_2} = (1 - \alpha) \cdot \frac{q_{smax_2} \cdot s_2}{K_{ss_2} + s_2} \cdot \left(1 - \frac{P - p_{is_2}}{p_{ms_2} - p_{is_2}}\right) \quad \textbf{(6.10)}$$

#### 6.3.3.3 *ETHANOL PRODUCTION ($r_p$)*

When the sugar consumption rate is affected by substrate limitation or competition, the ethanol production rate is affected in the same way (Rogers *et al.,* 2001; Zhang *et al.,* 1995a). Therefore, the ethanol production rate was expressed as follows:

$$r_p = \{\alpha \cdot \frac{q_{pmax_1} \cdot s_1}{K_{sp_1} + s_1} \cdot \left(1 - \frac{P - p_{ip_1}}{p_{mp_1} - p_{ip_1}}\right) + (1 - \alpha) \cdot \frac{q_{pmax_2} \cdot s_2}{K_{sp_2} + s_2} \cdot \left(1 - \frac{P - p_{ip_2}}{p_{mp_2} - p_{ip_2}}\right)\} \quad \textbf{(6.11)}$$

#### 6.3.3.4 *HYDRAULIC DILUTION RATE*

The hydraulic dilution rate is an indicator for mean residence time of liquid media in the MRB system. However, the residence time of the system is dependent on the filtration performance of the MFU. The relationship between the hydraulic dilution rate and the permeate flux is presented below:

$$D_H(t) = J(t) \cdot \frac{A_{mem}}{V_{tot}} \quad \textbf{(6.12)}$$

***J(t)*** is the permeate flux rate at time t [$L.m^{-2}.h^{-1}$], $\boldsymbol{A_{mem}}$ is the surface area of the membrane [$m^2$], $\boldsymbol{V_{tot}}$ is the total control volume [L].

Bacterial growth has been shown to severely impact the operation of MRBs due to membrane fouling effects and the subsequent decline in the permeate flux. Although many models and theories for simulating the decline in the permeate flux through the membrane have been proposed in literature, the simplest models assume that fouling is a first order mechanism (Moudeeb *et al.,*

1995). Therefore exponential type empirical models have been shown to fit experimental data well (Patel *et al.,* 1982). As a result, the following empirical function was adopted to describe the transient permeate flux rate through the MFU:

$$J(t) = J_0 t^{-b} \quad \textbf{(6.13)}$$

where $J_0$ is the flux at 1 min [L.m$^{-2}$.h$^{-1}$], and **b** is the fouling rate constant. When no fouling is present, b =0.

#### 6.3.3.5 *PERFORMANCE INDICATORS*

The performance of the MRB system was indicated by profiling the instantaneous substrate conversion (***Z***) and the instantaneous volumetric productivity (***Pr***).

***Instantaneous Glucose Conversion:*** $Z_1(t) = \frac{[s_1]_{Feed,0} - [s_1]_{Permeate,t}}{[s_1]_{Feed,0}}$ **(6.13)**

***Instantaneous Xylose Conversion:*** $Z_2(t) = \frac{[s_2]_{Feed,0} - [s_2]_{Permeate,t}}{[s_2]_{Feed,0}}$ **(6.14)**

***Instantaneous Ethanol Productivity:*** $VP(t) = r_p(t) \cdot x$ **(6.15a)**

$= D_H(t) \cdot P(t)$ **(6.15c)**

$\therefore VP(t) = J(t) \frac{A_{mem}}{V_{tot}} \cdot P(t)$ **(6.15b)**

where $D_H(t)$ is the instantaneous dilution rate at time *t*, and $r_p(t)$ is the instantaneous specific rate of ethanol production at time *t.*

At pseudo steady-state conditions, the change in the permeate flux rate with time can be considered negligible. Following Equation 6.12, the change in the hydraulic dilution rate ($D_H$) with time also becomes negligible. Therefore, simplifying equation 6.15, the volumetric ethanol productivity becomes the product of pseudo steady-state hydraulic dilution rate and the ethanol concentration in the permeate stream.

## 6.4. MRB SIMULATION

The solution to the ordinary differential equations (equations 6.4 – 6.7) was implemented numerically using the 4th Order Runga-Kutta numerical model. The numerical model was programmed in Microsoft Excel 2013, with Solver used as the goal-attaining tool. The simulation program was designed to achieve a goal of minimizing the total residuals sum of squares ($RSS_{total}$) with the kinetic parameters bound by their biological relevance. The $RSS_{total}$ was normalized such the error prediction for each profile was within the same order of magnitude. The $RSS_{total}$ function used is presented below:

$$RSS_{total} = RSS_{cellmass} + RSS_{glucose} + RSS_{xylose} + RSS_{ethanol} \quad \textbf{(6.16)}$$

$$RSS_a = \sum_{n=1}^{N} \left( \frac{i_{pred} - i_{exp}}{i_{exp}^{max}} \right)^2 \quad \textbf{(6.17)}$$

where $\boldsymbol{RSS_{total}}$ is the total sum of residuals, $\boldsymbol{RSS_{cellmass}}$ is the cell mass sum of residuals, $\boldsymbol{RSS_{glucose}}$ is the glucose sum of residuals, $\boldsymbol{RSS_{xylose}}$ is the xylose sum of residuals, $\boldsymbol{RSS_{ethanol}}$ is the ethanol sum of residuals, $\boldsymbol{a}$ is the designated variable (glucose, xylose etc.), $\boldsymbol{i_{pred}}$ is the predicted value, $\boldsymbol{i_{exp}}$ is the experimental value, $\boldsymbol{i^{max}_{exp}}$ is the maximum experimental value of a required to normalize the error prediction.

### 6.4.1 CONDITIONS FOR MODEL PARAMETER SIMPLIFICATION

To ascertain the biological relevance to the predicted model parameters, some of the model parameters were constrained. The table below presents a summary of the constrained model parameters:

**Table 16:** *The simplification of the model parameters for biological significance*

| ***CONDITIONS FOR INITIAL MODEL PARAMETER SIMPLIFICATION*** | | |
|---|---|---|
| | **CONDITION** | **CONSTRAINT** |
| ***1*** | $q_{pmax\_1} < 0.51\ q_{smax\_1}$<br>$q_{pmax\_2} < 0.51\ q_{smax\_2}$ | Based on the reaction stoichiometry, the theoretical yields of ethanol from glucose and xylose are both 0.51. |
| ***2*** | $K_{ss\_1} = K_{sp\_1}$<br>$K_{ss\_2} = K_{sp\_2}$ | When the rate of substrate consumption is affected by substrate limitation, the ethanol production rate is limited in the same way |
| ***3*** | $P_{ms\_1} = P_{mp\_1}$<br>$P_{ms\_2} = P_{mp\_2}$ | Complete inhibition of the substrate consumption rate by the ethanol concentration results in no further ethanol production |
| ***4*** | $P_{is\_1} = P_{ip\_1}$<br>$P_{is\_2} = P_{ip\_2}$ | The threshold ethanol concentration for substrate consumption also begins to inhibit ethanol production in the same way |
| ***5*** | $\alpha < 1$ | The proportionality constant must be less than unity. |
| **6** | $\mu_{max\_1} < 0.5$ | The max specific growth rate on glucose is $0.5h^{-1}$ (section 2.2.4) |

### 6.4.2 SIMULATION APPROACH

The simulation algorithm approach is highlighted in *Figure 41*. The simulation was initiated by defining a system of ODEs consisting of the combination of equations 6.4-6.7 with their respective rate expressions. The overall system of ODEs is summarised below:

$$f_1(t, x, s_1, s_2, P) = \frac{dx}{dt} = \left\{\left[k_1 \frac{k_2 s_1}{k_3 + s_1} \times \left(1 - \frac{p - p_{ix_1}}{p_{mx_1} - p_{ix_1}}\right) + (1 - k_1) \frac{k_4 s_2}{k_5 + s_2} \times \left(1 - \frac{p - p_{ix_2}}{p_{mx_2} - p_{ix_2}}\right)\right] - k_6\right\} * x - \beta D_H \quad \textbf{(6.18)}$$

$$g_1(t, x, s_1) = \frac{ds_1}{dt} = D_H(sf_1 - s_1) - \left\{\left[k_1 \frac{k_7 s_1}{k_8 + s_1}\right] \times \left(1 - \frac{p - p_{is_1}}{p_{ms_1} - p_{is_1}}\right)\right\} * x \quad \textbf{(6.19)}$$

$$g_2(t, x, s_2) = \frac{ds_1}{dt} = D_H(sf_2 - s_2) - \left\{\left[(1 - k_1) \frac{k_9 s_2}{k_{10} + s_2}\right] \times \left(1 - \frac{p - p_{is_2}}{p_{ms_2} - p_{is_2}}\right)\right\} * x \quad \textbf{(6.20)}$$

$$h_1(t, x, s_1, s_2, P) = \frac{dP}{dt} = D_H(P_f - P) - \left\{\left[k_1 \frac{k_{11} s_1}{k_8 + s_1} \times \left(1 - \frac{p - p_{ip_1}}{p_{mp_1} - p_{ip_1}}\right) + (1 - \alpha) \frac{k_{12} s_2}{k_{10} + s_2} \times \left(1 - \frac{p - p_{ip_2}}{p_{mp_2} - p_{ip_2}}\right)\right]\right\} * x \quad \textbf{(6.21)}$$

In the above equations, the kinetic parameters were substituted with variable constants $k_1$-$k_{12}$. A table illustrating the substituted parameters is presented in Appendix B.

The dilution rate was described as a piece-wise function. At start-up conditions, the MRB was operated in batch mode and therefore the dilution rate was set to zero. Then, at time $t_{start\text{-}up}$, the MRB was switched to continuous operation and thereafter the dilution rate was expressed by equation 6.12.

$$D_H = 0 \qquad \textbf{for } t < t_{start\text{-}up} \qquad \textbf{(6.22)}$$

$$D_H = \frac{A_{mem}}{V_{tot}} * J_0 * t^{-b} \qquad \textbf{for } t > t_{start\text{-}up} \qquad \textbf{(6.23)}$$

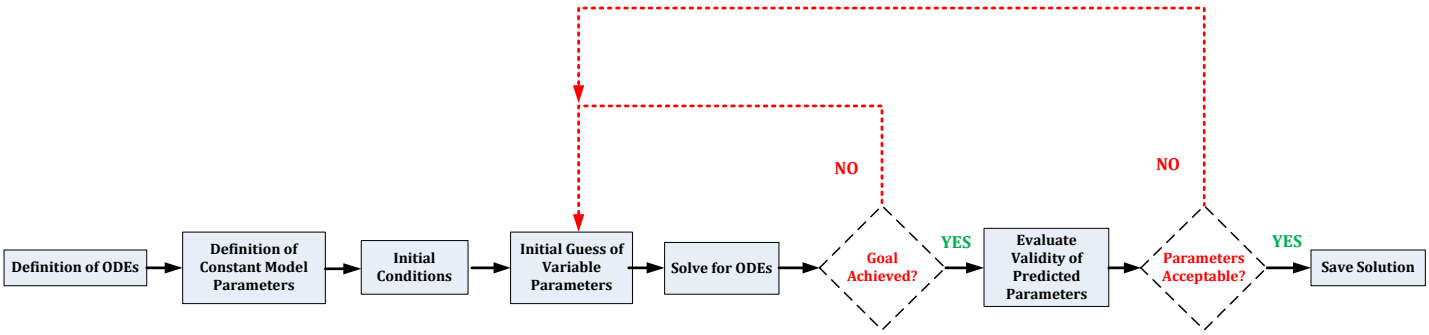


***Figure 41:*** *Simulation Approach used for solving the MBR system of ODEs*

The MRB algorithm is initiated by the definition of the system ODEs as indicated by equations 6.18-6.21. After the definition of the ODEs, the constant model parameters ($p_{ix}$, $p_{is}$, $p_{ip}$, $p_{mx}$, $p_{ms}$, $p_{mp}$, $A_{mem}$, $V_{tot}$) and the initial conditions for the ODEs were defined. The initial conditions for the ODE variables ($s_{1_0}$, $s_{2_0}$, $x_0$, $P_0$) were all measured experimentally. Initial guesses for the variable model parameters ($k_1$-$k_{12}$) were obtained from kinetic data obtained from the start-up phase or literature. Upon the solution of the ODEs, the algorithm evaluated the $RSS_{total}$ as the goal function. The algorithm was designed to change the variable model constants (within their constraints) such that the goal

function was minimized. The kinetic parameters predicted by the model were evaluated for biological relevance. Accepted kinetic parameters were subsequently stored.

### 6.4.3 Goodness of Model Fit

The goodness of model fit is the evaluation of how well the developed model predicts the behaviour of the proposed system. The adjusted correlation coefficient ($R^2_{adj}$) and the magnitude of the $RSS_{total}$ terms were used to evaluate the 'goodness' of the model prediction of the cell mass, glucose, xylose and ethanol profiles relative the experimental performance of the MRB.

The adjusted correlation coefficient eliminates bias caused by the evaluation of addition of parameters since it takes into account the random increase induced by these additional parameters. The correlation coefficient is given by the following correlation:

$$R^2_{adj} = 1 - (1 - R^2)\frac{data\ points}{datapoints - parameters - 1} \quad \textbf{(6.24)}$$

To validate the model, the proposed model was fitted to three different experimental conditions and the $R^2_{adj}$ of each experimental data set was evaluated. The three experimental conditions for model validation correspond with Experiments 5-6 in *section 5.3*.

# CHAPTER 7

# RESULTS AND DISCUSSIONS

*The results in this chapter will be discussed under the four main sections highlighted throughout this work: (1) optimization of the fermentations conditions, (2) the characterization of the microfiltration unit, (3) the quantification of the kinetics of Z. mobilis in continuous culture, (4) and process modelling. The discussion of the results was directed towards answering the relevant section key questions and consequently proving or disproving the project hypotheses.*

## 7.1 Optimization of the Fermentation Conditions

### 7.1.1 Experimental Method Validation

Prior to exploring into the optimization of the fermentation conditions, it is essential to consider the following parameters for ensuring accurate results analysis:

- ✓ Establishing whether pH control through the addition of a phosphate buffer to the fermentation medium is adequate.
- ✓ Verifying the microbial growth protocol through bench-marking the kinetic performance of the wild-type strain (*Z. mobilis* ZM4) with reported kinetic data from literature.
- ✓ Evaluate the reproducibility of the kinetic performance of the wild-type strain under the same fermentation conditions.

#### 7.1.1.1 pH Control through Phosphate Buffer Addition

As discussed in section *2.2.4.2*, organic acids such as acetate and lactate are potential fermentation by-products that may result in a reduction in the fermentation pH. In an attempt to attenuate the change in the fermentation pH in shake-flask experimental work, a phosphate buffer (consisting of a mixture of di-hydrogen ($KH_2PO_4$) and mono-hydrogen phosphates ($K_2HPO_4$)) was added to the fermentation media. However, at high buffer concentrations, potassium phosphates can become inhibitory towards the fermentation kinetics of bacteria or fungi (Bhave, 1996).Therefore, the buffer concentration that limited the change in the fermentation pH without inhibiting the fermentation kinetics was desired. The attenuation of the change in fermentation pH as a function of the buffer concentration is presented in *Figure 42* for the fermentation of 5% m/v glucose substrate by *Z. mobilis* ZM4. The data presented in this figure was obtained by removing 5mL samples from the

fermentation media and taking pH measurements of the sample at various times during the fermentation.

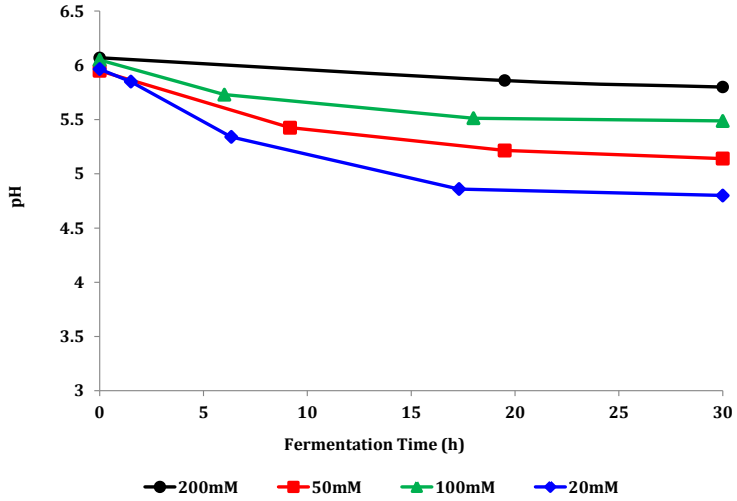


***Figure 42**: The effect of buffer addition for pH attenuation in shake-flask fermentation. **Experimental conditions:** T = 35 °C, $pH_0$ = 6, 5% (m/v) Glucose*

By inspection of *Figure 42*, it is evident that increasing the buffer concentration generally results in better buffering action and pH attenuation. At these higher buffer concentrations, there is a greater concentration of the slightly basic salt ($K_2HPO_4$). Whilst acidic metabolic by-products (organic acids) are produced during the fermentation, part of $K_2HPO_4$ is converted into the weakly acidic salt ($K_2HPO_4$) and subsequently the fermentation media resists changes to the hydrogen ion concentration (pH) (Bhave, 1996).

The effect of the higher potassium phosphate concentration on the kinetic performance of ZM4 was quantified by comparing the fermentation kinetics of the buffered media in a shake-flask relative to that of a pH controlled batch fermentation in the bioreactor. The analysis performance indicators were selected as: the cell yield ($Y_{xs}$), ethanol yield ($Y_{ps}$), and the volumetric productivity. The deviation of the these performance indicators due to the addition of the phosphate buffer relative to those obtained in a pH-controlled bioreactor is presented in *Figure 43*.

Through graphical and kinetic interpretation, it is apparent that performing the fermentation at a buffer concentration of 100mM leads to shake-flask fermentation kinetic parameters similar to those in the pH-controlled environment. At buffer concentrations lower than 100mM, the deviation of the performance indicators from the "control" was attributed to the insufficient resistance to changes in the fermentation pH. For buffer concentrations greater than 100mM, sufficient attenuation of the fermentation pH occurred. Yet, the significantly lower performance indicators suggest that the potassium phosphate concentration becomes inhibitory at these high

concentrations. Therefore, all shake-flask fermentation media were buffered at a concentration on 100mM.

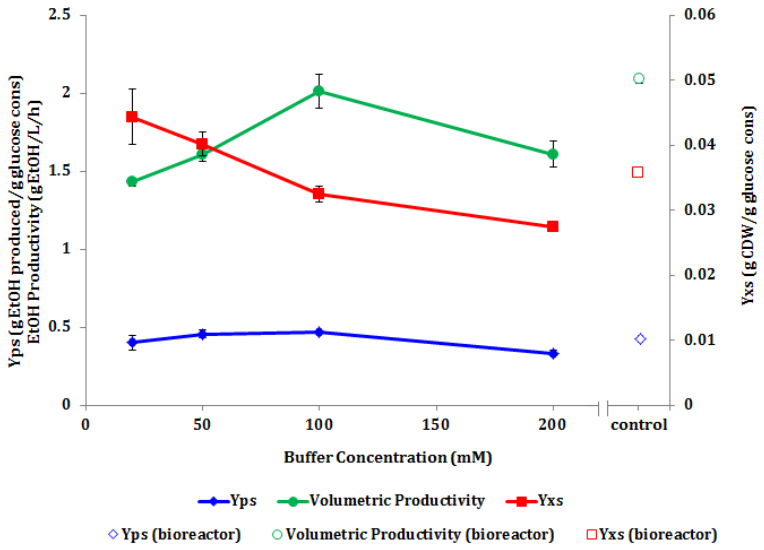


***Figure 43:*** *Kinetic quantification of the effect of the buffer concentration in shake-flask fermentation media.* ***Experimental conditions:*** *T = 35 °C, $pH_0$ = 6, 5% (m/v) Glucose.* ***Control*** *– pH-controlled in bioreactor at the same conditions*

### 7.1.1.2 BENCHMARKING EXPERIMENTAL KINETICS OF ZM4 TO LITERATURE

For the verification of the microbial growth protocol and analysis procedure, the fermentation kinetics obtained from experiments performed in a shake-flask and in an instrumented bioreactor (with pH control) in batch culture were benchmarked with those obtained in literature. The shake flask and bioreactor culture experiments were performed at an initial pH of 6 and a temperature of 30 °C. Due to the lack of literature kinetic data for *Z. mobilis* ZM4 at the aforementioned experimental conditions, the experimental results were compared to literature data executed in an instrumented bioreactor at a controlled pH of 5 and a temperature of 30 °C (Lee and Rogers, 1983).

The microbial growth and ethanol production profiles for the shake flask and bioreactor experiments can be seen in *Figure 44-A* and *Figure 44-B*. *Figure 44-C and Figure 44-D* provide kinetic analysis of the experimental fermentation data and for comparison literature data is included. Calculations for the specific rates of glucose consumption ($q_s$) and ethanol production ($q_p$) were determined in the exponential growth phase.

Benchmarking the experimental microbial growth and ethanol production profiles in the bioreactor to those reported by Lee and Rogers (1983), it is apparent that the experimental ethanol production profile closely resembles those reported in literature.

However, considering cell production, a discrepancy between the experimental and the literature reported final cell mass or more accurately the cell yield ($Y_{xs}$) was observed. At first inspection, it seems as if the lower experimental $Y_{xs}$ is a result of the literature fermentation being performed at

pH 5 instead of pH 6 units. This observation is echoed by analyzing the change in $Y_{xs}$ in *Figure 42* as the buffer concentration decreases. The low buffer concentrations correspond with a larger deviation from the initial value of 6 (*Figure 43*). For example, at a buffer concentration of 20mM, the final fermentation pH tends towards 5 units and the $Y_{xs}$ is higher than those obtained at higher concentrations were the pH tends towards a value of 6 units. Moreover, because of the lower $Y_{xs}$, the specific rates of glucose and xylose consumption were higher at pH 6 relative to those reported in literature.

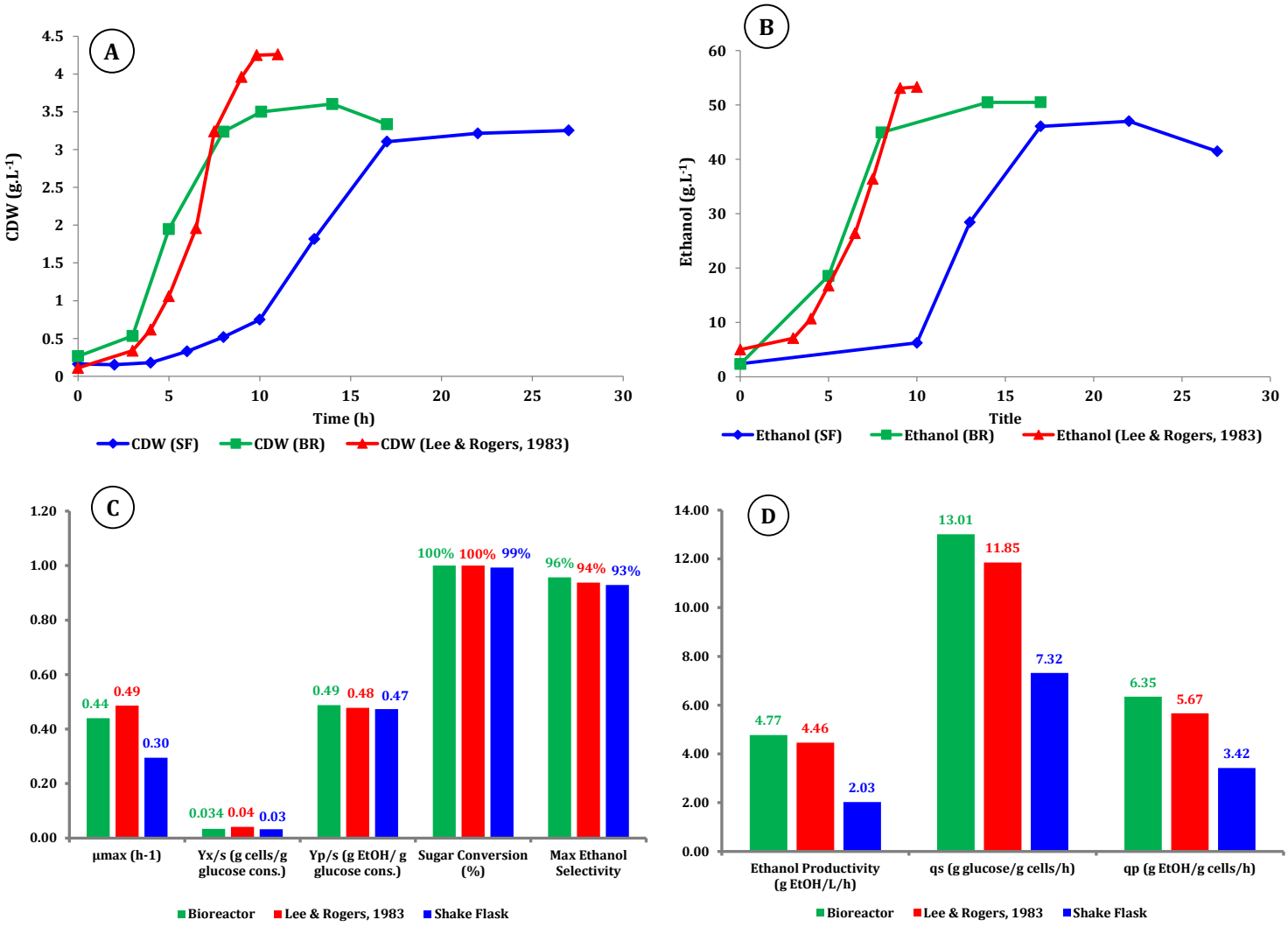


***Figure 44:*** *Benchmarking the experimental fermentation kinetics to literature data.* ***A****- Microbial growth profile,* ***B*** *– Ethanol Production Profile,* ***C****- Kinetic parameters,* ***D*** *– ethanol productivity and specific rates of substrate consumption ($q_s$) and ethanol production ($q_p$).* ***BR*** *– bioreactor,* ***SF*** *– Shake Flask*

Shake-flask fermentations were characterized by an extended lag-phase, lower overall volumetric productivity and lower specific rates of glucose consumption and ethanol production relative to bioreactor culture. The lower productivity and specific fermentation rates in the shake flask were attributed to non-ideal conditions of mixing within the shake-flask and subsequently leading to a longer adaptation period. However, the cell and product yields obtained from the shake-flask and

bioreactor culture experiments were essentially the same. Therefore, whilst shake-flask experiments require extended adaptation periods, the final product and cell yield are independent of whether the fermentation was performed in a shake-flask or in an instrumented bioreactor.

#### 7.1.1.3 *EXPERIMENT REPRODUCIBILITY*

In a bid to quantify the reproducibility shake-flask experiments, an error analysis was performed on experimental duplicates (each experiment performed twice). Three experimental conditions were evaluated for reproducibility and their respective experimental conditions are presented below:

***Table 17:*** *Experimental conditions used for evaluating reproducibility*

| Experiment No. | Biocatalyst | Initial Substrate Conc. ($g.L^{-1}$) | | Temperature (°C) | $pH_0$ |
|---|---|---|---|---|---|
| | | Glucose | Xylose | | |
| ***Experiment 1*** | ZM4 | 50 | 0 | 30 | 6 |
| ***Experiment 2*** | ZM4 | 50 | 0 | 35 | 7 |
| ***Experiment 3*** | 8b | 13 | 37 | 33.5 | 7 |

The reproducibility was evaluated by comparing the variance in $Y_{xs}$, $Y_{ps}$, $\mu_{max}$, and the volumetric productivity from the mean of the duplicate experiments and expressed as percentage reproducibility. The percentage reproducibility was calculated as follows:

$$\%\ Reproducibility_i = \left(1 - \frac{standard\ deviation_i}{mean_i}\right) * 100 \qquad \textbf{(7.1)}$$

Based on equation 7-1, a percentage reproducibility of 100% indicates perfect reproducibility. Contrary, a percentage reproducibility of 0% would indicate no reproducibility. The reproducibility results are presented in *Figure 45*. The error bars indicate the standard deviation from triplicate experiments all performed at the same conditions. According to *Figure 45*-D, it is apparent that the shake flask experiments indicate very good reproducibility as the percent reproducibility of most of the fermentation kinetic parameters were greater than 95%. Experimental error in the shake-flask experiments may have originated from the variance in the conditions surrounding the experiments, the implementation of the experimental protocol, and the execution of analytical techniques. Therefore, the slight differences in the percentage reproducibility can be attributed to either instrument precision or systematic error during sampling and/or handling of the experiment samples.

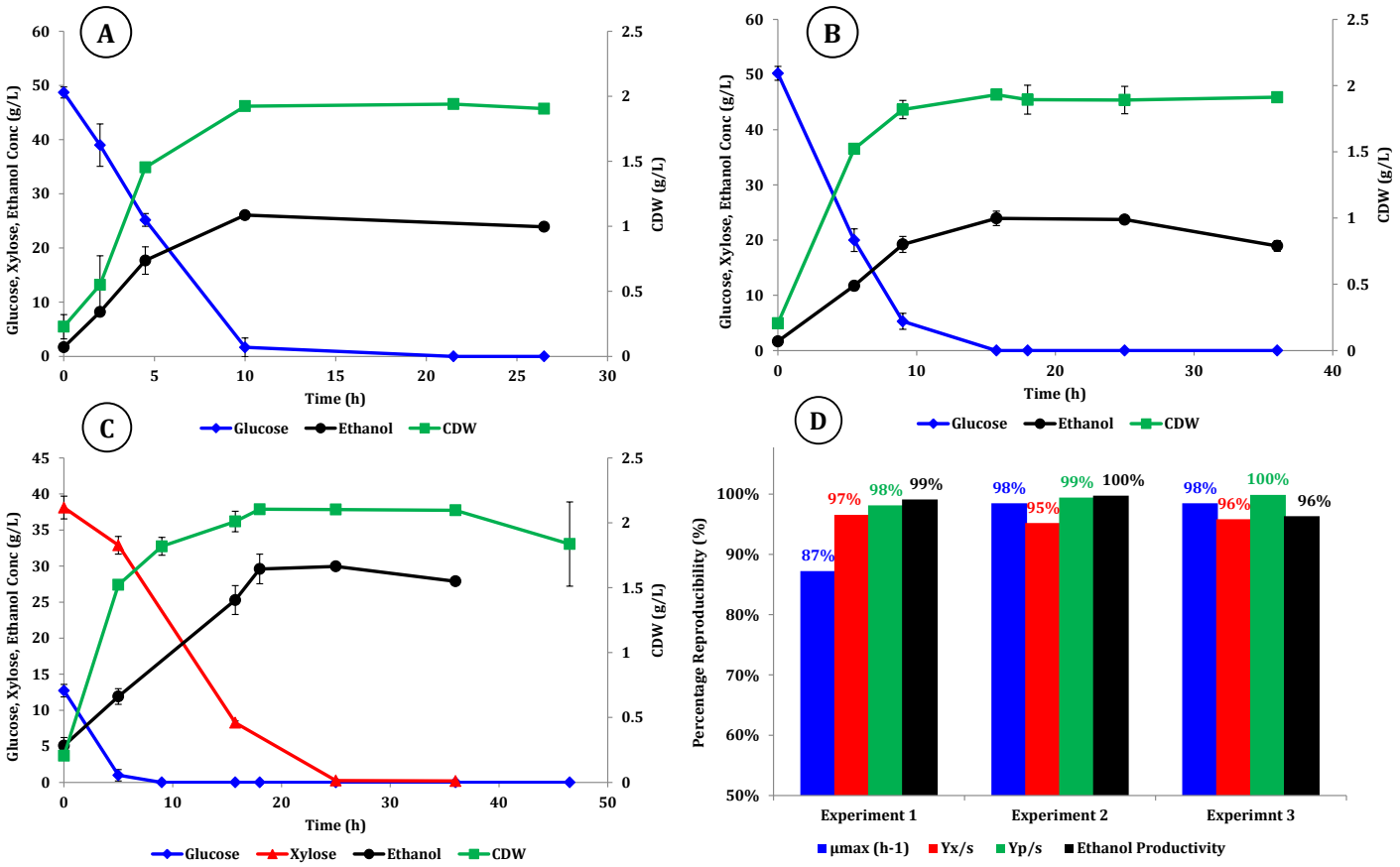


***Figure 45: A – Experiment 1****-Glucose, CDW and Ethanol concentration profiles during shake-flask fermentation.* ***B – Experiment 2*** *- Glucose, CDW and Ethanol concentration profiles during shake-flask fermentation.* ***C – Experiment 3*** *- Glucose, Xylose, CDW and Ethanol concentration profiles during shake-flask fermentation* ***D -*** *Percentage repeatability of fermentation kinetics at shake-flask level.*

## 7.1.2 Optimization of the Fermentation Temperature and Initial pH

### 7.1.2.1 Glucose Fermentation by *Z. mobilis* ZM4

Most of the glucose fermentations by *Z. mobilis* ZM4 in literature have been performed at a temperature of 30 °C, and a controlled pH of 5.5. In this work, a statistical approach was used to optimize the fermentation temperature and initial pH ($pH_0$) in shake-flask fermentation (*section 5.3.1.1* for experimental design). The experimental results from the statistical full factorial design are summarized in *Table 18*. The glucose, CDW, and ethanol concentration profiles for each experiment and an overall summary of the full factorial data are presented in Appendix C1.1.

The quantification of the effect of the fermentation temperature and $pH_0$ were performed under sugar-limited conditions to eliminate the effect of ethanol and substrate inhibition on the observed kinetics. In most experiments, the deviation of the fermentation pH from the initial value was less

than 0.5 units. Therefore, reference to a $pH_0$ represents a pH range within 0.5 units from the initial buffered value.

#### 7.1.2.1.1 Effect of the Fermentation Temperature and $pH_0$ on $Y_{ps}$ and Ethanol Productivity

According to the experimental data presented in *Table 18*, the highest $Y_{ps}$ and volumetric productivity (VP) were 98% and 2.439 $g.L^{-1}.h^{-1}$ respectively and were achieved at $pH_0$ 6 and 30 °C. Contrary, the lowest values for the two response factors were 68% and 0.626 $g.L^{-1}.h^{-1}$ respectively and were obtained at $pH_0$ 8 and 40 °C. In general, decreasing $pH_0$ and decreasing temperature had a positive effect on the $Y_{ps}$ and VP.

**Table 18:** *Ethanol Productivity and yields obtained from shake-flask cultures of Z. mobilis ZM4 as determined by a 3-level 2-factor factorial design*

| Glucose fermentation: $3^2$ Full Factorial Design | | | | |
|---|---|---|---|---|
| **Experiment No.** | ***Temperature (°C)*** | ***$pH_0$*** | ***$Y_{ps}$ (% Theo. EtOH Yield )*** | ***Volumetric Productivity ($g.EtOH.L^{-1}.h^{-1}$)*** |
| ***10 (C)*** | 35 | 7 | 89% | 1.815 |
| ***5 (C)*** | 35 | 7 | 88% | 1.628 |
| ***1*** | 30 | 6 | 98% | 2.439 |
| ***11 (C)*** | 35 | 7 | 87% | 1.623 |
| ***8*** | 40 | 7 | 76% | 1.255 |
| ***9*** | 40 | 8 | 68% | 0.626 |
| ***2*** | 30 | 7 | 98% | 2.048 |
| ***6*** | 35 | 8 | 80% | 1.246 |
| ***7*** | 40 | 6 | 82% | 1.339 |
| ***4*** | 35 | 6 | 93% | 2.015 |
| ***3*** | 30 | 8 | 94% | 1.298 |

The statistical significance of the fermentation temperature, $pH_0$ (process variables) and their interaction towards $Y_{ps}$ and the VP (response variables) was determined by fitting quadratic models to the experimental data and subsequently performing an ANOVA analysis on the fitted quadratic models. The unrefined quadratic models, which were expressed in terms of their uncoded process variables (actual values), consist of linear, quadratic and interaction terms (and coefficients). In general the sign of the regression coefficient defined whether the contribution of the model term was synergistic (positive effect) or antagonistic (negative effect).

The ensuing ANOVA analysis identified all the factors that affect both $Y_{ps}$ and VP with a certainty greater than 95% by analyzing the p-value of each model term. The ANOVA analysis for the unrefined response models is shown in Appendix C1.1.

A summary of the ANOVA analysis in the form of a Pareto chart and a surface plot representing the change in the response variables as a function of the independent process variables are presented in *Figure 46* below.

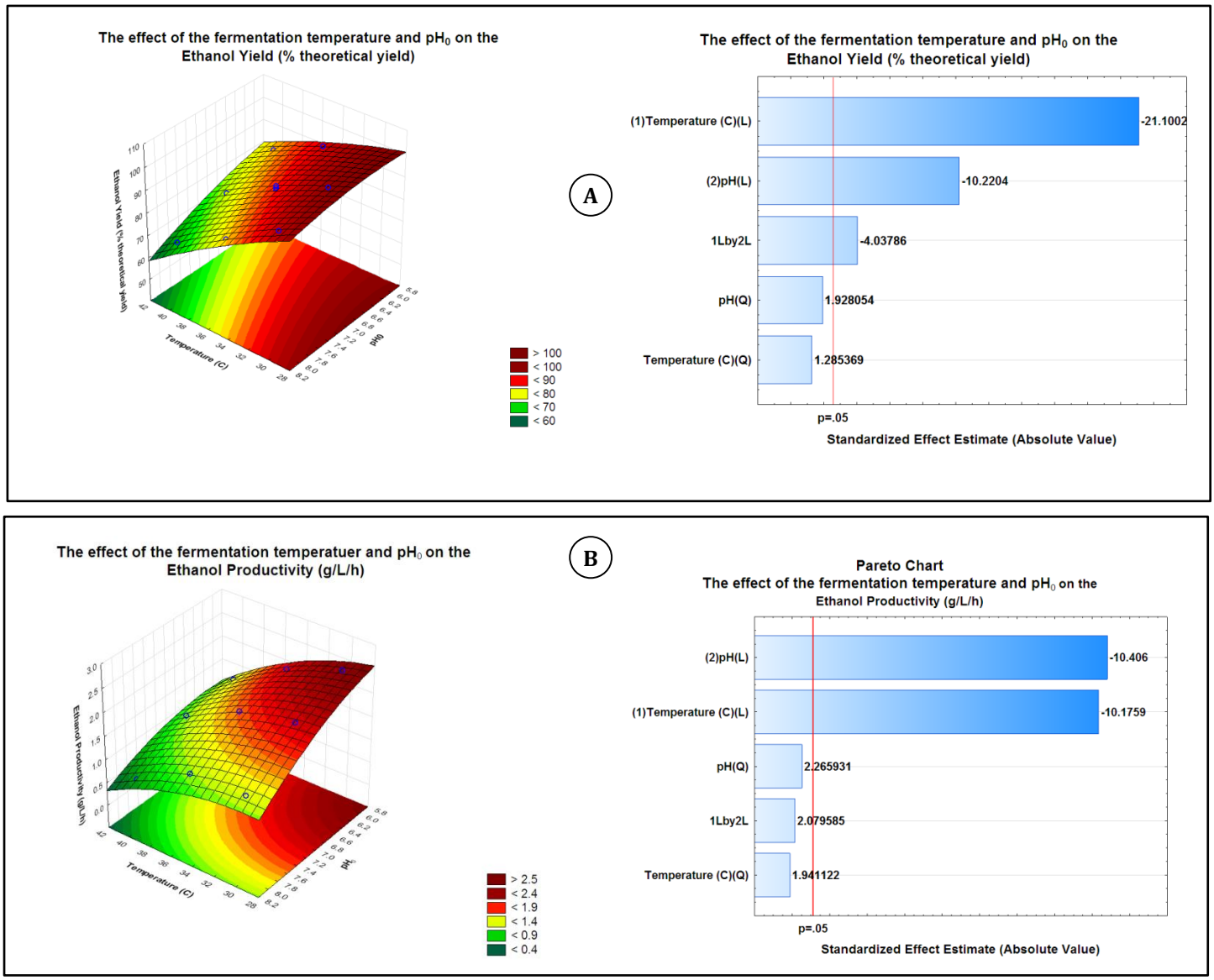


***Figure 46:*** *The surface plots and result of the ANOVA analysis for the effect of the fermentation temperature and $pH_0$ on glucose fermentation.* ***A -*** *Ethanol Yield (top);* ***B-*** *Volumetric Productivity (below). Pareto Chart Key:* ***(L)*** *– main effects,* ***(Q)*** *quadratic effects,* ***(1L by 2L)*** *– interaction effects*

Model terms with a significant contribution to the predicted response were quantified by a p-value smaller than 0.05. Using back-elimination, the two model predicted responses (VP and $Y_{ps}$) were refined such that only model terms that had a significant contribution for the predicted response were present (only parameters with p<<0.05). However, backward elimination was performed in such a way that the integrity of the model hierarchy was retained. The refined model equations and the order/degree of significance of each model term are summarized in *Table 19*.

***Table 19:*** *Refined response models and corresponding parameters for test of adequacy*

| Response Factor | Refined equation | Degree of significance (descending order) | $R^2_{adj}$ |
|---|---|---|---|
| **Ethanol Yield (% theoretical yield)** | $Y_1 = -10.633 + 1.37x_1 + 37.07x_2 - 1.767x_2^2 - 0.5x_1x_2$ | $x_1^{\Psi}$, $x_2^{\dagger}$, $x_1x_2$, $x_2^2$, | 0.96 |
| **Volumetric Productivity (g EtOH/L/h)** | $Y_2 = -0.31 + 0.86x_1 + 0.12x_2 - 0.15x_2^2$ | $x_2$, $x_1$, $x_2^2$ | 0.92 |
| **Ψ** | $x_1$ represents the fermentation temperature | | |
| **†** | $x_2$ represents the initial fermentation pH | | |

The adjusted $R^2$ values for both refined models were 0.96 and 0.92 respectively. The high magnitude of the $R_{adj}$ values indicated a high degree of model fit to the experimental data. Validation of the assumptions made during the development of the mathematical model is presented in Appendix C1.2.

By inspecting the predicted surface plots in *Figure 46*, it can be seen that both the $Y_{ps}$ and the VP increase with a decreasing fermentation temperature. Similarly, a reduction in the $pH_0$ had a positive effect on both response variables. From the Pareto chart of the standardized effects of the model parameters on $Y_{ps}$, it can be seen that the fermentation temperature, $pH_0$ and the temperature-$pH_0$ interaction are statistically significant towards the product yield. Likewise, the Pareto chart of the standardized effects of the model parameters on VP revealed that the VP was more sensitive to the fermentation temperature and $pH_0$. However, the temperature-$pH_0$ interaction was statistically insignificant within a 95% confidence interval. Due to the absence of statistical analysis of the effect of temperature and $pH_0$ on $Y_{ps}$ and VP by *Z. mobilis* ZM4 in literature, the observed statistical results could not be benchmarked. However, the general trends predicted by the quadratic models were compared to those observed in literature.

The increase in $Y_{ps}$ with a decrease in the fermentation temperature was consistent with literature findings in that the production of fermentation by-products by the *Z. mobilis* ZM4 become more pronounced at higher fermentation temperatures. The distribution of the by-products formed at various process conditions will be discussed later in *section 7.1.2.1.3*.

The reduction in the overall volumetric productivity with an increase in the fermentation temperature was attributed to the lower final ethanol concentration, longer adaptation periods and significant loss in cell viability at elevated fermentation temperatures. Moreover, the decline in $Y_{xs}$ with an increase in the fermentation temperature (not shown, see Appendix C1.1) indicated some extent of uncoupling of the growth and catabolism mechanisms during high temperature fermentation (Chen and Huang, 1987; Lawford, 1988; Rogers *et al.,* 1981). Rogers et al., (1981) reported similar results where it was found that catabolism and growth were closely coupled up to 33 °C but at higher temperatures (33-39 °C) decreasing biomass yields were found.

The increase in $Y_{ps}$ and VP with a decrease in the initial fermentation pH suggests that fermentations performed at higher pHs negatively affect growth and ethanol production. Although the exact effect of the high fermentation pH on the metabolism of *Z. mobilis* is unclear, generalized concepts were used to explain the observed decline in the microbial performance at these conditions.

Unfavourable fermentation pHs affect the ionic states of the media components, the solubility of proteins in the cell wall, the activity and stability of intracellular enzymes and induce undesirable intracellular-extracellular pH gradients (Nielsen *et al.,* 2003). As a result, the activity of enzymes in the cytoplasmic wall or those associated with the conversion of glucose-to-ethanol through the Entner-Doudoroff pathway may well be negatively impacted by indirect effects of undesirable fermentation pHs (Bhave, 1996). Moreover, some microbial cells have the ability to maintain constant intracellular pH levels even in the presence of large pH gradients. However, the maintenance of the intracellular pH often comes at the expense of significant substrate utilization for cell maintenance demands (Nielsen *et al.,* 2003).

Considering the both surface plots of the $Y_{ps}$ and VP as functions of the fermentation temperature and $pH_0$, it is not clear whether performing the fermentation at lower temperature or pH may result in an increase in both responses. However, it has been shown in literature when the fermentation is performed at temperatures lower than 30 $^{o}$C, the specific glucose uptake rate ($q_s$) and the specific ethanol production rate ($q_p$) are approximately two-fold lower than fermentations performed at temperatures greater than or equal to 30 $^{o}$C (Rogers *et al.,* 1981). Therefore, whilst fermentations at these lower temperatures were not performed in this work, it is assumed that the volumetric productivity under these fermentation conditions would be lower than those performed in the recommended temperature range.

#### 7.1.2.1.2 MULTIPLE-RESPONSE OPTIMIZATION

One of the most widely-used approaches for the optimization of multiple responses is the simultaneous optimization technique, i.e. desirability function approach (Derringer and Suich, 1980). In this approach, each response is transformed into an individual desirability function that varies over the range 0 to 1. Undesired responses are typically reflected by desirability values approaching 0 whilst those approaching ideal intervals attain desirability values towards of 1 (Fitrianto and Midi, 2011; Grahovac *et al.,* 2012). The overall desirability of all process responses is computed from the geometric mean of all the individual desirability functions (Fitrianto and Midi, 2011). The overall desirability characterizes the proximity of the response to its ideal value and usually lies between 0 and 1. In this work, a desirability function approach was used as the multiple response optimization tool for attaining a single combination of the temperature and pH that resulted in the optimum $Y_{ps}$ and VP for glucose fermentation by *Z. mobilis* ZM4 within the experimental range.

Since ethanol is a low-value high-volume product, greater emphasis was placed on the volumetric productivity than the ethanol yield. Therefore, a linear desirability function for the ethanol productivity was set up with the desirability value of zero selected for ethanol productivities below

1.533 g EtOH.$L^{-1}$.$h^{-1}$ and the maximum attainable volumetric productivity with a value of one. Considering the desirability function for $Y_{ps}$, a linear function was selected by setting a desirability value of zero for the experimental conditions that resulted in lowest $Y_{ps}$ and a value one for the conditions that produce the highest $Y_{ps}$. A surface plot and contour plot of the overall desirability of the VP and $Y_{ps}$ as a function of the fermentation conditions is presented in *Figure 47* (left and right respectively). The definition of the desirability functions and profiles is presented in Appendix C.1.3.

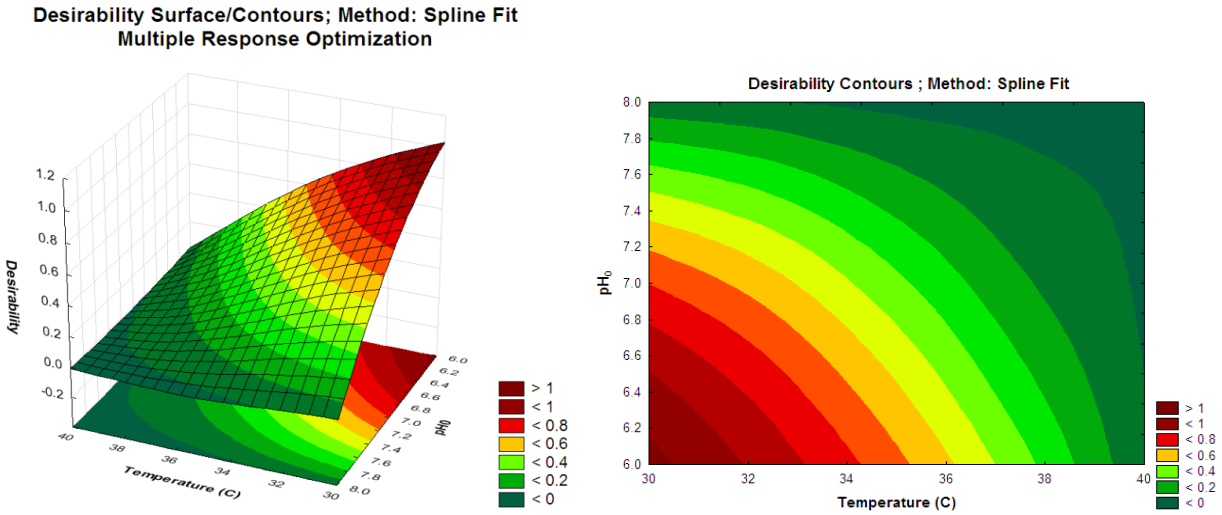


***Figure 47:*** *Multiple Response Optimization desirability for glucose fermentation. Surface Plot (left) and Contour plot (right)*

Based on the desirability optimization analysis, the optimum fermentation conditions for glucose-limited fermentation by *Z. mobilis* ZM4 are at 30 °C and $pH_0$ 6-5.5. Unsurprisingly, these optimum fermentation conditions are relatively close to the default fermentation conditions of 30 °C and pH 6 that are predominantly used in literature. However, the optimum conditions obtained here are only valid for the temperature and $pH_0$ range investigated. The optimized model suggests that fermentations performed at lower temperature and $pH_0$'s may possibly result in higher desirability. Therefore, future work should be done to investigate the fermentation kinetics at the lower temperatures and $pH_0$'s, not only to confirm that the statistically optimized conditions are indeed the best operating conditions, but to ascertain that lower temperature fermentations do indeed affect the specific rate of glucose consumption and specific rate of ethanol production.

Nonetheless, mathematical and graphical representation of the variation in the key performance indicators ($Y_{ps}$ and VP) with changing temperature and $pH_0$ presented here have significant implication for hexose fermentation systems, especially SSF processes. For example, consider a case whereby a SSF fermentation is performed with *Z. mobilis* ZM4 as the fermenting ethanologic biocatalyst. Since the optimum operating temperature and pH for the hydrolysis enzymes are expected to differ to that of ZM4, the deviation of the biological performance of ZM4 due to the SSF being performed at sub-optimal conditions can be predicted using the models established using the statistical approach. For example, SSF temperatures over 40 °C and pHs lower that 4.8 are required to facilitate an increase in the rate of cellulose hydrolysis (Mohagheghi *et al.,* 2004). This work has

illustrated that ZM4 performs better at lower temperatures and near neutral pHs. In effect, at temperatures higher than 35 $^{o}$C, the performance of this ethanologic biocatalyst decreases significantly.

#### 7.1.2.1.3 QUANTIFICATION OF BY-PRODUCT FORMATION BY CARBON BALANCE

Literature highlights that the major by-products during glucose fermentation by *Z. mobilis* are acetaldehyde, lactate, succinic acid, $CO_2$, glycerol and acetate. In this work, the major by-products produced during the fermentation were glycerol and acetate with their respective concentrations dependent on the fermentation conditions (*Figure 48*). *Table 20* presents a carbon balance calculation based on the initial sugar content and the residual soluble fermentation sugars and products that was used to quantify the carbon recovery from the shake-flask fermentation experimental runs[1]. The carbon recovery calculation was used as a tool for ensuring that the major fermentation products have been identified and for the confirmation that the concentration of the minor products such as lactate, xylitol and succinic acid were present in trace amounts.

The carbon balance analysis revealed that the carbon recovery at four different experimental conditions was between 96% and 99%. More importantly, the carbon recovery validated that the main fermentation by-products were indeed $CO_2$, acetate and glycerol. Through the inspection of the conditions at B and C (same $pH_0$), the effect of the fermentation temperature on the concentration of acetate and glycerol formed can be quantified. It is apparent that a 5% and 6% increase in acetate and glycerol concentrations was achieved by increasing the fermentation temperature from 35 $^{o}$C to 40 $^{o}$C. Literature reports that acetate inhibits/hinders the activity and the productivity of *Z. mobilis* for both glucose and xylose fermentation (Rogers *et al.,* 2000). Therefore, the reduction in the volumetric productivity with an increase in the fermentation temperature may well be caused or aggravated by the formation of acetate.

Similarly, by comparing the conditions at C and D (same temperature), acetate and glycerol concentrations increased approximately 3% and 16% respectively as the fermentation $pH_0$ was increased from 7 to 8. As a result, the observed increase in the amount of acetate produced in response to the increase in $pH_0$ suggests that the observed decrease in the volumetric productivity can be partially attributed to the higher degree of formation of the inhibitory compound (acetate) at fermentation conditions of high temperature and $pH_0$s. Moreover, the results of this analysis agree with the model predictions presented in *Figure 46*.

[1] The amount of carbon dioxide formed was calculated based on reaction stoichiometry using the actual concentration of ethanol formed. For glucose fermentation the amount of CO2 formed was calculated as follows: $C_{EtOH} * MW_{CO_2}/MW_{EtOH,}$ where $MW_i$ is the molecular weight of species i.

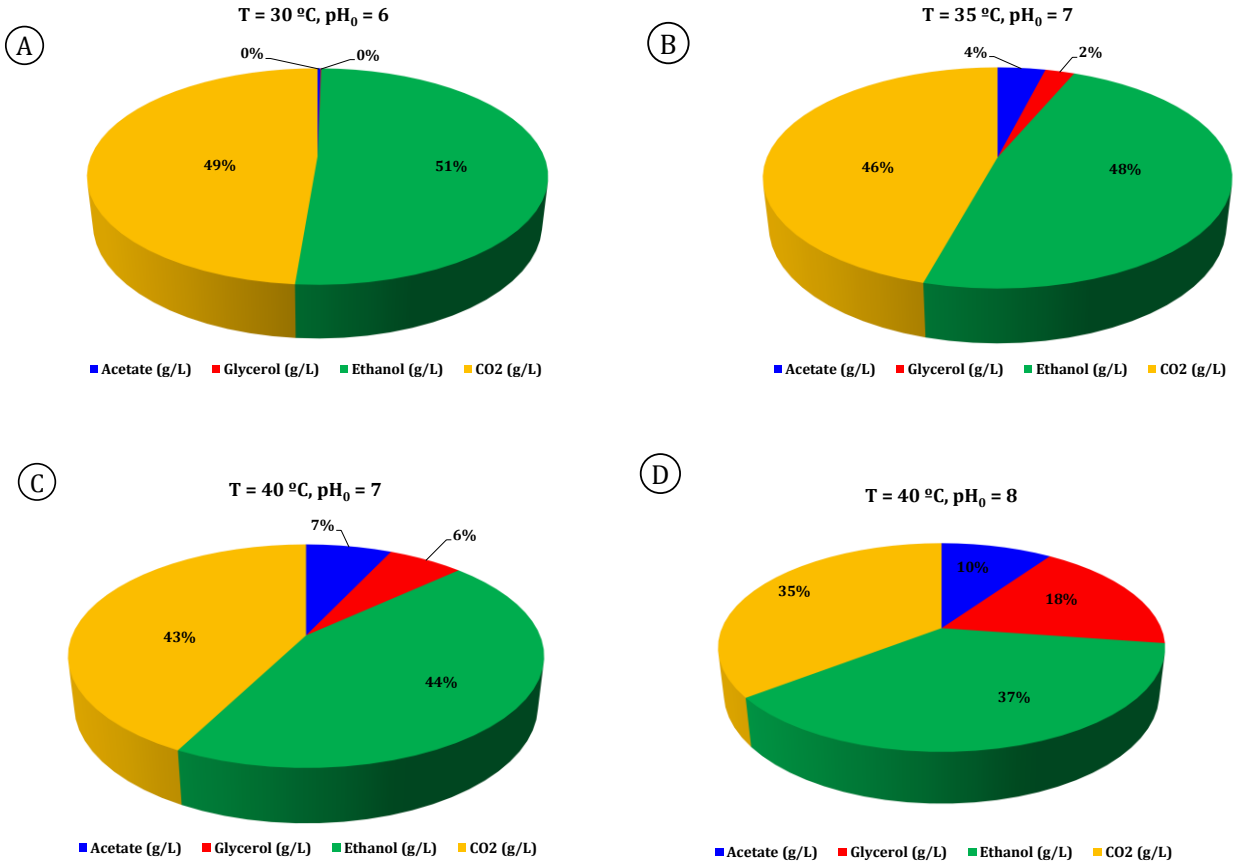


***Figure 48:*** *By-product evolution as a function of the fermentation conditions.*
***A** – 30 °C, $pH_0$ 6; **B** - 35 °C, $pH_0$ 7; **C** - 40 °C, $pH_0$ 7; **D** - 40 °C, $pH_0$ 8;*

***Table 20:*** *Carbon Balance for glucose fermentation by Z. mobilis ZM4 at various process conditions*

| Component(g.L$^{-1}$) | T = 30 °C, $pH_0$ = 6 | T = 35 °C $pH_0$ = 7 | T = 40 °C $pH_0$ = 7 | T = 40 °C $pH_0$ = 8 |
|---|---|---|---|---|
| | | ***Carbon in*** | | |
| ***Glucose*** | 49.71 | 51.35 | 53.13 | 51.82 |
| ***Xylose*** | - | - | - | - |
| ***Acetate*** | ~0 | ~0 | ~0 | ~0 |
| ***Glycerol*** | ~0 | ~0 | ~0 | 0.02 |
| ***Ethanol*** | 1.69 | 1.21 | 0.01 | 1.04 |
| ***Total Carbon in*** | 51.39 | 52.56 | 53.14 | 52.86 |
| | | ***Carbon out*** | | |
| ***Glucose*** | 0.00 | 0.00 | 0.00 | 0.00 |
| ***Xylose*** | - | - | - | - |
| ***Cell Mass***‡ | 0.03 | 0.030 | 0.01 | 0.01 |
| ***Acetate*** | 0.12 | 2.02 | 3.55 | 4.86 |
| ***Glycerol*** | 0.03 | 1.24 | 3.13 | 8.93 |
| ***Ethanol*** | 25.98 | 24.51 | 22.61 | 18.77 |
| ***$CO_2$*** | 24.81 | 23.41 | 21.59 | 17.92 |
| ***Total Carbon out*** | 50.98 | 51.21 | 50.89 | 50.49 |
| ***Carbon Recovery*** | **99%** | **97%** | **96%** | **96%** |

‡ The carbon attributed to cell mass production was based on an assumed carbon content of 44% of the CDW (Zhang *et al.,* 2009). The cell weight carbon contribution was calculated as follows: $m_{CDW} = Y_{xs}(CDW_{stationary} - CDW_{inoculum})*0.44$

### 7.1.2.2 *XYLOSE-RICH SUBSTRATE FERMENTATION BY Z. MOBILIS 8B*

The quantification of the effect of the fermentation temperature and $pH_0$ was performed on *Z. mobilis* 8b to identify the conditions whereby VP, $Y_{ps}$ and the overall rate of xylose consumption ($Q_{s\_xylose}$) were optimized. The effect of the fermentation temperature and $pH_0$ on the co-fermentation of a fixed sugar concentration (37g.$L^{-1}$ xylose and 13g.$L^{-1}$ glucose) by *Z. mobilis* 8b was studied using a 3-level 2-factor ($3^2$) full-factorial design. The ranges of the factorial points were defined in *section 5.3.1.1*. Two duplicate center point runs (T = 30 °C, $pH_0$ = 7)were added to the statistical design to increase the statistical inference of the quadratic model and to allow the model to make an unbiased estimate of the pure error term (Lawson and Erjavec, 2001).

#### 7.1.2.2.1 *EFFECT OF THE FERMENTATION TEMPERATURE AND $pH_0$ ON VP, $Y_{PS}$ AND $Q_{S\_XYLOSE}$*

The experimental results from this experiment are summarized in Table 21 and *Figure 49* below. Generally, as temperature and $pH_0$ increased from 30 °C to 37 °C and 6 to 8 respectively, all three performance indicators ($Y_{ps}$, VP and the overall rate of xylose consumption) initially increased, attained an optimum, and decreased again. Based on the experimental results, it is apparent that all three process indicators were highest at 33.5 °C and $pH_0$ 7. The lowest values in the factorial range were attained at 37 °C and pH 8.

**Table 21:** *Ethanol Productivity, ethanol yields and the overall rate of xylose consumption obtained from shake-flask cultures of Z. mobilis 8b as determined by a 3-level 2-factor factorial design*

| GLUCOSE: XYLOSE FERMENTATION: $3^2$ FULL FACTORIAL DESIGN | | | | | |
|---|---|---|---|---|---|
| **Experiment No.** | ***Process Variable*** | | ***Performance Indicators (Response variables)*** | | |
| | ***Temperature (°C)*** | ***$pH_0$*** | ***$Q_{s\_xylose}$ (g xylose cons.$L^{-1}$.$h^{-1}$)‡*** | ***% Theoretical Ethanol Yield*** | ***Volumetric Productivity (g EtOH.$L^{-1}$.$h^{-1}$)*** |
| **7** | 37 | 6 | 0.88 | 88 | 0.67 |
| **4** | 33.5 | 6 | 1.36 | 94 | 0.89 |
| **11(C)** | **33.5** | **7** | **1.44** | **94** | **0.96** |
| **6** | 33.5 | 8 | 0.76 | 69 | 0.7 |
| **8** | 37 | 7 | 0.7 | 82 | 0.55 |
| **1** | 30 | 6 | 1.24 | 93 | 0.78 |
| **10 (C)** | **33.5** | **7** | **1.47** | **95** | **0.97** |
| **5 (C)** | **33.5** | **7** | **1.44** | **95** | **1.02** |
| **3** | 30 | 8 | 0.77 | 77 | 0.41 |
| **2** | 30 | 7 | 1.09 | 90 | 0.66 |
| **9** | 37 | 8 | 0.12 | 66 | 0.13 |

‡ The overall rate of xylose consumption was calculated by the dividing the total amount of xylose consumed by the time taken when

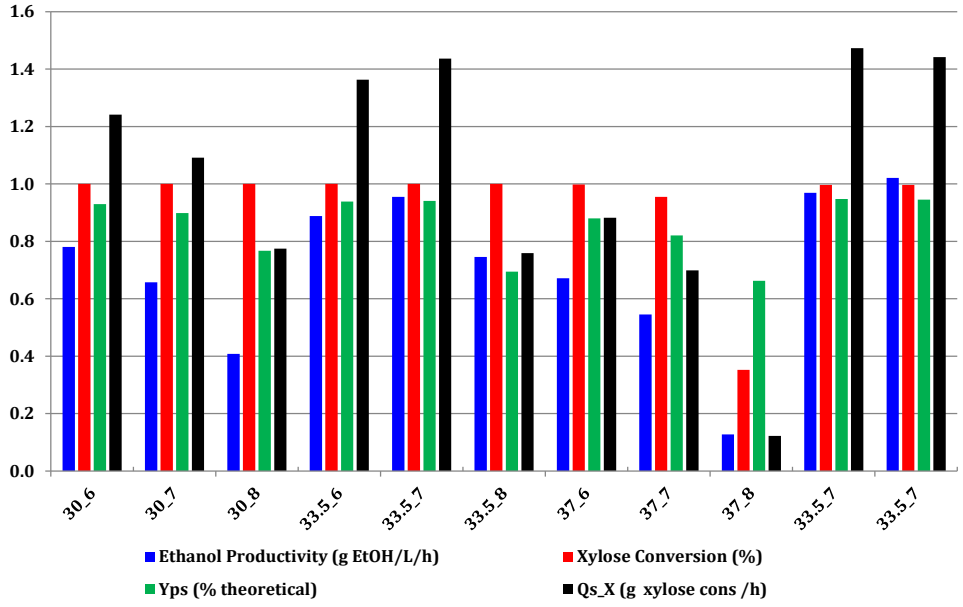


***Figure 49:*** *Effect of temperature on the ethanol yield ($Y_{ps}$), xylose conversion, ethanol productivity, and the overall rate of xylose consumption*

Similar to the quantification of the effect of temperature and $pH_0$ on glucose fermentation, the statistical significance of the temperature, $pH_0$ and their interaction towards response variables was determined by fitting quadratic models to the experimental data and subsequently performing an ANOVA analysis on the fitted quadratic models. The ANOVA analysis identified all the factors that affect both $Y_{ps}$, VP and $Q_{s\_xylose}$ with a certainty greater than 95%.

Using backward elimination, the three response models ($Y_1$, $Y_2$, $Y_3$) were refined such that only the model terms that had a significant contribution to the predicted response were present ($p<<0.05$). The refined model equations and the order/degree of significance of each model term are summarised in *Table 22*.

***Table 22:*** *Refined response models and corresponding parameters for test of adequacy*

| Response Factor | Refined equation | Degree of significance (descending order) | $R^2_{adj}$ |
|---|---|---|---|
| **Ethanol Yield (% theoretical yield)** | $Y_1 = -630.0 + 22.75x_1 - 0.36x_1^2 + 113.66x_2 - 8.86x_2^2$ | $x_2$, $x_2^2$, $x_1$,$x_1^2$ | 0.91 |
| **Volumetric Productivity (g EtOH/L/h)** | $Y_2 = -34.86 + 1.82x_1 - 0.0274x_1^2 + 1.86x_2 - 0.146x_2^2$ | $x_1^2$, $x_2$, $x_2^2$, $x_1$ | 0.91 |
| **Overall rate of xylose consumption (g xylose/L/h)** | $Y_3 = -45.87 + 2.26x_1 - 0.0347x_1^2 + 3.33x_2 - 0.26x_2^2$ | $x_2$, $x_1^2$, $x_1$, $x_2^2$ | 0.94 |

The adjusted $R^2$ values for the three models were 0.91, 0.91 and 0.94 respectively. The high magnitude of the $R_{adj}$ values indicated a high degree of model fit to the experimental data. Validation of the assumptions made during the development of the mathematical model along with a complete summary of the standardized effects is presented in Appendix C2.2.

A summary of the ANOVA analysis in the form of a Pareto chart and a graphical representation of the change in the response variables as a function of the independent process variables is presented in *Figure 50* below.

Considering $Y_{ps}$, the statistical analysis of the refined model revealed that the linear (main) and quadratic effects of $pH_0$ and temperature are statistically significant within a 95% confidence interval. The main effects define the significance of the process variable and the quadratic effects describe whether the response profile has curvature (a maximum or minimum). The positive sign of the linear term indicates that the ethanol yield is affected in a synergistic manner. Conversely, the ethanol yield was affected in an antagonistic manner by the quadratic terms of both temperature and $pH_0$, as indicated by negative sign of the quadratic terms. The relative sensitivity of $Y_{ps}$ to temperature and $pH_0$ is highlighted by the magnitude of the standardized effects in the Pareto chart. For example, since the main effect of $pH_0$ has the largest standardized effect, this indicates that strict pH control is required for maximizing $Y_{ps}$. Moreover, the large magnitude of the quadratic effect signifies $Y_{ps}$ has a high degree of curvature due a change in $pH_0$. This can be visualized graphically by the sharp decrease in $Y_{ps}$ as the $pH_0$ increases beyond a value of 7 in the surface plot. Similarly, the significance of the quadratic temperature term can be visually inspected by the significant decline of the ethanol yield at fermentation temperatures greater than 35°C. In addition, the temperature and $pH_0$ interaction was found to be statistically insignificant, as evidenced by the absence of the interaction term ($x_1x_2$) in the final refined model. A similar approach can be taken in analyzing the Pareto and surface plots of VP and $Q_{sxylose}$.

Comparing the operating conditions obtained in this study with work published in literature is challenging since the effect of temperature and pH have not been quantified for xylose-rich substrates. The surface plots obtained for the fermentation of a xylose-rich substrate in this work suggest that $Y_{ps}$, VP and $Q_{s\_xylose}$ are highest at 33.5 °C and $pH_0$ 6-7. Most of the fermentations reported in literature have been performed at 30 °C and pH 5-6 (controlled). However, most of these fermentations have been performed at a 1:1 glucose- xylose ratio that is not representative of the sugar distribution obtained from lignocellulose hydrolyzates. Hence, the results obtained in this work suggest that the fermentation conditions strongly dependent on the ratio of the fermentable sugars in the fermentation vessel. In-fact the literature reported fermentation conditions are indeed sub-optimal conditions for fermentation of the pentose rich liquid fraction SHF fermentations.

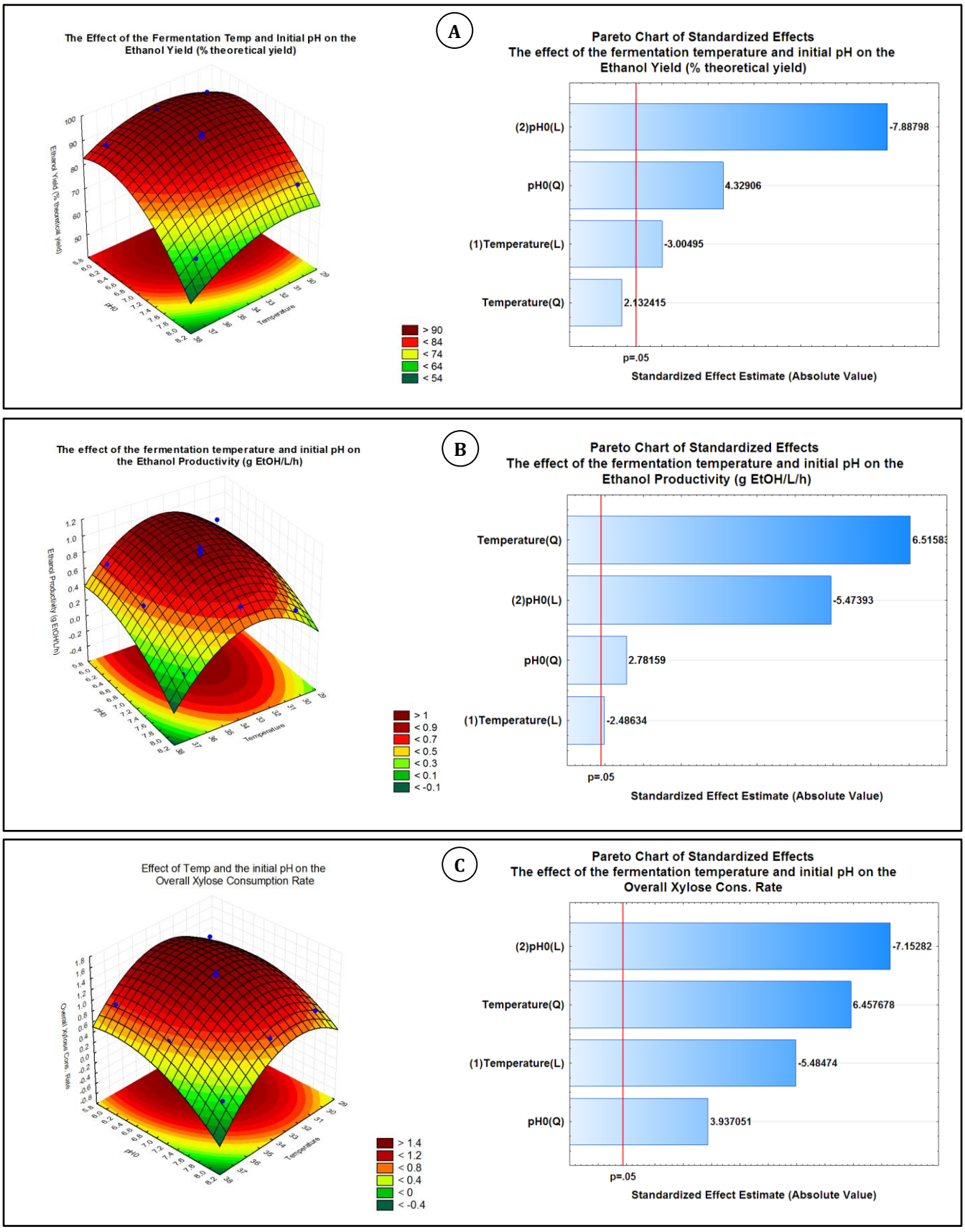


**Figure 50:** *The surface plots and result of the ANOVA analysis for the effect of the fermentation temperature and $pH_0$ on xylose-rich substrate fermentation.* ***A*** *- Ethanol Yield (top);* ***B*** *- Volumetric Productivity (middle);* ***C*** *– Overall rate of xylose consumption. Pareto chart Key:* ***(L)*** *– main effects,* ***(Q)*** *quadratic effects*

#### 7.1.2.2.2 MULTIPLE RESPONSE OPTIMIZATION (XYLOSE-RICH SUBSTRATE FERMENTATION)

The optimization of the fermentation conditions for a xylose-rich substrate was performed using a multiple response optimization approach. Similar to the optimization of the glucose fermentation condition, desirability functions were defined to constrain the fermentation conditions. Again, since ethanol is a low-value high volume product, the desirability was constraint such that the VP was optimized first, followed by the $Y_{ps}$ and then $Q_{s\_xylose}$. An additional constraint on $Y_{ps}$ was imposed in that the product yield should have a minimum value of 90%. The profiling and desirability functions are presented in *Appendix C.2.1.3*. The resultant surface and contour plots for the desirability functions are presented in *Figure 51*.

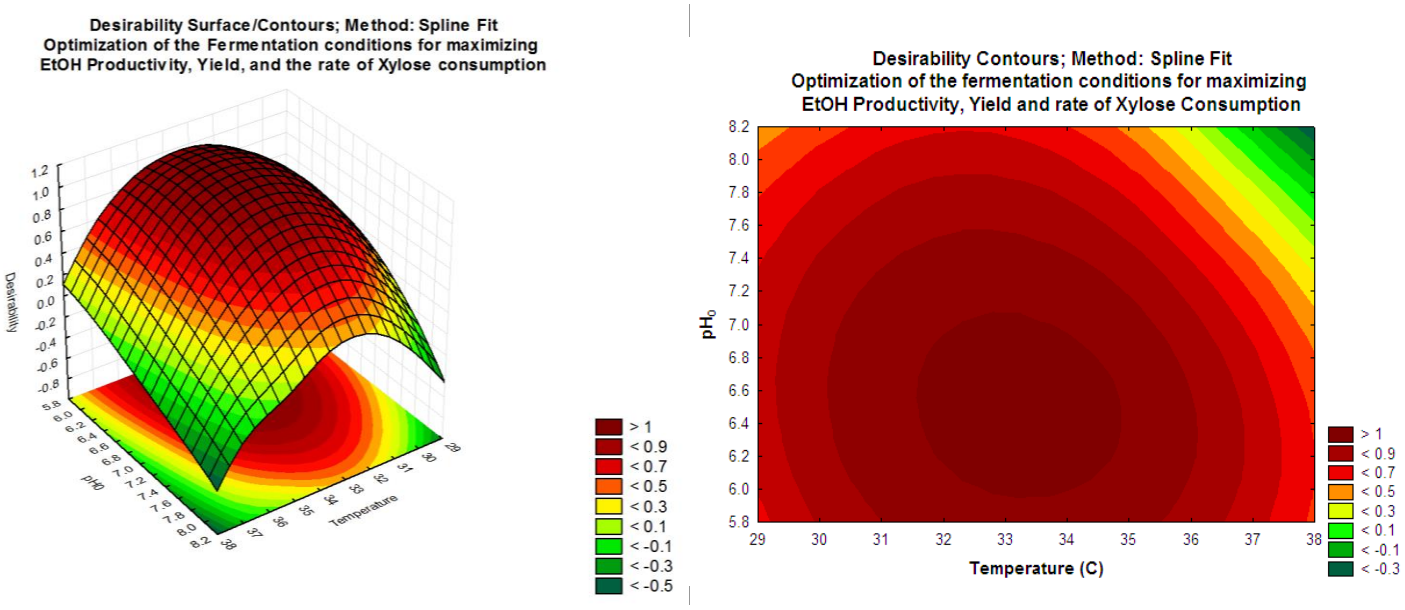


***Figure 51:*** *Multiple Response Optimization desirability for xylose-rich substrate fermentation. Surface Plot (left) and Contour plot (right)*

As evidenced from *Figure 51* the high overall desirability function values was achieved when the fermentation temperature and $pH_0$ were in the region of 32 - 34.5 $^oC$ and 7 - 6 respectively. However, the optimum conditions for the fermentation of a xylose rich substrate were at 33.5 $^oC$ and $pH_0$ 6.5, which corresponded to the highest desirability function of 0.999. At these optimum conditions, the individual responses were 94%, 1.02 g EtOH.$L^{-1}$.$h^{-1}$ and 1.486 g xylose.$L^{-1}$.$h^{-1}$, for the $Y_{ps}$, $Q_p$ and $Q_{s_{xylose}}$ respectively. In an attempt to explain the difference in optimum fermentation conditions for xylose-rich substrates, the kinetics of the parent strain (*Z. mobilis* ZM4) were consulted.

In *section 7.1.2.1.2* it was shown that the optimum fermentation conditions for glucose by ZM4 were at 30 $^oC$ and $pH_0$ 6. Therefore, assuming that the genetic engineering imposed on *Z. mobilis* 8b (recombinant strain of the parent strain ZM4) does not alter its glucose metabolizing action, the work done here suggests that the optimum conditions for xylose fermentation are different to those

of glucose fermentation. In effect, xylose consumption is highest near neutral pH and 33.5 °C. This indicates that in *Z. mobilis* 8b, xylose-fermenting enzymes are more active at a slightly higher pH and temperature than the generic glucose-fermenting enzymes. This observation reiterates that in maximizing VP, $Y_{ps}$ and $Q_{s\_xylose}$, the fermentation conditions are a function of the ratio of the fermentable sugars present in the hydrolyzate.

### 7.1.3 Quantification of Dual-Substrate Kinetics

The effect of the presence of glucose on the biological performance of *Z. mobilis* 8b was studied by performing fermentations at various the glucose to xylose ratios and maintaining the total sugar concentration constant. The objective was to establish whether the presence of glucose enhances, suppresses or has no effect on the overall rate of xylose consumption. The experimental data and a summary of the kinetic parameters obtained from the analysis are presented in *Figure 52* and *Table 23*.

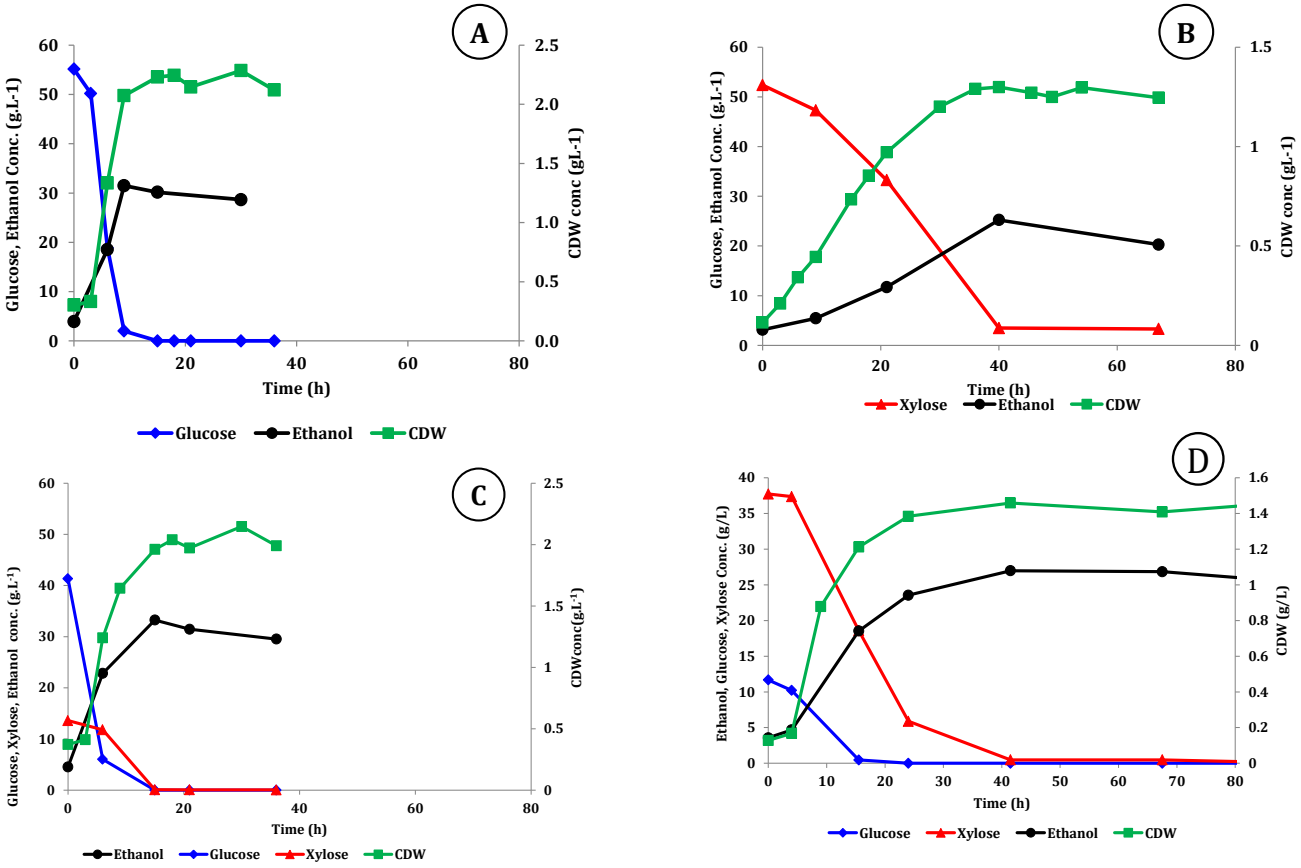


***Figure 52:*** *Substrate, Ethanol and CDW profiles for the quantification of the effect of glucose on xylose fermentation. A - 5% (m/v) Glucose, B - 5 % (m/v) Xylose, C - 3.7% Glucose, 1.3% Xylose; D - 1.3% Glucose, 3.7% Xylose*

The kinetic performance of the recombinant strain was compared to that of the parent strain (ZM4) to confirm that the high expression of the four xylose-fermenting genes in the host strain did not interfere with its glucose fermentation capabilities. As evidenced from *Table 23*, the kinetic parameters of the recombinant strain were within ±5% of the parameters of the control (parent

strain, ZM4). Considering the experimental error determined from the reproducibility experiments, it was shown that the standard deviation for the relevant kinetic parameters from triplicate samples was approximately ±5% (*section 7.1.1.3*). Thus, the small difference between the kinetic parameters obtained from the recombinant strain relative to the parameters obtained from the parent strain could be attributed to experimental error. Hence, the comparison of the kinetic parameters obtained from the recombinant strain to that of the parent strain confirmed that the biological performance of the recombinant strain was similar to that of the parent strain.

Two main observations were made from the glucose-xylose experiments. Firstly, by comparing pure glucose and pure xylose fermentation (A and B in *Figure 52*) it is apparent that glucose is consumed at a much faster rate than xylose. Secondly, the mixed substrate fermentations were characterized by two growth phases. The first phase consisted of simultaneous glucose-xylose consumption and was completed once glucose was completely consumed. The second phase was characterized by xylose consumption with minimal specific cell growth on xylose. Although no diauxic growth was observed and the glucose-xylose substrate was consumed simultaneously, most mixed substrate fermentations illustrated that a large portion of the xylose initially present in the media was consumed after the glucose is fermented. This result implied that even though glucose and xylose are fermented simultaneously during the first phase, the ethanologic microbe has higher affinity for glucose relative to xylose. The presence of a two-phase growth mechanism is a consequence of the change in the limiting nutrient from glucose to xylose as the fermentation progresses (Monod, 1949).

***Table 23:*** *Kinetic Parameter quantification for the fermentation of various substrate ratios by Z. mobilis 8b at 30 °C, $pH_0$ 6.*

| | Sugar Ratio (Glucose-Xylose) | | | | |
|---|---|---|---|---|---|
| **Strain** | **50-0‡ ZM4†** | **50-0‡ 8b** | **37-13‡ 8b** | **13-37‡ 8b** | **0-50‡ 8b** |
| **Kinetic Parameter Summary** | | | | | |
| ***Glucose/Xylose (1st Phase)*** | | | | | |
| $\mu max\ (h^{-1})$ | 0.48 | 0.47 | 0.37 | 0.33 | - |
| $q_{s\_max}{}^{(1)}$ *(g substrate/g/h)* | 12.58 | 13.20 | 12.49 | 9.28 | - |
| $q_{p\_max}{}^{(2)}$*(g EtOH/g/h)* | 6.27 | 6.60 | 6.07 | 4.58 | - |
| ***Xylose Phase (2nd phase)*** | | | | | |
| $\mu max\ (h^{-1})$ | - | - | 0.062 | 0.025 | 0.066 |
| $q_{s\_max}{}^{(2)}$ *(g substrate/g/h)* | - | - | 1.84 | 1.92 | 2.78 |
| $q_{p\_max}{}^{(2)}$*(g EtOH/g/h)* | - | - | 0.93 | 0.83 | 1.27 |
| ***Overall*** | | | | | |
| *VP (g EtOH/L/h)* | 2.429 | 2.504 | 1.791 | 0.780 | 0.552 |
| $Y_{xs}$ *(g CDW/g substrate cons)* | 0.038 | 0.035 | 0.032 | 0.027 | 0.023 |
| $Y_{ps}$ *(% theoretical)* | 98% | 98% | 96% | 93% | 83% |
| $Q_s$ *(g substrate/L/h)* | 4.80 | 5.01 | 3.66 | 1.63 | 1.22 |

† 50 g.L$^{-1}$ glucose fermentation with wild-type Z. mobilis ZM4 used as control

‡ The glucose-xylose substrate concentrations in g.L$^{-1}$

From *Table 23*, it is apparent that as the fraction of glucose increases in the fermentation media, an increase in the overall rate of substrate consumption and ethanol VP was observed. The rapid increase in cell mass from growth on glucose during the first phase (which is preferentially metabolized) and subsequently increasing the overall rate of xylose consumption most likely cause the increase in the overall rate of substrate consumption ($Q_s$). Additionally, the presence of glucose did not seem to increase ethanol yield from xylose. In fact, the ethanol yield in mixed sugar fermentations was almost proportional to the ratio of glucose to xylose initially present in the media. However, this observation is not expected hold at higher total substrate concentrations. At higher substrate concentrations, it is hypothesized that the overall ethanol yield from the fermentation of a glucose rich mixed sugar substrate would decrease slightly due to effects of ethanol and substrate inhibition. Nonetheless, it is evident that the presence of glucose in xylose-rich fermentation media indirectly enhances the overall rate of xylose consumption and the ethanol VP (relative to pure xylose fermentation) through increased cell mass from preferential consumption of glucose.

On an industrial scale and upstream of the fermentation stage, the glucose-xylose ratio present in hydrolyzate is highly dependent on the type of feedstock, process design, and the LC biomass pre-treatment technique. To this end, the effect of glucose on the overall rate of xylose fermentation may be surpassed by the effect of the concentration of inhibitory compounds present in the hydrolyzate. Therefore, even though the presence of glucose may potentially improve the overall rate of xylose fermentation, the removal or increase in the inhibitor tolerance of the fermenting biocatalyst becomes an even more essential step in maximizing the xylose-to-ethanol yield.

### 7.1.4 Batch Fermentation

#### 7.1.4.1 Fermentation at Optimized Conditions

As mentioned in the previous section, LC hydrolyzates generally consist of both glucose and xylose in ratios that are dependent on a multitude of effects. To demonstrate and evaluate the fermentation kinetics of *Z. mobilis* at the optimized temperature and $pH_0$, the kinetic performance of both Z. mobilis strains was evaluated at 100 $g.L^{-1}$ total sugar substrate. Considering glucose-only substrate fermentation, the batch fermentation of a 100 $g.L^{-1}$ glucose substrate by *Z. mobilis* ZM4 at controlled conditions (at 30 $^{o}C$, pH 6) was performed *Figure 55*. For dual-substrate fermentation, a 1:1 glucose-to-xylose ratio was selected as the substrate whilst maintaining the total sugar concentration at 100 $g.L^{-1}$. The batch fermentation profiles for the conversion of 50$g.L^{-1}$ glucose-50$g.L^{-1}$ xylose substrate to ethanol by *Z. mobilis* 8b are presented in *Figure 55*. The experimental conditions for this experiment were of 33.5 $^{o}C$, pH = 6.25.

The substrate concentration profiles presented in *Figure 55* highlight previous observations that dual-substrate fermentation occurs in two growth phases. Although the target substrate concentration was 50$g.L^{-1}$ glucose-50$g.L^{-1}$ xylose, the measured substrate concentration at initial

conditions was 45.43g.L$^{-1}$ glucose-50.27g.L$^{-1}$ xylose. Hence the total substrate concentration at initial conditions was 95.7 g.L$^{-1}$.

At the start of the fermentation, glucose and xylose are consumed simultaneously with glucose being preferentially consumed at a rapid rate (Phase I). During Phase I, approximately 10 g.L$^{-1}$ of xylose is consumed. This represents approximately 20% of the initial xylose concentration and therefore indicates that significant xylose consumption occurs during the first phase. Once glucose was completely depleted, the first phase was followed by the consumption of xylose alone, albeit at a slower rate relative to glucose (Phase II). The second phase was completed 36.5 hours after inoculation with the final ethanol concentration being 47.52 g.L$^{-1}$. However, after allowing the fermentation to continue after the depletion of both glucose and xylose, slight ethanol degradation was observed within a further 20 hours. In-fact, a proportional increase in acetate concentration was detected. The significance of ethanol degradation will become apparent when analyzing the performance of the MRB.

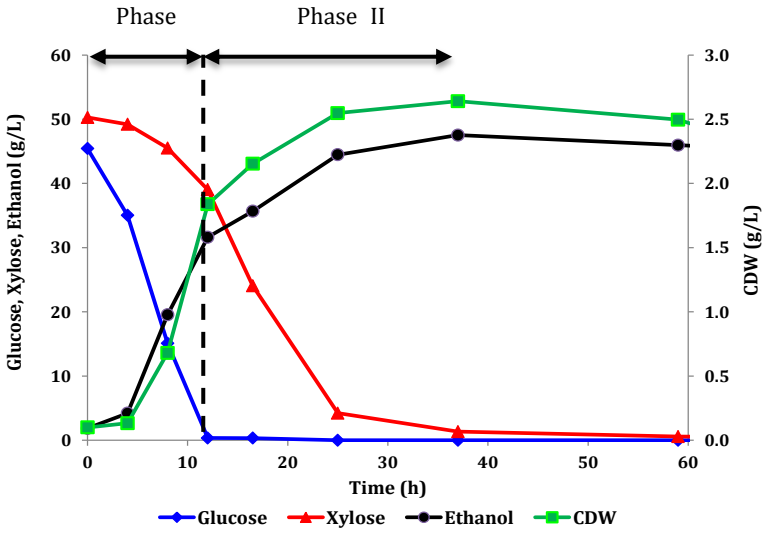


***Figure 53:*** *The batch fermentation of a 5% (w/v) glucose, 5% (w/v) xylose substrate by Z. mobilis 8b*

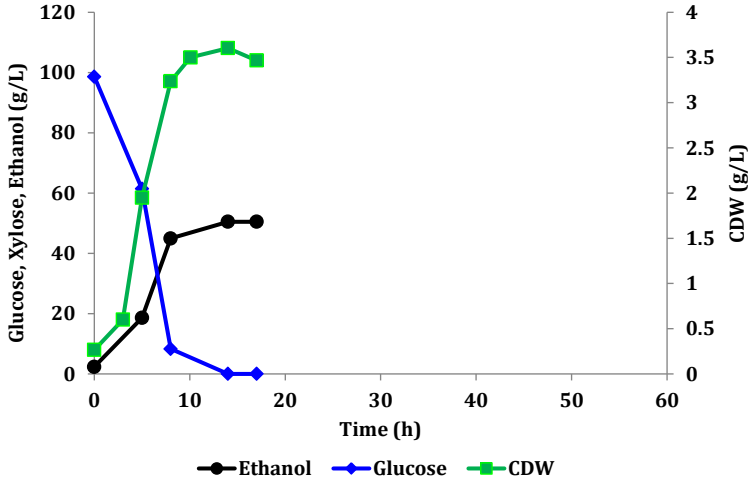


***Figure 54:*** *The batch fermentation of 10% (w/v) glucose by Z. mobilis ZM4*

The relevant kinetic parameters were calculated for both glucose-xylose fermentation in the first phase, followed by xylose only in the second phase. presents a summary of the kinetic parameters for the fermentation of 50g.L$^{-1}$ glucose-50g.L$^{-1}$ xylose substrate and for 100 g.L$^{-1}$ glucose fermentation. The glucose only kinetic parameters are presented to compare the range and magnitude of the dual substrate fermentation kinetic parameters. The significance of these parameters were already discussed in *section 7.1.1*. The calculation for the specific rates of sugar consumption ($q_{s\_max}$) and ethanol production ($q_{p\_max}$) were performed in the exponential segment of both growth phases. Sample calculations are presented in Appendix C.5.1.

***Table 24:*** *Kinetic parameters for glucose-xylose fermentation by Z. mobilis 8b at 33.5 °C, pH 6.25*

| Kinetic Parameters | Glucose-Xylose (g/L) | |
|---|---|---|
| | 50-50 | 100-0 |
| ***Glucose/Xylose (1st Phase)*** | | |
| $\mu_{max}$ ($h^{-1}$) | 0.33 | 0.43 |
| $q_{s\_max}^{(1)}$ (g substrate/g CDW/h) | 10.65 | 12.72 |
| $q_{p\_max}^{(1)}$ (g EtOH/g CDW/h) | 5.63 | 6.2 |
| ***Xylose (2nd Phase)*** | | |
| $\mu_{max}$ ($h^{-1}$) | 0.035 | N/A |
| $q_{s\_max}^{(2)}$ (g xylose/g CDW/h) | 2.115 | N/A |
| $q_{p\_max}^{(2)}$ (g EtOH/g CDW/h) | 0.875 | N/A |
| ***Overall*** | | |
| VP (g EtOH/L/h) | 1.47 | 4.8 |
| $Y_{xs}$ (g CDW/g substrate cons) | 0.025 | 0.034 |
| $Y_{ps}$ (g EtOH/g substrate cons) | 0.480 | 0.488 |
| $Y_{ps}$ (% theoretical) | 94% | 96% |

From *Table 23*, it is evident that microbial growth on a mixed substrate is slower relative to a glucose containing substrate. This observation was consistent with the findings presented in section 7.1.3.

The maximum specific rates of xylose consumption ($q_{s\_max}^{(2)}$) and ethanol production ($q_{p\_max}^{(2)}$) in the second phase were approximately 17% and 15% of the maximum specific glucose/xylose uptake rates in the first phase. The lower $q_{s\_max}^{(2)}$ and $q_{p\_max}^{(2)}$ in the second phase are most likely caused by a shift in the limiting nutrient from glucose to xylose after glucose is exhausted (at the end of Phase I). The effect of the shift in limiting nutrient can be evidenced graphically by the slower specific growth rate on xylose (during phase II) relative to glucose (during Phase I). Moreover, due to the elevated ethanol concentrations during the second phase, the overall rates of xylose consumption ($Q_s^{(2)}$) and ethanol production ($Q_p^{(2)}$) may be negatively impacted towards the end of the fermentation. The latter observation has been previously reported (Helle and Duff, 2004).

The overall ethanol yield remained high for dual-substrate fermentation ($Y_{ps}$ = 0.48 or 94% of the theoretical yield) whilst the volumetric productivity was 1.23 g.L$^{-1}$.

### 7.1.4.2 *OPTIMIZED Z. MOBILIS RELATIVE TO OTHER XYLOSE-FERMENTING STRAINS*

To put the fermentation kinetics of *Z. mobilis* 8b at the optimized conditions into perspective, a comparative study was performed whereby the ethanol yield and volumetric productivity of *Z. mobilis* 8b were compared to those of other strains of *Z. mobilis* and *S. cerevisiae* presented in literature. The benchmarking scope was limited to the batch fermentation of a of 50g.L$^{-1}$ glucose-50g.L$^{-1}$ xylose substrate (in defined mineral medium and not lignocellulose hydrolyzate), with the effects of different cell inoculum concentrations and hydrolyzate inhibitors not taken into account. Based on the benchmarking scope, the fermentation kinetics (reported in literature) of the following strains were compared to *Z. mobilis* 8b: three industrial yeast strains[2] (*S. cerevisiae* BH4, *S. cerevisiae* A4, *S. cerevisiae* TMB 3400), one laboratory recombinant yeast strain (*S. cerevisiae* 1400(pLNH33)), and two laboratory recombinant *Z. mobilis* strains (*Z. mobilis* CP4(pZB5), *Z. mobilis* ZM4(pZB5)). A summary of the kinetic parameters obtained from the comparative study is presented in *Table 25*. To eliminate bias in the overall VP (owing to inconsistencies in the actual sugar concentrations at initial conditions), the overall VP per mass substrate (at initial conditions) was included in the analysis. The glucose, xylose, and ethanol time dependent profiles for the respective strains are shown in *Figure 55*.

***Table 25:*** *Comparison of the kinetic parameters from the fermentation of a 50 g.L$^{-1}$ glucose 50 g.L$^{-1}$ xylose substrate in a batch fermenter*

| **Comparative Study** | | | | | | | | | |
|---|---|---|---|---|---|---|---|---|---|
| | **Initial Conditions** | | | | **Kinetic Performance** | | | | |
| **Strain** | Glucose (g.L$^{-1}$) | Xylose (g.L$^{-1}$) | Temp. (ºC) | pH | $Y_{xs}$ (g CDW.g subs.$^{-1}$) | $Y_{ps}$ (%theoretical) | Overall VP (g EtOH.L$^{-1}$.h$^{-1}$) | Overall VP per g substrate (g EtOH $^{-1}$.h$^{-1}$.g subs$^{-1}$) | **Reference** |
| ***S. cerevisiae* (pLHN33)** | 52.8 | 56.3 | 30 | 5.5 | 0.084 | 78% ᵞ | 1.22 ᵞ | 0.011 ᵞ | (Krishnan *et al.*, 1999) |
| ***S. cerevisiae* BH42**† | 50 | 50 | 30 | 5.5 | 0.040 | 71% | 0.30 | 0.003 | (Sauer *et al.*, 2004) |
| ***S. cerevisiae* A4**† | 50 | 50 | 30 | 5.5 | 0.060 | 69% | 0.29 | 0.004 | (Sauer *et al.*, 2004) |
| ***S. cerevisiae* TMB3400**† | 50 | 50 | 30 | 5.5 | 0.070 | 67% | 0.52 | 0.005 | (Sauer *et al.*, 2004) |
| ***Z. mobilis* CP4 (pZB5)** | 62 | 65 | 30 | 5 | 0.020 | 90% | 0.97 | 0.008 | (Rogers *et al.*, 1999) |
| ***Z. mobilis* ZM4 (pZB5)** | 50 | 50 | 30 | 5 | 0.025 | 94% | 1.60 | 0.016 | (Rogers *et al.*, 1999) |
| ***Z. mobilis* 8b** | **45** | **50** | **33.5** | **6.25** | **0.027** | **94%** | **1.43** | **0.015** | **This Work** |
| † | Industrial yeast strains | | | | | | | | |
| ᵞ | Recalculated from Fig. 6 at 36 h | | | | | | | | |

[2] Industrial yeast strains tolerate hydrolyzates better than laboratory strains and therefore provide the robustness required in an industrial context (Sauer *et al.*, 2004)

From the comparative study, it was found that the three recombinant industrial yeast strains were outperformed by the recombinant *S. cerevisiae* (pLNH33) strains with regards to $Y_{ps}$, the overall VP and the overall volumetric productivity per mass substrate. For *S. cerevisiae* (pLHN33), xylose was completely consumed after approximately 36.5 hours whereas for the industrial yeast strains xylose fermentation was incomplete after 60 hours. Hence, the laboratory strain pLHN33 displayed an overall volumetric productivity that was more than two-fold higher than the industrial yeast strains.

However, dual substrate fermentation by *Z. mobilis* ZM4 (pZB5) and *Z. mobilis* 8b (this work) were both slightly faster than the laboratory yeast strain *S. cerevisiae* (pLHN33). The overall volumetric productivity per mass initial substrate was 45% and 36% faster for *Z. mobilis* ZM4 (pZB5) and *Z. mobilis* 8b respectively. Moreover, both *Z. mobilis* strains (ZM4 (pZB5) and 8b) demonstrated higher ethanol selectivity relative to *S. cerevisiae* as evidenced by ethanol yields of 94% and 94% respectively.

With the same ethanol yield and overall volumetric productivity per mass initial substrate, both *Z. mobilis* ZM4 (pZB5) and *Z. mobilis* 8b were not only the fastest but most selective ethanologic biocatalysts from the comparative study (at least on a laboratory scale). However, *Z. mobilis* 8b has been shown to efficiently ferment dual substrates from waste paper sludge in SSCF in the presence inhibitory compounds (Zhang and Lynd, 2010) and through detoxified corn stover hydrolyzates (Mohagheghi *et al.,* 2006). Moreover, unlike Z. mobilis ZM4(pZB5), Z. mobilis does not require the addition of tetracycline to the fermentation media to maintain a selective pressure for plasmid (pZB5) maintenance. Hence, considering *Z. mobilis* 8b has potential for fermenting and tolerating xylose-rich hydrolyzates better than *Z. mobilis* ZM4 (pZB5), its efficient performance at the defined optimum conditions becomes essential considering its robustness in the industrial context.

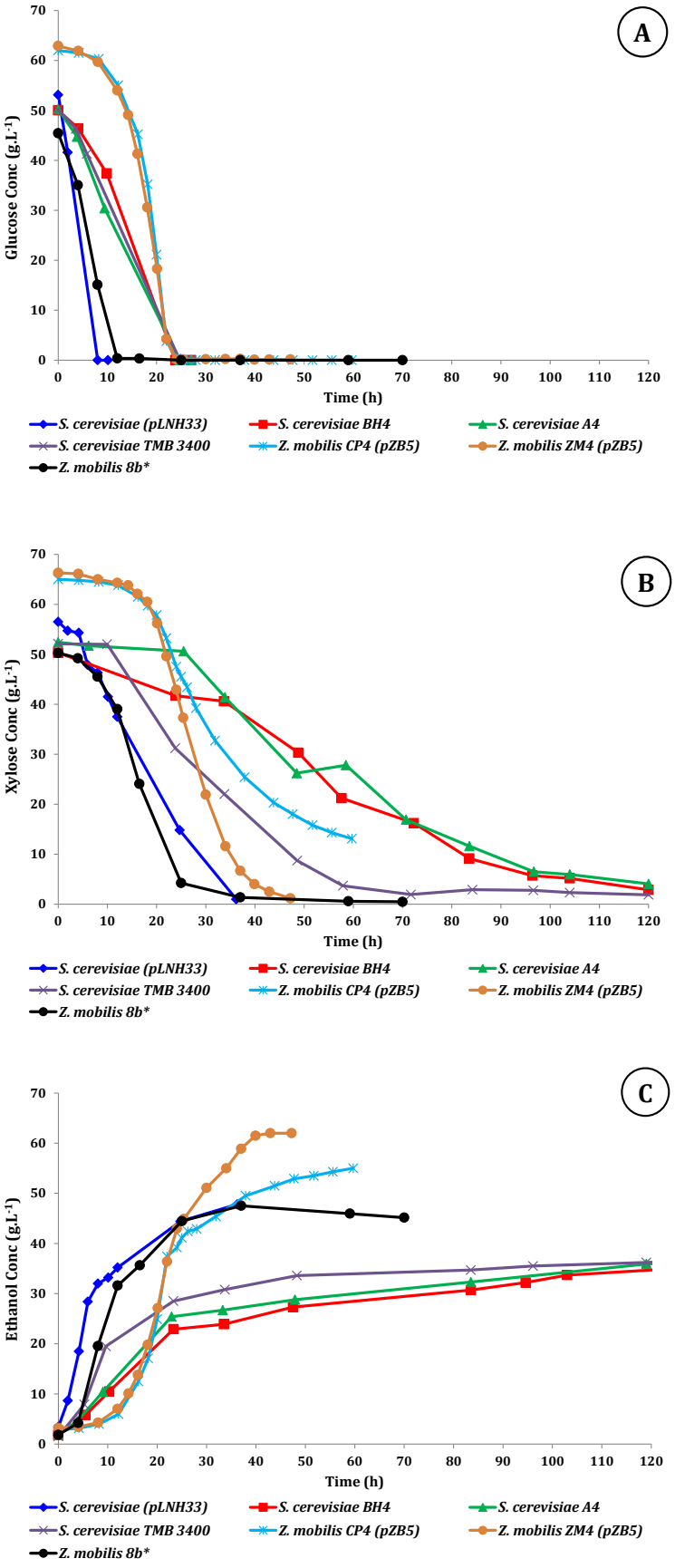


***Figure 55:*** *Batch fermentation of 50 g.L$^{-1}$ glucose-50 g.L$^{-1}$ xylose substrate by various ethanologic biocatalysts.* ***(A)*** *Glucose-time profiles,* ***(B)*** *Xylose-time profiles,* ***(C)*** *Ethanol-time profiles*

## 7.2 CHARACTERIZATION OF THE MICROFILTRATION UNIT

### 7.2.1 IDENTIFICATION OF THE SELECTED MEMBRANE

#### 7.2.1.1 SEM IMAGING

Because microfiltration is based on size exclusion at the membrane surface, scanning electron micrographs (SEM) of the cross-section of the α-$Al_2O3$ membrane were taken to identify the position of the permeable layer. For the selected membrane, the SEM micrograph confirmed that the permeable layer was indeed on the lumen side (*Figure 56*).

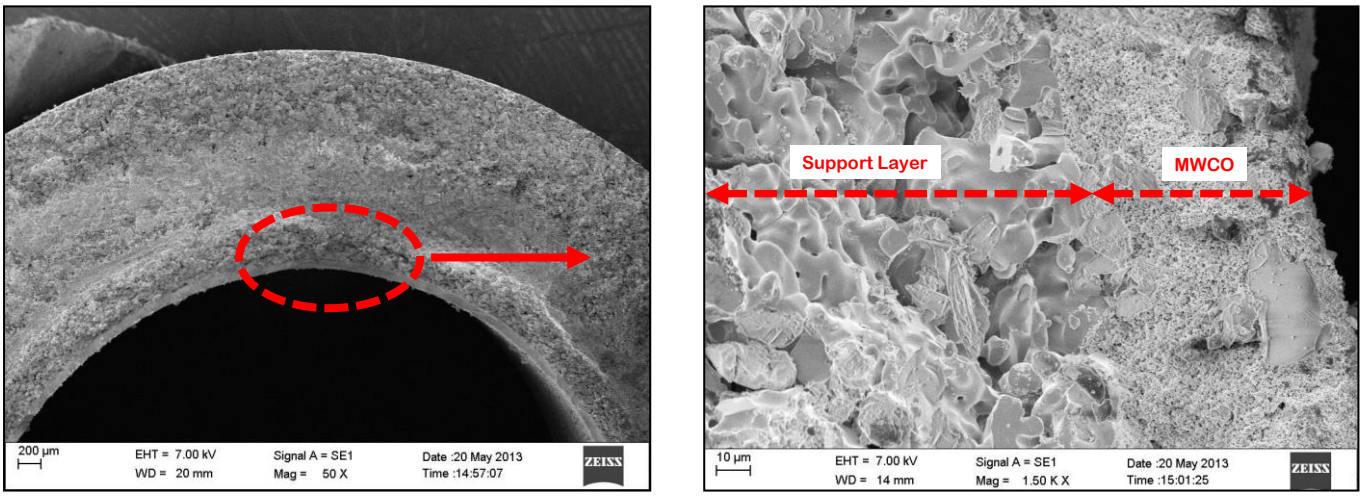


***Figure 56:*** *SEM micrograph of the membrane illustrating the cross section of the membrane with two distinct layers.*

The permeable layer was identified as the thin dense layer with a 0.2µm mean pore size (Atech Innovations, Germany). The support layer was characterized as the finger-like macroporous structure with a large mean pore size (6-8µm).

#### 7.2.1.2 CELL RETENTION EFFICIENCY

To ascertain whether the correct tubular membrane had been selected for retaining fermentation cultures of *Z. mobilis*, the particle size distribution (PSD) of the parent strain *Z. mobilis* ZM4 was quantified. The particle size distribution of the cell culture is shown in *Figure 57*. According to the PSD analysis, the cell length of the microbial cells had a narrow distribution with a mean length of 1.916 ± 0.05µm. The measured mean length was significantly higher than the mean pore size of the permeable layer and subsequently facilitating effective separation of the microbial cells from the fermentation liquid by size exclusion.

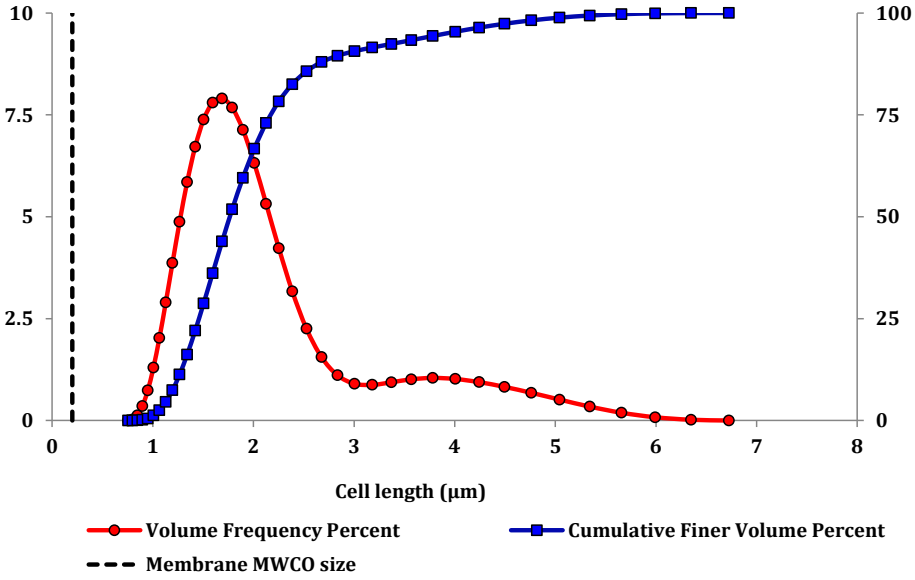


***Figure 57:*** *Particle size distribution for Zymomonas mobilis ZM4 sampled from continuous culture at 30 °C, $pH_0$ 6, $s_0$ = 100g.L$^{-1}$*

The retention efficiency (RE) of the tubular membrane was quantified by removing a sample of continuous culture broth, concentrating the cell mass and using the MFU to separate the whole cells from the broth liquid. The optical density of the broth was used as an indicator of the retention efficiency of the membrane using the following equation:

***Retention Efficiency:*** $$\% RE = \frac{OD_{feed} - OD_{permeate}}{OD_{feed}} x\ 100 \quad \textbf{(7.7)}$$

where **$OD_{feed}$** and **$OD_{permeate}$** are the culture optical density in the MFU feed and permeate respectively.From an initial culture feed concentration in the range 3-6.5g.L$^{-1}$, the retention efficiency of the MFU was 99.9±0.01%. The high retention efficiency highlighted the correct selection of the tubular membrane with a 0.2µm permeable layer.

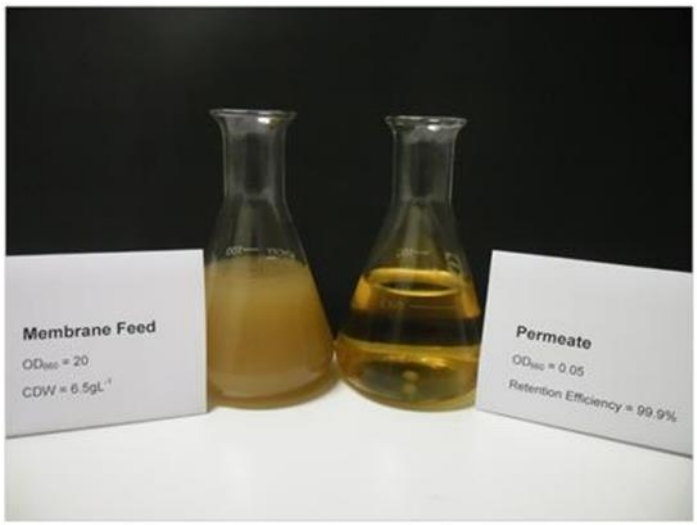


***Figure 58:*** *Optical examination of the retention efficiency of the MFU. Concentrated sample from culture mixture (left) and permeate (right)*

## 7.2.2 Determination of the Membrane Critical Flux

### 7.2.2.1 Effect of the Cross-Flow velocity on the Critical Flux

The effect of the CFV on the critical flux was investigated using cell-free fermentation media. Four different CFVs were evaluated, ranging from 0.0932 $m.s^{-1}$ to 0.4328 $m.s^{-1}$. The steady-state permeate flux rates as a function of the TMP for each of the four cross-flow velocities are plotted in *Figure 60*. All four experiments were performed at a constant temperature of 30 $^{o}C$, pH 6, and a substrate concentration of 10% (m/v) glucose.

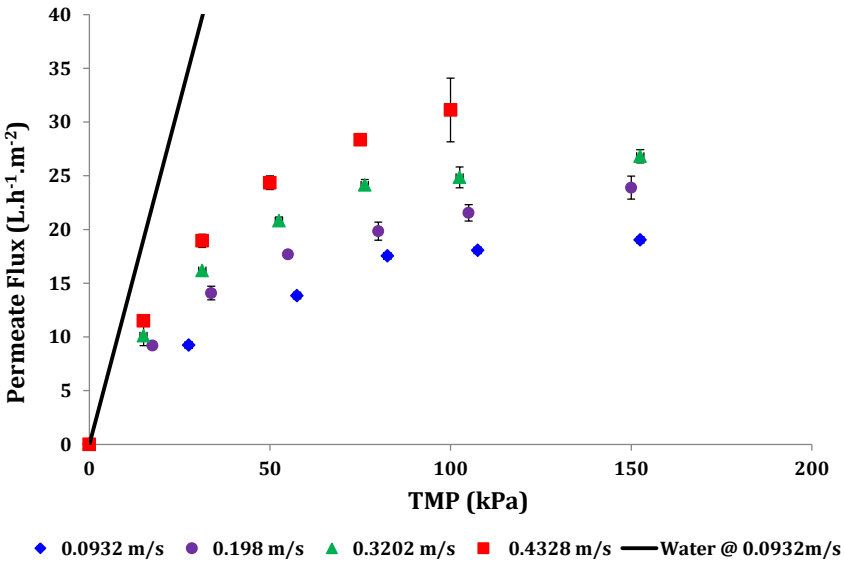


***Figure 60:*** *The effect of the cross-flow velocity on the critical flux*

The CFVs used in this work were relatively low for microfiltration with the media flow typically in the laminar flow regime. The low cross-flow velocities were a direct result of the use of industrial type ceramic membranes that are typically produced in finite sizes (large lumen diameters). Hence, for attaining high CFVs, high volumetric flowrates would be required. These ceramic membranes compare unfavourably to polymeric tubular membranes, which can have much smaller diameters (Li, 1999). Moreover, due to the equipment specifications, the upper limit cross-flow velocity was 0.4328 $m.s^{-1}$. Nonetheless, within the velocity limitations of the system, *Figure 60* shows that an increase in the cross-flow velocity increases the critical flux of the membrane. Again, the increase in the permeate flux was attributed to the increase in the turbulence at the membrane surface, which in this case enhances macrosolute (present in the fermentation media such as glucose) back-transport, limits the macrosolute cake layer thickness, and subsequently increase the critical flux (Belfort *et al.,* 1994; Ye, 2005; Cuperus and Smolders, 1991; Beier, 2008).

### 7.2.2.2 Effect of the substrate concentration on the Critical flux

The effect of increasing the substrate concentration in the fermentation media on the critical flux was investigated. The permeate flux profile as a function of the TMP was evaluated with

fermentation media solutions consisting of 5%, 10% and 15% (m/v) glucose. The cross flow velocity was maintained constant at 0.3202 $m.s^{-1}$ in all experiments.

Based on the permeate flux profiles in shown in *Figure 61*, it seems as though the critical flux decreases as the substrate concentration increases in the fermentation media. Moreover, a weak form of the critical flux definition was indicated by a deviation of the slope of the flux-pressure curves of the sugar-containing solutions from the slope of pure water (see *section 3.3.8* for weak form of the critical flux definition). The deviation of the slope of the sugar-containing solutions appeared to increase with an increase in the sugar concentration, suggesting that internal membrane fouling may potentially be a function of the sugar concentration.

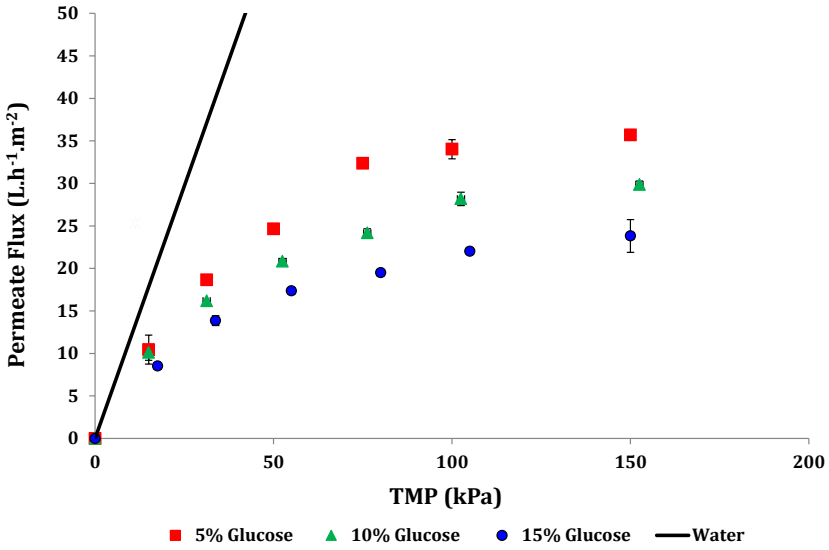


***Figure 61:*** *The effect of the substrate concentration on the critical flux*

The deviation of the permeate flux of the fermentation media relative to pure water flux can be a caused by a multitude of effects including:

- increased effect of internal fouling through the adsorption of macrosolutes in the media into the walls of the porous membrane,
- the build-up of the macrosolutes below the stagnant film near the membrane surface due to CP,
- physiochemical interactions between the media components and the membrane surface and,
- an increase in fluid viscosity with an increase in the sugar concentration, leading to deviation from Newtonian towards non-Newtonian behaviour and inevitably a drop in the permeation velocity.

However, based on the experimental data, it was not possible to establish whether the decrease in the permeability with increasing substrate concentration was a result of an increase in the fluid viscosity, internal fouling, CP or surface interactions. In an attempt to quantify whether the change in substrate concentration inflicted a significant difference on the fluid viscosity, the viscosity of four fermentation media solutions (0%, 5%, 10%, and 15% (m/v) glucose) was measured and compared

to the viscosity of water. The effect of the substrate concentration on the media viscosity is summarized in *Table 26*. Viscosity measurement data is presented in *Appendix C.3.1*.

***Table 26:*** *Quantification of the effect of the glucose concentration on the fluid viscosity*

| Fluid | Critical Flux ($L.m^{-2}.h^{-1}$) | μ (mPa.s) |
|---|---|---|
| *Water* | - | 1.05 ± 0.01 |
| *0% (m/v) Glucose* | - | 1.08± 0.01 |
| *5% (m/v) Glucose* | 31.5 | 1.2 ± 0.02 |
| *10% (m/v) Glucose* | 23.3 | 1.33 ± 0.01 |
| *15% (m/v) Glucose* | 18.8 | 1.5 ± 0.01 |

The addition of all the fermentation media components to water (0% (m/v) glucose) had an insignificant effect on the increase in the fluid viscosity. However, as suspected, an increase in the substrate concentration did result in a significant increase in the fermentation media viscosity (relative to pure water). Therefore, according to Darcy's law, the reduction in the membrane permeability (slope in *Figure 61*) at higher substrate concentrations can partially be attributed to the increase in the fermentation media viscosity.

As a result of the effect of the substrate concentration on the fluid viscosity, the hydraulic or total resistance to the permeate flux for the microfiltration of the fermentation media equals the sum of the membrane resistance and the adsorption resistance (see Darcy's Law in *Equation 3.1*). However, this simplification is based on the assumption that the membrane resistance is unaffected by the change in the fermentation media composition.

### 7.2.1 Permeate Flux Improvement by Back-flushing

As illustrated in *chapter 3*, permeate flux decline though macrosolute adsorption, surface membrane fouling and CP result in a significant reduction in the filtration performance of the MFU. In an attempt to control the effect of membrane fouling and establish continuous long-term operation at a sufficiently high permeate flux; operation with periodic back-flushing was investigated. Periodical back-flushing involves the reversal of the flow/ applied pressure through the membrane at a magnitude 1-3 fold higher than the forward flow (Pearce *et al.,* 2011). The efficiency of membrane back-flushing is strongly dependent on the type of bulk fluid to be treated, the dominant fouling mechanism caused by the bulk fluid and the frequency and amplitude of the pulses of the reverse pressure (Zhao *et al.,* 2000).

During operation, the membrane was backflushed at a TMP of 150 kPa for 1 min and at a frequency of 4-6 hours. An example of a permeate flux cycle for the filtration of a fermentation culture of approximately 5.3 $g.L^{-1}$ with periodic back-flushing is presented in *Figure 65*. The permeate flux cycle consists of two phases, a low TMP phase (operating TMP = 50kPa) and a high TMP phase (operating TMP = 100kPa). Both phases were characterized by a rapid decline in the permeate flux rate and thereafter stabilizing to a pseudo-steady state value.

As shown in *Figure 65*, periodic back-flushing the membrane did not have a significant effect on recovering the permeate flux. Operating at both low TMP (50kPa) and high TMP (100kPa) resulted in a permeate flux decline greater than 50% before the flux stabilized and reached pseudo steady-state. In-fact, for practical considerations, the fouling mechanism is most likely to be dominated by the formation of compressible and highly adhesive cake layer on the membrane surface that can be considered irreversible.

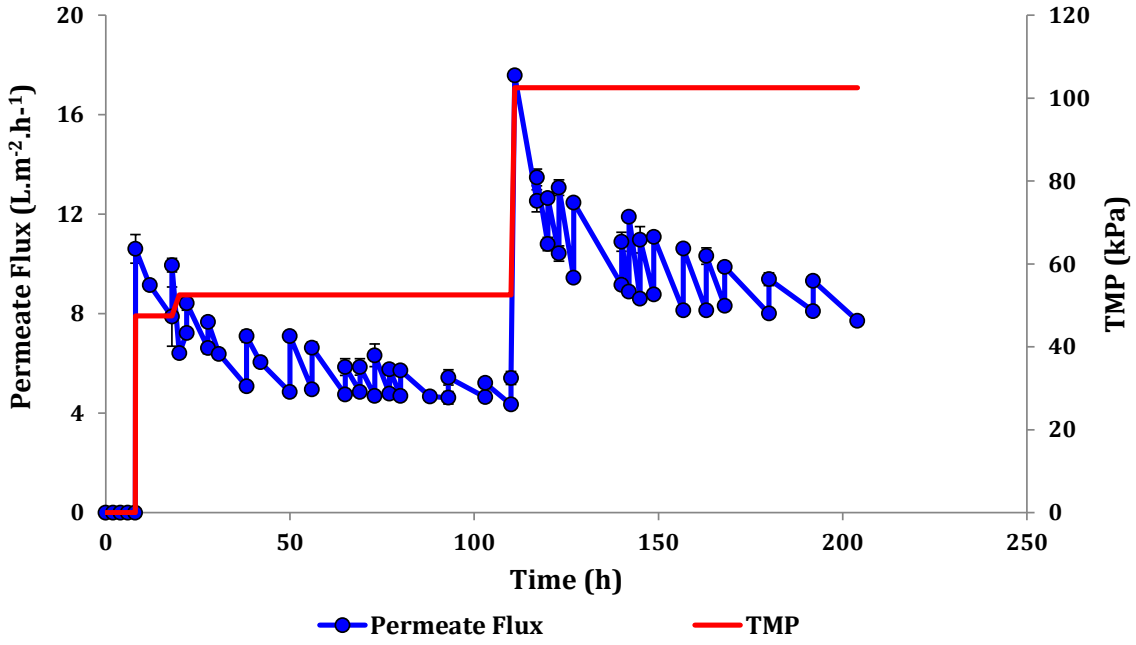


***Figure 62:*** *Permeate flux cycle for the filtration of 5.3 g.L$^{-1}$ fermentation culture with periodic back-flushing after every 4-6 hours*

The apparent negligible effect of the periodic back-flushing may be attributed to a number of causes. First, the operating CFV or shear forces on the membrane surface may be so low (laminar flow regime) that a thick and highly adhesive cake layer is formed whilst operating in filtration mode. Hence, upon switching to back-flushing mode, either a small percentage of the cake forming microbial cells are removed from the surface and back into the bulk fermentation culture or upon switching back to filtration mode the fouling rate is so rapid that the permeate flux decreases almost immediately back to its pseudo-steady state value. Benkahla *et al.,* (1995) studied the reversibility of a $CaCO_3$ cake formed during CF filtration through periodic back-flushing and found that the $CaCO_3$ cake was virtually irreversible due to strong cohesive forces keeping the particles together (Ye, 2005; Benkahla *et al.,* 1995).

The negligible effect of back-flushing may also be attributed to the low frequency and amplitude of the pulses of reverse pressure used in this work. Levesley and Hoare, (1999) reported the greater the amplitude and duration of the back pulses though the membrane, the higher the potential for removing/ clearing foulants off the pores and surface of porous membranes. Moreover, it has been shown that back-flushing for 0.5 sec at 5 sec intervals yielded 20-30 fold increase in the pseudo steady-state permeate flux for the microfiltration of washed yeast cells (Redkar and Davis, 1995).

Therefore, operating at high frequencies and amplitudes of the reverse pressure are viable options to the recovery of the permeate flux for biological retention systems. However, operating at these conditions was not possible within the available equipment in this work.

As a result, future work should be directed towards expanding the limitations of the current experimental set-up in view of increasing the back-flushing frequency and amplitude capabilities. Moreover, the improvement of the filtration hydrodynamics, such as improving surface turbulence by operating at higher CFVs, is necessary for operating at sufficiently high permeate flux rates. The effect of increasing the CFV is also highlighted by its positive and linear effect in the quadratic model. Therefore, by increasing the CFV or membrane surface shear stresses, the thickness of the foulant cake layer would be minimized and CP would be minimized through the enhancement of the back-transport of microbial cells back into the bulk fluid (cell suspension) phase. However, the effect of the CFV would only be significant if the shear forces are significant enough to overcome possible cohesive forces binding the compressible microbial cake layer and would have no effect on internal fouling.

Nonetheless, the extent of limitation imposed by the declining permeate flux on the performance of MRB was studied and is presented in the next section. Even though membrane fouling was a significant problem during operation, flux recovery was attained (within 5% of the original water permeability) through high temperature chemical cleaning after the completion of each experiment.

### 7.2.2 Statistical Determination of the Pseudo Steady-State Permeate Flux Rate of Fermentation Broth with Cell Culture Suspension

Having established in *section 7.2.2.2* that the substrate concentration of the fermentation media influences the permeability and critical flux of the microfiltration membrane, the presence of bacterial cells was expected to further decrease the filtration performance of MFU due to membrane fouling. To quantify the extent and significance of the presence of the bacterial cells on the pseudo-steady state permeate flux rate, a black-box approach in the form of a face-centered central composite design (CCD) was used. The cross-flow velocity, TMP, and cell concentration were used as the process variables with the response variable a being the pseudo-steady state permeate flux. The CCD statistical design was defined in *section 5.3.2.3*.

#### 7.2.3.1 Empirical Permeate Flux Model

The refined quadratic model obtained from the statistical analysis for the prediction of the pseudo-steady state permeate flux is presented below:

$$Flux = 1.977 - 1.39(Cell\ Conc) + 0.199(Cell\ Conc)^2 + 0.11(TMP) + 8.79(CFV) - 0.01(Cell\ Conc \cdot TMP) \quad \textbf{(7.8)}$$

All statistically insignificant parameters were excluded from the model and considered as model error. The accuracy of the refined quadratic fit to the experimental data was highlighted by an

adjusted $R^2$ value of 0.903. The high magnitude of the $R_{adj}$ value indicated a high degree of model fit to the experimental data. Validation of the assumptions made during the development of the mathematical model and the ensuing ANOVA analysis are presented in Appendix C4.1.

A graphical representation of the change in the pseudo-steady state permeate flux as predicted by the mathematical quadratic model is presented in *Figure 63*. A Pareto chart summarizing the standardized effects of all the factors considered in the ANOVA analysis from the refined quadratic model is illustrated in the *Figure 63*. According to an ANOVA analysis, the cell concentration, TMP, the quadratic effect of the cell concentration, the TMP-cell concentration interaction and the CFV have a significant effect on the permeate flux within a 95% confidence interval.

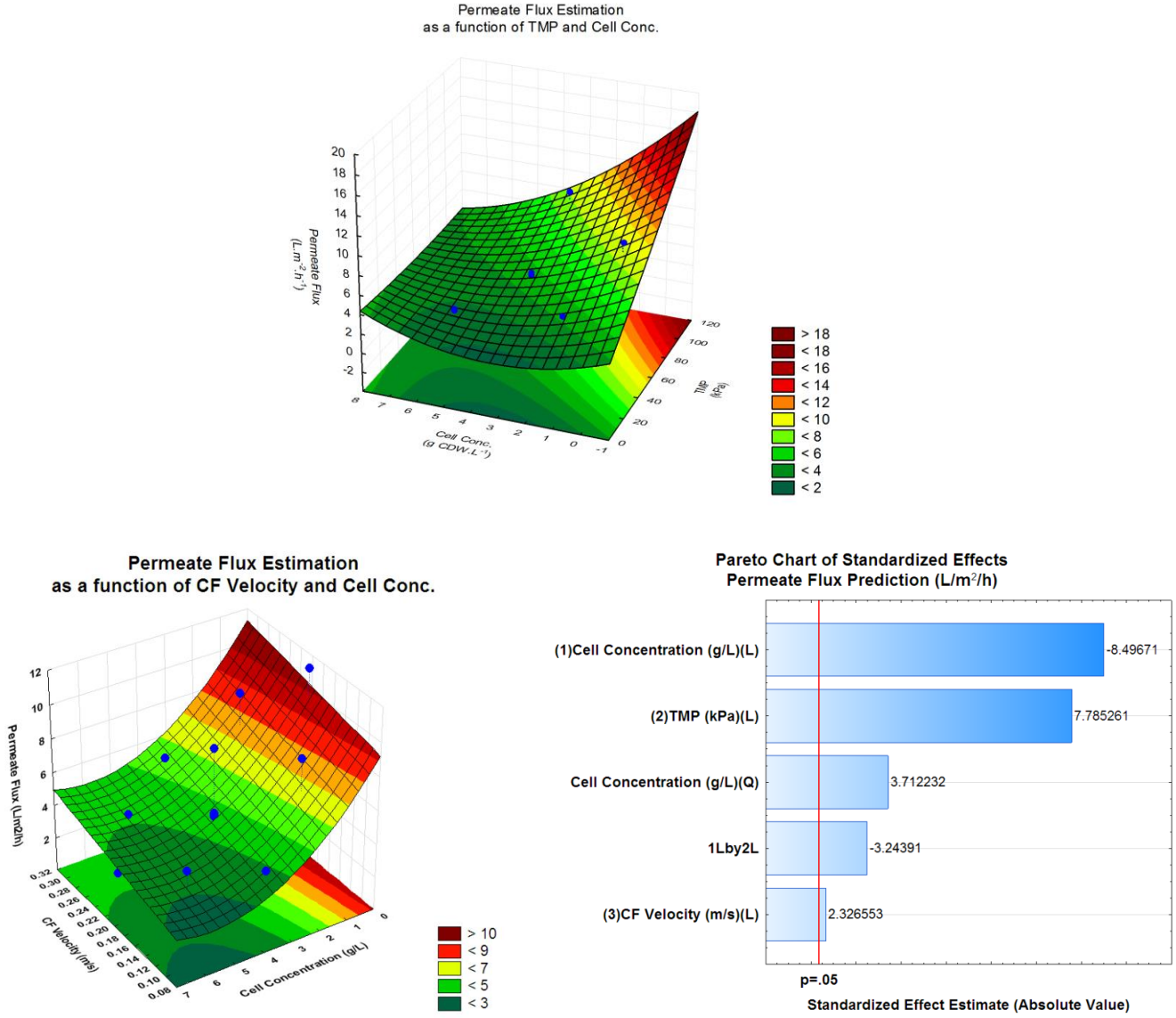


***Figure 63:*** *Surface plots of the quadratic model predicting the pseudo-steady state flux as a function of the TMP, CFV and cell concentration (top and bottom left) and Pareto chart of standardized effects of quadric model (bottom right).*

### 7.2.3.2 *EFFECT OF THE CELL CONCENTRATION*

According to the quadratic model, the pseudo-steady state permeate flux declines sharply with an increase in the cell concentration and thereafter becomes independent of the cell concentration at concentrations greater than 5g.$L^{-1}$.

The cell concentration has a multitude of effects on the filtration performance of microfiltration membranes. First, increasing the cell concentration in the bulk fluid to the MFU has the undesirable effect of increasing effective viscosity of the bulk fluid. As reported in the *section 7.2.2.2*, increasing the bulk fluid viscosity contributed to a reduction in the permeate flux rate to some degree. For example, an increase in the fluid viscosity because of the addition of cells to the bulk-fluid decreases the actual shear or turbulence on the membrane surface and effectively increasing CP and cake layer thickness (Bhave, 2003).

Secondly, since the bacterial cells in the bulk fluid suspension are too large to enter the membrane pores, the retained cells accumulate on the membrane surface and subsequently form a growing and compressible cake layer. The accumulated cells impede permeate flux through either blocking the pores at the membrane surface, the reduction of the effective pore size of the membrane through the formation of the compressible cake layer, or the development of a highly concentrated layer near the membrane surface due to CP (Belfort et al., 1994; Zhao et al., 2000). Bhave (2003) suggested that permeate flux decrease with an increase in the solids concentration in the bulk fluid is largely due to concentration polarization and can be minimized through efficient fluid hydrodynamics or periodic high-pressure back-flushing. Additionally, the higher the cell concentration in the bulk fluid, the higher the probability of forming a thick cake layer due to particulate accumulation and subsequently providing a high resistance to the permeate flux through the membrane.

However, the propagation of the cake layer does not continue indefinitely. Instead, it is arrested by the shear forces/ turbulence induced by the CFV at the membrane surface. Therefore, the eventual stabilization of the permeate flux at cell concentrations higher than 5g.$L^{-1}$ can be attributed to the limitation of the thickness of the cake-layer by the CFV at the operating TMP.

### 7.2.3.3 *EFFECT OF THE CROSS-FLOW VELOCITY*

The quadratic model predicts that an increase in the cross-flow velocity increases the pseudo-steady state permeate flux linearly within the experimental range. The significance of the CFV in the mathematical correlation shows that the effect of the CFV is pronounced even in the laminar flow regime investigated. It is well documented that the cross-flow velocity provides shear or turbulence at the surface and subsequently promotes back diffusion and transport of foulants at the membrane surface into the bulk fluid phase (Beier, 2008; Belfort et al., 1994; Pearce et al., 2011; van den Berg and Smolders, 1990; Ye, 2005)

. Therefore, increasing the CFV arrests cake layer formation, limits the thickness of foulant layer on the membrane surface and subsequently improves the mass transfer coefficient of the fluid through the membrane. However, the CFV has limited effect on minimizing internal fouling.

Nonetheless, as evidenced by the Pareto chart, the CFV has a less significant effect on the permeate flux relative to the cell concentration and the TMP. For example, an increase in the cross-flow velocity would improve the permeate flux but the model suggests that a greater improvement in the flux can be imposed by operating at higher TMPs and/or lower cell concentrations.

#### 7.2.3.4 *EFFECT OF THE TRANS-MEMBRANE PRESSURE*

The TMP provides the driving force for the permeation velocity for inflicting the size-based exclusion at the membrane surface. The quadratic model predicts that the permeate flux increases linearly with an increase in the TMP. However, in addition to providing the driving force, increasing the TMP also increases the fouling rate. High TMP generally offset the effect of turbulence induced by the CFV due to the greater convective flux across the membrane. Therefore, even though the quadratic model indicated that the CFV-TMP interaction was statistically insignificant, the observed effect of the CFV may have been offset by operating at high TMPs.

#### 7.2.3.5 *QUADRATIC MODEL VALIDATION*

The accuracy and limitations of the quadratic model was evaluated by comparing model predictions to experimentally obtained pseudo-steady state permeate flux rates. Randomly selected experimental conditions and results of the validation of the quadratic model are presented in *Table 27* and *Figure 64* respectively.

As evidenced in *Figure 64*, the within the selected experimental range, the empirical model accurately predicted the pseudo-steady state permeate flux obtained experimentally. Therefore, within the validated region, this model provides a tool for estimating the pseudo-steady state permeate flux rate as a function of only operating conditions and not the complex fouling mechanism. The significance and application of this model will be become evident in the MRB kinetic modeling section (*section 7.4*). However, implications pertaining to the extrapolation of this model beyond the validated conditions are unknown. Therefore, future work should be done in extending the range of this model.

***Table 27:*** *Experimental conditions for pseudo-steady state flux model validation*

| | Experimental Conditions | | | | Model Prediction |
|---|---|---|---|---|---|
| **Experiment No.** | **CFV ($m.s^{-1}$)** | **TMP (kPa)** | **CDW ($g.L^{-1}$)** | **Flux ($L.m^{-2}.h^{-1}$)** | **Flux ($L.m^{-2}.h^{-1}$)** |
| **1** | 0.141 | 45 | 2.8 | 4.2±0.124 | 4.60 |
| **2** | 0.169 | 15 | 2.8 | 2.3±0.381 | 2.35 |
| **3** | 0.255 | 50 | 4.9 | 4.9±0.234 | 5.23 |
| **4** | 0.255 | 50 | 2.47 | 5.4±0.423 | 6.26 |
| **5** | 0.255 | 100 | 5.3 | 8.1±0.211 | 8.15 |

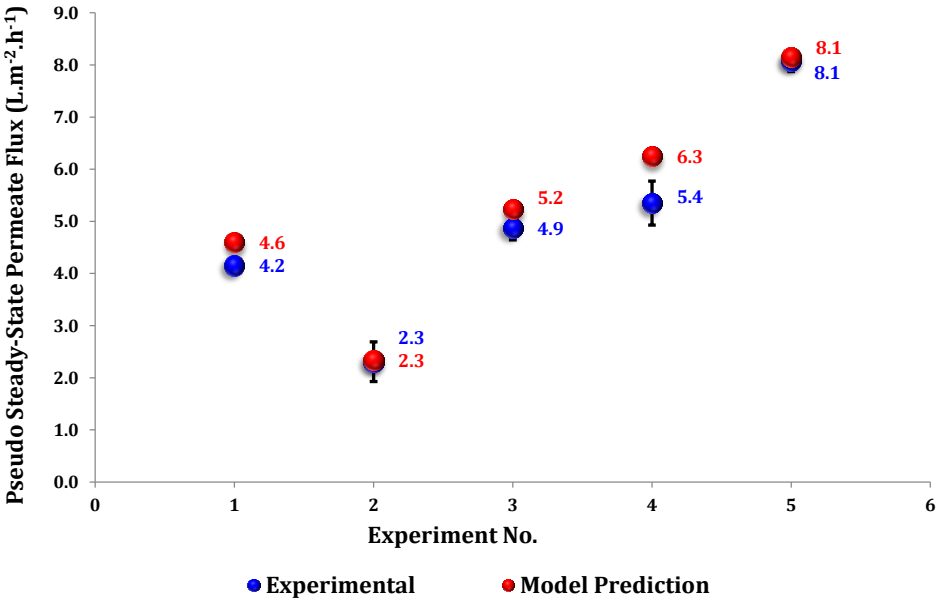


***Figure 64**: Validation of the statistically derived empirical model with experimental data*

## 7.3 QUANTIFICATION OF THE KINETIC PERFORMANCE OF *Z. MOBILIS* IN CONTINUOUS CULTURE

The kinetic performance of *Z. mobilis* in continuous culture was investigated by comparing the continuous culture (without cell retention) to continuous culture with cell retention fermentation strategies, both performed at the same experimental conditions. Continuous culture with cell retention was evaluated using two fermentation strategies, i.e. cell immobilization and cell retention via an external cross-flow microfiltration membrane (or MRB) (*Figure 66*). From this point forth, continuous culture (without cell retention) will be referred to as continuous culture and continuous culture with cell retention via an external cross-flow microfiltration membrane will be referred to as a membrane recycle bioreactor (or MRB).

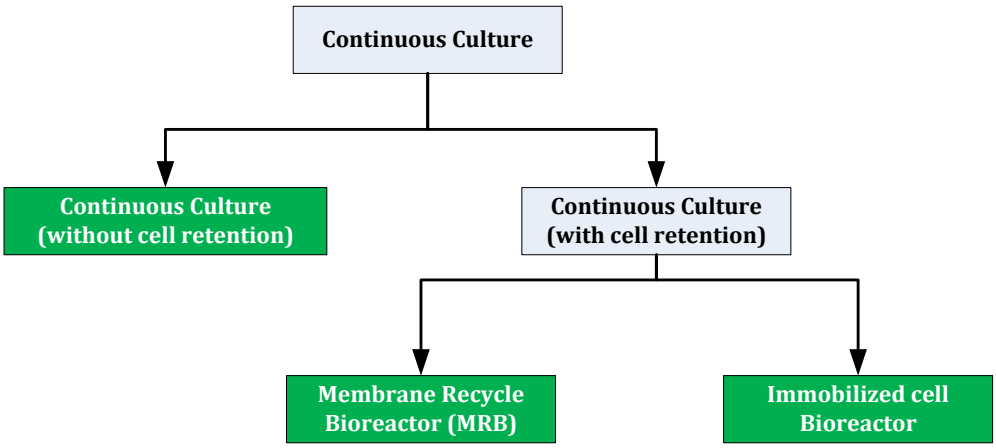


***Figure 66:*** *Block Diagram for the quantification of the kinetic performance of Z. mobilis in Continuous Culture*

The performance of the three fermentation strategies was compared using a 1:1 glucose-xylose substrate at the optimum fermentation conditions for *Z. mobilis* 8b (controlled at 33.5 $^{o}$C, pH 6.25). The fermentation performance indicators (PI) were selected as the overall volumetric productivity, the ethanol yield (as a percentage of the theoretical yield) and the final ethanol concentration. The batch-culture PI's for *Z. mobilis* 8b were compared to the PI's obtained from the continuous culture and MRB fermentation strategies at the same operating conditions. The PI's of *Z. mobilis* 8b at the optimum conditions in batch culture were discussed in *section 7.1.3*.

### *7.3.1 CONTINUOUS CULTURE*

#### 7.3.1.1 *GLUCOSE FERMENTATION*

The conversion of a 10% (w/v) glucose substrate to ethanol by the parent strain (ZM4) was evaluated in continuous culture. The aim of this experiment was to determine the PI's of *Z. mobilis* ZM4 for a glucose substrate with an increase in the dilution rate and to establish the microbial maintenance energy requirements at the optimized conditions. The continuous culture CDW and

dilution rate profile during the experimental run are presented at discreet dilution rates of 0.04, 0.1, 0.3, 0.33 $h^{-1}$, in *Figure 67* below. Steady state was assumed after a minimum of four-to-six volume changes as indicated by the circular broken red line.

Once a minimum of four volume changes had been achieved, the last three data points (indicated in the circular red broken line in *Figure 67*) were assumed to be at steady state and were consequently analyzed for sugar and product concentrations. The average value at each steady state was plotted as a function of the dilution rate in *Figure 68*.

For lower dilution rates (D = 0.04- 0.11 $h^{-1}$), glucose was nearly completely utilized and the ethanol concentration achieved was within 5% of the theoretical concentration. However, within the same dilution rate range, the steady state cell concentration increased with an increase in the dilution rate (where D is equivalent to μ). This behaviour is typically indicative of the significance of the utilization of the substrate for cell maintenance instead of cell growth at lower dilution rates. Maintenance energy describes energy expenditure for maintaining an energized membrane and for essential metabolic functions such as the repair of damaged cellular structures (Shuler and Kargi, 2008). Unlike glucose fermentation with yeasts where ethanol production is almost completely growth associated (tight energetic coupling of the catabolic and anabolic processes), glucose fermentation in continuous culture with *Z. mobilis* is less regulated and ethanol production is not necessarily coupled with the anabolic processes (which include bacterial growth) (Belaich and Senez, 1965). Therefore, considering that ethanol production remains essentially constant during this dilution range, the experimental data suggests some degree of energetic uncoupling whereby non-growth associated ethanol production was observed (Lawford 1988).

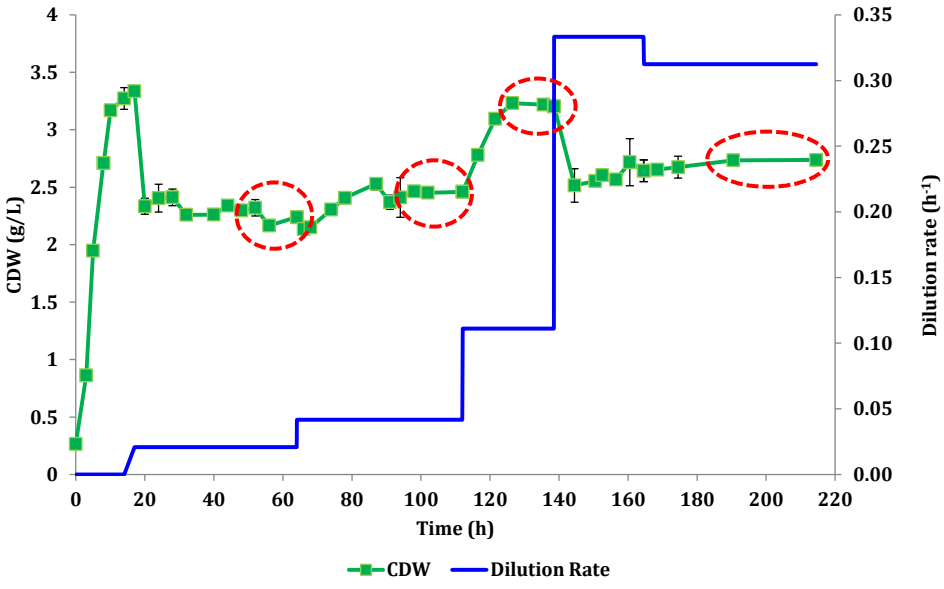


***Figure 67:*** *Continuous Culture CDW and dilution rate profiles for 10% (w/v) glucose fermentation by Z. mobilis ZM4 at controlled conditions of 30 °C, pH 6.*

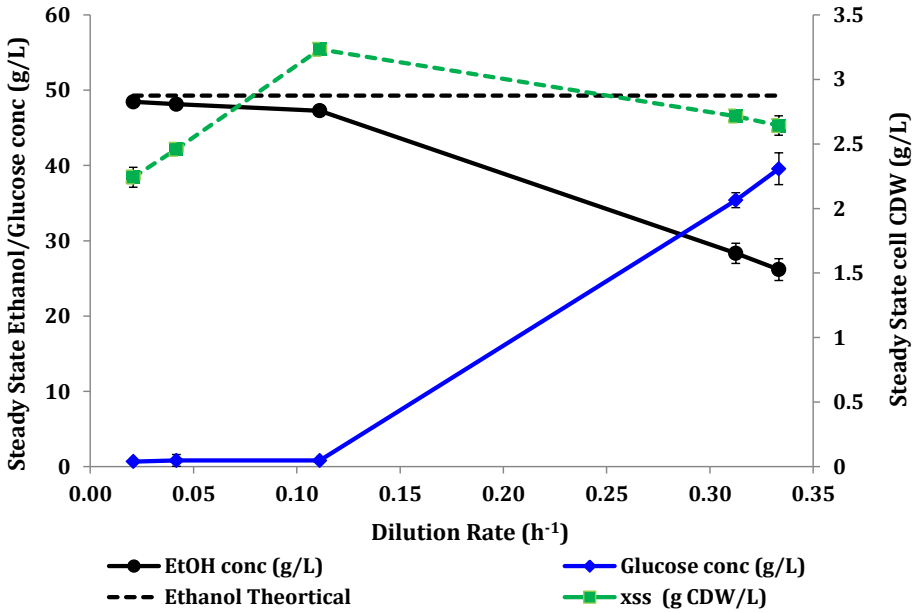


***Figure 68:*** *Steady-State continuous fermentation profiles of ZM4 on 10% (w/v) glucose at various dilution rates (pH 6, 30 °C, 500rpm)*

At dilution rates higher than 0.11 $h^{-1}$, the steady-state cell and ethanol concentrations decrease with an increase in the dilution rate, primarily due to the decrease in the substrate residence time within the fermenter. Additional analyses of the continuous culture data is presented in *Figure 69* whereby the specific glucose consumption rate, ethanol production rate and the volumetric ethanol productivity are plotted as functions of the dilution rate.

The maintenance energy coefficient was calculated by extrapolating the $q_s$ vs D profile to zero dilution rate according to the following equation (Pirt, 1976):

$$q_s = \frac{D}{Y_{x/s}^{max}} + m \qquad \textbf{(7.8)}$$

where $Y_{x/s}^{max}$ is the maximum cell yield coefficient (in the absence of maintenance energy or endogenous respiration) and m is the maintenance energy coefficient. Through graphical inspection, the maintenance coefficient and the maximum cell yield coefficient was calculated as 0.62g glucose.g $CDW^{-1}.h^{-1}$ and 0.0416 g CDW.g $glucose^{-1}$ respectively.

The optimum volumetric ethanol productivity was calculated as 8.82 g $EtOH.L^{-1}.h^{-1}$ at a dilution rate of 0.3 $h^{-1}$. As expected, the volumetric productivity of the continuous culture was significantly higher relative to batch culture at the same experimental conditions (VP batch = 4.8 g $EtOH.L^{-1}.h^{-1}$).

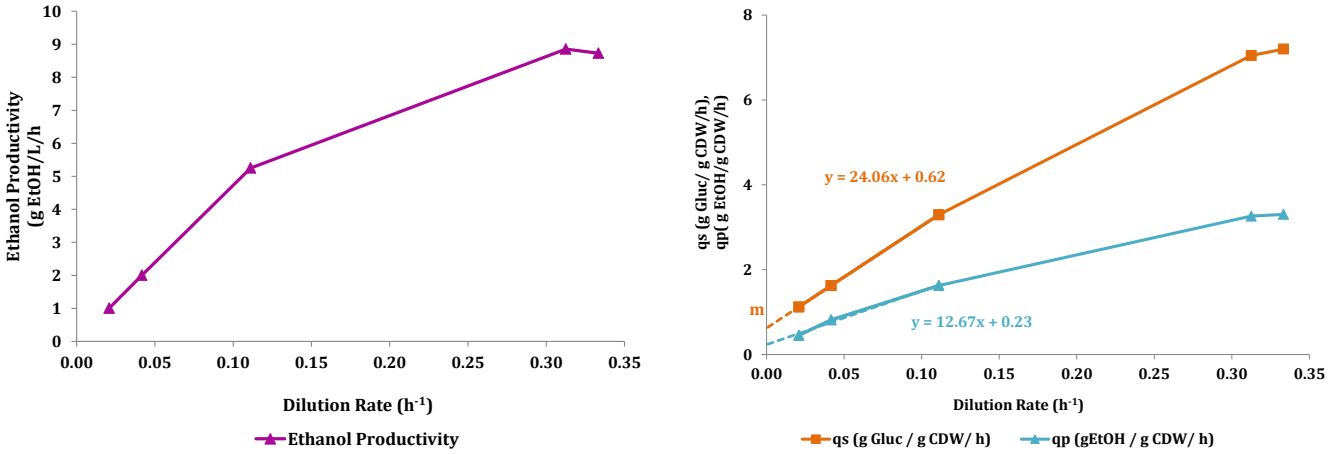


***Figure 69:*** *Steady-State volumetric productivity (left),and specific glucose consumption rate and specific ethanol production rate profiles at various dilution rates (right)*

### 7.3.1.2 *DUAL-SUBSTRATE FERMENTATION*

The continuous culture fermentation of a 50g.L$^{-1}$ glucose and 50g.L$^{-1}$ xylose substrate by *Z. mobilis* 8b was investigated over the dilution rate range 0.04-0.2 h$^{-1}$. The continuous culture and dilution rate profiles during the experimental run are presented in *Figure 70*. Steady state was assumed after a minimum of four-to-six volume changes. Steady state cell, glucose, xylose and ethanol concentrations within the fermenter are shown in *Figure 71*. For the entire dilution rate range used in this experiment, the residual glucose concentration was essentially zero. However, as the dilution rate increased from 0.04-0.2h$^{-1}$, the residual xylose concentration increased nearly linearly from 1.6-12.6 g.L$^{-1}$. Because glucose is preferentially metabolized by *Z. mobilis* 8b (shown in *section 7.1.3*), xylose conversion decreases as the dilution rate increases due to a reduction in the residence time of substrate in the fermenter. Therefore, at higher dilution rates, higher residual xylose concentrations were attained.

Similar to the case of glucose consumption by the parent strain (ZM4), at lower dilution rates (D = 0.04-0.11 h$^{-1}$), the steady-state cell concentration increased with an increase in the dilution rate, indicating the significance of maintenance energy requirements at these low dilution rates. In the dilution rate range D = 0.11-0.2 h$^{-1}$, the steady-state cell concentration slightly decreased with an increase in the dilution ate. This was primarily due to the decrease in the conversion of xylose at dilution rates greater than 0.11 h$^{-1}$.

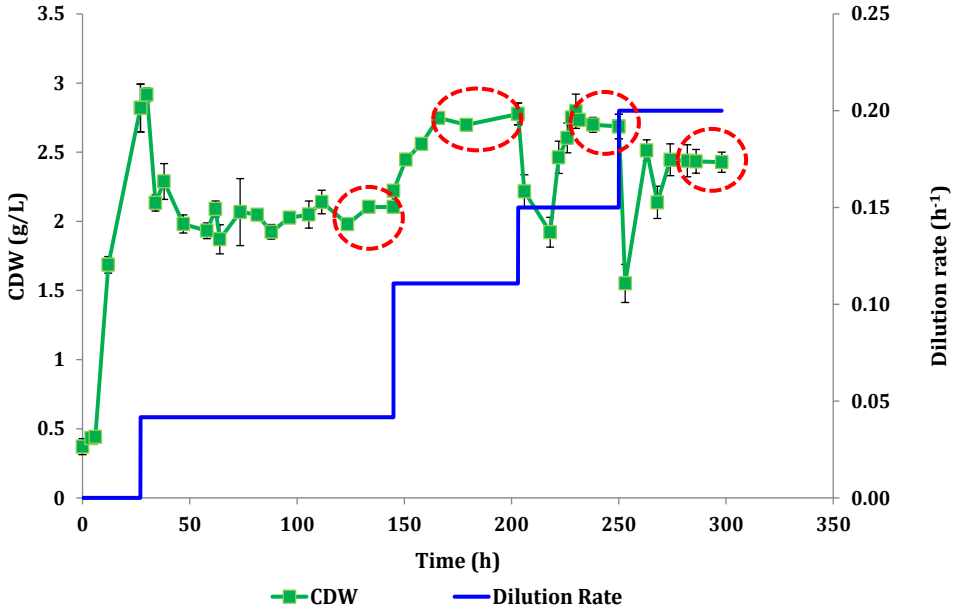


***Figure 70:*** *Continuous Culture CDW and dilution rate profiles for 5% (w/v) glucose and 5% (w/v) xylose fermentation by Z. mobilis 8b at controlled conditions of 33.5 ºC, pH 6.25.*

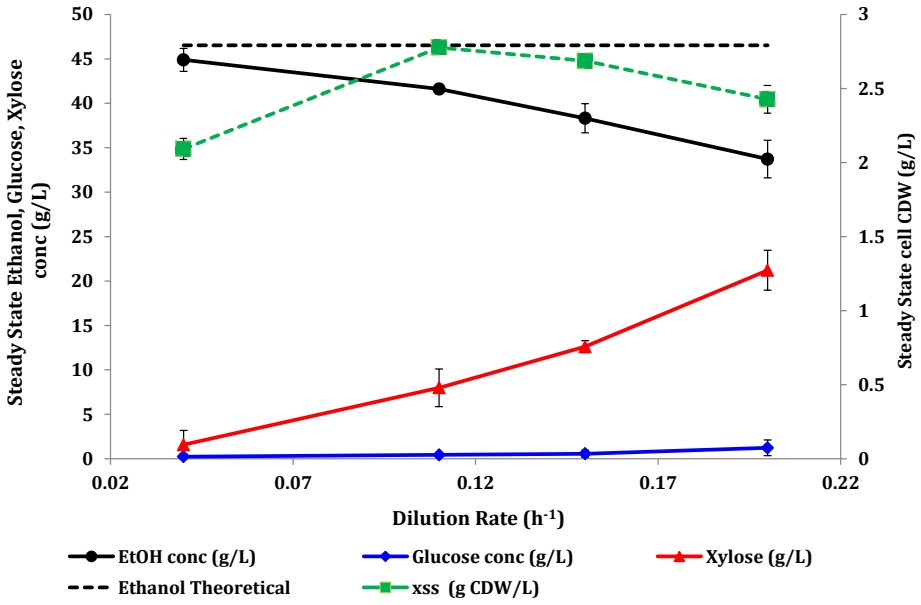


***Figure 71:*** *Steady-State continuous fermentation profiles of Z. mobilis 8b on 5% (w/v) glucose and 5% (w/v) xylose at various dilution rates (33.5 ºC, pH 6.25, 500rpm)*

To quantify the maintenance requirements of *Z. mobilis* 8b, the steady-state specific sugar consumption rate ($q_s$) and the specific ethanol production rate ($q_p$) were quantified at various dilution rates. Using *Equation 7.8* and extrapolating the $q_s$-D plot by means of regression analysis at D = 0 $h^{-1}$, it was found that maintenance coefficient was 0.68 g glucose-xylose.g $CDW^{-1}.h^{-1}$ (*Figure 72*). $Y_{x/s}^{max}$ was estimated from the reciprocal of the slope of the $q_s$-D regression line, and subsequently determined to be 0.041g CDW.g glucose-$xylose^{-1}$.

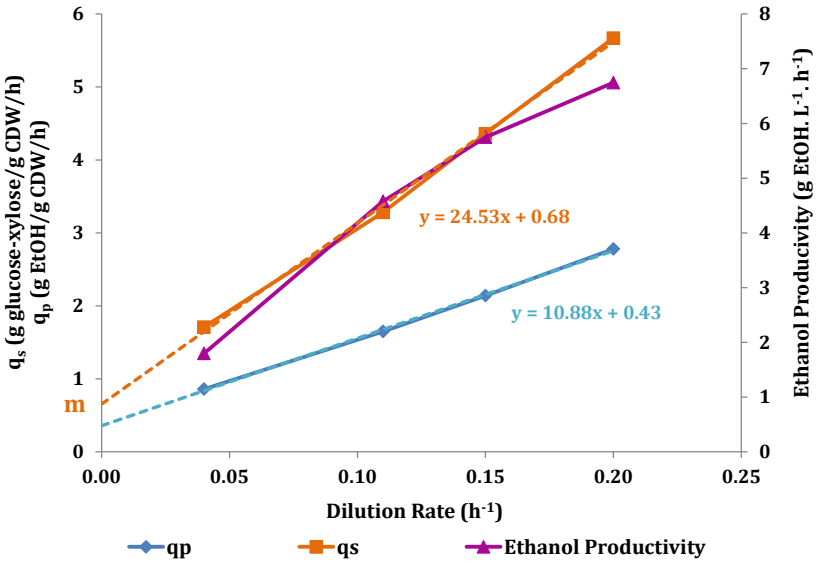


**Figure 72:** *Steady-State volumetric productivity, overall specific glucose-xylose consumption rate and specific ethanol production rate profiles at various dilution rates*

Comparing the maintenance requirements of the recombinant strain (*Z. mobilis* 8b) to those of the parent strain (*Z. mobilis* ZM4) in continuous culture (both at a 100g.L$^{-1}$ total substrate feed), it is evident that the maintenance energy coefficient of both strains was essentially the same. In fact, the slight difference may be attributed to the two experiments being performed at different fermentation temperatures and pHs (Lawford, 1988). This result indicates that the encoding of the genes necessary for xylose fermentation did not have a significant effect on the maintenance requirements of the parent strain (ZM4). This observation is consistent with literature reports for the xylose-fermenting strain *Z. mobilis* ZM4 (pZB5) (Rogers *et al.,* 1999). In the investigated dilution rate range, the highest volumetric ethanol productivity observed was 6.74 g EtOH.L$^{-1}$.h$^{-1}$ at D = 0.2 h$^{-1}$. Although this productivity may not necessarily be the optimum productivity, it is more than 5-fold greater than that obtained in batch culture (VP = 1.427 g EtOH.L$^{-1}$.h$^{-1}$).

At the dilution rate whereby the highest volumetric productivity was observed (D = 0.2h$^{-1}$) it was found that the steady state ethanol concentration was 33.7 g.L$^{-1}$. As one of the PI's, it had to be taken into consideration in determining the best dilution rate for operating the continuous culture fermenter. Considering that energy input to distillation in the ethanol production process is primarily proportional to final ethanol concentration from fermentation, the selection of the optimum fermentation dilution rate in continuous culture is not only determined by the highest productivity but the combination of a minimum ethanol concentration (required for distillation) and the highest volumetric productivity obtained from the continuous culture. Zacchi and Axelsson (1989) reported that ethanol recovery by distillation becomes economically feasible when the ethanol concentrations from the fermentation step is greater than 4% (w/v) (or 40g.L$^{-1}$). For example, assuming some pretreated hydrolyzate has a sugar concentration of 50g.L$^{-1}$ glucose and 50g.L$^{-1}$ xylose, the recommended operating dilution rate would be between 0.11 and 0.15 h$^{-1}$ in view of maintaining a minimum ethanol concentration of 4% (w/v) whilst maintaining a relatively high volumetric productivity. Within this recommended dilution rate range, the volumetric productivity

would be in the range 4.58 – 5.75 g EtOH.$L^{-1}$.$h^{-1}$, which is still more than 3-fold higher than the productivity in batch culture.

However, it can be seen that whilst fermentation by continuous culture is an attractive prospect, there is approximately 10 g.$L^{-1}$ unconverted xylose being continuously removed from the system. Therefore, there lies potential in increasing the rate of substrate conversion through the cell retention in view of minimizing the residual xylose concentration and subsequently maximizing the ethanol concentration and productivity from the fermenter to distillation.

## 7.3.2 Continuous Culture with Cell Retention

### 7.3.2.1 Cell Retention through Cell Immobilization

The extent of sugar conversion within an immobilized cell bioreactor was evaluated by immobilizing the bacterial cells within the macroporous structure of the tubular membrane and using the permeable layer to prevent the cells from leaking to the permeate stream. For this experiment, the experimental set-up indicated in *Figure 34* was used. In this instance, the MFU was used as an "immobilized cell bioreactor" and the 1.5L bioreactor was used as an unused substrate recirculation vessel (RV). A diagram of the immobilized cell bioreactor in operation is presented in *Figure 73*. A cell-free 5% (w/v) glucose substrate was fed through the lumen-side and permeated through a cell-containing macroporous support through the application of a TMP. Cell-free product was recovered from the permeate stream (shell-side). The immobilized cell bioreactor was operated at a constant TMP of 50kPa.

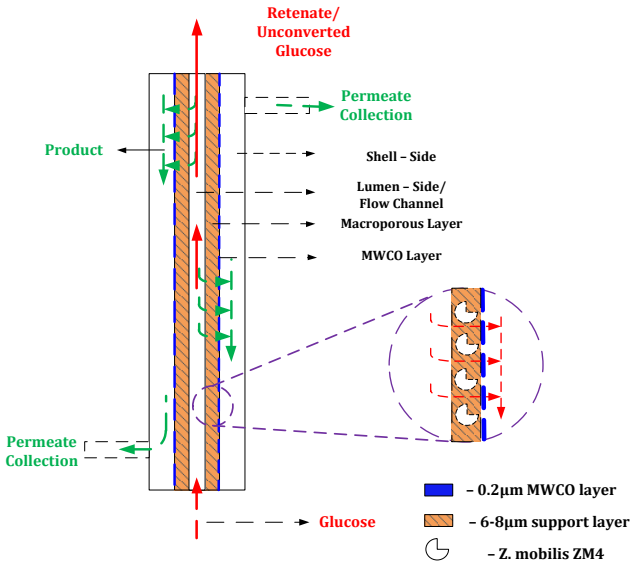


***Figure 73:*** *Immobilized cell bioreactor operating with lumen to shell flow configuration*

The amount of cells immobilized within the semi-permeable membrane at initial conditions was calculated by means of a mass balance around the entire system (*Figure 74*):

$$m_{immobilized} = m_{inoculum} + m_{substrate-feed} - m_{bleed} + m_{permeate} \qquad \textbf{(7.9)}$$

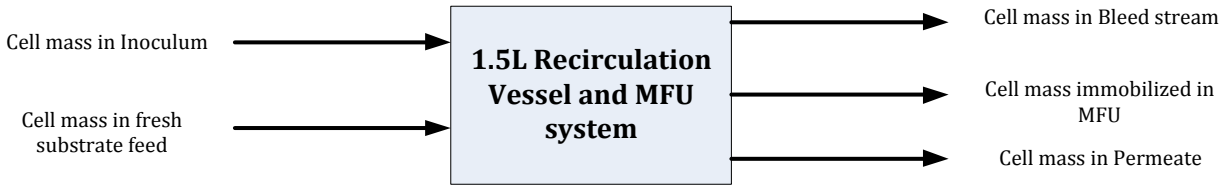


***Figure 74:*** *Block flow diagram of the mass balance around integrated membrane and bioreactor system for determining the initial mass of cells immobilized within the pores of the semi-permeable membrane*

Based on the proposed mass balance equation (Equation 7.9), it was determined that at initial conditions the mass of cells immobilized within the macroporous structure of the membrane was 0.188 g CDW. This mass represented 5.8% of the cell mass initially present in the inoculum. Sample calculations for the mass balance are presented in Appendix C.5.2.

After immobilizing the cells in the membrane, substrate was permeated through the membrane, essentially contacting the bacterial cells on the way through the membrane. In order to ensure that there was no cell growth in the RV and process tubing, the optical density of the RV was monitored continuously. Cell growth in the RV would indicate a loss of cells from the immobilization surface and subsequently result in a microbial growth in the RV. Cell growth in the RV would indicate a crossover in operation from cell immobilization to cell retention through cell recycling (or MRB operation). Therefore, by profiling the cell mass concentration in the RV, the point of departure from cell immobilization to cell retention (MRB operation) can be identified.

The cell mass concentration profile within the recirculation vessel and the change in the permeate flux throughout the entire experiment is presented in *Figure 76*. As shown by the cell concentration profile, fermentation through cell immobilization commenced for approximately 50 hours, followed MRB operation for the next 90 hours. During the cell immobilization phase, there was virtually no statistically significant change in the glucose concentration both in the RV and in the permeate stream. The statistical insignificance of the change in the glucose concentration during the cell immobilization phase was confirmed by a t-test. Moreover, within this timespan, the ethanol concentration in the membrane permeate stream was less than 1±0.12 $g.L^{-1}$. Additionally, the permeate flux had declined by approximately 30% to 7.5 $L.m^{-2}.h^{-1}$.

After 50 hours in operation, cell mass was detected in the RV. The evolution in cell mass in the RV suggested that the biocatalysts might have escaped from the macroporous support into the bulk substrate in the lumen section of the membrane and into the RV. However, based on the experimental data, the precise mechanism of the evolution in cell mass in the RV remained unclear.

Considering the glucose and ethanol concentrations within the cell retention phase (*Figure 75*), the ethanol concentration detected in the permeate stream increased towards the theoretical yield. This observation (near theoretical ethanol yield during cell retention by recycling phase) indicated that

not only were the immobilized cells active, but also ruled out the probability of the observed cell concentration increase in the RV being due to contamination by external microorganisms.

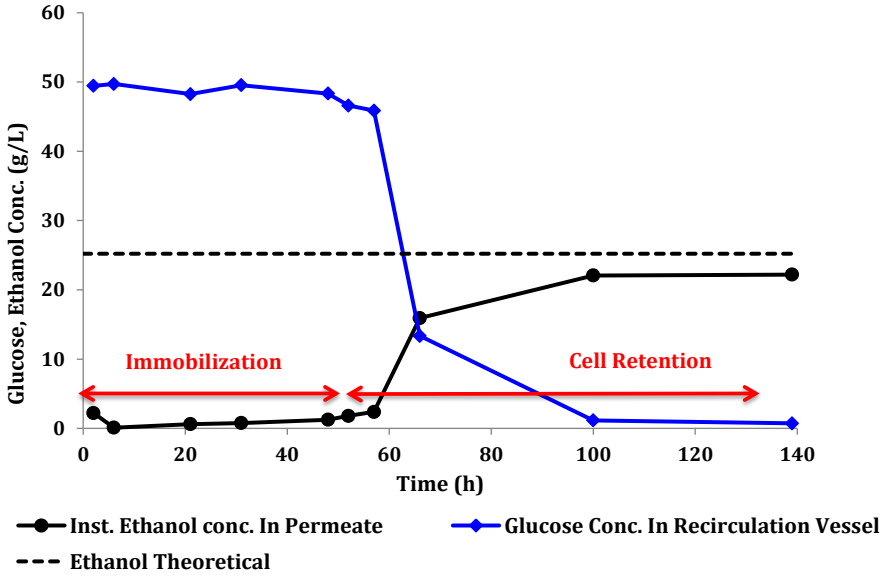


***Figure 75:*** *Glucose concentration in recirculation vessel and instantaneous ethanol concentration in permeate during crossover from cell immobilization to cell retention*

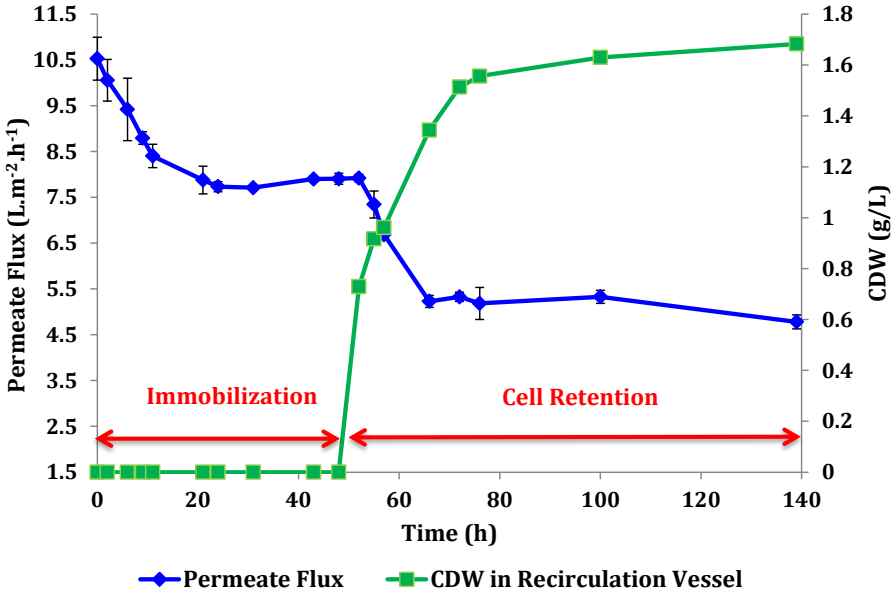


***Figure 76:*** *Change in the permeate flux and CDW during crossover from cell immobilization to cell retention*

Nevertheless, this experiment illustrated that the conversion of glucose by immobilized cells was essentially zero. The low substrate conversion could possibly be attributed to the low residence time of the substrate through the cell containing macroporous support (high characteristic time relative to the specific growth rate). Under the current filtration conditions, the extent of reaction within the MFU could be assumed to be zero.

### 7.3.2.2 *MRB FERMENTATION*

#### *7.3.2.2.1 HYDRAULIC DILUTION RATE*

The hydraulic dilution rate ($D_H$) represents the inverse residence time of the substrate/product within the MRB system. As a result, the hydraulic dilution rate directly affects the volumetric productivity of the MRB system. In the current system, $D_H$ was highly dependent on the filtration performance (indicated by the permeate flux) of the MFU. As indicated by the CCD statistical design, the cell concentration and the TMP were the most significant parameters concerning the permeate flux obtained by the MFU. The TMP was an independent parameter that could be varied in an attempt to increase hydraulic dilution rate range of the system. However, since the cell concentration was dependent on the substrate concentration in the fermenter feed stream and the fermentation conditions (such as temperature, pH, and ethanol concentration), it could not be varied as an independent parameter. Therefore, in the investigation of the effect of the process conditions on the hydraulic dilution rate, only the TMP was varied as an independent variable.

The variation of the permeate flux during the fermentation of the 50 $g.L^{-1}$ glucose-50 $g.L^{-1}$ xylose substrate was shown in *Figure 65* in *section 0*. The change in the hydraulic dilution rate in response to the change in the permeate flux due to membrane fouling and periodic back-flushing is presented in *Figure 77*.

In this experiment, start-up conditions were defined by operating the MRB system in batch culture mode for the first 8 hours until the cell concentration in the fermenter was approximately 2.5$g.L^{-1}$. Thereafter, cell recycle was initiated, with the MFU operated at a TMP of 50kPa and a 0.255$m.s^{-1}$. During this phase, the cell concentration in the system rapidly increased to approximately 5.5-5.3 $g.L^{-1}$. However, the $D_H$ of the system experienced a sharp decrease from initial value of 0.03 $h^{-1}$ to 0.014 $h^{-1}$ (a 53% drop) (*Figure 77*). The decrease in the dilution rate due to membrane fouling corresponded with a 2-fold increase in the substrate/product residence time from 33.3 h to approximately 71 h. Pseudo-steady state conditions were reached after approximately 50 hours. Fermentation was allowed to continue for an additional 60 hours after pseudo-steady state had been achieved.

To increase the system $D_H$, after 110 hours in operation, the TMP across the MFU was increased to 100kPa (CFV maintained at its highest possible setting of 0.433$m.s^{-1}$) and maintained constant for 90 hours. The increase in the TMP and CFV resulted in an initial increase in the $D_H$ to 0.055 $h^{-1}$. However, due to the significance of membrane fouling, the dilution rate decreased sharply to approximately 0.025 $h^{-1}$ (a 55% drop). The drop in $D_H$ corresponded with an increase in substrate/ethanol residence time from 18.2 h to 40 h. Nevertheless, pseudo steady-state conditions were realized after approximately 145 hours of operation.

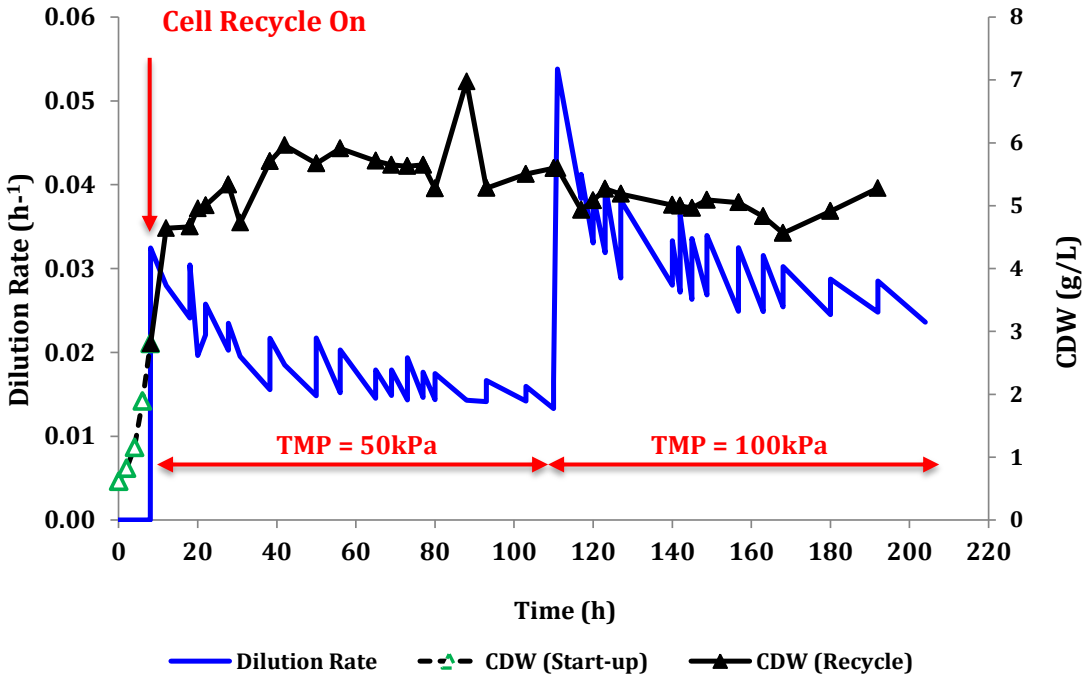


***Figure 77:*** *Change in the dilution rate in response to change in the cell concentration, TMP and periodic back-flushing*

In summary, operation at higher TMP (above the critical TMP) resulted in an increase in the hydraulic dilution rate. However, even though operation at the higher TMP resulted in an increase in the pseudo-steady state $D_H$ (from 0.014 $h^{-1}$ at 50kPa to 0.025 $h^{-1}$ at 100kPa), the increased $D_H$ was still significantly lower than the dilution rates achieved during continuous culture (D = 0.04-0.3 $h^{-1}$). This already indicated that in order to make the MRB process strategy feasible for ethanol production, the addition of a MFU to continuous culture should be justified by its ability to achieve dilution rates higher than continuous culture (without cell retention) whilst maintaining a substrate high conversion rate. As a result, improving the hydrodynamic conditions (e.g. operating at higher CFVs) in view of alleviating membrane fouling or increasing the MFU surface area are required in order to increase the achievable dilution rates of the system at the current fermentation conditions.

In addition, operating the MFU at the higher TMP resulted in decreased water permeability after chemically cleaning the membrane. This indicated that permanent membrane fouling had occurred during operation at the higher TMP. However, water permeability was recovered within ± 5% of its original permeability whilst operating the MFU within the MRB system at 50kPa. Therefore, all the subsequent MRB fermentations were limited to operating the MFU at 50kPa in view of extending the lifetime of the tubular membranes.

#### 7.3.2.2.2 ETHANOL PRODUCTION

The fermentation kinetics of the MRB system were evaluated at the conditions described in the previous section. The glucose, xylose and ethanol residual concentrations from the MRB system are shown in *Figure 78*.

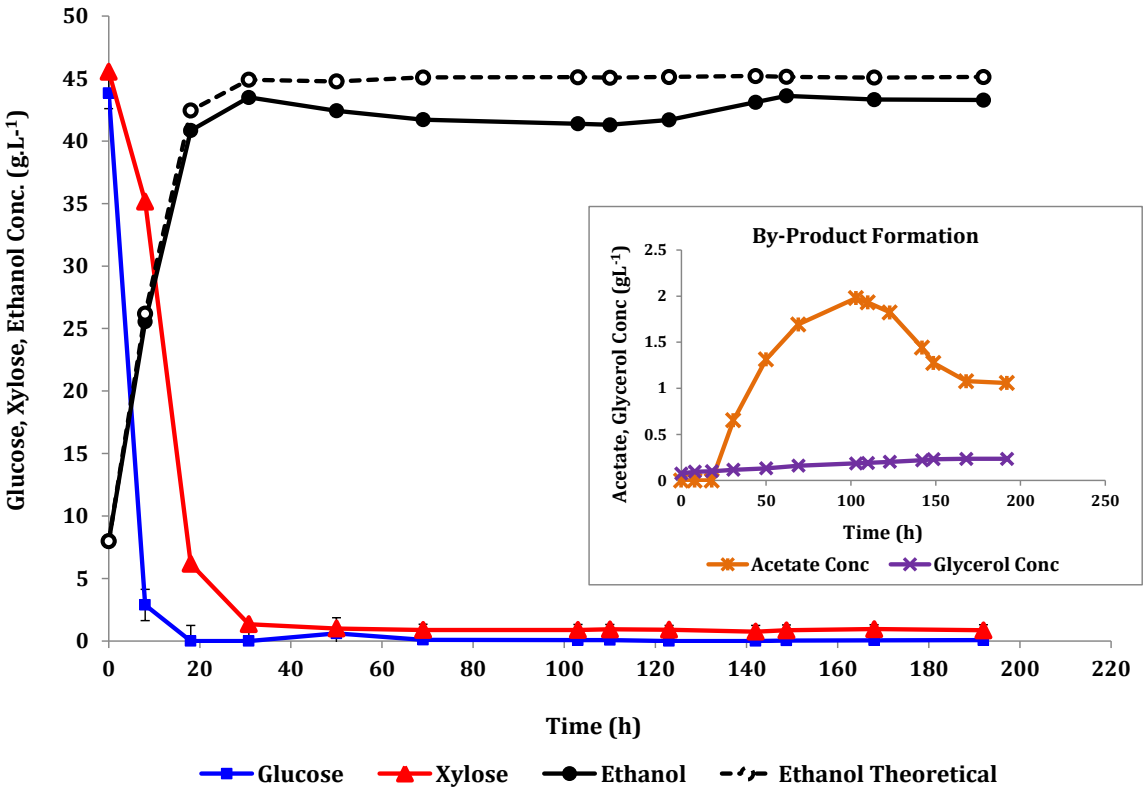


***Figure 78:*** *The residual glucose, xylose and ethanol concentrations during MBR fermentation of a 50-50 glucose-xylose substrate by Z. mobilis 8b at 33.5 °C, pH 6.25.*

The theoretical ethanol concentration was calculated by assuming the selectivity of the biocatalyst was 100% based on the amount of sugar consumed (*Figure 78*). Based on residual concentrations sampled from the fermenter, it is evident that both glucose and xylose consumption were complete after approximately 28 hours. The time required to reach complete glucose-xylose consumption in the MRB was approximately 5 hours faster relative to batch fermentation even at the low dilution rate. Moreover, after 20 hours of operation, the residual xylose concentration is approximately 5 $g.L^{-1}$. This residual xylose concentration is significantly lower than the residual xylose concentration obtained in batch culture at the same time (*Figure 53*). This observation indicates that the MRB improved the overall rate of xylose consumption. The faster conversion rate can be attributed to the higher cell density of the MRB relative to the batch culture. The higher cell density facilitates higher substrate-cell contact and subsequently increases the overall rate of substrate conversion. However, throughout the entire experimental run the average residual xylose concentration at pseudo-steady state was approximately 0.875 $g.L^{-1}$ (corresponding to a xylose conversion of 98%).

Profiling the ethanol concentration during the low TMP operation phase (t = 8-110 h in *Figure 78*), it is apparent that the ethanol concentration closely followed the theoretical concentration for the first 30 hours until both glucose and xylose were exhausted. Thereafter, the ethanol concentration decreased slightly and subsequently deviated from the theoretical ethanol concentration profile. As the ethanol concentration decreased, an increase in acetate and glycerol concentrations was detected. The possible reduction in the ethanol concentration after the complete substrate utilization may be attributed by degradation of ethanol in the system at the low dilution rates. However, the mechanism of ethanol degradation remains unclear based on the experimental data. Once, the acetate concentration stabilized at approximately 1.9±0.15 $g.L^{-1}$, the ethanol concentration had decreased to 41.7±0.3 $g.L^{-1}$ (corresponding to a yield of 0.471 g EtOH/g glucose-xylose or 92.5% of the theoretical yield).

Operating at the higher TMP (t = 110-200 h in *Figure 78*), the concentration of the by-product acetate decreased approximately 50% to 1.05 ± 0.05 $g.L^{-1}$. The reduction in the residual acetate concentration corresponded with a higher final ethanol concentration of 43.41 ± 0.18 $g.L^{-1}$ and an ethanol yield of 0.49 g/g (96% of the theoretical yield). This result suggests that decreasing ethanol residence time in the system resulted in lower degradation of ethanol and subsequently facilitated a higher final ethanol concentration. Nevertheless, at pseudo-steady state conditions, a stable ethanol concentration of 43.41 ± 0.18 $g.L^{-1}$ was produced at the low dilution rate of 0.025 $h^{-1}$ for at least 45 hours.

#### 7.3.2.2.3 VOLUMETRIC PRODUCTIVITY

In response to the change in the hydraulic dilution rate due to membrane fouling, the volumetric productivity was expected to change proportionally to the dilution rate (see *Equation 2.6*). The change in the volumetric productivity during the fermentation of the 50 $g.L^{-1}$ glucose- 50 $g.L^{-1}$ xylose substrate at the same experimental conditions mentioned in *sections 7.3.2.2.1* and *7.3.2.2.2* is shown in *Figure 79*.

Considering the low TMP operation phase (t = 8-110 h in *Figure 79*), the volumetric productivity initially declined sharply and stabilized at a value of approximately 0.6 g $EtOH.L^{-1}.h^{-1}$. Since the volumetric productivity is the product of the ethanol concentration and the hydraulic dilution rate, the low volumetric productivity achieved by the MRB clearly illustrates that the permeate flux through the membrane is the bottleneck of the productivity obtainable from the current system.

Even though operating at the higher TMP (t = 110-200 h in *Figure 79*) did result in an increase in the pseudo-steady state volumetric productivity (VP = 1.13 g $EtOH.L^{-1}.h^{-1}$), the increase was still below that of both batch (VP = 1.23 g $EtOH.L^{-1}.h^{-1}$ and continuous culture (without cell retention) (VP = 4.58 – 5.75 g $EtOH.L^{-1}.h^{-1}$ at D = 0.11-0.15 $h^{-1}$). However, comparing the volumetric productivity of the MRB to that of fermentation in continuous culture (without cell retention) at different dilution rates is not a clear indicator in determining which process strategy is better.

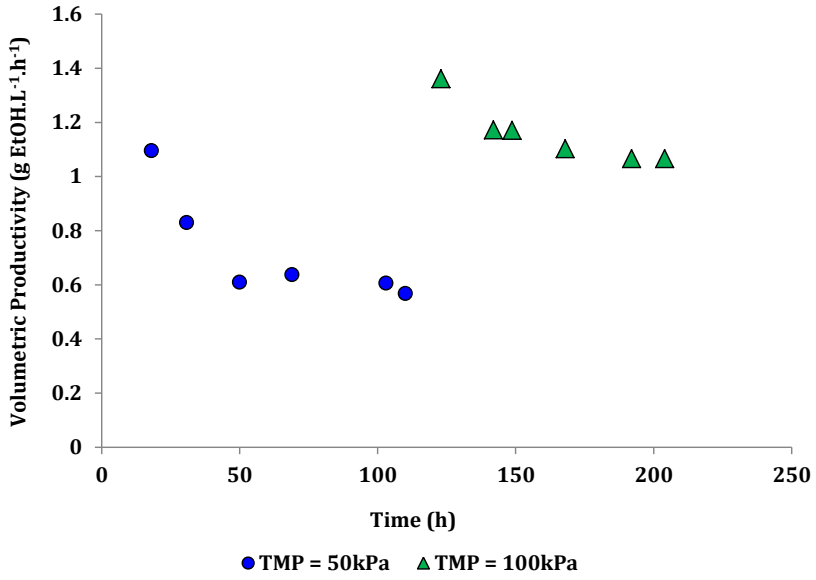


***Figure 79:*** *Volumetric productivity change during 50-50 g.L$^{-1}$ glucose-xylose fermentation by Z. mobilis 8b at 33.5 °C, pH 6.25, TMP 50-100kPa*

To put the performance of the MRB relative to that of continuous culture into perspective, the volumetric productivity of both process strategies as a function of the dilution rate (pseudo-steady state $D_H$ in the case of MRB) is shown in *Figure 80*. Since continuous culture experiments were performed in the dilution rate range 0.04-0.2 h$^{-1}$, the productivity in continuous culture at lower dilution rates was extrapolated from the experimental data using regression.

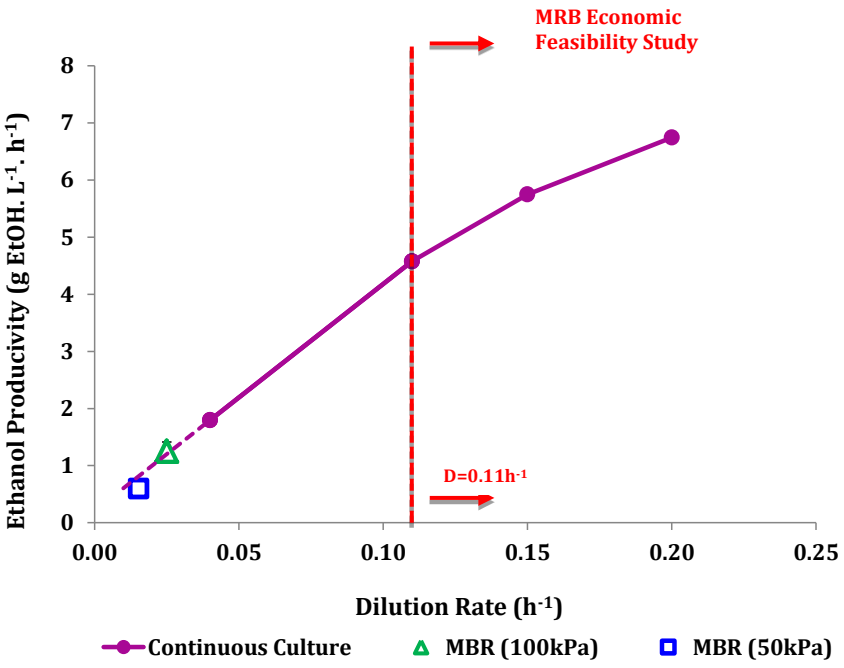


***Figure 80:*** *The comparison of the volumetric productivity of fermentation performed in continuous culture and in MBR as a function of the dilution rate*

Based on the extrapolation of the volumetric productivity for dual substrate fermentation in continuous culture, it is evident that the volumetric productivity of the MRB system was essentially the same as that achieved in continuous culture at low dilution rates. This indicates that at dilution rates lower than 0.11 $h^{-1}$, where near theoretical yields were obtained in both continuous culture and the MRB system; both systems would achieve the same volumetric productivity. However, in this dilution rate range, continuous culture would be the more favourable process strategy from an economic perspective considering the absence capital costs for the microfiltration unit, its maintenance and energy input to drive and operate the recirculation stream through the MFU.

In order to evaluate feasibility of the MRB system, the dilution rate achieved by the MRB should be greater than 0.11$h^{-1}$. For at dilution rates greater than 0.11$h^{-1}$, the steady-state ethanol concentration in continuous culture was lower than 40$g.L^{-1}$, which is the required concentration for enabling ethanol recovery by distillation to be economically feasible. Hence, assuming the MRB system would facilitate an increase the rate of substrate conversion and maintain near theoretical pseudo-steady state ethanol concentrations at higher dilution rates, an economic analysis would be necessary to evaluate the viability of the MRB process as an alternative fermentation strategy to continuous culture. The economic feasibility would take into account the required capital cost for the MFU and its maintenance relative to the increase in the overall operational revenue generated based on the projected improved volumetric productivity.

#### 7.3.2.3 *Effect of the substrate composition on the MRB Performance*

The analysis reported in *section 7.3.2.2* holds only for a 50 $g.L^{-1}$ glucose-50 $g.L^{-1}$ xylose substrate. It is well known that continuous culture is very sensitive to upstream changes in the substrate concentration and composition. Moreover, since hydrolyzates are hardly maintained at the same sugar concentrations, the fermentation of hydrolyzates with varying glucose-xylose composition would be much simpler in MRB systems where cell washout conditions are avoided by retaining the biocatalysts. To investigate the fermentation performance of the MRB at different substrate compositions, two hypothetical cases were considered. First, the fermentation of a glucose rich substrate was evaluated by selecting the sugar composition (75-25 $g.L^{-1}$ glucose-xylose) reported for the Iogen process (see *Figure 13*). Similarly, the fermentation of a xylose-rich substrate was evaluated by selecting a sugar composition reported for pre-treated corn stover in the Aden *et al.,* (2010) process design (*see Figure 14*). Both fermentations were performed at 33.5 $^{o}$C, pH 6.25, TMP = 50kPa, and CFV = 0.255$m.s^{-1}$.

The residual glucose, xylose and ethanol concentration profiles for xylose-rich substrate fermentation are shown in *Figure 81*. At start-up conditions, the MRB was operated in batch culture mode for the first 19 hours until the cell concentration was approximately 2.2$g.L^{-1}$. After switching to cell retention mode, the permeate flux declined and reached pseudo-steady state conditions after approximately 50 hours. Similar to the case of 50 $g.L^{-1}$ glucose-50 $g.L^{-1}$ xylose substrate fermentation, the permeate flux dropped to an average value of 5.58 $L.m^{-1}.h^{-1}$. This permeate flux corresponded to

an average dilution rate of 0.017$h^{-1}$ (or a substrate/product mean residence time of 58 hours). However, even at this low dilution rate, the pseudo-steady state ethanol concentration was approximately 51.34 ±0.65 g.$L^{-1}$ and the ethanol yield was maintained above 90% throughout the experimental run.

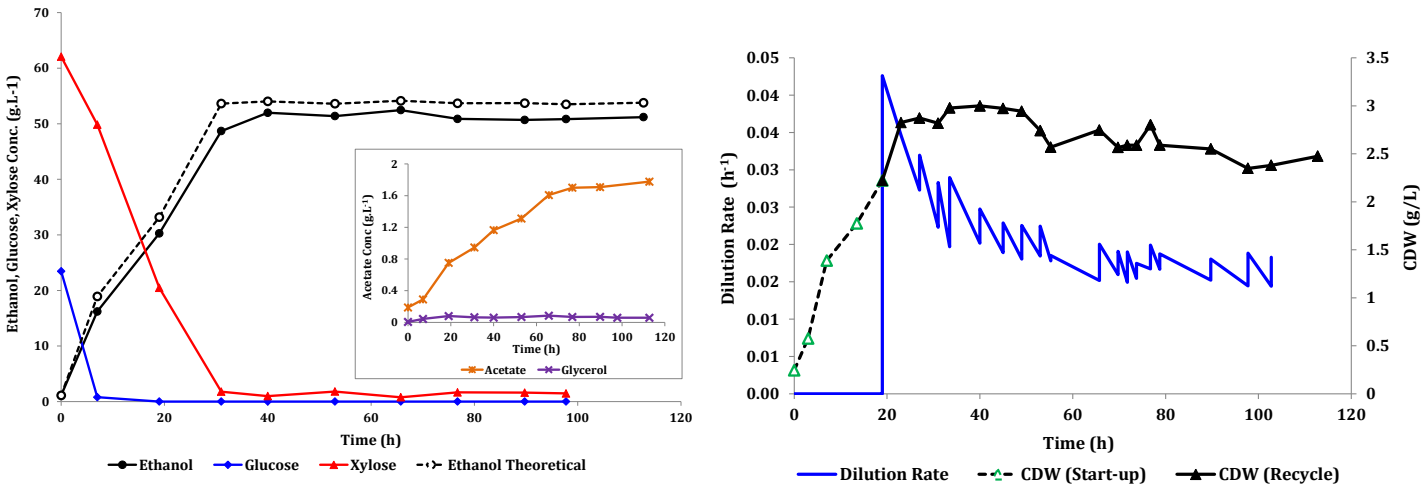


***Figure 81:*** *Residual glucose, xylose and ethanol concentrations from MBR fermentation of xylose rich substrate (left), dilution rate decline (right). Experimental conditions: $s_{f1}$ = 29.32g.$L^{-1}$, $s_{f2}$ = 77.6 g.$L^{-1}$, T = 33.5 °C, pH 6.25.*

The high theoretical yields were maintained even in the presence of 1.8 ± 0.2 g.$L^{-1}$ of the inhibitory compound acetate. The maintenance of high microbial activity in the presence of acetate indicates that either *Z. mobilis* 8b is naturally tolerant of this inhibitory compound at these concentrations or the recycled cells are become adapted to the toxic environment and subsequently maintain high microbial activity. The recycling of fermentation biocatalysts has been reported to improve yeast tolerance to hydrolyzate inhibitors through adaptation and subsequently reducing detoxification requirements prior to the fermentation step (Jeffries and Sreenath, 2000; Purwadi *et al.,* 2007).

Similarly high ethanol yields were achieved during glucose-rich substrate fermentation (see *Figure 82*). However, the ethanol yield from the glucose rich substrate fermentation was slightly lower than the previous two cases (92% of the theoretical yield after 116 hours in operation). The residual acetate concentration was approximately 3.4 ±0.3 g.$L^{-1}$ by the time the fermentation was stopped. Similar to the previous two cases, acetate production after the complete utilization of glucose and xylose coincided with a reduction in the residual ethanol concentration in the fermenter. Hence, for maximizing ethanol recovery from fermentation, it is essential that the residence time of ethanol in the MRB be minimized in view of preventing/minimizing ethanol degradation.

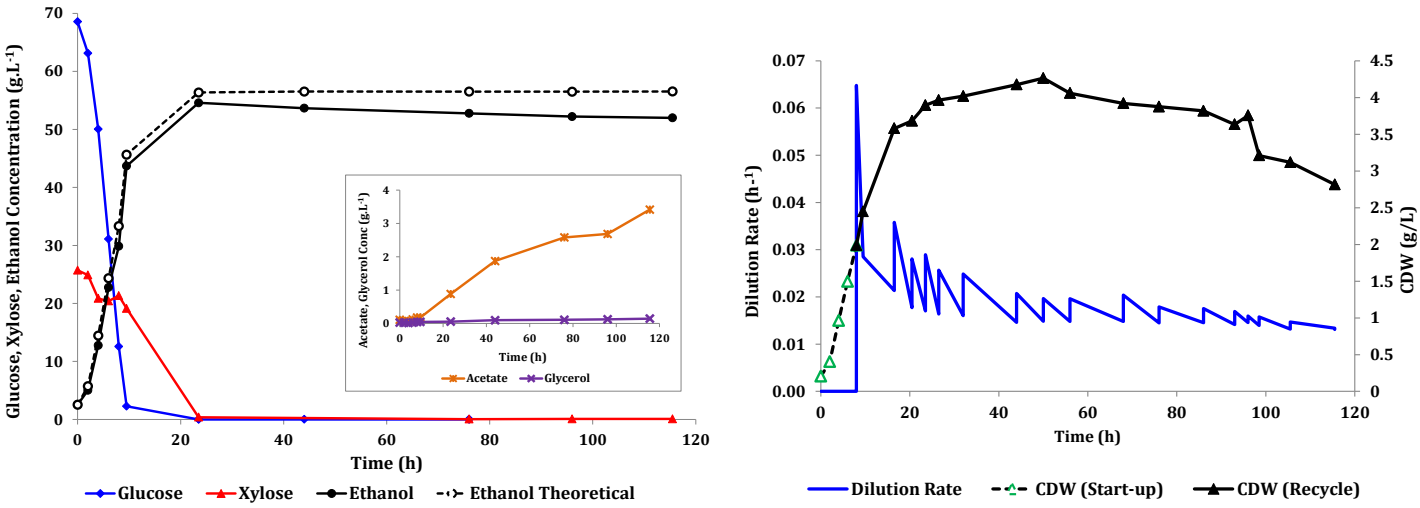


***Figure 82:*** *Residual glucose, xylose and ethanol concentrations from MBR fermentation of xylose rich substrate (left), dilution rate decline (right). Experimental conditions: $s_{f1}$ = 80.64 g.L$^{-1}$, $s_{f2}$ = 30.25 g.L$^{-1}$, T = 33.5 ºC, pH 6.25.*

Considering all three substrate compositions, the MRB system facilitated complete glucose and xylose consumption with ethanol yields greater than 92%. In *section 7.1.3* it was shown that the overall rate of xylose consumption is positively affected be the fraction of glucose present in the fermentation media. Following this result, it was expected that the volumetric productivity in the MRB would be higher for the glucose-rich substrate fermentation relative to the systems with higher xylose concentrations. However, the volumetric productivity achieved from the MRB fermentation was essentially the same for all three tested mixed sugar substrates i.e. 0.61±0.18 g. EtOH.L$^{-1}$.h$^{-1}$ (all at low pressure). This indicated that under the current operating conditions, the volumetric productivity of the MRB system was not reaction limited but limited by the low dilution rate of the system. Therefore, there exists potential for enhancing the volumetric productivity by improving the hydrodynamic conditions (higher CFVs and optimizing the TMP), increasing the membrane surface area and/or utilizing more complex permeate flux recovery techniques.

## 7.4 Kinetic Modeling of MRB Fermentation System

### 7.4.1 Permeate Flux Prediction

Prior to simulating the MRB kinetic model, the simulation of the transient permeate flux was required in order to describe the change in the MRB system hydraulic dilution rate with time. The transient permeate flux rate was predicted by fitting a semi-empirical correlation (Equation 6.13) to experimental data using regression analysis and least squares to estimate the fouling rate constant (b). Since the MFU was subject to periodic back-flushing during operation, the semi-empirical model was fitted to the average of the flux before and after back-flushing. The model fit to the permeate

flux data for the 50 $g.L^{-1}$ glucose-50 $g.L^{-1}$ xylose substrate (or 50-50 G-X) fermentation experiment is shown in *Figure 83*. The transient model fitted the experimental data relatively well throughout the experimental data range. The high degree of model fit was indicated by an $R^2_{adj}$ value above 0.9. The fouling rate constant was determined to be 0.3 units. The fouling rate constant defines the magnitude of rate at which the permeate flux decreases due to membrane fouling.

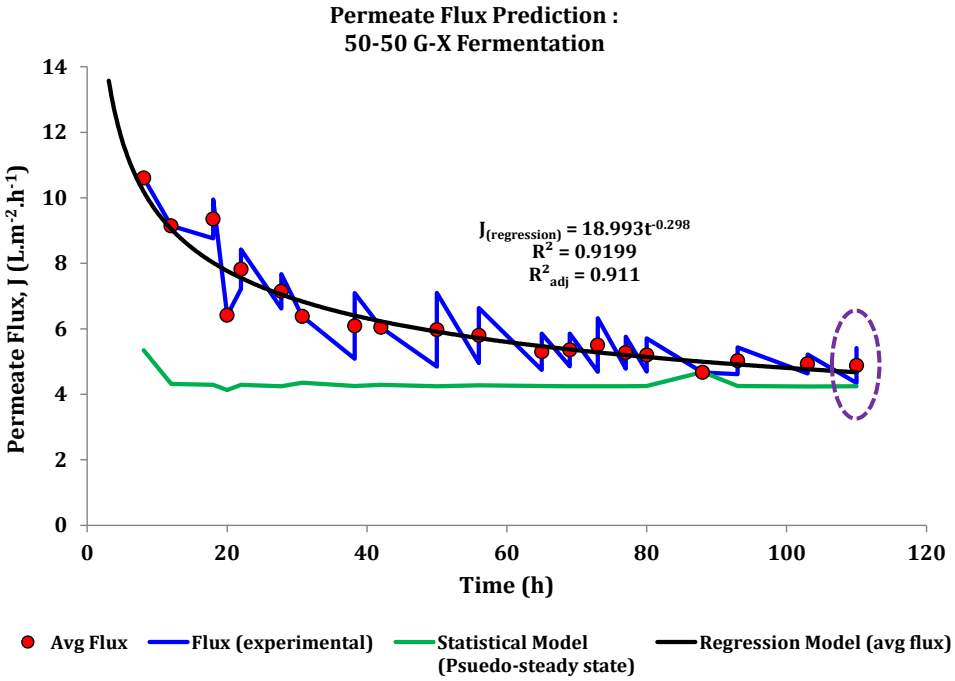


***Figure 83:*** *Transient and pseudo-steady state permeate flux prediction using semi-empirical model and statistical model respectively*

The fitted model was also compared to the pseudo-steady state statistical model developed in section *7.2.3.1.* Ideally, the statistical model should intersect the semi-empirical model at pseudo-steady state conditions defined by a permeate flux decline of less than 5%. As evidenced in *Figure 83*, both the experimental data and the intersection of the statistical and empirical models suggest that pseudo-steady state conditions were reached at approximately 90 hours. After 90 hours of operation, the flux recovery through membrane back-flushing became insignificant, thus indicating that membrane fouling became "irreversible" at approximately 90 hours.

The validation of the semi-empirical model was performed by fitting the semi-empirical model to the permeate flux experimental data extracted from both the xylose-rich and glucose-rich substrate MRB fermentations (*Figure 84*). Considering the model fit to both sets of the permeate flux experimental data, the model was significantly inaccurate in predicting the permeate flux during the initial phase (first 10-15 hours) of each experiment. The initial phase corresponds to the rapid deposition of the microbial cells onto the membrane surface (phase I-III in the fouling mechanism in *section 3.3.3*). Nevertheless, the model accurately predicted the transient change in the permeate flux once the rate of cellular sub-layer deposition had stabilized and subsequently results in a slow decline the permeation rate.

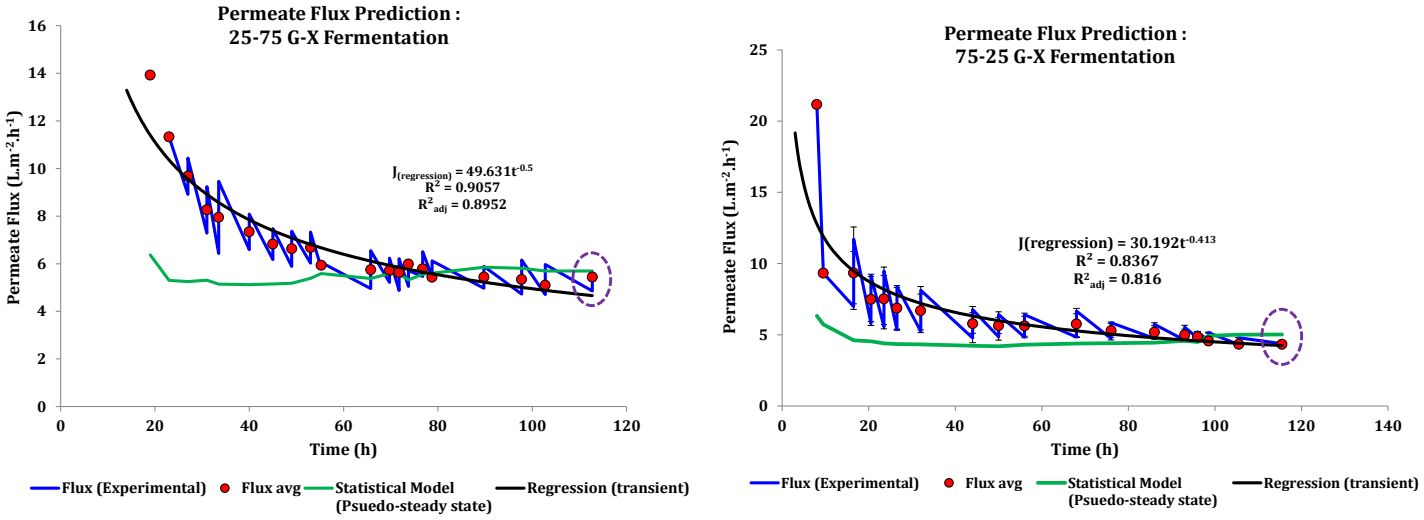


***Figure 84:*** *Permeate flux prediction for xylose-rich substrate fermentation (left) and glucose-rich substrate fermentation (right)*

In both instances, the pseudo-steady state permeate flux predicted by the statistical model was within 5% of the experimentally determined permeate flux (at the end of each run). The significance of the statistical model will become apparent in the discussion of the requirements for MRB process optimization using the kinetic model.

Once it was established that the empirical model was sufficient to predict the transient permeate flux rate, the hydraulic dilution rate was related to the permeate flux using Equation 6.12.

### 7.4.2 SIMULATION RESULTS

The simulation of the kinetic model was initially performed on the 50-50 G-X substrate fermentation system. The model was applied thereafter to the 25-75 G-X and 75-25 G-X substrate fermentations as a means of validating the model at different experimental conditions.

#### 7.4.2.1 MODEL SIMULATION

The initial values for estimating the variable model kinetic parameters were calculated during the "start-up or batch" phase of the MRB system operation. The calculation procedure for the initial parameters was similar to the approach adopted in *section 7.1.4*. The simulated profiles for the cell concentration (CDW), glucose, xylose, and ethanol predicted by the kinetic model in conjunction with the experimental data are shown in *Figure 85*. A sample of the excel spreadsheet for the solution of the system of ODEs (equations 6.18-23) using the 4$^{th}$ order Runga-Kutta and the minimization of $RSS_{total}$ using Excel$^{TM}$'s Solver are presented in Appendix C.5.3 and C.5.4 respectively. The solution algorithm previously presented in section 6.4.2 was applied.

Similar to the analysis of the batch kinetic data, the model predicts that the fermentation of glucose and xylose occurs in two phases. The model describes that the first phase is characterized by a high rate of ethanol production with preferential glucose consumption, followed by a slower rate of

ethanol production on xylose as the primary substrate (after glucose is exhausted) during the second phase. However, the developed model performed poorly for the prediction of the residual ethanol concentration as evidenced by the deviation of the predicted ethanol concentration from the experimental value at fermentation time greater than 40 hours. The current model did not take into account the formation of acetate, which is a fermentation by-product. In the analysis of the batch fermentation data, it was experimentally observed that when the ethanol residence time was increased in the fermenter, ethanol degraded to acetate to some extent. Therefore, to further improve the model prediction for accurate ethanol concentration prediction, the formation of acetate needs to be taken into account. The following mass balance equation was, therefore, added to the system of ODEs defined in *section 6.4.2*:

$$y_1\,(t, x, s_1, s_2) = \frac{dAc}{dt} = D(\,-Ac) - \{\,\alpha \frac{q_{pmax_{Ac_1}} * s_1}{K_{sp_{Ac1}} + s_1} + (1-\alpha)\frac{q_{pmax_{Ac_2}} * s_2}{K_{sp_{Ac2}} + s_2} * x \qquad \textbf{(7.9)}$$

In equation 7.9, **Ac** denotes the acetate concentration, $\mathbf{q_{p\_max_{AC_1}}}$ is the maximum specific acetate production rate in the first growth phase, $\mathbf{K_{sp_{AC1}}}$ is the saturation limitation for acetate production at low glucose concentrations, $\mathbf{q_{p\_max_{AC_2}}}$ is the specific acetate production rate in the second growth phase, and $\mathbf{K_{sp_{AC1}}}$ is the saturation limitation for acetate production at low xylose concentrations.

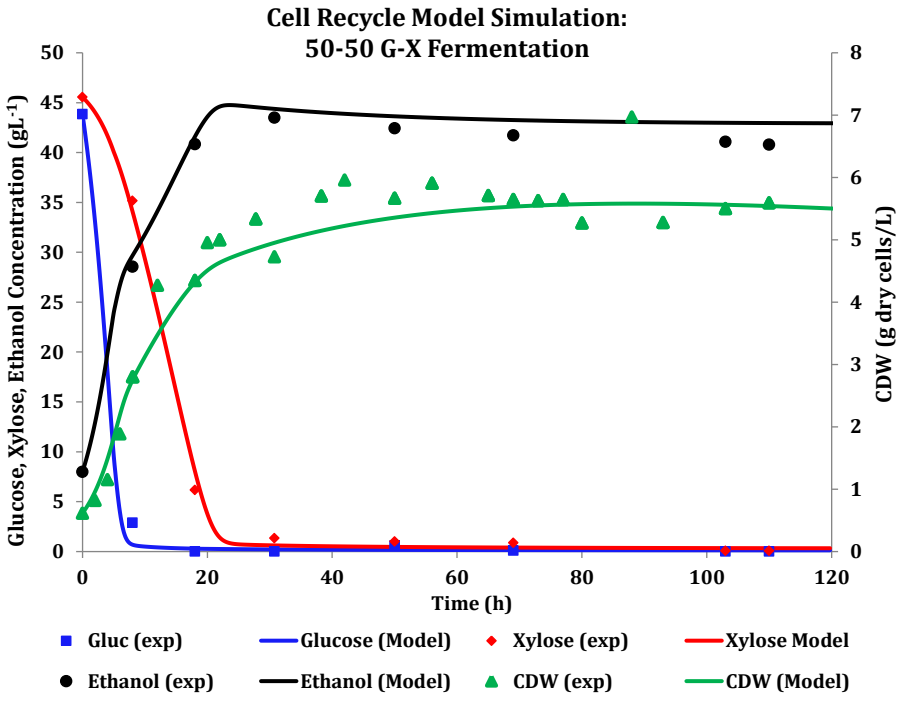


***Figure 85:*** *Cell recycle experimental data and model simulation of the 50-50 G-X substrate fermentation by Z. mobilis 8b*

Graphical analysis of *Figure 86* illustrates that the model prediction with the inclusion of acetate formation into the kinetic model is in good agreement with the experimentally determined results. On a statistical basis, the comparative degree of model fit was highlighted through the calculation of

the adjusted correlation coefficient's ($R^2_{adj}$) of the model predicted CDW, glucose, xylose and ethanol profiles relative the experimental data. $R^2_{adj}$ values of 0.995, 0.997, 0.936 and 0.998 were obtained for each of the four aforementioned profiles respectively. The minimum $RSS_{total}$ as predicted by the model was found to be 0.08. A small $RSS_{total}$ (<0.1) indicates close agreement of the model prediction with the experimentally determined data.

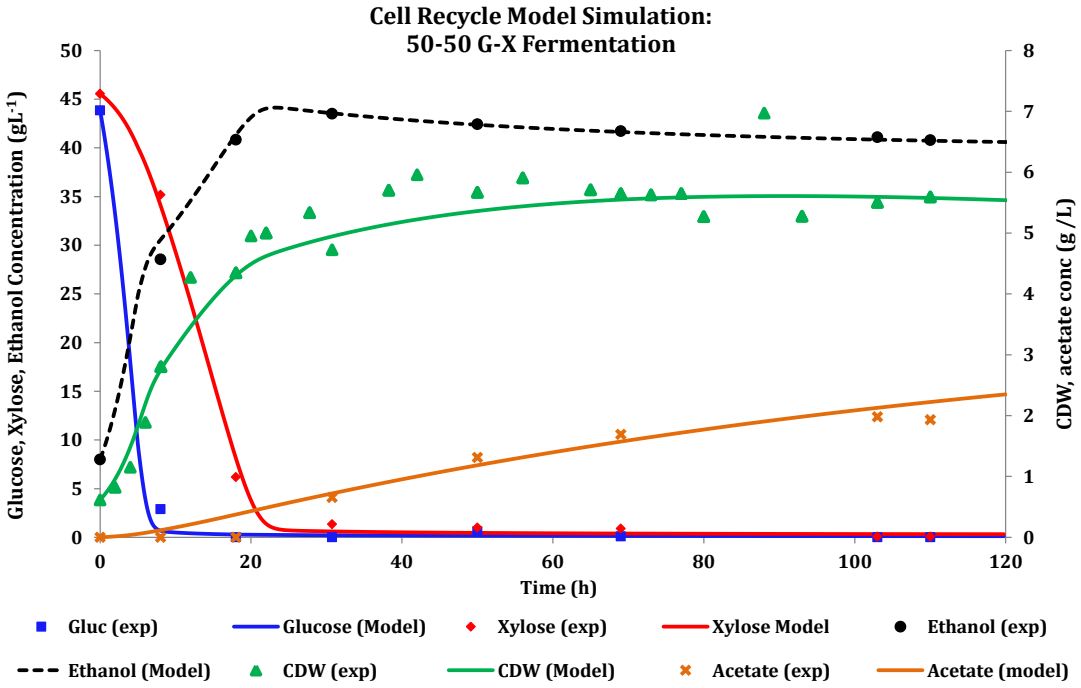


***Figure 86:*** *Cell recycle experimental data and model simulation of the 50-50 G-X substrate fermentation by Z. mobilis 8b with acetate formation taken into account*

Within the parameter constraints (to ascertain biological relevance), the kinetic parameters estimated from the minimization of the $RSS_{total}$ of the model prediction relative to experimental data are shown in *Table 28*. The model simulation procedure to obtain the kinetic parameters in *Table 28* was previously described in section 6.4. The parameter constraints form the upper and lower bounds for the predicted kinetic parameters so as to ensure that the parameters obtained from the numerical estimator are biologically sensible.

According to the predicted model parameters, the saturation limitation constant for cell production on xylose ($K_{sx_2}$) was found to be approximately 3-fold larger than for the glucose ($K_{sx_1}$). The higher $K_{sx_2}$ suggests that *Z. mobilis* 8b has a low affinity for xylose as the growth carbon source in the presence of glucose. The high affinity of glucose is further highlighted by the much higher maximum specific glucose consumption rate ($q_{smax_1}$) relative to the maximum specific xylose consumption rate ($q_{smax_2}$).

The proportionality constant ($\alpha$) was used to define the preference for sugar consumption and the relative rates of ethanol and cell mass production from glucose and xylose. The proportionality constant was found to be 0.65. For example, when both glucose and xylose are present in a 50-50 G-X substrate, *Z. mobilis* 8b consumes glucose at 65% of its maximum specific glucose consumption

rate, whilst xylose is consumed at 35% of its maximum specific xylose consumption rate. The proportionality constant obtained in this work agrees with literature reported kinetic data for 25-25 G-X fermentation with *Z. mobilis* ZM4 (pZM5) in batch culture (Rogers *et al.,* 2001).

Considering the acetate formation kinetic parameters, the model estimated that the maximum specific acetate formation rate was approximately 10-fold higher on glucose ($q_{p\_maxAC_1}$) than on xylose ($q_{p\_maxAC_2}$). Therefore, the model suggests that acetate formation is more likely to occur in the presence of high glucose concentrations. Indeed, this result corroborates with the higher acetate concentration formed during the glucose-rich substrate fermentation (*Figure 81* and *Figure 82*). Moreover, the model estimated the endogenous respiration coefficient ($k_D$) as 0.012 $h^{-1}$. Even though the magnitude of $k_D$ seems small or negligible, it is very significant within the current MRB, which operates at low dilution rates.

***Table 28:*** *Kinetic parameter estimation by the MRB kinetic model for 50-50 G-X fermentation. Feed conditions: $s_{f1}$ = 43.8g.$L^{-1}$ glucose, $s_{f2}$ = 45.55 g.$L^{-1}$xylose (sample calculations in Appendix C.5.3 and C.5.4)*

| MRB Fermentation simulation: 50-50 G-X Fermentation | | | | | | | | |
|---|---|---|---|---|---|---|---|---|
| Model simulation parameters | | | | Sensitivity Analysis† | | | | |
| Notation | Parameter | Quantity | Units | 50% | 75% | 100%‡ | 125% | 150% |
| $k_1$ | alpha,α | 0.650 | | 0.33 | 0.49 | 0.650 | 0.81 | 0.98 |
| $k_2$ | $\mu_{max._1}$ | 0.330 | $h^{-1}$ | 0.17 | 0.25 | 0.330 | 0.41 | 0.50 |
| $k_3$ | $K_{sx_1}$ | 1.791 | g/L | 0.90 | 1.34 | 1.791 | 2.24 | 2.69 |
| $k_4$ | $\mu_{max._2}$ | 0.100 | $h^{-1}$ | 0.05 | 0.08 | 0.100 | 0.13 | 0.15 |
| $k_5$ | $K_{sx_2}$ | 5.76 | g/L | 2.88 | 4.32 | 5.76 | 7.20 | 8.63 |
| $k_6$ | $k_D$ | 0.012 | $h^{-1}$ | 0.01 | 0.01 | 0.012 | 0.02 | 0.02 |
| $k_7$ | $q_{s,max._1}$ | -13.38 | $g_{substrate}/g_{cells}.h$ | -6.69 | -10.03 | -13.38 | -16.72 | -20.06 |
| $k_8$ | $K_{ss_1}$ | 9.50 | g/L | 4.75 | 7.13 | 9.50 | 11.88 | 14.25 |
| $k_9$ | $q_{s,max._2}$ | -2.98 | $g_{substrate}/g_{cells}.h$ | -1.49 | -2.24 | -2.98 | -3.73 | -4.47 |
| $k_{10}$ | $K_{ss_2}$ | 2.684 | g/L | 1.34 | 2.01 | 2.684 | 3.35 | 4.03 |
| $k_{11}$ | $q_{pmax._1}$ | 5.117 | $g_{product}/g_{cells}.h$ | 2.56 | 3.84 | 5.117 | 6.40 | 7.68 |
| $k_{12}$ | $q_{pmax._2}$ | 1.520 | $g_{product}/g_{cells}.h$ | 0.76 | 1.14 | 1.520 | 1.90 | 2.28 |
| $k_{13}$ | $q_{pmax\_AC_1}$ | 0.015 | $g_{Acetate}/g_{cells}.h$ | 0.01 | 0.01 | 0.015 | 0.02 | 0.02 |
| $k_{14}$ | $q_{pmax\_AC_2}$ | 0.001 | $g_{Acetate}/g_{cells}.h$ | 0.00 | 0.00 | 0.001 | 0.00 | 0.00 |
| $k_{15}$ | $K_{spAC_1}$ | 0.1 | g/L | 0.04 | 0.06 | 0.1 | 0.10 | 0.12 |
| $k_{16}$ | $K_{spAC_2}$ | 10.1 | g/L | 5.07 | 7.61 | 10.1 | 12.69 | 15.22 |
| Constrained Parameters | | | | | | | | |
| | $K_{sp_1}$ | 9.50 | g/L | 4.75 | 7.13 | 9.50 | 11.88 | 14.25 |
| | $K_{sp_2}$ | 2.68 | g/L | 1.34 | 2.01 | 2.68 | 3.35 | 4.03 |
| | β | 0.05 | | 0.03 | 0.04 | 0.05 | 0.06 | 0.08 |

† Univariant sensitivity analysis

‡ Represents the base case parameters as predicted by the simulator

The model was further extended with the view to predict the transient (or instantaneous) and pseudo-steady state volumetric productivities. The instantaneous and the pseudo-steady state productivities were estimated using Equation 6.15 and the statistical quadratic model respectively. Both productivity predictions are presented in *Figure 87*.

As expected, the instantaneous productivity was characterized by a decline proportional to the decrease in the system dilution rate and the MFU permeate flux. Nevertheless, the instantaneous productivity predicted by the kinetic model fitted the experimental data relatively well. The goodness of fit was quantified by a $R^2_{adj}$ value of 0.937. Moreover, the predicted pseudo-steady state productivity was in good agreement with the experimental data.

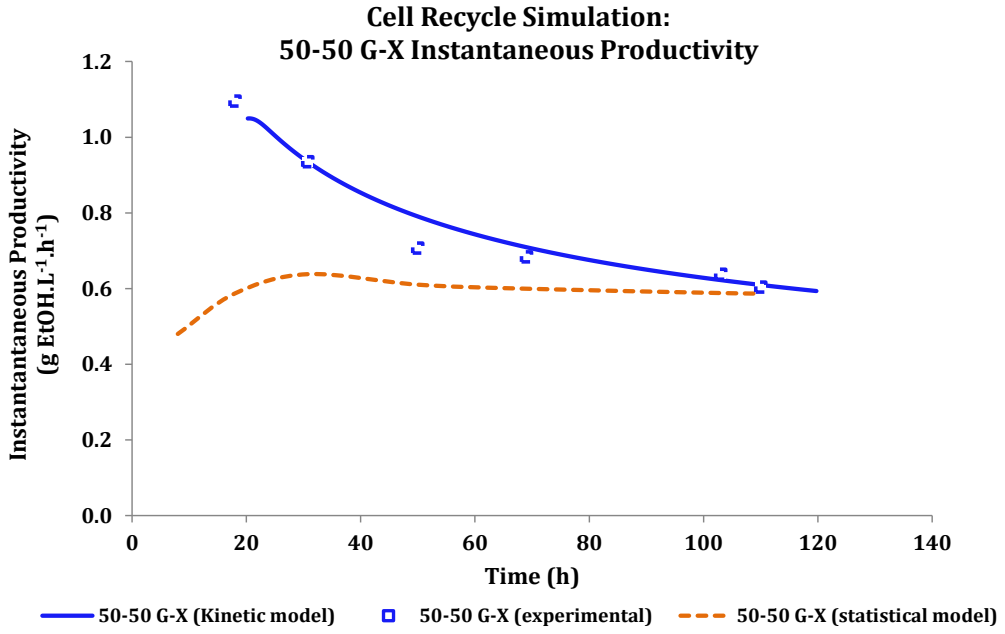


***Figure 87:*** *Volumetric productivity estimation using the kinetic model and the statistical model*

Even though both models fit the experimental data relatively well, they both fulfill different purposes. For example, the instantaneous volumetric productivity obtained through the kinetic model is highly dependent on the fouling mechanism and the membrane-fouling rate, which can be challenging to predict without the use of empirical formulations. However, even though the statistical model only estimates the pseudo-steady state productivity, it is only dependent on the final ethanol concentration and operating conditions, i.e. TMP, CFV, cell concentration. Therefore, the statistical approach is a useful tool for obtaining rough estimates of the expected MRB system productivity when target ethanol concentrations have been set. For detailed analysis of the kinetic performance of the MRB system, the kinetic model provides an important tool for estimating the MRB system productivity at any time during operation. However, the performance of the kinetic model is highly dependent on the accuracy of the prediction of the rate of membrane fouling or the change in the instantaneous hydraulic dilution rate.

### 7.4.2.2 *PARAMETER SENSITIVITY ANALYSIS*

A sensitivity analysis was performed on the kinetic parameters estimated by the kinetic model so as to establish:

- whether the $RSS_{total}$ obtained by the model is indeed at its minimum, and
- which parameters are most influential in affecting the behaviour of the model simulation.

A univariant (or single-factor) approach was adopted whereby the estimated kinetic parameters were varied within ±50% of the values given by the model (whilst all the other parameters were held constant). The $RSS_{total}$ was used as the response/output in an attempt to ascertain that the minimization was successful and to identify the order of parameter significance with regards to the simulation performance. The sensitivity analysis was performed in SensIt™ (Middleton, 2014). A spider-chart of the univariant sensitivity analysis is shown in *Figure 88*.

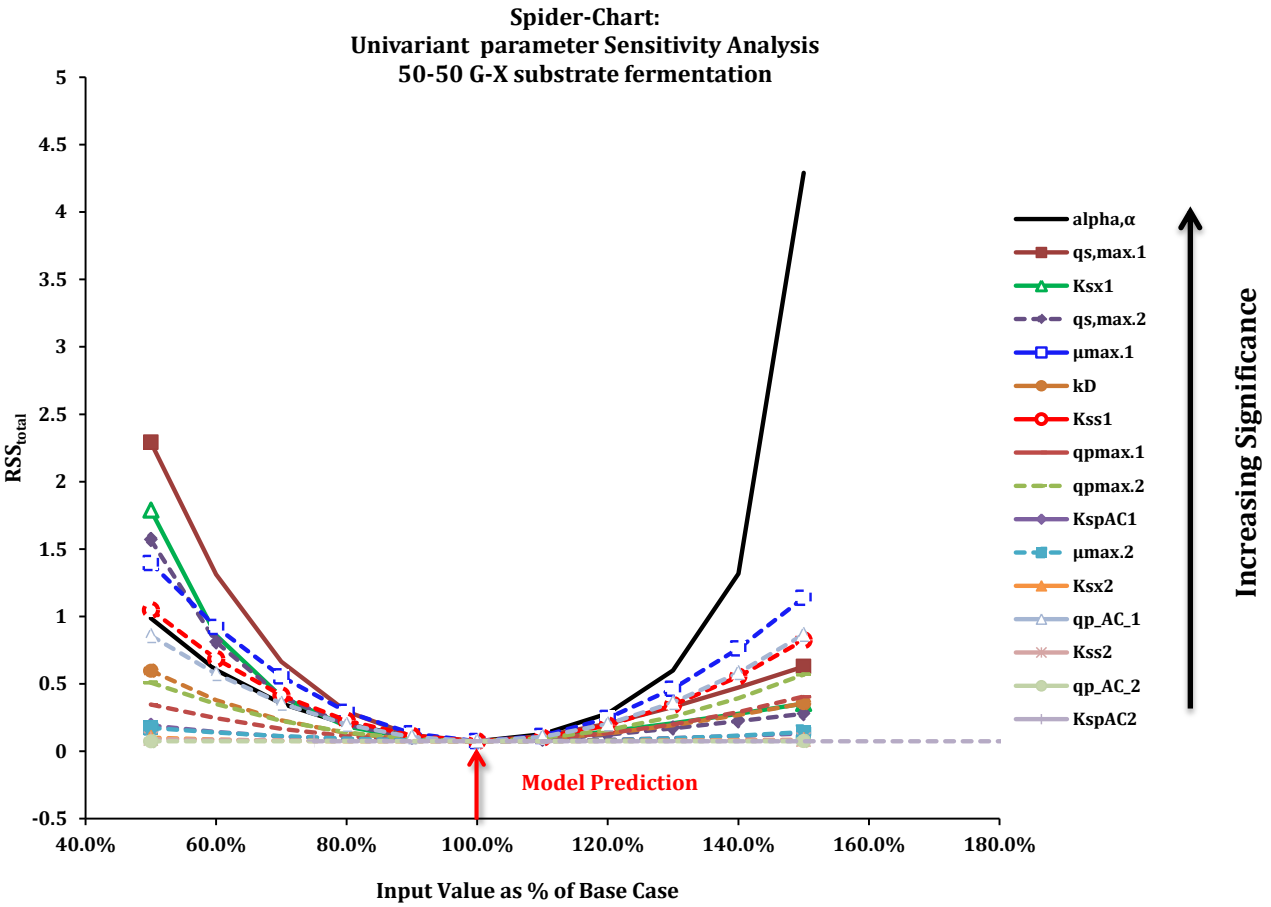


***Figure 88:*** *Uni-variant parameter sensitivity analysis for 50-50 G-X substrate fermentation*

On spider-charts, lines that are horizontal typically define parameters that result in an insignificant change in the response/output variable with small changes in the estimated model parameters. On the contrary, the more vertical the line is, the more significant small changes in estimated model parameters are on the response variable. Considering the kinetic model parameters, the order of

significant parameters is shown on the legend in *Figure 88*. Hence, within the range 90-110% of the estimated model parameters, the change in $RSS_{total}$ is small. This indicates that the model response is stable within this parameter range. However, on either side of this range, a number of parameters (such as the proportionality constant) significantly affect the model performance.

Nevertheless, the combination of the kinetic parameters estimated by the kinetic model did result in what appears to be a minimum $RSS_{total}$. More accurate sensitivity analysis can be performed using a bivariant analysis whereby the significance of the interaction between the model parameters is determined.

### 7.4.3 Model Validation

#### 7.4.3.1 Fermentation Profiles

The MRB kinetic model was validated by comparing the predicted profiles of CDW, glucose, xylose, acetate and ethanol to experimental results obtained during glucose-rich (75-25 G-X) and xylose-rich (25-75 G-X) substrate fermentations. The model simulation profiles and the corresponding experimental data for these two experimental runs are shown in *Figure 89* and *Figure 90*.

Through graphical inspection of *Figure 89*, it can be seen, that in both cases, the predicted results are in good agreement with the experimental MRB fermentation data. The actual goodness of model fit to the experimental data was quantified by determining the adjusted correlation coefficients for each of the model profiles. A summary of the adjusted correlation coefficients for all three MRB experiments is presented in *Figure 90*. The high degree of the MRB kinetic model fit to experimental data was highlighted by adjusted correlation coefficients for CDW, glucose, xylose and ethanol concentration that were greater than 0.98 for all three MRB fermentation experimental runs.

The validation results of the MRB kinetic model suggest that the model is sufficient for predicting the performance of the MRB system, at least for fermentation simulation within the investigated experimental range. However, extrapolating or applying the MRB kinetic model to experimental conditions outside the investigated range is not trivial. Since the change in experimental conditions result in change in the kinetic model parameters (such as saturation constant ($K_{sx}$)), model extrapolation requires the calculation of these new kinetic parameters. Nevertheless, the model does provide a means for estimating the kinetic parameters of glucose-xylose substrate fermentation with *Z. mobilis* 8b in a MRB fermentation system. The subsequent estimation of the process kinetic parameters provides an insight into the various factors that influence and/or bottleneck the fermentation performance of the MRB.

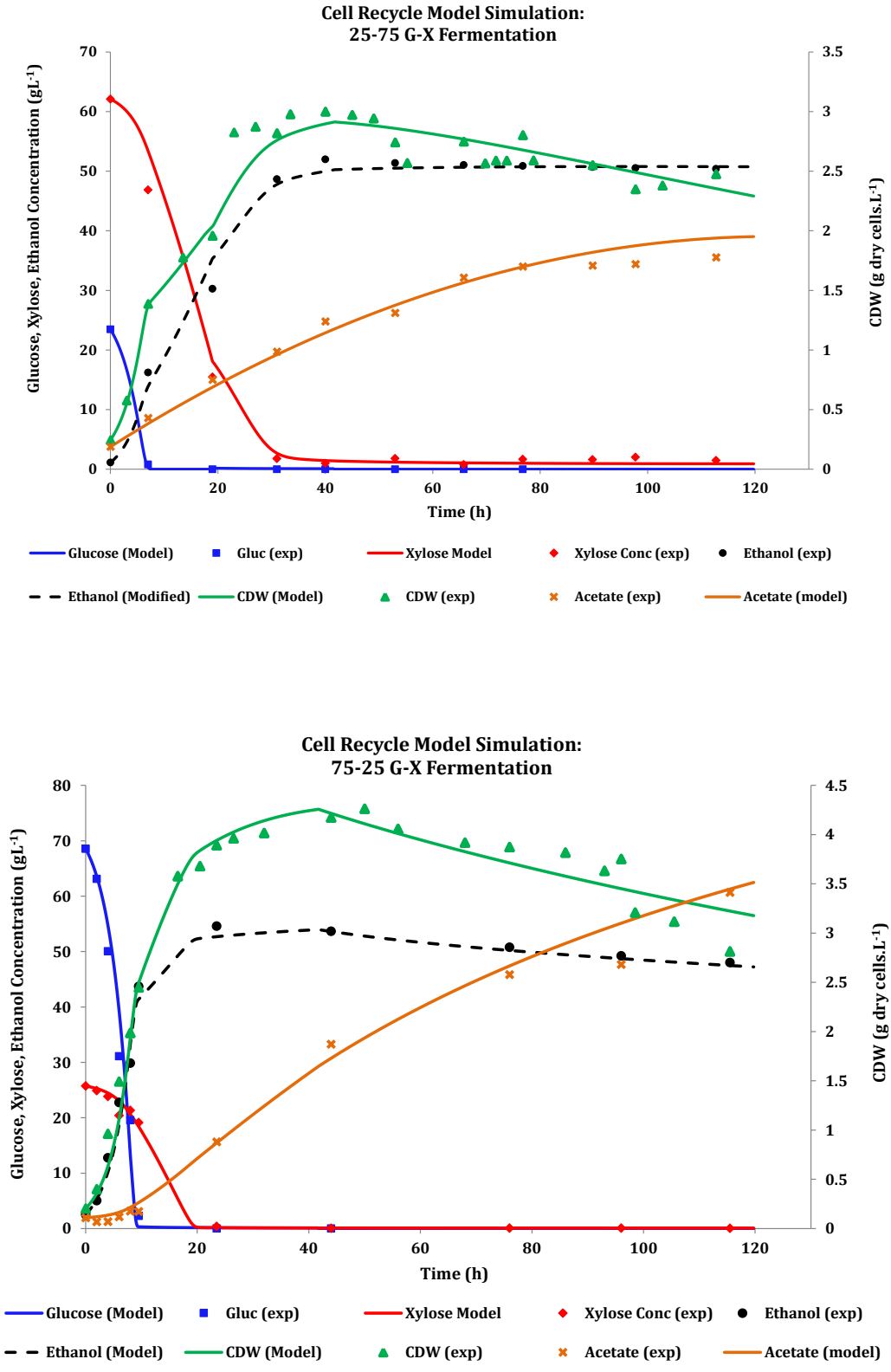


***Figure 89:*** *Cell recycle experimental data and model simulation of 25-75 G-X (top) and 75-25 G-X substrate fermentation (bottom) by Z. mobilis 8b at 33.5 °C, pH 6.25.*

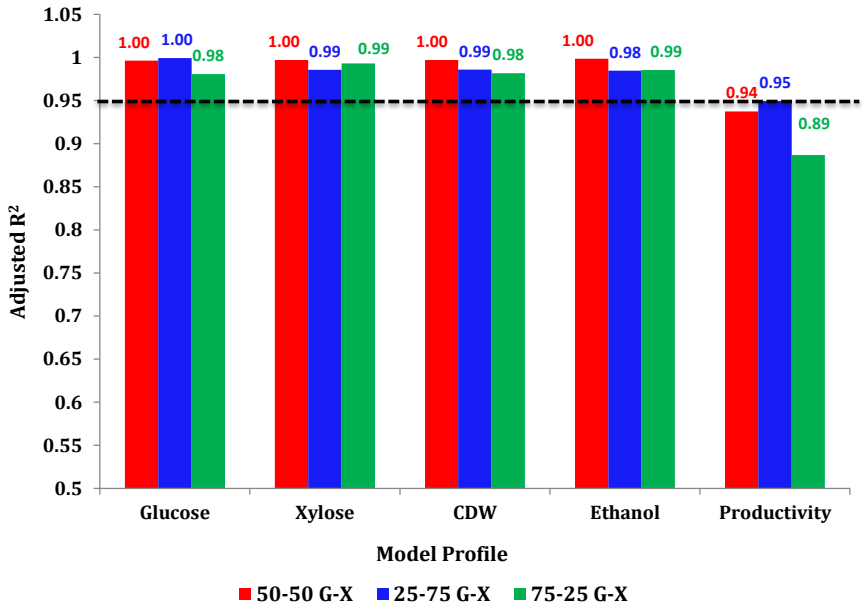


***Figure 90:*** *A summary of the adjusted correlation coefficients for all the model profiles obtained from the three MBR fermentations*

### 7.4.3.2 *VOLUMETRIC PRODUCTIVITY PROFILES*

Either coupling the MRB kinetic model with an empirical/fundamental transient permeate flux rate prediction model or statistical pseudo-steady state model provides a basis for understanding the response of the MRB system volumetric productivity as the process conditions are varied. The two experiments used in the previous section were used to validate the volumetric productivity calculation model where the MRB kinetic model was coupled with either the semi-empirical permeate flux prediction model or the pseudo-steady state statistical model. Both model predictions for the transient and pseudo-steady state productivities are shown in *Figure 91*.

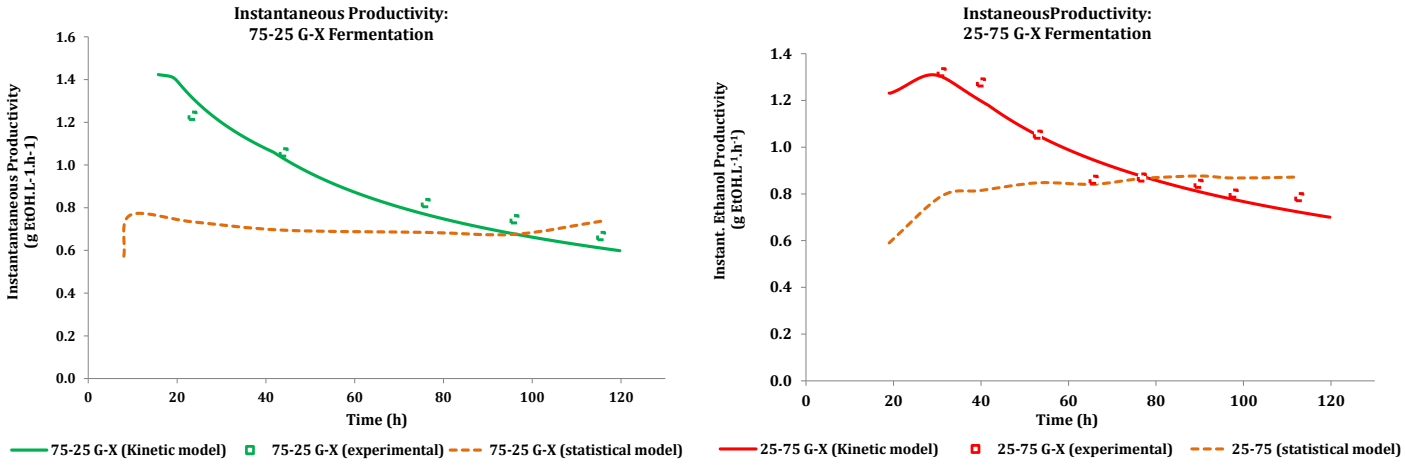


**Figure 91:** *Cell recycle experimental data and model simulation of the 75-25 G-X substrate fermentation by Z. mobilis 8b (left), volumetric productivity estimation using the kinetic model and the statistical model (right)*

In both the xylose-rich and glucose-rich substrate fermentation experiments, the transient steady-state volumetric productivity predicted by the kinetic model fitted the experimental data relatively

well. The degree of model fit was quantified by $R^2_{adj}$ values of 0.95 and 0.89 respectively. Since the volumetric productivity was calculated as the product of the instantaneous hydraulic dilution rate and the instantaneous ethanol concentration, the deviation of the model prediction from experimental data was attributed the slight error in the prediction of the transient permeate flux rate by the semi-empirical model (*Figure 84*).

Analyzing the pseudo-steady state volumetric productivity prediction, it is apparent that in both cases the statistical model over-predicts the volumetric productivity after approximately 115 hours of operation. The pseudo-steady state volumetric productivity is only dependent on the final ethanol concentration and the operating conditions, i.e. TMP, CFV and cell concentration. Therefore, the pseudo-steady state volumetric productivity over-prediction was attributed to the decline in the measured cell concentration with time due to the significance of endogenous respiration at these low operating hydraulic dilution rates (*Figure 89*). Based on the statistical model, decreases in the cell concentration result in an increase in the pseudo steady state permeate flux rate and ultimately an increase in the volumetric productivity. Nevertheless, even with this limitation, the model over-prediction of the volumetric productivity after 115 hours in operation was approximately 10% and 11% for xylose-rich and glucose-rich substrate fermentation respectively.

In light of the proposed MRB kinetic model, the only requirements for model simulation are the estimation of the initial model parameters by performing a kinetic analysis during the start-up phase and the accurate prediction of the transient permeate flux rate. Further, the challenge of predicting the membrane fouling rate or the transient permeate flux rate can be circumvented by operating the membrane under constant permeate flux conditions (with variable TMP).

### 7.4.4 Application of Kinetic Model for MRB Process Optimization

The kinetic model confirmed that the bottleneck to the process was not the activity of the biocatalysts, but the low hydraulic dilution rate achieved by the system due to membrane fouling. It has previously been established that the region whereby the MRB could be considered for an economic feasibility was defined by operating the MRB at hydraulic dilutions rates greater than 0.11 $h^{-1}$, whilst maintaining an ethanol concentration greater than 4 (w/v) %.

One of the classical methods for improving the volumetric flow from a MFU is to increase filtration surface area by increasing the number of membranes in the MFU. Consider a hypothetical case whereby the surface area of the MFU used in this work could be increased by increasing the number of membranes in a parallel configuration in the MFU. Due to the cell retention action and probability of increasing the cell density at high hydraulic dilution rates, it could be assumed MRB would maintain an ethanol concentration greater than the minimum requirement even at hydraulic dilution rates. Moreover, it could be assumed that since the membranes would be placed in a parallel formation, the extent of membrane fouling on each membrane would be the same.

In this hypothetical case, the pseudo-steady state model can be used to approximate the minimum number of membranes required such that the volumetric productivity of the current MRB system is greater than the one achieved in continuous culture at the same dilution rate. An approximation of the minimum number of membranes required to increase the volumetric productivity of the MRB system is shown in *Figure 92*. In *Figure 92*, the hashed bars indicate the number of membranes that result in a volumetric productivity that is lower to that achieved in continuous culture at D = 0.11 $h^{-1}$.

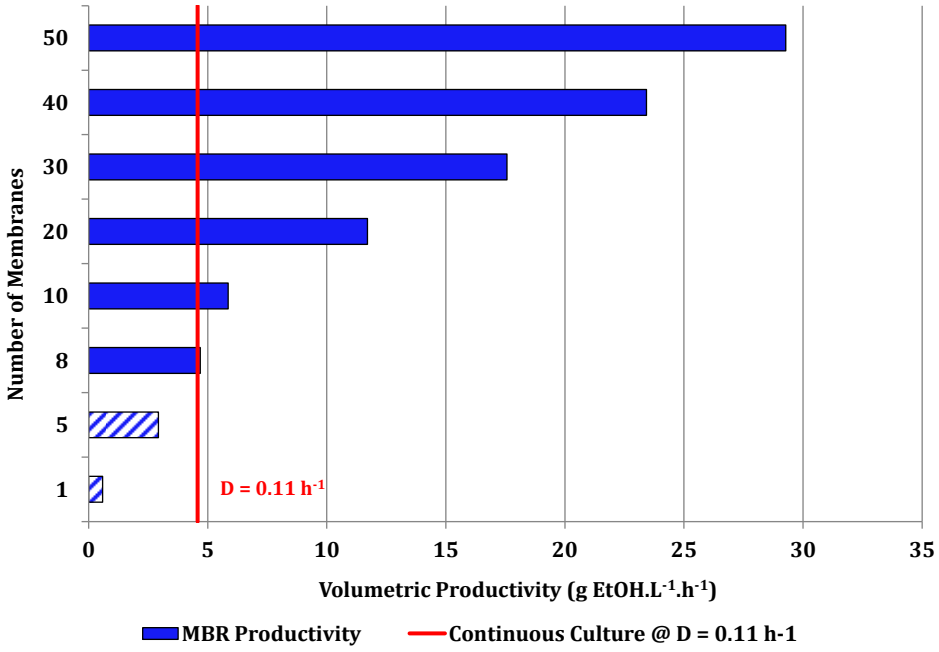


***Figure 92:*** *Application of statistical and MRB kinetic model for determining the effect of the number of MFU membranes on the volumetric productivity (membranes in parallel formation).*

Based on the model output, it is projected that a minimum of eight membranes would be required to sufficiently increase the volumetric productivity of the MRB as an alternative fermentation strategy. Moreover, it is also projected that the use of 50 membranes in the MFU has the potential for a 6-fold increase in the MRB the volumetric productivity relative to continuous culture strategy.

The potential for increasing the microfiltration surface area is further emphasized by investigating literature reported dilution rates obtained from glucose MRB fermentation systems with large filtration surface area to working volume ratio's ($a_{s/v}$ in *Table 5*). The $a_{s/v}$ used in this work was approximately 1.4 $m^{-1}$. This ratio is significantly lower than those presented in literature (in the range 23-575 $m^{-1}$, see *Table 5*). Consequently, increasing the membrane surface area in the MFU would provide an ideal area for increasing the MRB ability to achieve high hydraulic dilution rates and subsequently high volumetric productivities.

Nevertheless, the method of estimating the pseudo-steady state volumetric productivity provides a tool for investigating the effect of various process parameters (provided they do not interfere in the biocatalyst activity) on the volumetric productivity of the MRB system.

# CHAPTER 8

# CONCLUSIONS AND RECOMMENDATIONS

A critical literature analysis highlighted that both the efficient conversion of all hydrolyzate sugars to ethanol and the ethanol concentration in the fermentation broth prior to distillation have the most significant impact on the second generation ethanol production cost. To this end, the primary objective of this work was to develop, model and assess the viability of using a membrane recycle bioreactor (MRB) as a vehicle for efficiently converting a synthetic glucose-xylose substrate into ethanol in addition to improving the volumetric productivity of the fermentation process.

The research approach undertaken in this work involved the division of the project into four main segments, i.e. the optimization of the fermentation conditions, the design and characterization of a microfiltration unit, the quantification of the kinetics of *Z. mobilis* in continuous culture and the kinetic modeling of the MRB system. The conclusions from this work will be discussed in an order corresponding to these four segments.

## 8.1 CONCLUSIONS

### 8.1.1 OPTIMIZATION OF THE FERMENTATION CONDITIONS

Two $3^2$ full-factorial designs were employed in light of establishing whether the fermentation temperature and pH had a significant effect on the ethanol yield and volumetric productivity of a glucose substrate with *Z. mobilis* ZM4 and a xylose-rich substrate using *Z. mobilis* 8b. The ensuing ANOVA analysis revealed that both the fermentation temperature and pH had a significant effect on the ethanol yield and productivity of a glucose substrate (*Z. mobilis* ZM4) and a xylose-rich substrate (*Z. mobilis* 8b). Interestingly, considering the ethanol yield, the interactive effect of temperature and pH was statistically significant within a 95 % confidence interval.

The optimum combination of the fermentation temperature and pH was determined using a multiple response optimization statistical tool. Considering glucose substrate fermentation, the optimum fermentation temperature and pH *for Z. mobilis* ZM4 corresponded with literature default values of 30 $^{o}$C, pH = 6-5.5. However, for a xylose-rich substrate, the optimum fermentation temperature and pH for *Z. mobilis* 8b were at 33.5 $^{o}$C, pH = 6.5-6. As a result, it was concluded that the optimum fermentation temperature and pH for mixed-sugar hydrolyzate fermentation is dependent on the sugar composition.

In an attempt to quantify whether xylose fermentation is suppressed, improved or is independent of the glucose fraction in the fermentation media; the overall and specific rates of xylose consumption were analyzed at varying glucose fractions. It was found that the overall rate of xylose consumption increased with an increase in the glucose fraction in a glucose-xylose batch fermentation system. However, the presence of glucose did not have a significant effect on the specific xylose consumption rate nor the ethanol yield from xylose.

The fermentation kinetics of *Z. mobilis* 8b (at the optimized conditions) were benchmarked with those of three industrial yeast strains (*S. cerevisiae* BH4, *S. cerevisiae* A4, *S. cerevisiae* TMB 3400), one laboratory recombinant yeast strain (*S. cerevisiae* 1400(pLNH33)), two laboratory recombinant *Z. mobilis* strains (*Z. mobilis* CP4(pZB5), *Z. mobilis* ZM4(pZB5)). Considering the fermentation of a 50-50g.$L^{-1}$ glucose-xylose substrate, it was found that the optimal volumetric productivity from batch culture was 1.42 g EtOH.$L^{-1}$.$h^{-1}$. From the comparative study, it was found that both *Z. mobilis* 8b and *Z. mobilis* ZM4(pZB5) outperformed the industrial and laboratory yeast strains. However, considering *Z. mobilis* 8b has potential for fermenting and tolerating hydrolyzates better than *Z. mobilis* ZM4 (pZB5), its efficient performance at the defined optimum conditions becomes essential considering its robustness in the industrial context.

### 8.1.2 Characterization of the Microfiltration Unit

In light of quantifying whether the cell-free fermentation media components contributed towards internal membrane fouling and the membrane critical flux, preliminary experiments were performed. Considering the filtration of the cell-free fermentation media, it was found that increasing the cross-flow velocity (CFV) and decreasing the substrate concentration resulted in an increase in both the membrane permeability and the membrane critical flux.

With regards to the filtration of cell-containing fermentation broth, a black-box approach was undertaken whereby the effect of the fermentation broth cell concentration, TMP and the CFV were analysed using a CCD statistical design. The ensuing ANOVA analysis revealed that the cell concentration, TMP, CFV and the TMP-cell concentration interaction all had a significant effect on the pseudo-steady state permeate flux through the microfiltration unit. Moreover, a quadratic mathematical model fitted by regression to the CCD experimental data was sufficient to predict the pseudo-steady state concentration as a function of the TMP, CFV and cell concentration. The quadratic model was validated within the experimental conditions, which limited by the experimental apparatus.

Considering the filtration of a cell-containing fermentation suspension, permeate flux recovery through membrane back-flushing did not have a significant effect. Therefore, the compressible fouling cake layer on the membrane surface was considered “irreversible”. Moreover, internal fouling by the fermentation media components did significantly affect the membrane permeability and ultimately resulted in a decline in the permeate flux.

### 8.1.3 Quantification of the kinetics of Z. mobilis in Continuous Culture

The kinetic performance of *Z. mobilis* in continuous culture was investigated by comparing the continuous culture (without cell retention) to continuous culture with cell recycle fermentation strategies, both performed at the same experimental conditions. Considering the fermentation of a 50-50g.$L^{-1}$ glucose-xylose substrate, it was found that the optimal volumetric productivity from continuous culture (without cell retention) was 4.58 g EtOH.$L^{-1}$.$h^{-1}$ (at D = 0.11$h^{-1}$). The optimal volumetric productivity of the latter was limited by the decrease in the ethanol concentration below the minimum concentration of 40.g. $L^{-1}$ (or 4% (w/v)) at dilution rates greater than D = 0.11$h^{-1}$. The minimum concentration is mandatory for minimizing energy and economic requirements for ethanol recovery by distillation.

At the same feed substrate composition, the volumetric productivity of the continuous culture with cell recycle (or MRB) was limited to 1.15 g EtOH.$L^{-1}$.$h^{-1}$ whilst operating the microfiltration unit at a TMP of 100kPa and a CFV of 0.433m.$s^{-1}$. The volumetric productivity of the MRB was limited by membrane fouling in the MFU and subsequently the low hydraulic dilution rate obtained from the MRB system. As a result, it was concluded that the volumetric productivity of the MRB system was not limited by the rate of ethanol production but by the system hydraulic dilution rate (i.e. rate of ethanol removal from the system).

Nevertheless, comparing the continuous culture (without cell retention) to the MRB system at the same dilution rate and feed substrate composition, it was determined that the volumetric productivity of both systems was indeed the same. Moreover, it was determined that for the MRB to be considered as an alternative continuous culture (without cell retention) fermentation strategy, its minimum hydraulic dilution rate must be greater than 0.11$h^{-1}$.

In another experiment, the ethanol yield and volumetric productivity were found to be unaffected by the feed sugar composition to the MRB. Although this observation was unexpected, it stemmed from the volumetric productivity limitation by the achievable hydraulic dilution rate and not the rates of substrate consumption.

### 8.1.4 Kinetic Modelling of MRB Fermentation System

The MRB kinetic model consisted of two sections, i.e. the prediction of the transient decline in the permeate flux and a system of ordinary differential equations defined by the mass balance of the major fermentation components in the MRB system. The transient permeate flux rate could be successfully modelled by fitting a semi-empirical model to experimental data using regression analysis. Moreover, the quadratic mathematical model determined from the CCD statistical design (in the second segment of this work) was sufficient to predict the pseudo-steady state permeate flux rate within 5-10% of the experimental data.

Considering the fermentation of a 50-50 $g.L^{-1}$ glucose-xylose substrate, the MRB kinetic model accurately predicted the CDW, glucose, xylose, acetate and ethanol concentrations. The high degree of model fit was highlighted by adjusted correlation coefficients ($R^2_{adj}$) consistently greater than 0.98. The MRB kinetic model achieved similar results for 25-75 $g.L^{-1}$ and 75-25 $g.L^{-1}$ glucose-xylose substrate fermentation.

Extrapolation using the MRB kinetic model outside the experimental conditions was not trivial due to the sensitivity of the model parameters to changing operating and feed substrate conditions. The transient permeate flux relationship with the system hydraulic dilution rate was specific to the exact experimental system used in this work. Therefore, the use of the kinetic model for estimating the pseudo-steady state cell, substrate and ethanol concentrations for MRB systems with different membrane permeate flux profiles is not applicable.

However, kinetic model was useful for estimating the MRB fermentation kinetic parameters and subsequently for identification of areas that can potentially improve the MRB system volumetric productivity. Moreover, using the pseudo-steady state statistical model, it was projected that a minimum of eight membranes would be required to meet the minimum ethanol concentration and exceed the volumetric productivity of the continuous culture fermentation strategy.

### 8.1.5 SUMMARY

In summary, the global objectives of this project were met through:

- ✓ the development and characterization of the MRB system,
- ✓ the quantification of its fermentation kinetic performance relative to batch and continuous culture (without cell recycle) at optimized fermentation conditions,
- ✓ the development and validation of a kinetic model for the prediction of the system kinetic parameters
- ✓ and the identification of the process limitations that the process hinder the viability of the MRB system as an alternative mixed-sugar fermentation strategy.

## 8.2 RECOMMENDATIONS

Overall, whilst most of the project objectives were met, the limitation of the MRB system performance due to a combination of membrane fouling and low filtration surface area provides cause for future work in exploiting ways of minimizing membrane fouling, increasing the available filtration area or the use of a different filtration module. In light of these aspects, the following recommendations were made in view of guiding future work:

### 8.2.1 IMPROVE HYDRODYNAMIC CONDITIONS THROUGH THE MFU

Prior to considering the option of improving the volumetric flow from the MFU by increasing the filtration surface area, the minimization of the primary source for attaining low volumetric flows remains first priority. The most convenient starting point is the improvement of the hydrodynamic conditions through the MFU. Whilst long-term operation could only be ensured at CFVs less than 0.3202 $m.s^{-1}$ with the existing experimental equipment, increasing the CFV would result in an increase in the shear rate at the membrane surface and subsequently reduce membrane fouling. Within the current system, higher CFVs can be achieved through either selecting tubular membranes with a smaller diameter or redesigning the piping system such that both high volumetric flows and easy sterilization are facilitated.

### 8.2.2 IMPROVE FERMENTATION MEDIA SOLUTION CHEMISTRY

However, increasing the CFV would have minimal effect on internal membrane fouling caused by some of the fermentation media components, especially the sugars. To combat the adsorption of these media components, future work should be directed towards the improvement of the solution chemistry such that the electrostatic interactions between the membrane and media foulants are minimized.

### 8.2.3 IMMOBILIZING THE CELL CULTURE THROUGH ENTRAPMENT IN A STABLE MATRIX

It is well known that larger particles are sterically hindered from depositing and accumulating at the membrane surface and are subsequently easier to remove away from the membrane surface (Shiraz, 2010). Therefore, the bacterial cells could be immobilized by entrapping them within a matrix such as calcium alginate beads (CABs) in light of increasing the size of the cell culture towards the MFU. Therefore, high cell densities can be obtained within CABs of approximately 1mm diameter. This configuration has great potential for decreasing membrane fouling through the minimization of cake layer formation and requiring mild CFVs for arresting accumulation of CABs at the membrane surface. However, immobilizing the microbial cells in CABs could result in the sugar-to-ethanol conversion reaction to be mass transfer limited rather than kinetically limited. Moreover, the stability of the CABs at various hydrodynamic conditions would have to be quantified.

### 8.2.4 Alternative Fouling Control Techniques

Provided membrane fouling through the formation a compressible cake layer is still a major problem even at improved hydrodynamic conditions, economic intensive anti-fouling measures should be investigated. Since ceramic membranes are known to be good reflectors of ultrasonic waves, submerging the MFU within an ultrasonic bath provides an alternative option for minimizing membrane fouling through cake-layer formation. In fact, many authors have reported that in liquid medium ultrasound creates shock waves and localized regions of low and high pressure that not only prevent particulate deposition on the membrane surface but also instigate the removal of foulants on the membrane surface (Dhariwal, 2007; Kyllonen *et al.,* 2005; Chen *et al.,* 2006). However, the effect of the ultrasound waves on the activity or the biocatalysts would have to be thoroughly investigated.

### 8.2.5 Expansion of the Filtration surface area

It was highlighted in the results section that increasing the number of membranes within the MFU could facilitate a significant improvement the hydraulic dilution rate and consequently the volumetric productivity achieved by the MRB fermentation system. However, increasing the number of membranes would directly increase the capital expenses required for the MFU. Hence, process economics would be required to quantify whether the improvement in the volumetric productivity through cell retention is economically feasible or not. Moreover, in light of process economics, polymeric membranes would provide a better option. However, due to their temperature instability, alternative sterilization techniques would be required.

### 8.2.6 Expanding Experimental Conditions for MRB Operation

Operating at constant flux rather than constant TMP would simplify the kinetic model by ensuring steady throughput from the MFU and subsequently negate the requirement for complex transient permeate flux models. Nevertheless, constant flux operation (below the subcritical flux) would require justification through ensuring that the system hydraulic dilution rate would not be too low to limit the volumetric productivity of the MRB system.

The experimental range for which the model was evaluated should be extended to evaluate its response to a multitude of feed conditions. Moreover, instead of evaluating the effect of various substrate compositions and concentrations, the MRB system should be evaluated for fermentation the liquid fraction of actual hydrolyzates obtained from various LC feedstocks such as sugarcane bagasse and corn stover. The use of hydrolyzates would provide an indication of the advantages and limitations of the MRB system and subsequently establish a benchmark for determining the viability of this system for larger scale ethanol production.

### 8.2.7 EXPANSION OF KINETIC MODEL

In light of extending the accuracy of the MRB kinetic model for a multitude of feed conditions, the model should be extended such that the effects of substrate and acetate inhibition are taken into consideration. In this work, the total substrate concentration was limited to concentrations whereby substrate inhibition is insignificant. However, in practice, the total sugar concentration present in hydrolyzates could be significantly higher. Moreover, the initial parameters of the model were estimated from the start-up phase of the MRB experimental runs. The accuracy of the predicted kinetic parameters should be evaluated by assessing the solution of the model simulation at different sets of initial conditions.

# CHAPTER 9

## REFERENCE LIST

Achyuthan, K.E., Achyuthan, A.M., Adams, P.D., Dirk, S.M., Harper, J.C., Simmons, B.A., Singh, A.K., 2010. Supramolecular self-assembled chaos: polyphenolic lignin's barrier to cost-effective lignocellulosic biofuels. Molecules 15, 8641–88. doi:10.3390/molecules15118641

Ackerson, M.., Clausen, E.., Gaddy, J.., 1991. Production of ethanol from MSW via concentrated acid hydrolysis of the lignocellulosic fraction, in: Energy from Biomass Wastes. Institute of Gas Rechnology, Chicago, IL, pp. 725–743.

Aden, A., Dutta, A., Dowe, N., Ibsen, K.N., Schell, D.J., 2010. An economic comparison of different fermentation configurations to convert corn stover to ethanol using Z. mobilis and Saccharomyces. Biotechnol. Prog. 26, 64–72. doi:10.1002/btpr.311

Anon, G., 2012. Solubility of Gases in Water [WWW Document]. Eng. Toolbox.

Asghari, A., Bothast, R.J., Doran, J.., Ingram, L.O., 1996. Ethanol production from hemicellulose hydrolyzates of agricultural residues using genetically engineered Escherichia coli strain KO11. J. Ind. Microbiol. 16, 42–47.

Bacchin, P., Aimar, P., Field, R., 2006. Critical and sustainable fluxes: Theory, experiments and applications. J. Memb. Sci. 281, 42–69. doi:10.1016/j.memsci.2006.04.014

Beier, S.P., 2008. Dynamic Microfiltration- Critical Flux and Macromolecular Transmission. Technical University of Denmark.

Belaich, J.-P., Senez, J.C., 1965. Influence of Aeration and of Pantothenate Growth Yields of Zymomonas mobilis. J. Bacteriol. 89, 1195–1200.

Belfort, G., Davis, R.H., Zydney, A.L., 1994. The behavior of suspensions and macromolecular solutions in crossflow microfiltration. J. Memb. Sci. 96, 1–58.

Belhocine, D., Mokrane, H., Grib, H., Lounici, H., Pauss, A., Mameri, N., 2000. Optimization of enzymatic hydrolysis of haemoglobin in a continuous membrane bioreactor. Measurement 76, 189–196.

Benkahla, Y.K., Jaffrin, M.Y., Ould-Dris, A., Si-Hassen, D., 1995. Cake growth mechanism in cross-flow microfiltration of mineral suspensions. J. Memb. Sci. 98, 107–117.

Bhave, R.R., 1996. Cross-Flow Filtration, in: Vogel, H.C., Todaro, C.L. (Eds.), Fermentation and Biochemical Engineering Handbook. Noyes Publication, pp. 271–347.

Bothast, R.J., Nichols, N.N., Dien, B.S., 1999. Fermentations with New Recombinant Organisms. Biotechnol. Prog. 15, 867–875.

Bringer, S., Finn, R.K., Sahm, H., 1984. Effect of oxygen on the metabolism of Zymomonas mobilis. Arch. Microbiol. 139, 376–381.

Burton, S.G., 2001. Development of bioreactors for application of biocatalysts in biotransformations and bioremediation *. Symp. A Q. J. Mod. Foreign Lit. 73, 77–83.

Burton, S.G., Boshoff, A., Edwards, W., Rose, P.D., 1998. Biotransformation of phenols using immobilised polyphenol oxidase. J. Mol. Catal. B Enzym. 5, 411–416. doi:10.1016/S1381-1177(98)00020-4

Cardona, C. a, Sánchez, O.J., 2007. Fuel ethanol production: process design trends and integration opportunities. Bioresour. Technol. 98, 2415–57. doi:10.1016/j.biortech.2007.01.002

Carrère, H., Blaszkow, F., Roux, H., Balmann, D., 2001. Modelling the clarification of lactic acid fermentation broths by cross-flow microfiltration 186, 219–230.

Carstensen, F., Apel, A., Wessling, M., 2012. In situ product recovery : Submerged membranes vs . external loop membranes. J. Memb. Sci. 394-395, 1–36. doi:10.1016/j.memsci.2011.11.029

Catapano, G., Eibl, R., Eibl, D., Pörtner, R., Czermak, P., 2009. Bioreactor Design and Scale-Up, in: Catapano, G., Eibl, R., Eibl, D., Pörtner, R., Czermak, P. (Eds.), Cell and Tissue Reaction Engineering, Principles and Practice. Springer, Berlin, Heidelberg, pp. 173–246. doi:10.1007/978-3-540-68182-3

Chaabane, F. Ben, Aldiguier, A.., Alfenore, S., Cameleyre, X., Blanc, P., Bideaux, C., Guillouet, S.E., Roux, G., Molina-Jouve, C., 2006. Very high ethanol productivity in an innovative continuous two-stage bioreactor with cell recycle. Bioprocess Biosyst. Eng. 29, 49–57. doi:10.1007/s00449-006-0056-1

Chander, R., Gupta, R., Pal, Y., Singh, A., Zhang, Y.P., 2011. Bioethanol production from pentose sugars: Current status and future prospects. Renew. Sustain. Energy Rev. 15, 4950–4962. doi:10.1016/j.rser.2011.07.058

Chang, H.N., Lee, W.G., Kim, B.S., 1993. Cell retention culture with an internal filter module: continuous ethanol fermentation. Biotechnol. Bioeng. 41, 677–81. doi:10.1002/bit.260410612

Charcosset, C., 2006. Membrane processes in biotechnology: an overview. Biotechnol. Adv. 24, 482–92. doi:10.1016/j.biotechadv.2006.03.002

Chen, D., Weavers, L.K., Walker, H.W., 2006. Ultrasonic control of ceramic membrane fouling by particles : Effect of ultrasonic factors. Ultrason. Sonochem. 13, 379–387. doi:10.1016/j.ultsonch.2005.07.004

Cheryan, M., Mehaia, M.A., 1983. A High-Performance Membrane Bioreaqctor for Continuous Fermentaiton of Lactose to Ethanol. Biotechnol. Lett. 5, 519–524.

Cuperus, F.., Smolders, C.., 1991. Characterization of UF Membranes: Membrane Characteristics and Characterization Techniques. Adv. Colloid Interface Sci. 34, 135–173.

Daubert, I., Mercier-Bonin, M., Maranges, C., Goma, G., Fonade, C., Lafforgue, C., 2003. Why and how membrane bioreactors with unsteady filtration conditions can improve the efficiency of biological processes. Ann. N. Y. Acad. Sci. 984, 420–35.

Davison, B.H., Scott, C.D., 1988. Operability and Feasibility of Ethanol Production by Immobilized Zymomonas mobilis in a Fluidized-Bed Bioreactor. Biotechnol. Bioeng. 19–34.

Deanda, K., Zhang, M.I.N., Eddy, C., Picataggio, S., 1996. Development of an Arabinose-Fermenting Zymomonas mobilis Strain by Metabolic Pathway Engineering. Appl. Environ. Microbiol. 62, 4465–4470.

Derringer, G., Suich, R., 1980. Simultaneous Optimization of Several Response Variables. J. Qual. Technol. 12, 214–219.

Dhariwal, A., 2007. The significance of Submerged Ceramic Membrane systems for production oriented Bioprocesses. Univ. Saarland, Ger. University of Saarland, Germany.

Dien, B.S., Cotta, M.., Jeffries, T.., 2003. Bacteria engineered for fuel ethanol production : current status. Environ. Microbiol. 63, 258–266. doi:10.1007/s00253-003-1444-y

Dien, B.S., Nichols, N.N., O'Bryan, P.J., Bothast, R.J., 2000. Development of new ethanologenic Escherichia coli strains for fermentation of lignocellulosic biomass. Appl. Biochem. Biotechnol. 84-86, 181–96.

Ding, S., Tan, T., 2006. l-lactic acid production by Lactobacillus casei fermentation using different fed-batch feeding strategies. Process Biochem. 41, 1451–1454. doi:10.1016/j.procbio.2006.01.014

Donkoh, E., Degenstein, J., Tucker, M., Ji, Y., 2012. Optimization of Enzymatic Hydrolysis of Dilute Acid Pretreated Sugar Beet Pulp Using Response Surface Design. J. Sugarbeet Res. 49, 26–38. doi:10.5274/jsbr.49.1.26

Doran, P.M., 1995. Reactor Engineering, in: Bioprocess Engineering Principles. Academic Press, Amsterdam, pp. 335–359.

Drioli, E., Curcio, E., Fontananova, E., 2010. Mass Transfer Operation. Encycl. Life Support Syst.

Drioli, E., Giorno, L., 1999. Biocatalytic Membrane Reactors: Applications in biotechnology and the pharmaceutical industry, 1st ed. Taylor & Francis Ltd, London.

Du Preez, R., 2008. Development of a Membrane Immobilised Amidase Bioreactor System. Univ. Stellenbosch. University of Stellenbosch.

Escobar, J.M., Rane, K.D., Cheryan, M., 2001. Ethanol Production in a Membrane Bioreactor. Appl. Biochem. Biotechnol. 91-93, 283–296.

Ezeji, T.., Li, Y., 2010. Advanced Product Recovery Technologies, in: Biomass to Biofuels: Strategies for Global Industries. pp. 331–343.

Feldmann, S.D., Sahm, H., Sprenger, G.A., 1992. Biotechnology App ed Pentose metabolism in Zymomonas mobilis wild-type and recombinant strains. Cell 354–361.

Feltenstein, A.J., 1983. The behaviour of Zymomonas Mobilis in Continuous Culture. Univ. Cape T. 11–120.

Ferraz, H.C., Alves, T.L.M., Borges, C.P., 2001. Coupling of an electrodialysis unit to a hollow fiber bioreactor for separation of gluconic acid from sorbitol produced by Zymomonas mobilis permeabilized cells. J. Memb. Sci. 191, 43–51.

Fitrianto, A., Midi, H., 2011. Multi-Response Optimization via Desirability Functionfor the Black Liquor DATA. J. Sci. Technol. 91–102.

Galbe, M., Zacchi, G., 2002. A review of the production of ethanol from softwood. Appl. Microbiol. Biotechnol. 59, 618–28. doi:10.1007/s00253-002-1058-9

Giorno, L., Drioli, E., 2000. Biocatalytic membrane reactors: applications and perspectives. Trends Biotechnol. 18, 339–49.

Grahovac, J., Dodić, J., Jokić, A., Dodić, S., Popov, S., 2012. Optimization of ethanol production from thick juice: A response surface methodology approach. Fuel 93, 221–228. doi:10.1016/j.fuel.2011.10.019

Groot, W.J., Lans, R.G.J.M. Van Der, Luyben, K.C.A.M., 1993. Process engineering for a membrane recycle fermentor. Bioprocess Eng. 8, 235–246.

Gunasekaran, P., Chandra, R.K., 1999. Ethanol fermentation technology. Curr. Sci. 77, 56–69.

Gupta, R., Beg, Q.K., Khan, S., Chauhan, B., 2002. An overview on fermentation , downstream processing and properties of microbial alkaline protease. Appl. Microbiol. Biotechnol. 60, 381–395.

Hahn-Hägerdal, B., Karhumaa, K., Fonseca, C., Spencer-Martins, I., Gorwa-Grauslund, M.F., 2007. Towards industrial pentose-fermenting yeast strains. Appl. Microbiol. Biotechnol. 74, 937–53. doi:10.1007/s00253-006-0827-2

Hahn-Hägerdal, B., Stanley, G., 2010. Fuel Ethanol Production From Lignocellulosic Raw Materials Using Recombinant Yeasts, in: Vertes, A., Qureshi, N., Blaschek, H., Yukawa, H. (Eds.), Biomass to Biofuels: Strategies for Global Industries. John Wiley and Sons Ltd., West Sussex, United kingdom, pp. 261–291.

Hamann, M.L., 2010. System hydrodynamics to reduce fouling of air-sparged immersed flat-sheet microfiltration membranes. University of Stellenbosch.

Helle, S., Duff, S.J.B., 2004. Supplementing Spent Sulfite Liquor with a Lignocellulosic Hydrolysate to Increase Pentose / Hexose Co-fermentation Efficiency and Ethanol Yield. Vancouver, B.C.

Hill, T., Lewicki, P., 2007. Statistica.

Howard, R.L., Abotsi, E., Jansen Van Rensburg, E.L., Howard, S., 2003. Lignocellulose biotechnology : issues of bioconversion and enzyme production. African J. Biotechnol. 2, 602–619.

Huang, S., Chen, J., 1988. Analysis of the kinetics of ethanol fermentation with Zymomonas mobilis considering temperature effect. Enzym. Microbiol. Technol. 10, 431–439.

Ingram, L.., Clark, T., Sewell, G.., Preston, J.., 1987. Genetic Engineering of ethanol production by Escherichia coli. Appl. Environ. Microbiol. 53, 2420–2425.

Ingram, L.., Conway, T., 1988. Expression of different levels of ethanologenic enzymes from Zymomonas Mobilis in recombinant strains of Escherichiea coli. Appl. Environ. Microbiol. 54, 397–404.

Inui, M., Vertes, A.A., Yukawa, H., 2010. Advances Fermentation Technologies, in: Vertes, A.A., Qureshi, N., Blaschek, H.P., Yukawa, H. (Eds.), Biomass to Biofuels: Strategies for Global Industries. John Wiley and Sons Ltd., West Sussex, United kingdom, pp. 311–330.

Ishikawa, H., Nobatashi, H., Tanaka, H., 1990. Mechanism of Fermentation Performance of Zymomonas mobilis under Oxygen Supply in Batch Culture *. J. Ferment. Bioeng. 70, 34–40.

Jeffries, T.W., Jin, Y.-S., 2004. Metabolic engineering for improved fermentation of pentoses by yeasts. Appl. Microbiol. Biotechnol. 63, 495–509. doi:10.1007/s00253-003-1450-0

Karsch, T., Stahl, U., Esser, K., 1983. Ethanol Production by Zymomonas and Saccharomyces , Advantages and Disadvantages known. Eur. J. Appl. Microbiol. 18, 387–391.

Kelsey, J., Pillarella, M.R., Zydney, A.L., 1990. Theoretical analysis of convective flow profiles in a hollow-fiber membrane bioreactor. Chem. Eng. Sci. 45, 3211–3220.

King, F.G., Hossain, M.A., 1982. The effect of Temperature, pH, and initial Glucose concentration on the kinetics of ethanol production by Zymomonas Mobilis in batch Fermentation. Biotechnol. Lett. 4, 531–536.

Krishnan, M.S., Ho, N.W.., Tsao, G.T., 1999. Fermentation Kinetics of Ethanol Production from Glucose and Xylose by Recombinant Saccharomyces 1400 (pLNH33). Appl. Biochem. Biotechnol. 77, 373–388.

Kyllonen, H.M., Pirkonen, P., Nystrom, M., 2005. Membrane filtration enhanced by ultrasound : a review. Desalination 181, 319–335. doi:10.1016/j.desal.2005.06.003

Lafforgue, C., Malinowski, J., Goma, G., 1987. High Yeast Concentration in Continuous Fermentation with cell recycle obtained by tangential microfiltration. Biotechnol. Lett. 9, 347–352.

Lafforgue, G., Delorme, C., Goma, P., 1994. Continuous Alcoholic Fermentation with Sacchuromyces cerevisiue Recycle by Tangential Filtration : Key Points for Process Modelling. Biotechnol. Lett. 16, 741–746.

Lau, M.W., Gunawan, C., Balan, V., Dale, B.E., 2010. Comparing the fermentation performance of Escherichia coli KO11 , Saccharomyces cerevisiae 424A ( LNH-ST ) and Zymomonas mobilis AX101 for cellulosic ethanol production. Biotechnol. Biofuels 3, 1–10.

Lawford, H.., Rousseau, J.D., 2002. Performance Testing of Zymomonas mobilis Metabolically Engineered for Cofermentation of Glucose , Xylose , and Arabinose. Appl. Biochem. Biotechnol. 98, 429–448.

Lawford, H.., Rousseau, J.D., 2003. Cellulosic Fuel Ethanol. Appl. Biochem. Biotechnol. 105, 457–469.

Lawford, H.G., 1988. A New Approach to Improving the Performance of Zymomonas in Continuous Ethanol Fermentations. Biotechnol. Bioeng. Vol 33, 203–219.

Lawson, J., Erjavec, J.., 2001. Response Surface Methodology, in: Modern Statistics for Engineering and Quality Improvement. Duxbury., p. 465.

Le Clech, P., Jefferson, B., Chang, I.S., Judd, S.J., 2003. Critical flux determination by the flux-step method in a submerged membrane bioreactor. J. Memb. Sci. 227, 81–93. doi:10.1016/j.memsci.2003.07.021

Lee, C.W., Gu, M.B., Chang, H.N., 1989. High-density culture of Escherichia coil carrying recombinant plasmid in a membrane cell recyde fermenter. Enzyme Microb. Technol. 11, 49–54.

Lee, K.J., Rogers, P.L., 1983. The Fermentation Kinetics of Ethanol Production by Zymomonas mobilis. Chem. Eng. J. 27, B31–B38.

Lee, K.Y., Park, J.M., Kim, T.Y., Yun, H., Lee, S.Y., 2010. The genome-scale metabolic network analysis of Zymomonas mobilis ZM4 explains physiological features and suggests ethanol and succinic acid production strategies. Microb. Cell Fact. 9, 94. doi:10.1186/1475-2859-9-94

Levesley, J.A., Hoare, M., 1999. The effect of high frequency backflushing on the microfiltration of yeast homogenate suspensions for the recovery of soluble proteins. J. Memb. Sci. 158, 29–39.

Li, K., 1999. Novel Ceramic Hollow Fibre Membranes for Separation and Reaction. London.

Libicki, B., Karel, S.F., Robertson, C.R., 1985. The Immobilization of Whole Cells: Engineering Principles. Chem. Eng. Sci. 40, 1321–1354.

Lievenspiel, O., 1999. Chemical Reaction Engineering, 3rd ed, Distribution. John Wiley and Sons Ltd., New York.

Lin, Y., Tanaka, S., 2006. Ethanol fermentation from biomass resources : current state and prospects. Appl. Microbiol. 69, 627–642. doi:10.1007/s00253-005-0229-x

Liu, S., 2010. Conversion of Biomass to Ethanol by Other Organisms, in: Vertes, A., Quereshi, N., Blascheck, H.P., Yukawa, H. (Eds.), Biomass to Biofuels: Strategies for Global Industries. John Wiley and Sons Ltd., West Sussex, United kingdom, pp. 293–310.

McCrady, E., 1991. The Nature of Lignin [WWW Document]. Alkaline Pap. Advocate. URL http://cool.conservation-us.org/byorg/abbey/ap/ap04/ap04-4/ap04-402.html (accessed 4.5.12).

McKendry, P., 2002. Energy production from biomass (part 1): overview of biomass. Bioresour. Technol. 83, 37–46.

Melzoch, K., Rychetara, M., Markovichov, N.., Pospichalova, V., Basarora, G., Manakov, M.., 1991. Applicatiobn of a membrane recycle bioreactor for continuous ethanol production. Appl. Microbiol. Biotechnol. 34, 469–472.

Menon, V., Rao, M., 2012. Trends in bioconversion of lignocellulose: Biofuels, platform chemicals & biorefinery concept. Prog. Energy Combust. Sci. 38, 522–550. doi:10.1016/j.pecs.2012.02.002

Mercier-bonin, M., Daubert, I., Le, D., Maranges, C., Fonade, C., Lafforgue, C., 2001. How unsteady filtration conditions can improve the process efficiency during cell cultures in membrane bioreactors. Sep. Purif. Technol. 23, 601–615.

Middleton, M., 2014. SensIt.

Mohagheghi, A., Dowe, N., Schell, D., Chou, Y.-C., Eddy, C., Zhang, M., 2004. Performance of a newly developed integrant of Zymomonas mobilis for ethanol production on corn stover hydrolysate. Biotechnol. Lett. 26, 321–5.

Mohagheghi, A., Evans, K., Chou, Y.-C., Zhang, M., 2002. Cofermentation of Glucose , Xylose , and Arabinose by Genomic DNA – Integrated Xylose / Arabinose Fermenting Strain of Zymomonas mobilis AX101. Appl. Biochem. Biotechnol. 98-100, 885–898.

Mohagheghi, A., Ruth, M., Schell, D.J., 2006. Conditioning Hemicellulose Hydrolysates for Fermentation: Effects of Overliming pH on Sugar and Ethanol Yields. Process Biochem. 41, 1806–1811. doi:10.1016/j.procbio.2006.03.028

Monod, J., 1949. The Growth of Bacterial Cultures. Annu. Rev. Microbiol. 3, 371–394.

Nakao, S., Osada, H., Kurata, H., Tsuru, T., Kimura, S., 1988. Separation of Proteins by Charged Ultrafiltration Membranes. Desalination 70, 191–205.

Nellaiah, H., Karunakaran, T., Gunasekaran, P., 1988. Ethanol fermentation by an efficient Strain, NRRL B-4286, of Zymomonas mobilis. J. Ferment. Technol. 66, 219–223.

Nielsen, J., Villadsen, J., Liden, G., 2003. From Cellular Function to Industrial Products, 2nd ed, Bioreaction Engineering Principles. Kluwer Acadewmic/Plenum Publishers, New York, Boston, Dordrecht,London, Moscow.

Nipkow, A., Sonnleitner, B., Fiechter, A., 1985. Effect of carbon dioxide on growth of Zymomonas mobilis in continuous culture. Appl. Microbiol. Biotechnol. 21, 287–291.

Nishiwaki, a, Dunn, I.., 1999. Analysis of the performance of a two-stage fermentor with cell recycle for continuous ethanol production using different kinetic models. Biochem. Eng. J. 4, 37–44. doi:10.1016/S1369-703X(99)00029-7

Nunez J., S., Lopez, A.V.G., Lema, J.., 1989. The D-Xylose Fermenting Capacities of Immobilized Pichia stipitis and Pachysolen tannophilus. Biotechnol. Lett. ii, 353–358.

Olsson, L., Hahn-Hagerdal, B., 1996. Fermentation of lignocellulosic hydrolysates for ethanol production. Appl. Microbiol. 18, 312–331.

Panesar, P.S., Marwaha, S.S., Kennedy, J.F., 2006. Zymomonas mobilis : an alternative ethanol producer. Chem. Technol. 635, 623–635. doi:10.1002/jctb.1448

Paterson, S.., Fane, A.., Fell, C.., 1988. Sorbitol and gluconate production in a hollow fibre membrane reactor by immobilized. Biocatalysis 1, 217–229.

Pearce, G., Stepheson, T., Daigger, G., Verrecht, B., Germain, E., Hill, G., 2011. Membrane Fundamentals, in: Pearce, G., Stepheson, T., Daigger, G., Verrecht, B., Germain, E., Jefferson, B. (Eds.), The Membrane Bioreactor Book. Elsivieer Ltd, pp. 55–207. doi:10.1016/B978-0-08-096682-3.10002-2

Persson, a, Jönsson, a S., Zacchi, G., 2001. Separation of lactic acid-producing bacteria from fermentation broth using a ceramic microfiltration membrane with constant permeate flow. Biotechnol. Bioeng. 72, 269–77.

Pirt, S.., 1976. Principles of Microbe and Cell Cultivation. AIChE J. 22, 621.

Postma, D., 2012. Modification of hemicellulose using chemical and physical methods for use in the pulp and paper industry. University of Stellenbosch.

Purwadi, R., Brandberg, T., Taherzadeh, M.J., 2007. A Possible Industrial Solution to Ferment Lignocellulosic Hydrolyzate to Ethanol : Continuous Cultivation with Flocculating Yeast. Int. J. Mol. Sci. 8, 920–932.

Redkar, S.G., Davis, R.H., 1995. Cross-flow microfiltration with high-frequency reverse filtration. AIChE J. 41, 501–508.

Refaat, A.A., 2012. Biofuels from Waste Materials, in: Comprehensive Renewable Energy. Elsevier Ltd., Giza, Egypt, pp. 217–262. doi:10.1016/B978-0-08-087872-0.00518-7

Roberts, G.W., 2009. Chemical Reactions and Chemical Reactors, 1st ed. John Wiley and Sons Ltd., New Jersey.

Roca, C., Olsson, L., 2003. Increasing ethanol productivity during xylose fermentation by cell recycling of recombinant Saccharomyces cerevisiae. Appl. Microbiol. Biotechnol. 60, 560–3. doi:10.1007/s00253-002-1147-9

Rogers, P.., Lee, K.J., Tribe, D.., 1979. Ethanol Production by Zymomonas Mobilis in Continuous Culture at High Glucose Concentrations. Biotechnol. Lett. 1, 421–426.

Rogers, P.., Lee, K.J., Tribe, D.., 1981. Kinetics of Alcohol production by Zymomonas mobilis at high sugar concentrations. Biotechnol. Lett. 3, 165–170.

Rogers, P.L., Jeon, Y.J., Svenson, C.J., Joachimsthal, E.L., 2002. Kinetic analysis of ethanol production by an acetate-resistant strain of recombinant Zymomonas mobilis. Biotechnol. Lett. 24, 819–824.

Rogers, P.L., Joachimsthal, E.L., 2000. Characterization of a High-Productivity Recombinant Strain of Zymomonas mobilis for Ethanol Production from Glucose / Xylose Mixtures. Appl. Biochem. Biotechnol. 84, 343–356.

Rogers, P.L., Joachimsthal, E.L., Haggett, K.D., 1999. Evaluation of Recombinant Strains of Zymomonas mobilis for Ethanol Production from Glucose / Xylose Media. Appl. Biochem. Biotechnol. 77, 147–157.

Rogers, P.L., Lee, K.J., Lefebvre, M., Tribe, D.E., 1980. High Productivity Ethanol Fermentations with Zymomonas Mobilis using Continuous Cell Recycle. Biotechnol. Lett. 492, 487–492.

Rogers, P.L., Lee, K.J., Skotnicki, M.L., 1981. The effect of temperature on the kinetics of Ethanol Production by strains of Zymomonas mobilis. Biotechnol. Lett. 3, 291–296.

Rogers, P.L., Leksawasdi, N., Joachimsthal, E.L., 2001. Mathematical modelling of ethanol production from glucose / xylose mixtures by recombinant Zymomonas mobilis. Biotechnol. Lett. 23, 1087–1093.

Rudolf, A., Alkasrawi, M., Zacchi, G., Lidén, G., 2005. A comparison between batch and fed-batch simultaneous saccharification and fermentation of steam pretreated spruce. Enzyme Microb. Technol. 37, 195–204. doi:10.1016/j.enzmictec.2005.02.013

Russotti, G., Goklen, K.., 2001. Vortex Flow Filtration for Cell Separation in Bioreactor, in: Wang, W. (Ed.), Membrane Separations in Biotechnology. Mercel Dekker, Inc., New York and Based, pp. 85–173.

Saroj, D.P., Guglielmi, G., Chiarani, D., Andreottola, G., 2008. Modeling and simulation of membrane bioreactors by incorporating simultaneous storage and growth concept: an especial attention to fouling while modeling the biological process. Desalination 221, 475–482. doi:10.1016/j.desal.2007.01.108

Sauer, U., Sonderegger, M., Jeppsson, M., Larsson, C., Gorwa-grauslund, M.A., Boles, E., Olsson, L., Spencer-martins, I., Hahn-Hagerdal, B., 2004. Fermentation Performance of Engineered and Evolved Xylose-Fermenting Saccharomyces cerevisiae Strains. Biotechnol. Bioeng. 87, 90–98. doi:10.1002/bit.20094

Schreder, K., Brunner, R., Hampe, R., 1934. The anaerobic and aerobic fermentation of Pseudomonas lindneri Klyver in glucose-containing inorganic nutruient solution. Biochem. Eng. J. 237, 223–242.

Scott, C.D., 1987. Immobilized cells : a review of recent literature. Enzyme Microb. Technol. 9, 57–61.

Senthilkumar, V., Gunasekaran, P., 2005. Bioethanol production from cellulosic substrates : Engineered bacteria and process integration challenges. J. Sci. Ind. Res. 64, 845–853.

Shirazi, S., Lin, C.-J., Chen, D., 2010. Inorganic fouling of pressure-driven membrane processes — A critical review. Desalination 250, 236–248. doi:10.1016/j.desal.2009.02.056

Shuler, M.L., Kargi, F., 2008. Operating Considerations for bioreactors for Suspension and Immobilized Cultures, in: Bioprocess Engineering: Basic Concepts. Prentice Hall, pp. 263–275.

Skotnicki, M.L., Lee, K.J., Tribe, D.E., Rogers, P.L., 1981. Comparison of Ethanol Production by Different Zymomonas Strains Comparison of Ethanol Production by Different Zymomonas Strains. Appl. Environ. Microbiol. 41, 889–893.

Slininger, P.J., Bothast1, R.J., Ladisch, M.R., Okos, M.R., 1990. Optimum ph and temperature conditions for xylose fermentation by Pichia stipitis. Biotechnol. Bioeng. 35, 727–731.

Sreekumar, O., Chand, N., Basappa, S.C., 1999. Optimization and interaction of media components in ethanol production using Zymomonas mobilis by response surface methodology. J. Biosci. Bioeng. 88, 334–8.

Sreenath, H., Jeffreis, T., 2000. Production of ethanol from wood hydrolysate by yeasts. Bioresour. Technol. 72, 253–260.

Steynberg, D.L., 2012. Characterisation and desalination of typical South African Abalone farm effluent sea water. University of Stellenbosch.

Strathmann, H., Giorno, L., Drioli, E., 2006. Introduction, in: An Introduction to Membrane and Science Technology. Institute of Membrane Technology, Roma, pp. 3–13.

Sweere, A.P.J., Luyben, K.C.A.M., Kossen, N.W.F., 1987. Regime analysis and scale-down: Tools to investigate the performance of bioreactors. Enzyme Microb. Technol. 9, 386–398. doi:10.1016/0141-0229(87)90133-5

Swings, J., De Ley, J., 1977. The Biology of Zymomonas. Bacteriol. Rev. 41, 1–46.

Tolan, J., 2002. Iogen's process for producing ethanol from cellulosic biomass. Clean Technol. Environ. Policy 3, 339–345. doi:10.1007/s10098-001-0131-x

Vaija, J., Lagaude, A., Ghommidh, C., 1995. Evaluation of image analysis and laser granulometry for microbial cell sizing. Antonie Van Leeuwenhoek. 67, 139–49.

Van den Berg, G.B., Smolders, C. a., 1990. Flux decline in ultrafiltration processes. Desalination 77, 101–133. doi:10.1016/0011-9164(90)85023-4

Vázquez, M., Oliva, M., Téllez-Luis, S.J., Ramírez, J. a, 2007. Hydrolysis of sorghum straw using phosphoric acid: evaluation of furfural production. Bioresour. Technol. 98, 3053–60. doi:10.1016/j.biortech.2006.10.017

Wimpenny, J.W.., 1997. The validity of models. Adv. Dent Res 11, 150–159.

Wyman, C.E., Spindler, D.D., Grohmann, K., 1992. Simultaneous Saccharification and Fermentation of several lignocellulosic feedstocks to fuel ethanol. Biomass and Bioenergy 3, 301–307.

Ye, Y., 2005. Macromolecular fouling during membrane filtration of complex fluids. University of New South Wales.

Zacchi, G., 2006. Bio-ethanol – the fuel of tomorrow from the residues of today. Trends Biotechnol. 24. doi:10.1016/j.tibtech.2006.10.004

Zacchi, G., Anders, W., Galbe, M., 2003. Techno-Economic Evaluation of Producing Ethanol from Softwood: Comparison of SSF and SHF and Identification of Bottlenecks. Biotechnol. Prog. 19, 1109–1107.

Zacchi, G., Axelsson, A., 1989. Economic evaluation of preconcentration in production of ethanol from dilute sugar solutions. Biotechnol. Bioeng. 34, 223–233.

Zacchi, G., Bura, R., Lesnicki, G., Saddler, J., Karin, O., 2007. A comparison between simultaneous saccharification and fermentation and separate hydrolysis and fermentation using steam-pretreated corn stover. Process Biochem. 42, 834–839. doi:10.1016/j.procbio.2007.02.003

Zhang, J., Lynd, L.R., 2010. Ethanol production from paper sludge by simultaneous saccharification and co-fermentation using recombinant xylose-fermenting microorganisms. Biotechnol. Bioeng. 107, 235–44. doi:10.1002/bit.22811

Zhang, M., 2003. Zymomonas mobilis: Microbial Pentose metabolism, Microbial Pentose Metabolism. National Renewable Energy Laboratory, Colorado, USA.

Zhang, M., Chou, Y.-C., Picataggio, S., Finkelstein, M., 1998. Single Zymomonas Mobilis strain for xylose and arabinose fermentation. 5843760.

Zhang, M., Chou, Y.-C., William, H., Eddy, C., Evans, K., Mohagheghi, A., 2007. Zymomonas pentose-sugar fermenting strains and uses thereof. 7,223,575.

Zhang, M., Eddy, C., Deanda, K., Finkelstein, M., Picataggio, S., 1995. Metabolic engineering of a pentose metabolism pathway in ethanologenic Zymomonas mobilis. Science (80-. ). 267, 240–243.

Zhang, M., Eddy, C., Deanda, K., Finkelstein, M., Picataggio, S., n.d. Metabolic Engineering of a Pentose Metabolism Pathway in Ethanologenic Zymomonas mobilis. Science (80-. ). 267, 240–243. doi:10.1126/science.267.5195.240

Zhang, M., Franden, M.A., Newman, M., Mcmillan, J., Finkelstein, M., Picataggio, S., 1995. Promising Ethanologens for Xylose Fermentation Scientific Note. Appl. Biochem. Biotechnol. 51, 527–536.

Zhao, Y., Wu, K., Wang, Z., Zhao, L., Li, S., 2000. Fouling and cleaning of membrane--a literature review. J. Environ. Sci. 12, 241–251.

Zhu, Y., 2007. Chapter 14 . Immobilized Cell Fermentation for Production of Chemicals and Fuels. Adsorpt. J. Int. Adsorpt. Soc. 373–396.

# APPENDIX A

## ADDITIONAL LITERATURE GRAPHS

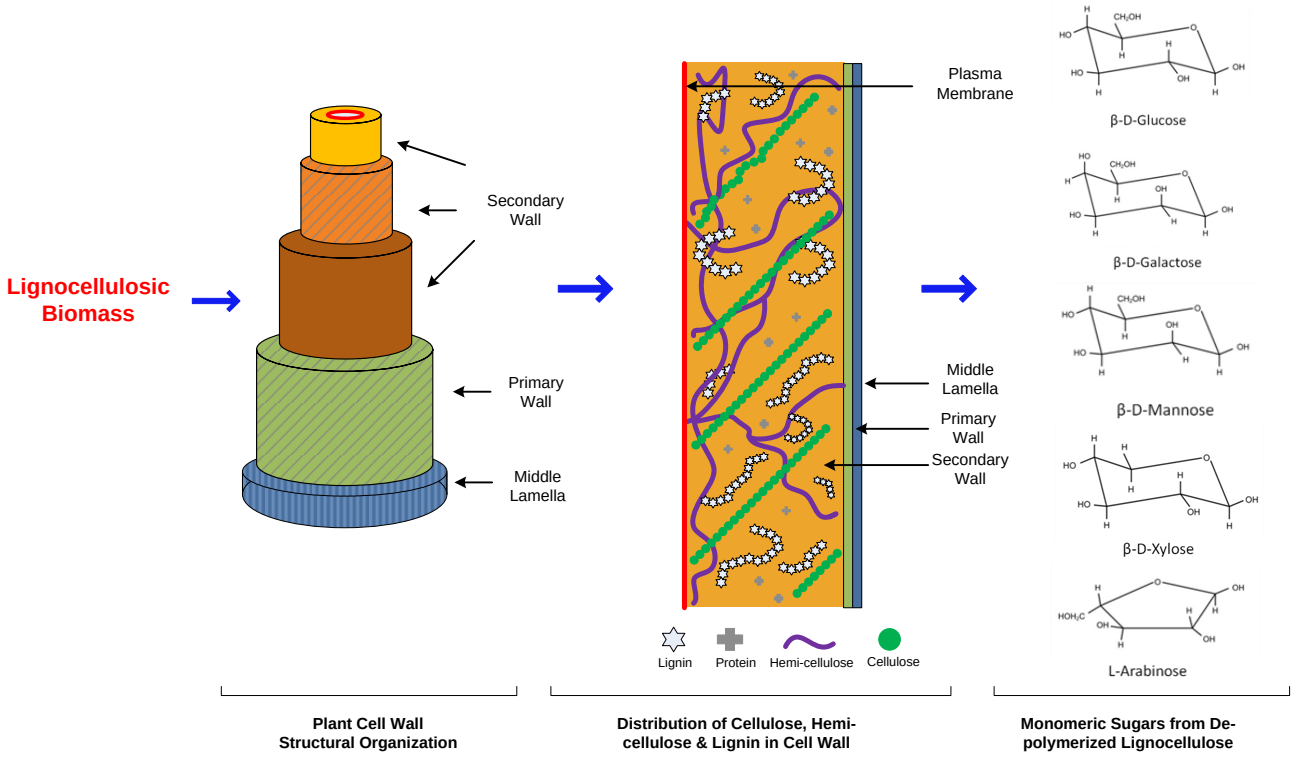


***Figure 93:*** *Breakdown or framework of lignocellulosic biomass (redrawn from Menon & Rao, 2012)*

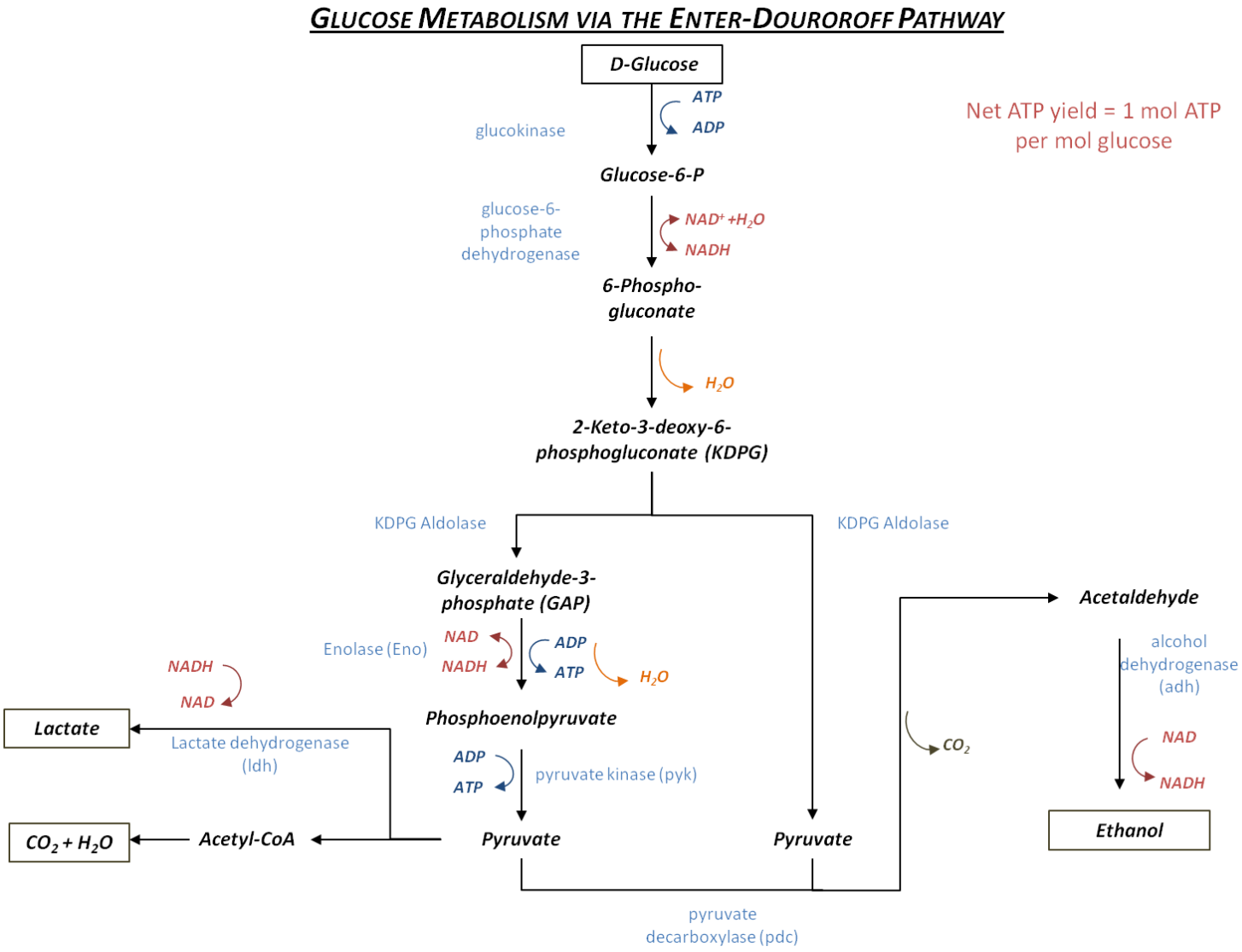


***Figure 94:*** *Z. mobilis Glucose Metabolism via the Enter-Douroroff Pathway [Redrawn from Shuler and Kargi, 2008)*

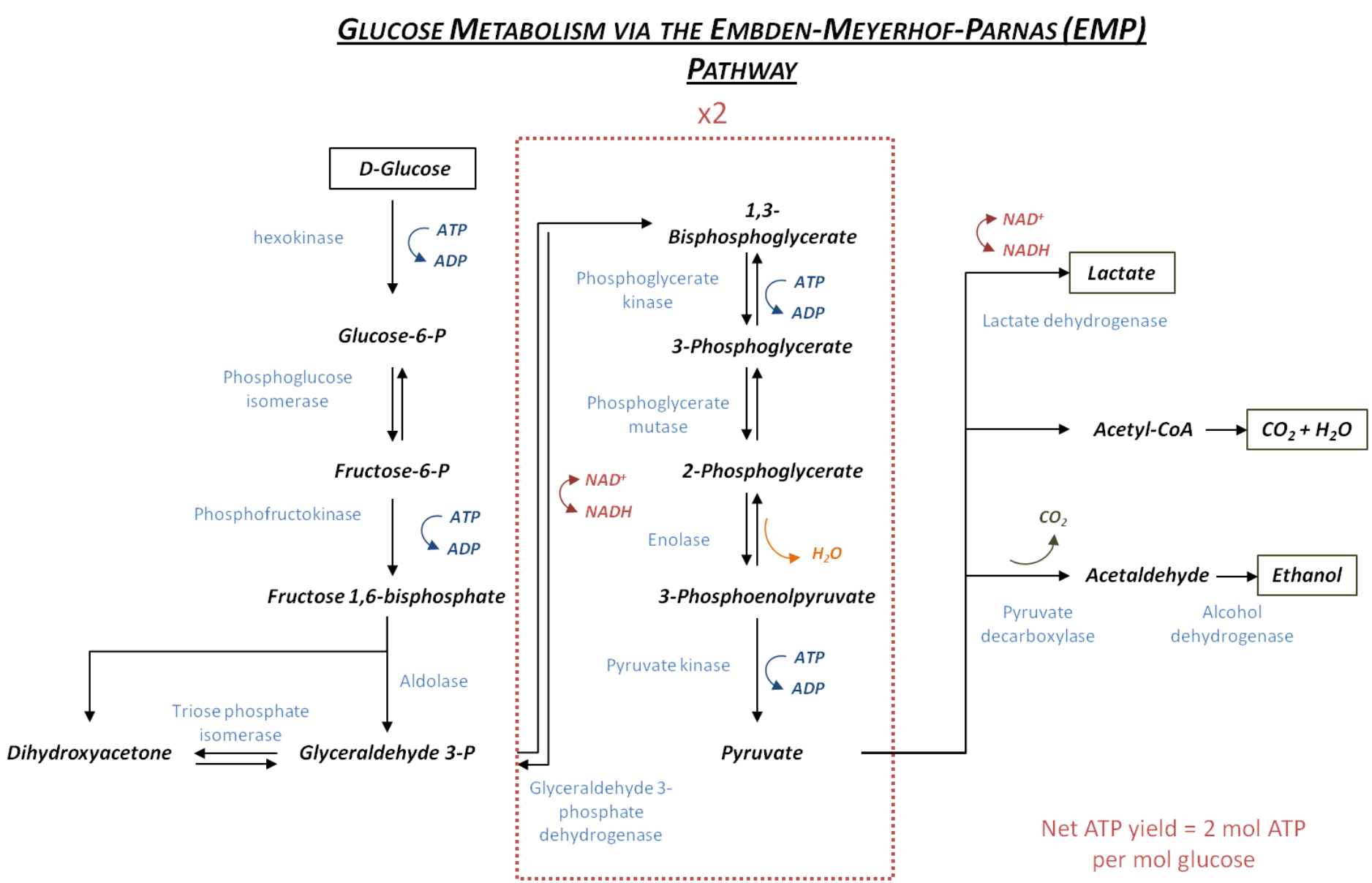


***Figure 95:*** *Glucose metabolism via the Embden-Meyerhof-Parnas (EMP) Pathway [redrawn from Shuler and Kargi, 2008)*

# APPENDIX B

## EXPERIMETAL DATA FOR ANALYSIS

## B.1. LIST OF CHEMICALS USED

The list presented below presents all the chemicals and nutrients necessary for seed preparation, ethanol synthesis, membrane maintenance and the respective analytical procedure for the reaction products.

- ***Seed Preparation and Ethanol Synthesis***
  - Yeast Extract
  - D-Glucose Monohydrate ($C_6H_{12}O_6.H_2O$) (Reagent grade) (Kimix, South Africa)
  - D-(+)-Xylose (≥99%) ($C_5H_{10}O_5$) (Reagent grade) (Sigma-Aldrich, South Africa)
  - Sorbitol ($C_6H_{14}O_6$) (≥ 98%) (Sigma-Aldrich, South Africa)
  - De-ionized water ($H_2O$)
  - Potassium Hydroxide (KOH) (uniVAR) (Merck, South Africa)
  - Dipotassium Phosphate ($K_2HPO_4$) (uniVAR) (Merck, South Africa)
  - Potassium Phosphate Monobasic ($KH_2PO_4$) (uniVAR) (Merck, South Africa)
- ***Membrane Maintenance***
  - Sodium Hydroxide pellets (uniVAR) (NaOH)
  - Nitric Acid (55% solution uniVAR) ($HNO_3$)
- **HPLC Sample Preparation**
  - Perchloric Acid ($HClO_4$) (70% solution uniVAR)
  - Potassium Hydroxide (KOH) (uniVAR) (Merck, South Africa)
- **HPLC Sample Analysis**
  - D-(+)-Glucose (≥99.5%) (HPLC grade) (Sigma-Aldrich, South Africa)
  - D-(+)-Xylose (≥99%) (HPLC grade) (Sigma-Aldrich, South Africa)
  - L-(+)-Arabinose (≥99%) (HPLC grade) (Sigma-Aldrich, South Africa)
  - D-(+)-Cellobiose (≥99%)
  - Acetic Acid (ReagentPlus®, ≥99%) (Sigma-Aldrich, South Africa)
  - Formic Acid (ACS reagent, ≥96%) (Sigma-Aldrich, South Africa)
  - Ethanol (denatured, CHROMASOLV, for HPLC) (Sigma-Aldrich, South Africa)
  - Glycerol (BioXtra, ≥99% GC) (Sigma-Aldrich, South Africa)

## B.2. PUMP CALIBRATION CURVE (P-201)

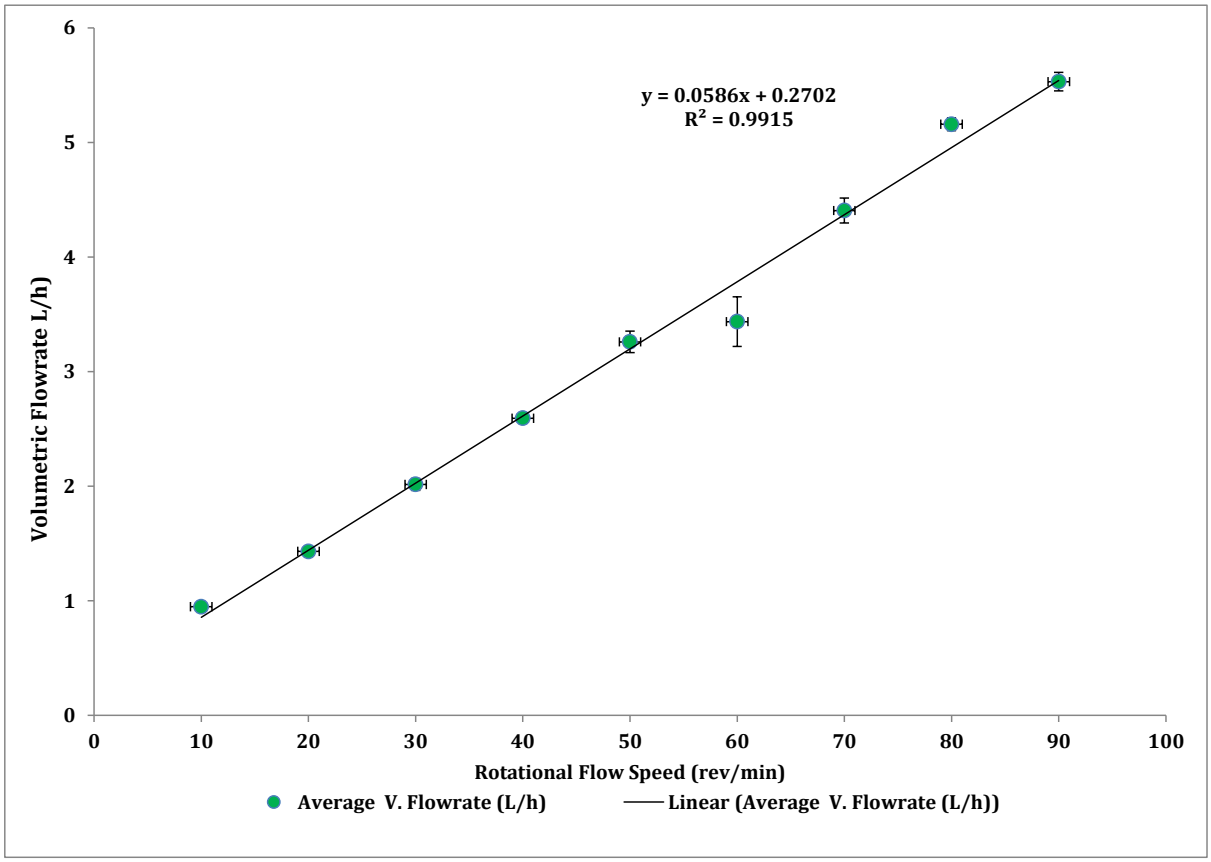


***Figure 96:*** *Calibration curve for the fresh substrate feed pump (P-201)*

## B.3 MODEL KINETIC PARAMETER NOTATION

***Table 29:*** *Model Kinetic Parameter Notation*

| Notation | Parameter | Units |
|---|---|---|
| $k_1$ | alpha,α | |
| $k_2$ | $\mu_{max.1}$ | $h^{-1}$ |
| $k_3$ | $K_{sx1}$ | g/L |
| $k_4$ | $\mu_{max.2}$ | $h^{-1}$ |
| $k_5$ | $K_{sx2}$ | g/L |
| $k_6$ | $k_D$ | $h^{-1}$ |
| $k_7$ | $q_{s,max.1}$ | $g_{substrate}/g_{cells}.h$ |
| $k_8$ | Kss1 | g/L |
| $k_9$ | $q_{s,max.2}$ | $g_{substrate}/g_{cells}.h$ |
| $k_{10}$ | Kss2 | g/L |
| $k_{11}$ | $q_{pmax.1}$ | $g_{product}/g_{cells}.h$ |
| $k_{12}$ | $q_{pmax.2}$ | $g_{product}/g_{cells}.h$ |
| $k_{13}$ | $q_{p\_AC\_1}$ | $g_{Acetate}/g_{cells}.h$ |
| $k_{14}$ | $q_{p\_AC\_2}$ | $g_{Acetate}/g_{cells}.h$ |
| $k_{15}$ | $K_{spAC1}$ | g/L |
| $k_{16}$ | $K_{spAC2}$ | g/L |

## B.4 IMAGES OF EXPERIMENTAL SET-UP

***Figure 97:*** *Experimental Set-up for MBR operation*

***Figure 98:*** *Custom built 1.5L fermenter, water bath, and fresh substrate reservoirs*

***Figure 100:*** *Single tubular membrane microfiltration unit (indicated by red ellipse), permeate reservoir, and backflush pump*

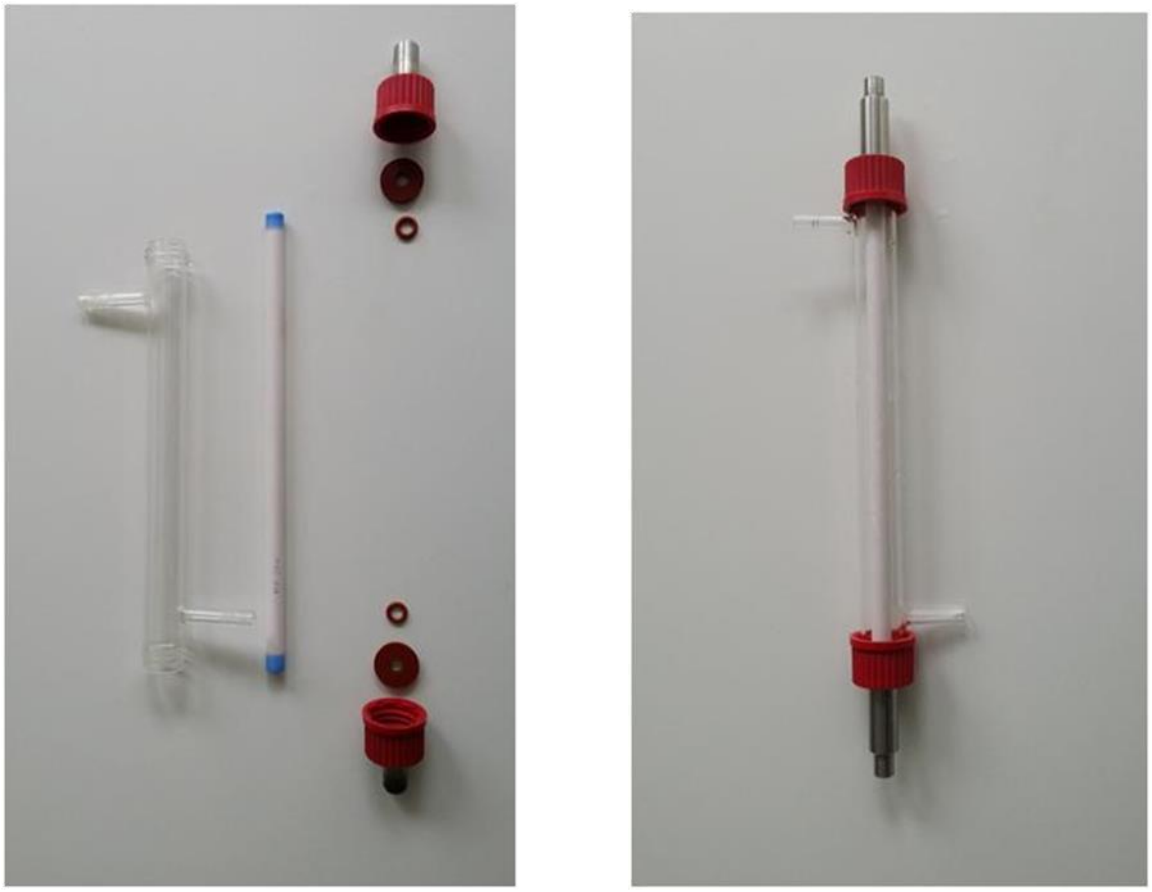

***Figure 99:*** *Parts used to construct the MFU (left), assembled MFU (right)*

# APPENDIX C

## ADDITIONAL RESULTS

### C.1.1 PROFILES FOR GLUCOSE FERMENTATION FULL FACTORIAL DESIGN

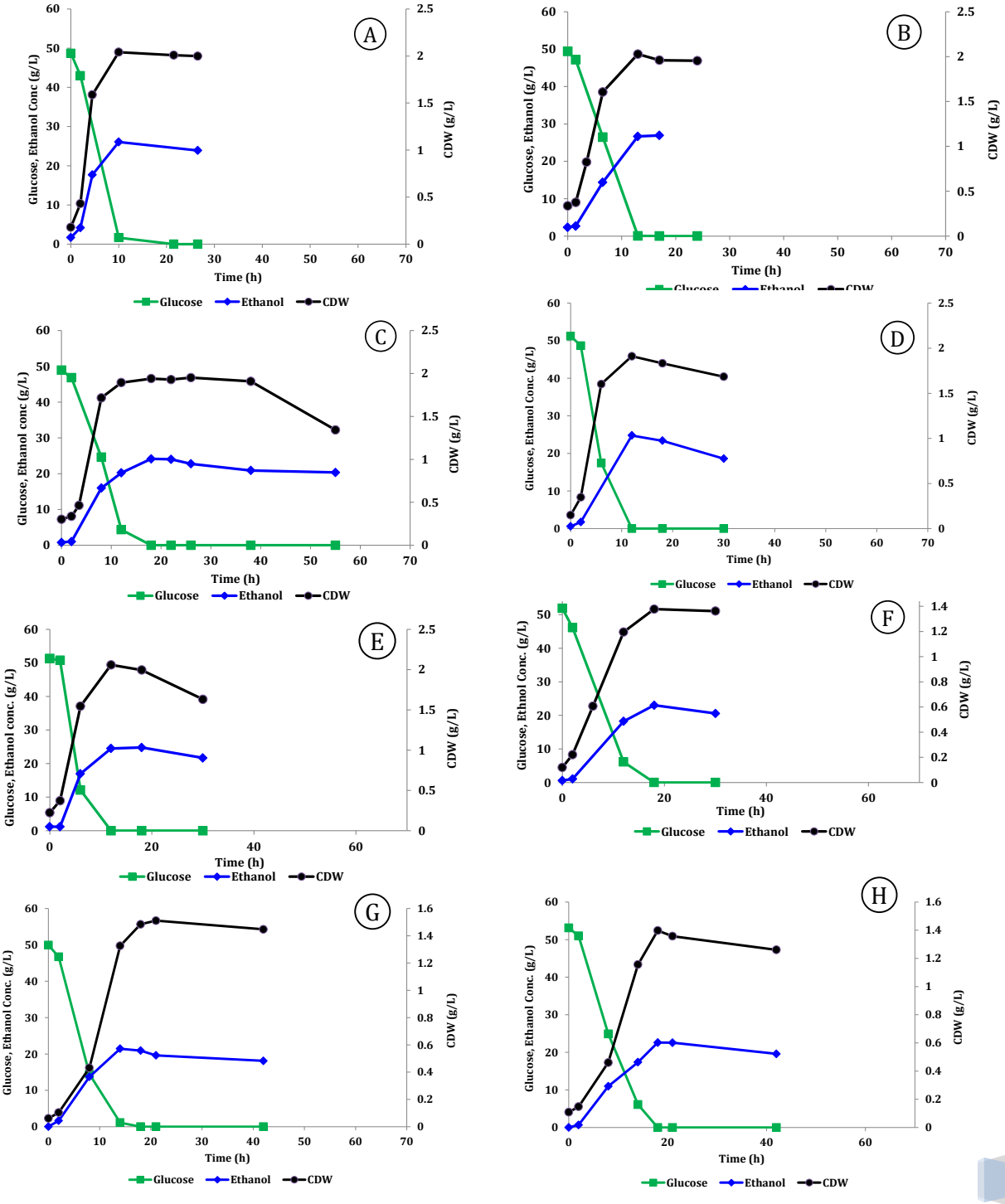

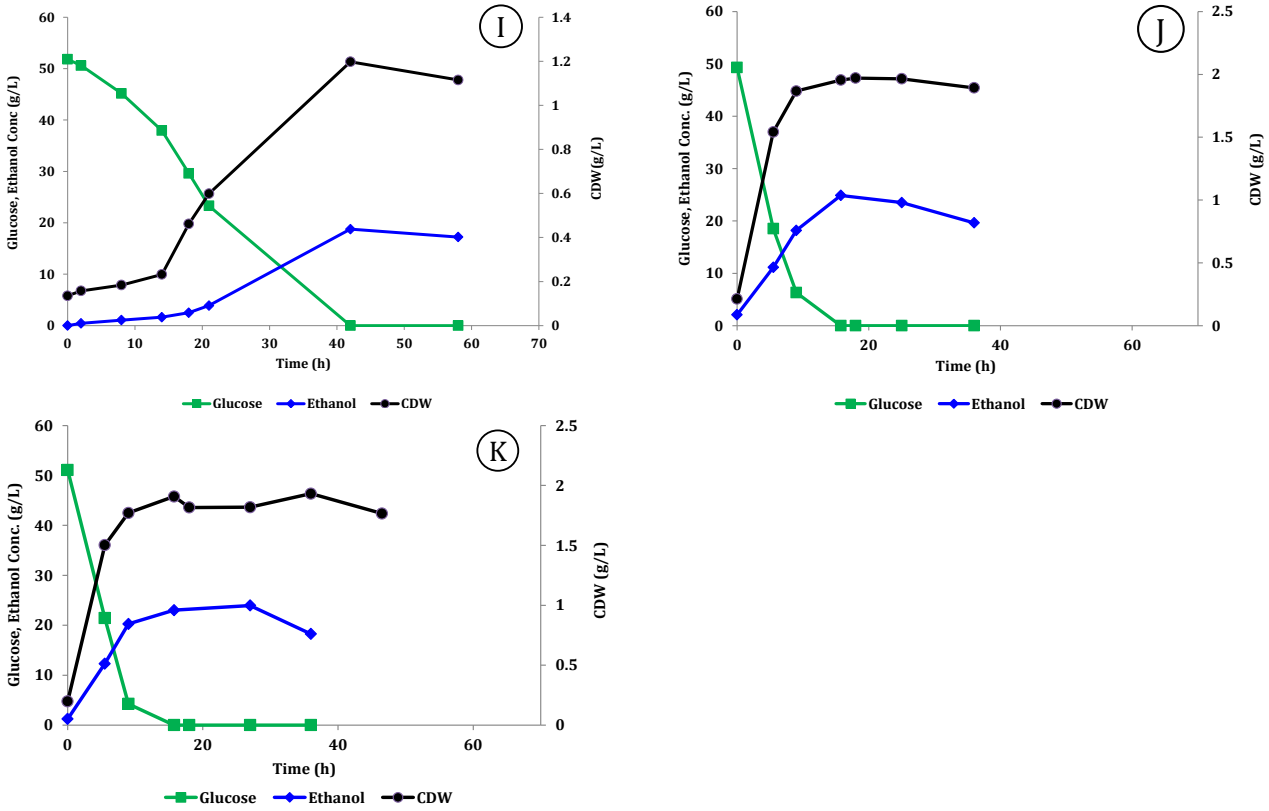


***Figure 101:*** *Glucose fermentation Full factorial experimental Data.* ***A*** *– Temp. = 30 °C, $pH_0$ = 6;* ***B*** *– Temp. = 30 °C, $pH_0$ = 7;* ***C*** *– Temp. = 30 °C, $pH_0$ = 8;* ***D*** *– Temp. = 35 °C, $pH_0$ = 6;* ***E*** *– Temp. = 35 °C, $pH_0$ = 7;* ***F*** *– Temp. = 35 °C, $pH_0$ = 8;* ***G*** *– Temp. = 40 °C, $pH_0$ = 6;* ***H*** *– Temp. = 40 °C, $pH_0$ = 7;* ***I*** *– Temp. = 40 °C, $pH_0$ = 8;* ***J*** *– Temp. = 35 °C, $pH_0$ = 7;* ***K*** *– Temp. = 35 °C, $pH_0$ = 7;*

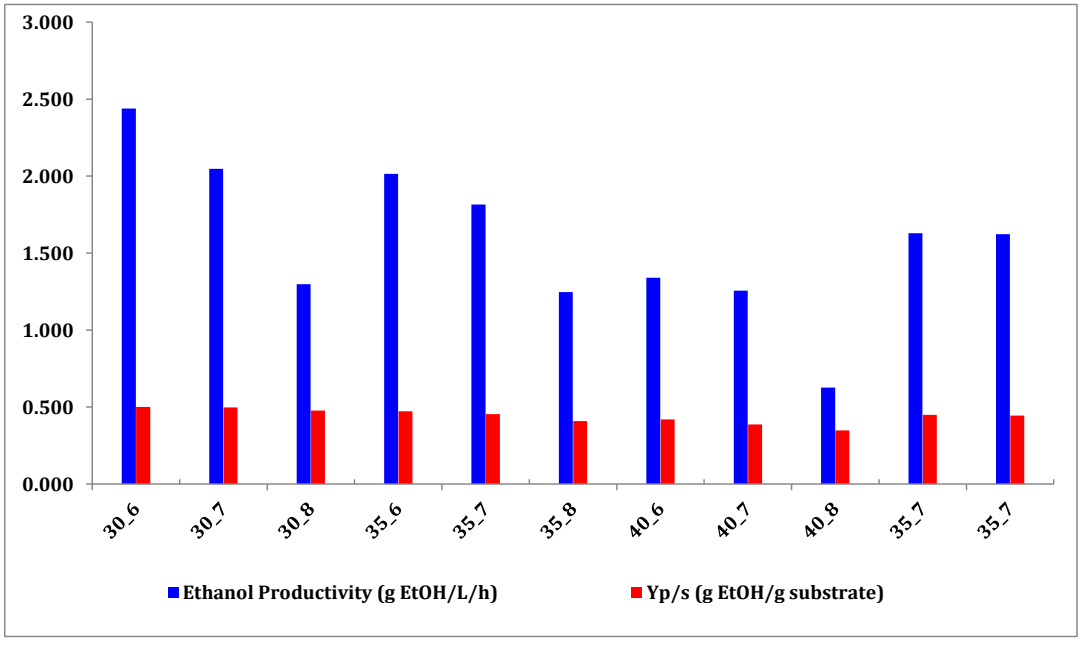


**Figure 102:** *Summary of the glucose fermentation full factorial design data*

***Table 30:*** *ANOVA analysis for ethanol productivity estimation for glucose fermentation by Z. mobilis ZM4*

| Factor | ANOVA; Var.:Yps (% theo. EtOH yield); R-sqr=.99135; Adj:.9827 (3**(2-0) full factorial design, 1 block , 9 runs (Design: 2 3-level factors, 1 Blocks, 11 Runs (3**(2-0) full factorial design, 1 block , 9 runs (Spreadsheet1) in GG_FFx(paper).stw) in Workbook3_(Recovered)) in GG_redone.stw) 2 3-level factors, 1 Blocks, 11 Runs; MS Residual=1.533333 DV: Yps (% theo. EtOH yield) | | | | |
|---|---|---|---|---|---|
| | SS | df | MS | F | p |
| **(1)Temperature (°C) (L)** | 682.6667 | 1 | 682.6667 | 445.2174 | 0.000004 |
| **Temperature (°C) (Q)** | 2.5333 | 1 | 2.5333 | 1.6522 | 0.254978 |
| **(2)$pH_0$ (L)** | 160.1667 | 1 | 160.1667 | 104.4565 | 0.000154 |
| **$pH_0$ (Q)** | 5.7000 | 1 | 5.7000 | 3.7174 | 0.111769 |
| **1L by 2L** | 25.0000 | 1 | 25.0000 | 16.3043 | 0.009944 |
| **Error** | 7.6667 | 5 | 1.5333 | | |
| **Total SS** | 886.5455 | 10 | | | |

**Table 31:** *ANOVA analysis for ethanol yield estimation for glucose fermentation by Z. mobilis ZM4*

| Factor | ANOVA; Var.:Volumetric Productivity (g EtOH/L/h); R-sqr=.97857; Adj:.95713 (3**(2-0) full factorial design, 1 block , 9 runs (Design: 2 3-level factors, 1 Blocks, 11 Runs (3**(2-0) full factorial design, 1 block , 9 runs (Spreadsheet1) in GG_FFx(paper).stw) in Workbook3_(Recovered)) in GG_redone.stw) 2 3-level factors, 1 Blocks, 11 Runs; MS Residual=.0105895 DV: Volumetric Productivity (g EtOH/L/h) | | | | |
|---|---|---|---|---|---|
| | SS | df | MS | F | p |
| **(1)Temperature (°C) (L)** | 1.096538 | 1 | 1.096538 | 103.5498 | 0.000157 |
| **Temperature (°C) (Q)** | 0.039901 | 1 | 0.039901 | 3.7680 | 0.109913 |
| **(2)$pH_0$ (L)** | 1.146688 | 1 | 1.146688 | 108.2857 | 0.000141 |
| **$pH_0$ (Q)** | 0.054371 | 1 | 0.054371 | 5.1344 | 0.072809 |
| **1L by 2L** | 0.045796 | 1 | 0.045796 | 4.3247 | 0.092110 |
| **Error** | 0.052947 | 5 | 0.010589 | | |
| **Total SS** | 2.470201 | 10 | | | |

## C.1.2 VALIDATION OF THE EFFECT OF TEMPERATURE AND $PH_0$ ON GLUCOSE FERMENTATION BY *Z. MOBILIS* ZM4

### *Test for Model Adequacy*

Prior to the optimization of the fermentation temperature and pH for the each response model, the adequacy of the generated models for the prediction of the true response variables was tested. The validity of the analysis of variance was tested by checking whether none of the least squares regression assumptions are violated. To this end, the adequacy of the analysis of variance was validated by confirming that the residuals from the predicted response variables exhibited homogeneity of variances, independence and normality.

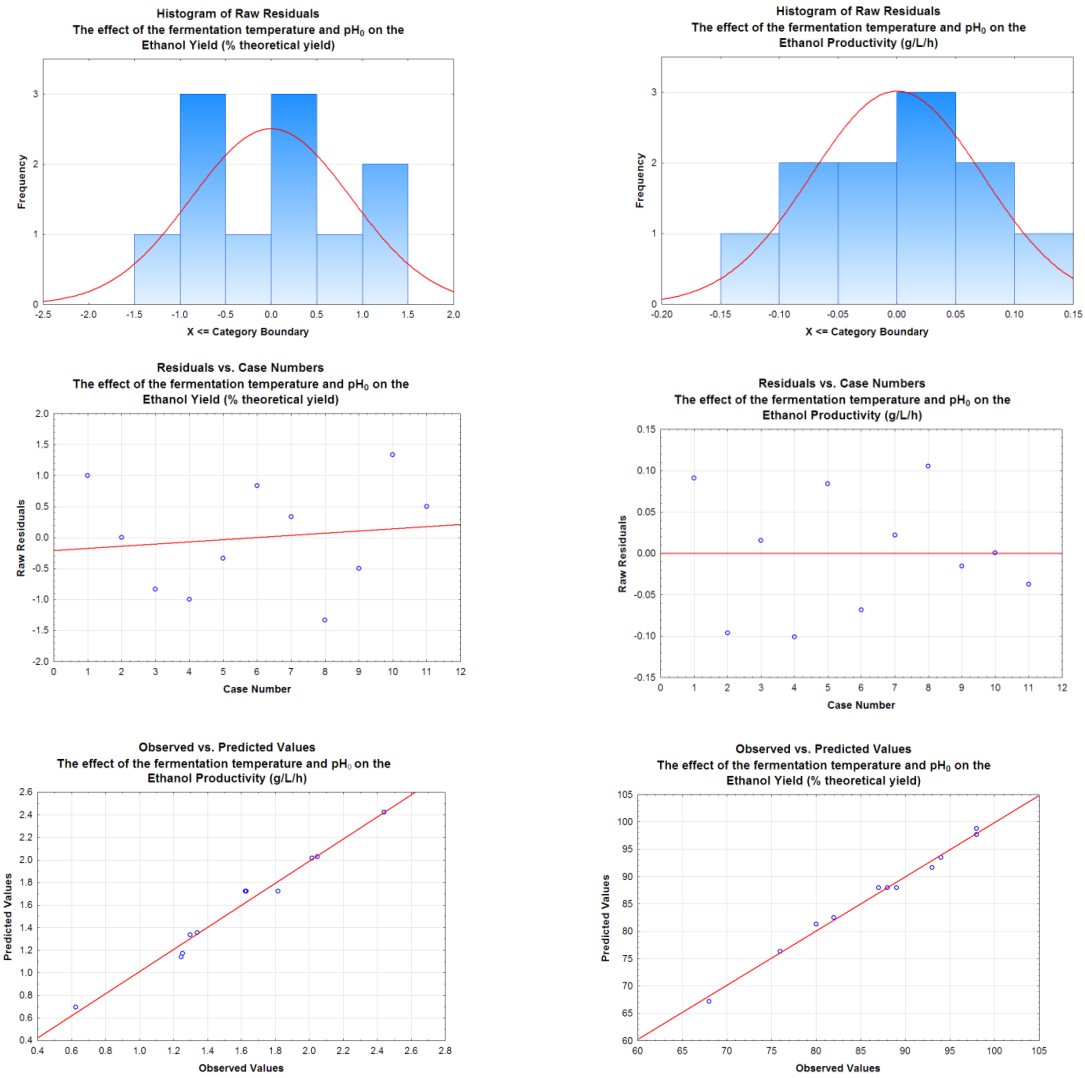


***Figure 103:*** *Validation of the ANOVA assumptions for glucose fermentation by Z. mobilis response models*

A histogram plot of the raw residuals approximated normal distribution curve for both response models, suggesting that the normality assumption was satisfied. Moreover, plotting the residuals as a function of the predicted response, it was found that the residuals scattered randomly, thereby confirming the homogeneity of the variances and independence of the input parameters. Moreover, a graphical representation of the comparative goodness of the model fit was demonstrated by plotting the predicted response as a function of the observed values. The close approximation of predicted vs observed values plot to linearity highlights the high magnitude of fit of the response models to the experimentally determined terms.

## C.1.3 MULTIPLE RESPONSE OPTIMIZATION FOR GLUCOSE FERMENTATION PROFILING

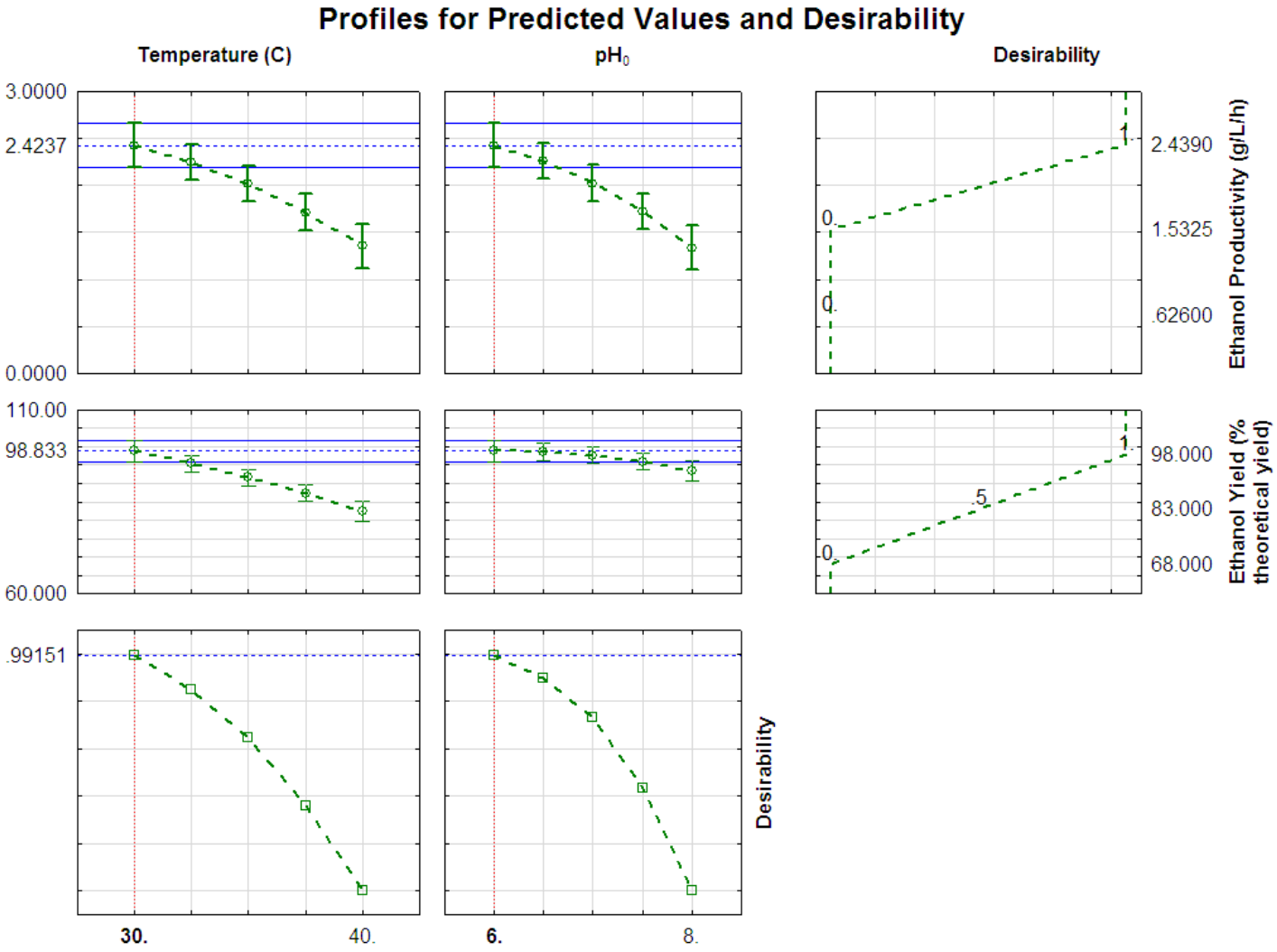


***Figure 104:*** *Desirability functions for glucose fermentation optimization*

## C.2.1 PROFILES FOR GLUCOSE-XYLOSE FERMENTATION FULL FACTORIAL DESIGN

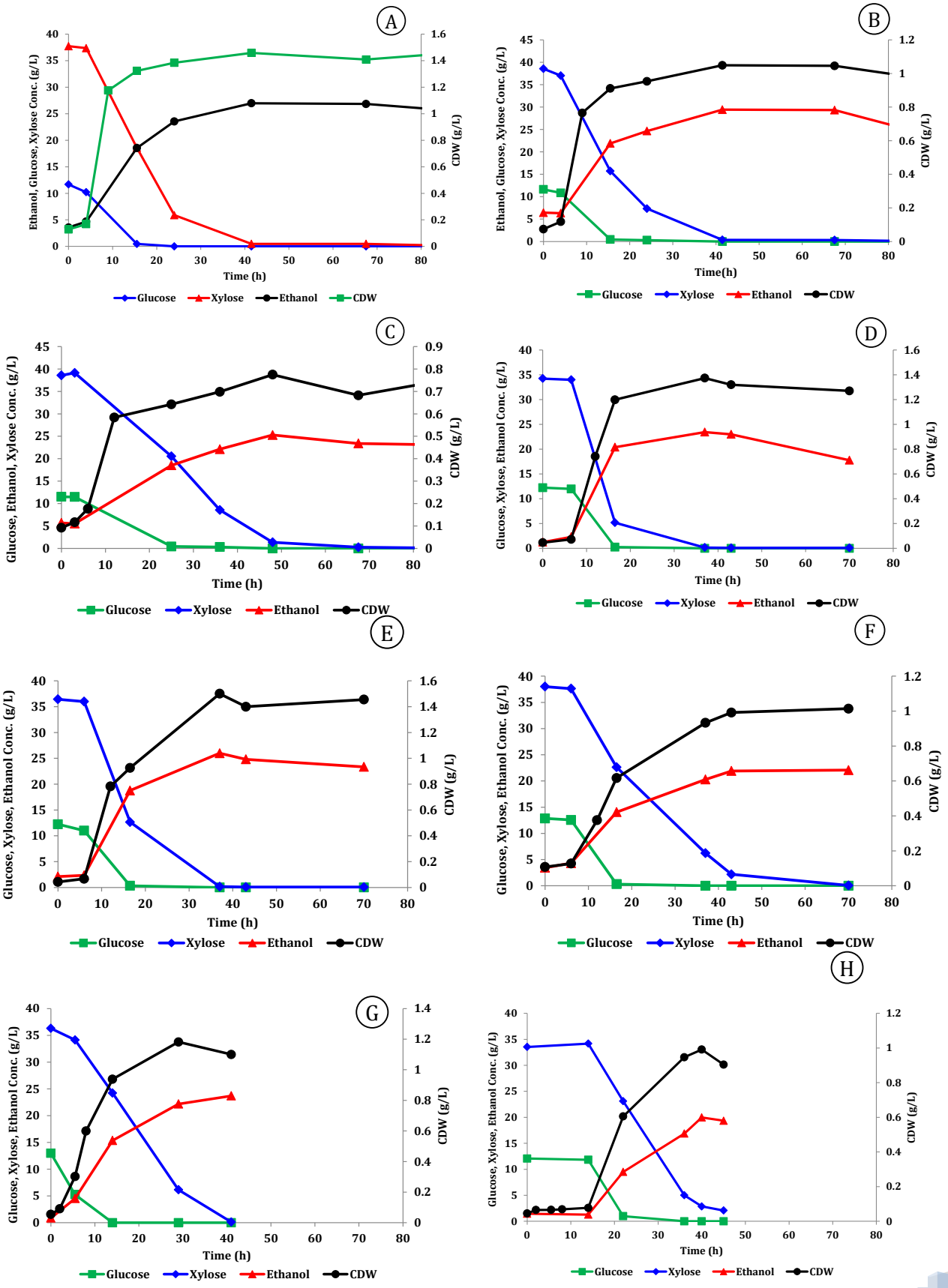

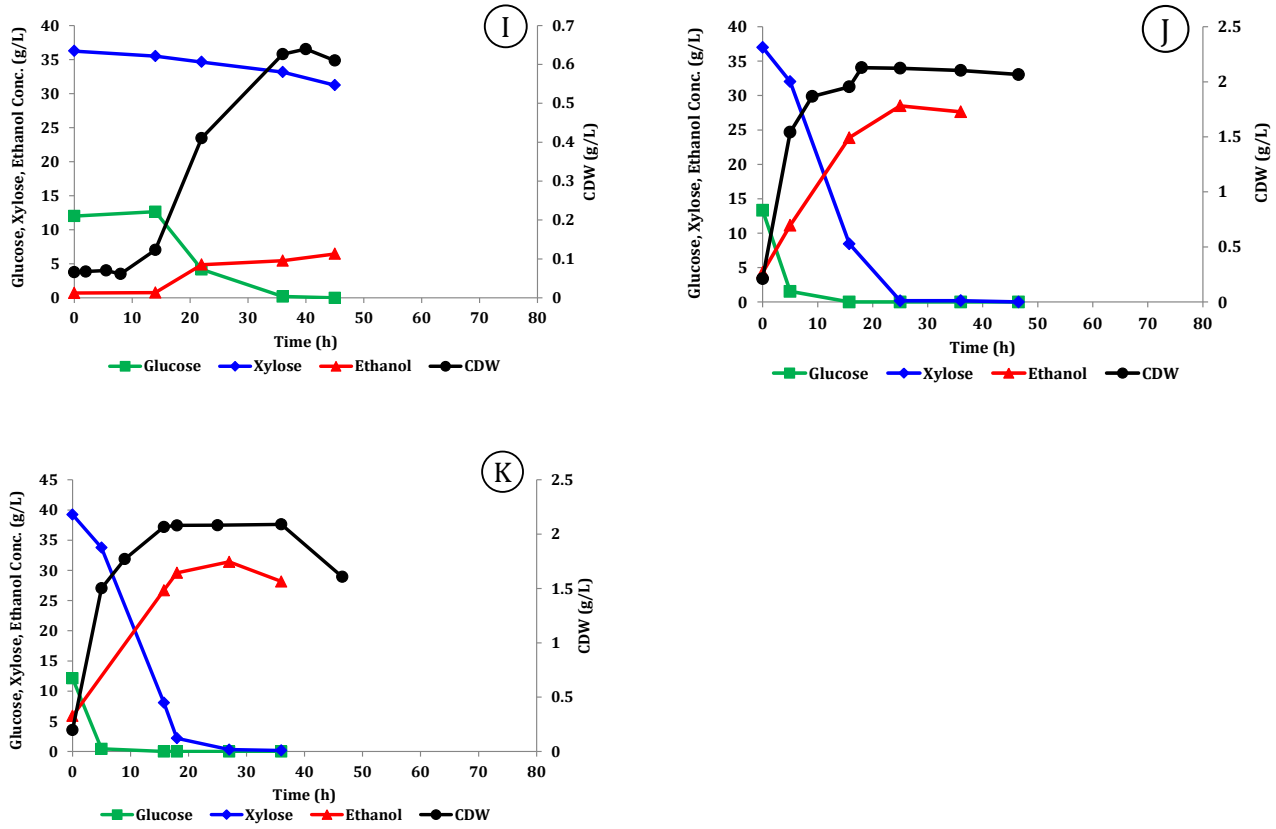


**Figure 105:** *Glucose-Xylose fermentation Full factorial experimental Data.* ***A*** *– Temp. = 30 °C, $pH_0$ = 6;* ***B*** *– Temp. = 30 °C, $pH_0$ = 7;* ***C*** *– Temp. = 30 °C, $pH_0$ = 8;* ***D*** *– Temp. = 35 °C, $pH_0$ = 6;* ***E*** *– Temp. = 35 °C, $pH_0$ = 7;* ***F*** *– Temp. = 35 °C, $pH_0$ = 8;* ***G*** *– Temp. = 40 °C, $pH_0$ = 6;* ***H*** *– Temp. = 40 °C, $pH_0$ = 7;* ***I*** *– Temp. = 40 °C, $pH_0$ = 8;* ***J*** *– Temp. = 35 °C, $pH_0$ = 7;* ***K*** *– Temp. = 35 °C, $pH_0$ = 7;*

***Table 32:*** *ANOVA analysis for the overall rate of xylose consumption for glucose-xylose fermentation by Z. mobilis 8b*

| Factor | ANOVA; Var.:Overall Xylose cons. rate (g xyl./L/h); R-sqr=.97549; Adj:.95099 (3**(2-0) full factorial design, 1 block , 9 runs (Spreadsheet1) in GG_FFx(paper).stw) 2 3-level factors, 1 Blocks, 11 Runs; MS Residual=.0087543 DV: Overall Xylose cons. rate (g xyl./L/h) | | | | |
|---|---|---|---|---|---|
| | SS | df | MS | F | p |
| **(1)Temperature(L)** | 0.326667 | 1 | 0.326667 | 37.31500 | 0.001703 |
| **Temperature(Q)** | 0.457017 | 1 | 0.457017 | 52.20485 | 0.000792 |
| **(2)pH (L)** | 0.558150 | 1 | 0.558150 | 63.75725 | 0.000497 |
| **pH (Q)** | 0.170907 | 1 | 0.170907 | 19.52262 | 0.006902 |
| **1L by 2L** | 0.021025 | 1 | 0.021025 | 2.40168 | 0.181894 |
| **Error** | 0.043771 | 5 | 0.008754 | | |
| **Total SS** | 1.786073 | 10 | | | |

***Table 33:*** *ANOVA analysis for the ethanol yield estimation for glucose-xylose fermentation by Z. mobilis 8b*

| Factor | ANOVA; Var.:Ethanol Yield (% theo. yield); R-sqr=.95211; Adj:.90423 (3**(2-0) full factorial design, 1 block , 9 runs (Spreadsheet1) in GG_FFx(paper).stw) 2 3-level factors, 1 Blocks, 11 Runs; MS Residual=10.95789 DV: Ethanol Yield (% theo. yield) | | | | |
|---|---|---|---|---|---|
| | SS | df | MS | F | p |
| **(1)Temperature (L)** | 96.000 | 1 | 96.0000 | 8.76081 | 0.031524 |
| **Temperature (Q)** | 48.344 | 1 | 48.3439 | 4.41178 | 0.089705 |
| **(2)pH (L)** | 661.500 | 1 | 661.5000 | 60.36744 | 0.000565 |
| **pH (Q)** | 199.244 | 1 | 199.2439 | 18.18268 | 0.007983 |
| **1L by 2L** | 9.000 | 1 | 9.0000 | 0.82133 | 0.406346 |
| **Error** | 54.789 | 5 | 10.9579 | | |
| **Total SS** | 1144.182 | 10 | | | |

***Table 34:*** *ANOVA analysis for the ethanol volumetric estimation for glucose-xylose fermentation by Z. mobilis 8b*

| Factor | ANOVA; Var.:Ethanol Productivity (g EtOH/L/h); R-sqr=.9555; Adj:.91099 (3**(2-0) full factorial design, 1 block , 9 runs (Spreadsheet1) in GG_FFx(paper).stw) 2 3-level factors, 1 Blocks, 11 Runs; MS Residual=.006402 DV: Ethanol Productivity (g EtOH/L/h) | | | | |
|---|---|---|---|---|---|
| | SS | df | MS | F | p |
| **(1)Temperature (L)** | 0.041667 | 1 | 0.041667 | 6.50836 | 0.051194 |
| **Temperature (Q)** | 0.285645 | 1 | 0.285645 | 44.61795 | 0.001136 |
| **(2)pH (L)** | 0.201667 | 1 | 0.201667 | 31.50049 | 0.002484 |
| **pH (Q)** | 0.053845 | 1 | 0.053845 | 8.41062 | 0.033787 |
| **1L by 2L** | 0.007225 | 1 | 0.007225 | 1.12855 | 0.336678 |
| **Error** | 0.032010 | 5 | 0.006402 | | |
| **Total SS** | 0.719255 | 10 | | | |

## C.2.2 VALIDATION OF THE EFFECT OF TEMPERATURE AND $PH_0$ ON XYLOSE-RICH SUBSTRATE FERMENTATION BY *Z. MOBILIS* 8B

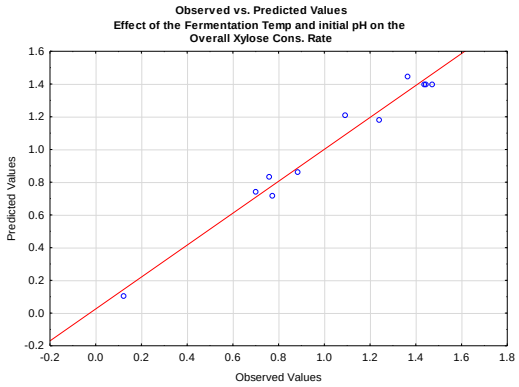


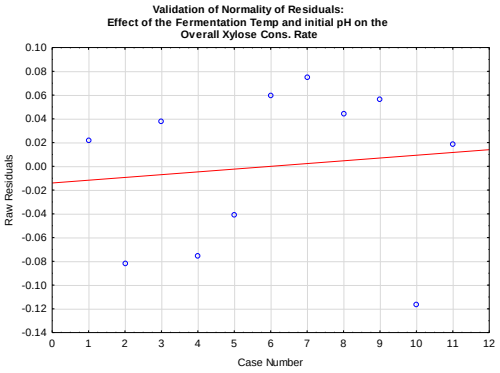


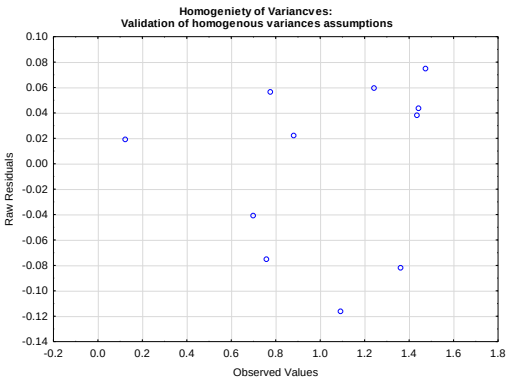


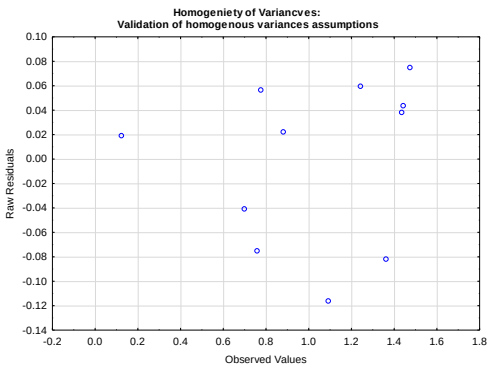


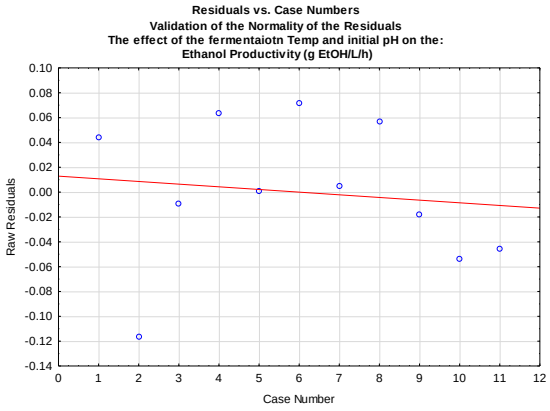


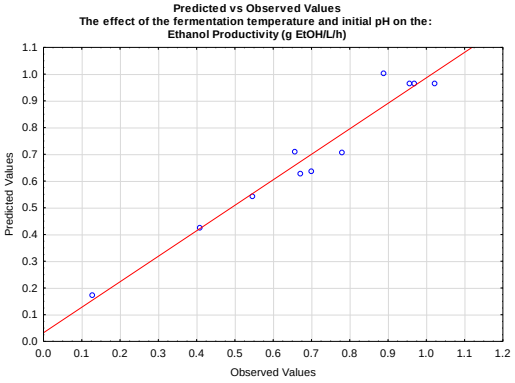

## C.2.3 MULTIPLE RESPONSE OPTIMIZATION FOR GLUCOSE-XYLOSE FERMENTATION PROFILING

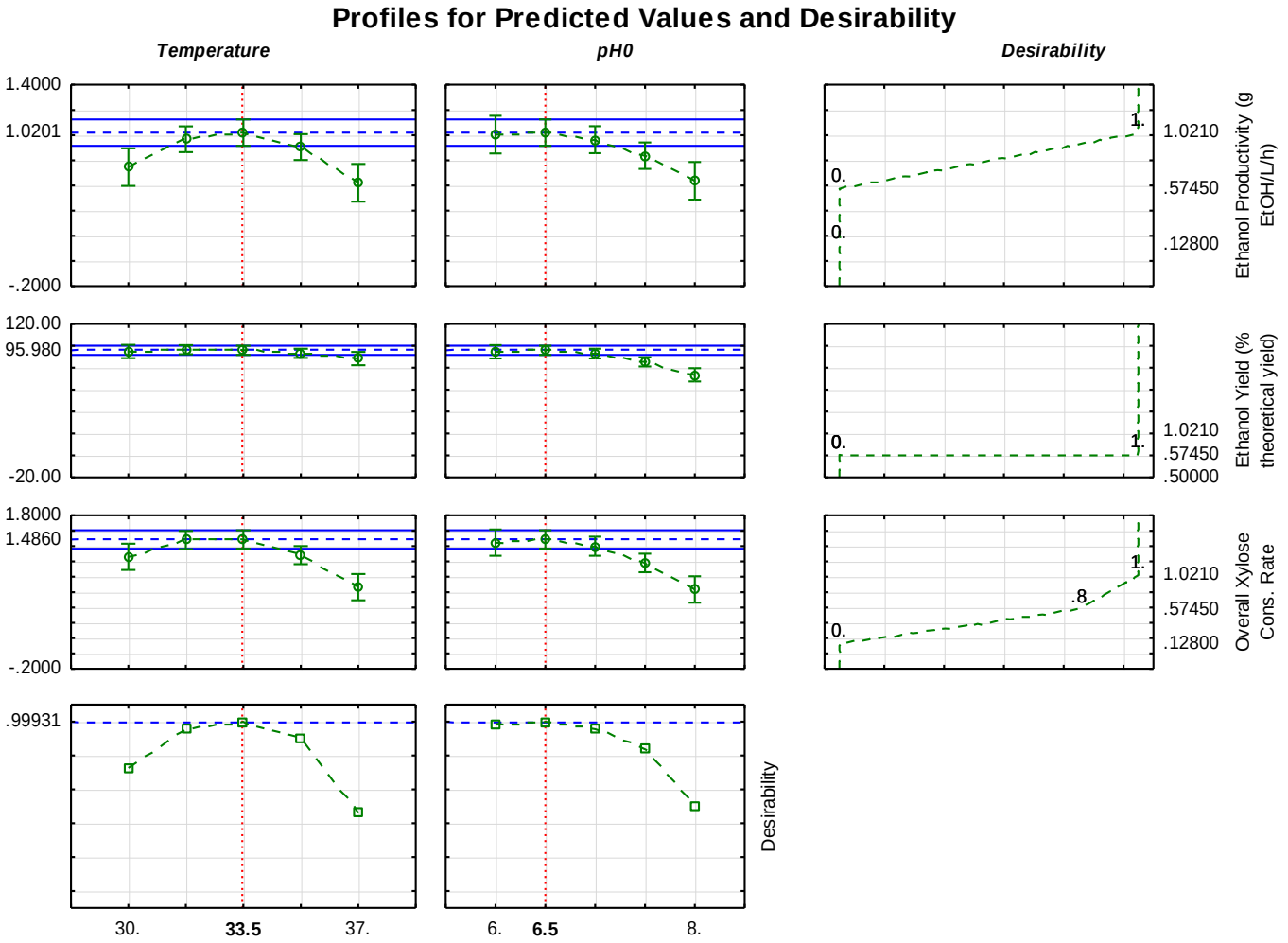


**Figure 106:** *Desirability functions for glucose-xylose fermentation optimization*

## C.3.1 FERMENTATION MEDIA VISCOSITY RESULTS

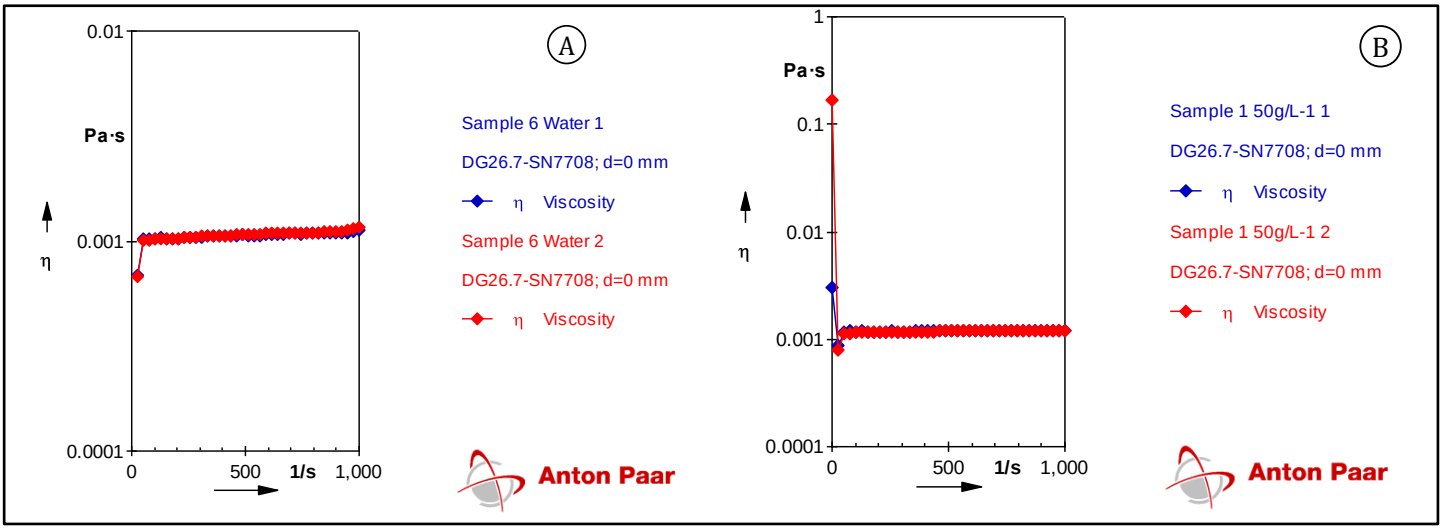


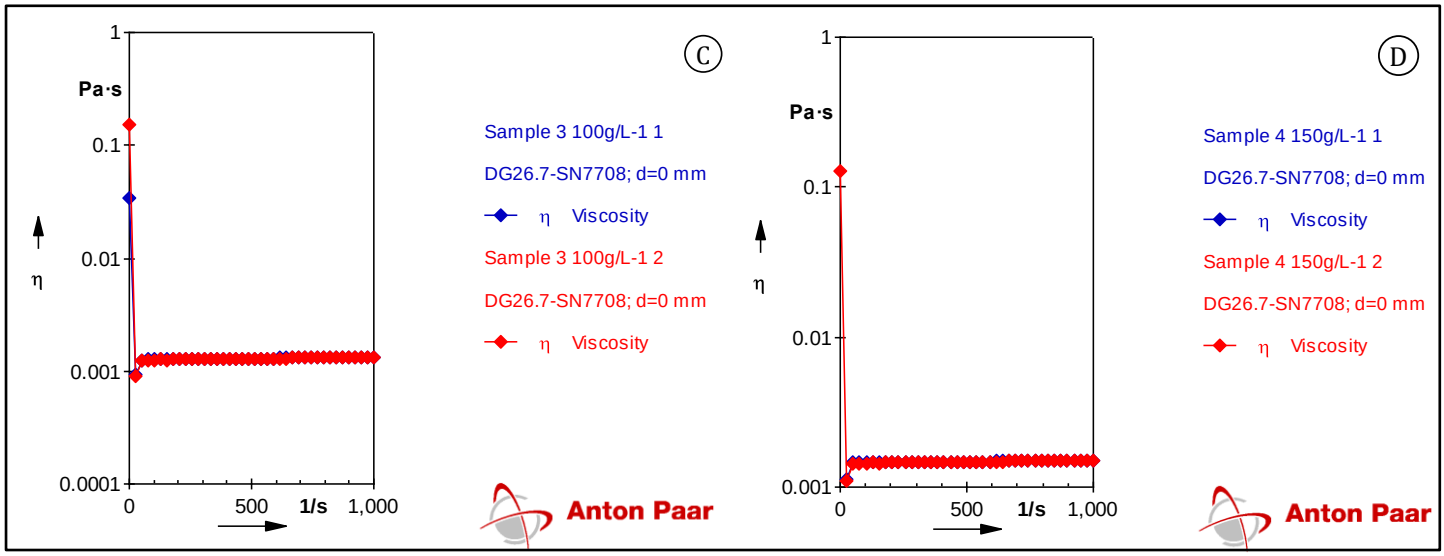


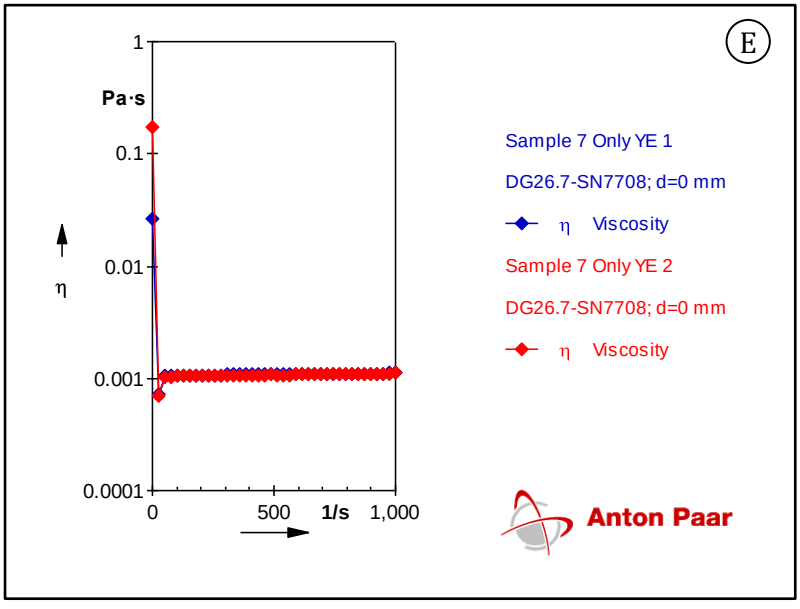


***Figure 107:*** *Viscosity measurements for fermentation media with various sugar concentrations.* ***A*** *- De-ionized water only,* ***B*** *- 5 %(m/v) glucose,* ***C*** *- 10% (m/v) glucose,* ***D*** *- 15% (m/v) glucose,* ***E*** *- Water, yeast extract, and minerals*

## C.4.1. VALIDATION OF THE ANOVA ASSUMPTIONS

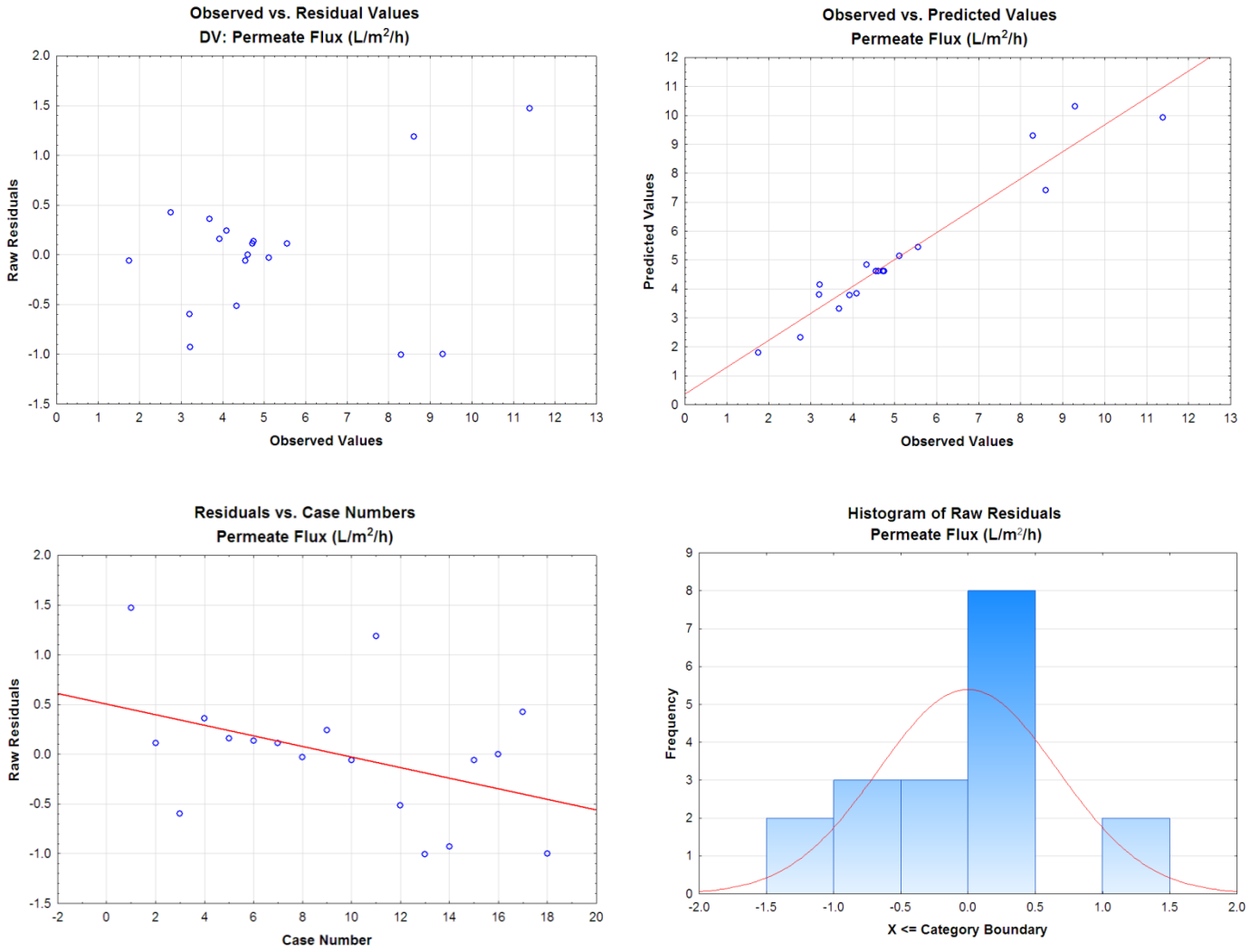


***Figure 108:*** *Validation of the ANOVA assumptions for the selection of the significant factors towards the MFU pseudo-steady state permeate flux*

The adequacy of the analysis of variance was validated by confirming that the residuals from the predicted response variables exhibited homogeneity of variances, independence and normality. A histogram plot of the raw residuals approximated normal distribution curve for both response models, suggesting that the normality assumption was satisfied. Moreover, plotting the residuals as a function of the predicted response, it was found that the residuals scattered randomly, thereby confirming the homogeneity of the variances and independence of the input parameters. Moreover, a graphical representation of the comparative goodness of the model fit was demonstrated by plotting the predicted response as a function of the observed values. The close approximation of predicted vs observed values plot to linearity highlights the high magnitude of fit of the response models to the experimentally determined terms.

## C.5.1. KINETIC PARAMETER CALCULATION FOR GLUCOSE-XYLOSE FERMENTATION

The sample calculation methodology presented below was applied to the 50-50 g.L$^{-1}$ glucose-xylose batch fermentation (as presented in *section 7.3.1*). As previously mentioned, *Z. mobilis* 8b was found to metabolize a glucose-xylose substrate in two growth phases. As a result, the growth kinetics were calculated in two separate phases, i.e. a simultaneous glucose-xylose consumption phase (phase I) and a xylose consumption phase (phase II). The figure below demarcates the division of the growth curve into these two phases.

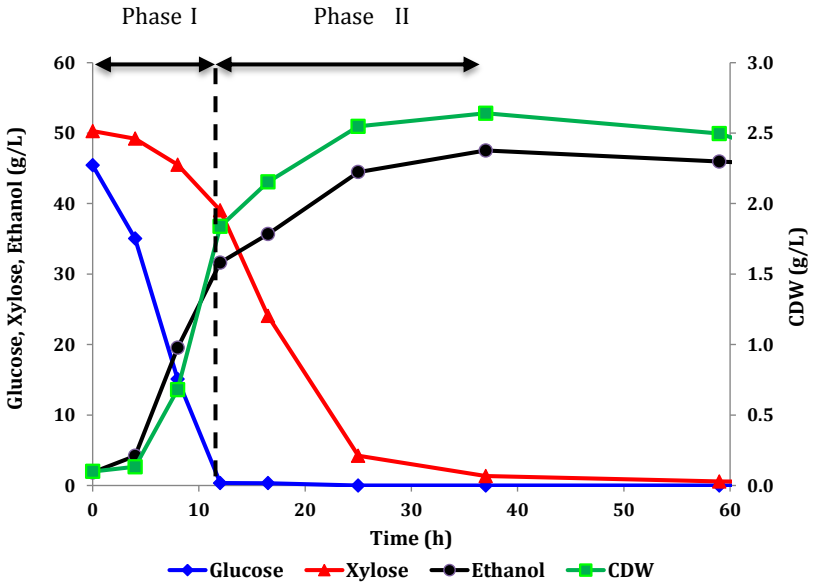


***Figure 109:*** *Growth curve used for sample calculation*

***Maximum Specific Growth Rate***

The maximum specific growth rate from the first phase ($\mu_{max}^{(1)}$)was calculated from the exponential growth phase of Z. mobilis on both glucose and xylose as the substrate. Considering the maximum specific growth rate in the second phase ($\mu_{max}^{(2)}$), ($\mu_{max}^{(2)}$) was calculated in the exponential growth phase after glucose was exhausted. The natural logarithm method was used to calculate $\mu_{max}$ in the respective exponential growth phases using the following formulae:

$$\mu_{max} = \frac{\ln(x_{t2}) - \ln(x_{t1})}{t_2 - t_1} \quad \textbf{(C.1)}$$

A minimum of three data points was used to calculate μmax in each phase.

***Maximum Specific Glucose, Xylose and Ethanol production rates***

Similar to the calculation of $\mu_{max}$, the specific glucose ($q_{s\_glucose}$), xylose ($q_{s\_xylose}$) and ethanol production rates ($q_{pmax}$) were calculated in each phase. Considering the first phase, the maximum specific glucose-xylose consumption and ethanol production rates were calculated in the exponential phase as follows:

$$q_{s_{max}}{}^{(1)} = \frac{ds^{(1)}}{dt} * \frac{1}{x} = \frac{\mu_{max}{}^{(1)}}{Y_{x/s}{}^{(1)}} \quad \textbf{(C.2)}$$

$$q_{p_{max}}{}^{(1)} = \frac{ds^{(1)}}{dt} * \frac{1}{x} = \frac{\mu_{max}{}^{(1)}}{Y_{p/x}{}^{(1)}} \quad \textbf{(C.3)}$$

where $Y_{x/s}{}^{(1)}$ and $Y_{p/x}{}^{(1)}$ define the cell and product yields within the exponential phase respectively.

***Overall Cell and Product Yields***

The overall cell and product yields were calculated at the point whereby xylose metabolization was complete (time $t_{end}$) relative to the time of culture inoculation (time $t_{initial}$) as follows:

$$Y_{x/s} = \frac{x_{end} - x_{initial}}{S_{initial} - S_{end}} \quad \textbf{(C.4)}$$

$$Y_{p/s} = \frac{P_{end} - P_{initial}}{S_{initial} - S_{end}} \quad \textbf{(C.5)}$$

***Table 35:*** *Sample calculation for determination of kinetic parameters for 50-5 g.L-1 glucose-xylose fermentation*

| Sample Calculation and Experimental Data | | | | | | | |
|---|---|---|---|---|---|---|---|
| **Time** | **OD (AU)** | **CDW ($g.L^{-1}$)** | **ln (CDW) ($g.L^{-1}$)** | **μ ($h^{-1}$)** | **Glucose ($g.L^{-1}$)** | **Xylose ($g.L^{-1}$)** | **Ethanol ($g.L^{-1}$)** |
| **0.0** | 0.303 | 0.100 | -1.195 | | 45.435 | 50.274 | 1.851 |
| **4.0** | 0.402 | 0.133 | -0.911 | 0.071 | 35.021 | 49.213 | 4.214 |
| **8.0** | 2.060 | 0.680 | 0.723 | 0.409 | 15.098 | 45.518 | 19.543 |
| **12.0** | 5.570 | 1.838 | 1.717 | 0.249 | 0.358 | 39.021 | 31.618 |
| **16.5** | 6.525 | 2.153 | 1.876 | 0.035 | 0.333 | 24.070 | 35.668 |
| **25.0** | 7.720 | 2.548 | 2.044 | 0.020 | 0.0 | 4.220 | 44.467 |
| **37.0** | 8.002 | 2.641 | 2.080 | 0.003 | 0.0 | 1.348 | 47.519 |
| **59.0** | 7.565 | 2.496 | 2.024 | -0.003 | 0.0 | 0.578 | 45.958 |
| **70.0** | 6.743 | 2.225 | 1.909 | -0.010 | 0.0 | 0.468 | 45.157 |

***Table 36:*** *Calculated kinetic parameters for 50-50 g.L-1 glucose-xylose fermentation*

| **Calculated Kinetic Parameters** | Quantity |
|---|---|
| ***Glucose/Xylose (1st Phase)*** | |
| $\mu_{max}$ $(h^{-1})$ | 0.33 |
| $q_{s\_max}{}^{(1)}$ *(g substrate/g CDW/h)* | 10.65 |
| $q_{p\_max}{}^{(1)}$ *(g EtOH/g CDW/h)* | 5.63 |
| ***Xylose (2nd Phase)*** | |
| $\mu_{max}$ $(h^{-1})$ | 0.027 |
| $q_{s\_max}{}^{(2)}$ *(g xylose/g CDW/h)* | 1.46 |
| $q_{p\_max}{}^{(2)}$ *(g EtOH/g CDW/h)* | 0.683 |
| ***Overall*** | |
| *VP (g EtOH/L/h)* | 1.43 |
| $Y_{xs}$ *(g CDW/g substrate cons)* | 0.027 |
| $Y_{ps}$ *(g EtOH/g substrate cons)* | 0.480 |
| $Y_{ps}$ *(% theoretical)* | 94% |

## C.5.2. MASS BALANCE FOR THE CALCULATION OF THE CELL MASS OF IMMOBILIZED CELLS AT INITIAL CONDITIONS

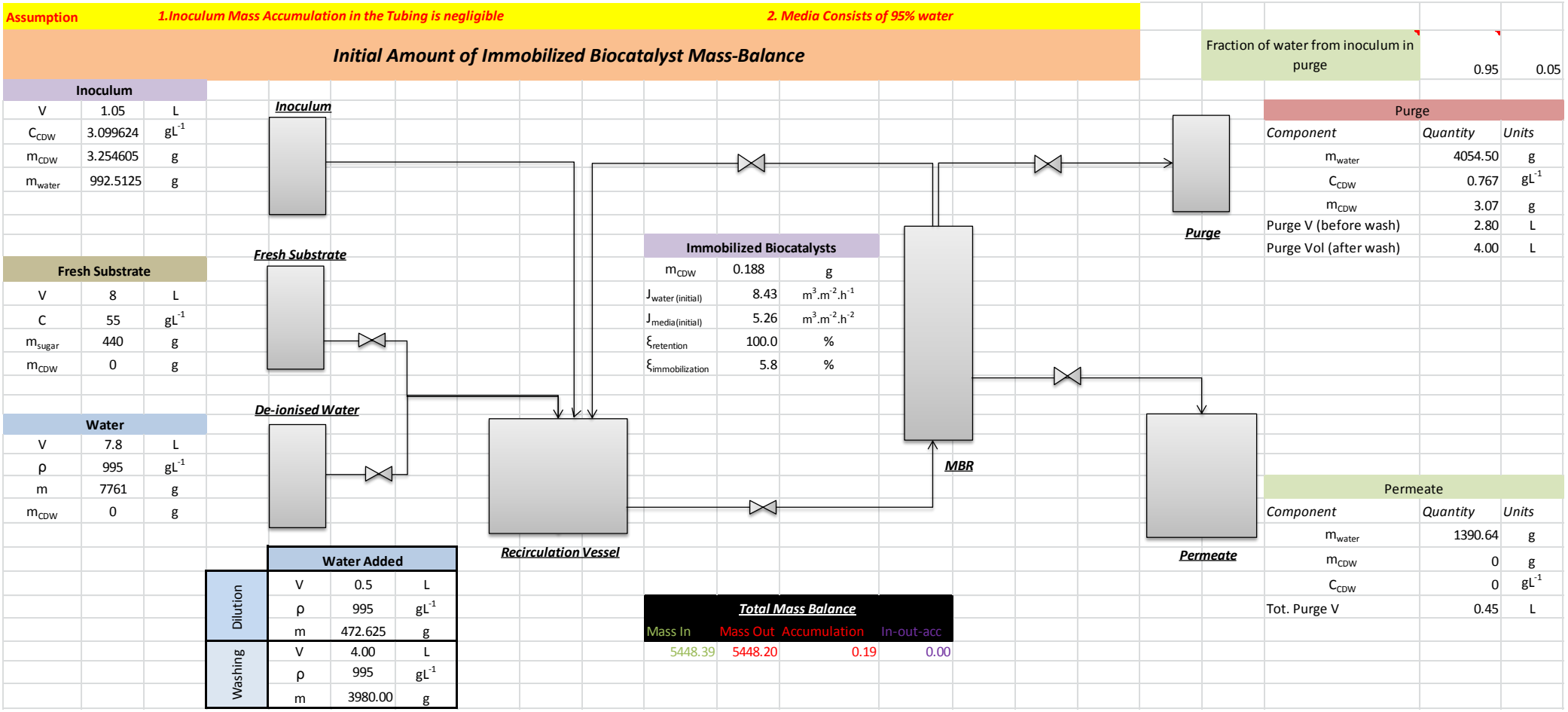


***Figure 110:*** *Mass Balance for determining the initial amount of immobilized biocatalyst*

## C.5.3. SAMPLE 4TH ORDER RUNGA-KUTTA CALCULATION

*Table 37* below presents sample calculation for the 4th order Runga-Kutta numerical method for the glucose, xylose, ethanol, cell mass, and acetate ODEs. The initial values for solving the ODEs were calculated from the experimental data obtained during start-up conditions. The time step-length of 0.25h was used. Although the data presented in Table XX proceeds to 8h, the actual solution simulating the system of ODEs was stopped about 10h after the last experimentally measured data point.

***Table 37:*** *Sample calculation of the 4th order Runga-Kutta with the definition of the initial values*

| 4th order Runga-Kutta Initial Values | | | | | |
|---|---|---|---|---|---|
| RK Step-length (h) | S10 (g/L) | S20 (g/L) | x0 (g/L) | P0 (g/L) | Ac0 (g/L) |
| 0.25 | 43.843 | 45.552 | 0.614 | 7.984 | 0 |

| Feed Conditions | | | | | |
|---|---|---|---|---|---|
| $S_{1\_f}$ | 43.84 | $g.L^{-1}$ | $A_{mem}$ | 0.00153 | $m^2$ |
| $S_{2\_f}$ | 45.55 | $g.L^{-1}$ | $V_{reactor}$ | 0.5 | L |
| $P_{\_f}$ | 0 | $g.L^{-1}$ | | | |

| Concentrations at Exit | | | | | | | | RUNGA-KUTTA CONSTANTS (4TH ORDER) | | | | | | | | | | | | | | | |
|---|---|---|---|---|---|---|---|---|---|---|---|---|---|---|---|---|---|---|---|---|---|---|---|
| | | | | | | | | Substrate 1 (Glucose) | | | | Substrate 2 (Xylose) | | | | Biomass (CDW) | | | | Product (Ethanol) | | | | Acetate | | | |
| time | $S_1$ | $S_2$ | x | J | D | P | Acetate | $G_{S1.1}$ | $G_{S1.2}$ | $G_{S1.3}$ | $G_{S1.4}$ | $X_{S1.1}$ | $X_{S2}$ | $X_{S3}$ | $X_{S4}$ | $V_{X1}$ | $V_{X2}$ | $V_{X3}$ | $V_{X4}$ | $P_{E1}$ | $P_{E2}$ | $P_{E3}$ | $P_{E4}$ | $Ac_{E1}$ | $Ac_{E2}$ | $Ac_{E3}$ | $Ac_{E4}$ |
| 0 | 43.84305688 | 45.55239565 | 0.614064 | 0 | 0 | 7.983786 | 0 | -4.38941 | -4.50278 | -4.50592 | -4.50601 | -0.60528 | -0.622261385 | -0.62273 | -0.62274 | 0.138258 | 0.142081 | 0.142187 | 0.14219 | 2.109805 | 2.164938 | 2.16646571 | 2.166507956 | 0.006133746 | 0.0063062 | 0.006310968 | 0.0063111 |
| 0.25 | 42.72168883 | 45.39747852 | 0.649438 | 0 | 0 | 8.522916 | 0.00157 | -4.62067 | -4.73877 | -4.74204 | -4.74213 | -0.64003 | -0.657962748 | -0.65846 | -0.65847 | 0.146077 | 0.150105 | 0.150216 | 0.150219 | 2.222321 | 2.27987 | 2.281460971 | 2.281504849 | 0.006486721 | 0.006668899 | 0.006673922 | 0.00667406 |
| 0.5 | 41.54150514 | 45.23367261 | 0.686811 | 0 | 0 | 9.090687 | 0.00323 | -4.86144 | -4.98421 | -4.98759 | -4.98769 | -0.67673 | -0.695661443 | -0.69618 | -0.6962 | 0.154313 | 0.158553 | 0.15867 | 0.158673 | 2.339713 | 2.399673 | 2.401327397 | 2.401372863 | 0.006859572 | 0.007051988 | 0.007057275 | 0.007057421 |
| 0.75 | 40.30014126 | 45.06048055 | 0.726287 | 0 | 0 | 9.688315 | 0.004986 | -5.11156 | -5.23885 | -5.24235 | -5.24245 | -0.71547 | -0.735460678 | -0.73601 | -0.73602 | 0.162983 | 0.167445 | 0.167567 | 0.16757 | 2.461958 | 2.524296 | 2.526011868 | 2.526058852 | 0.007253344 | 0.00745653 | 0.007462092 | 0.007462245 |
| 1 | 38.99529076 | 44.87737922 | 0.767978 | 0 | 0 | 10.31701 | 0.006842 | -5.3707 | -5.50226 | -5.50588 | -5.50598 | -0.75637 | -0.777467302 | -0.77804 | -0.77806 | 0.172104 | 0.176794 | 0.176922 | 0.176926 | 2.588969 | 2.653611 | 2.655385981 | 2.655434377 | 0.007669117 | 0.007883625 | 0.007889472 | 0.007889631 |
| 1.25 | 37.62475077 | 44.6838189 | 0.811997 | 0 | 0 | 10.97794 | 0.008805 | -5.6383 | -5.77379 | -5.77750 | -5.77760 | -0.79953 | -0.821791499 | -0.82239 | -0.82241 | 0.18169 | 0.186617 | 0.186751 | 0.186754 | 2.720572 | 2.787393 | 2.789223533 | 2.789273193 | 0.00810801 | 0.008334408 | 0.008340548 | 0.008340715 |
| 1.5 | 36.18648057 | 44.47922239 | 0.858463 | 0 | 0 | 11.67224 | 0.01088 | -5.91357 | -6.05244 | -6.05624 | -6.05635 | -0.84507 | -0.868546336 | -0.86918 | -0.8692 | 0.191756 | 0.196926 | 0.197065 | 0.197069 | 2.856483 | 2.925291 | 2.927171424 | 2.92722215 | 0.008571173 | 0.008810042 | 0.008816482 | 0.008816657 |
| 1.75 | 34.67867724 | 44.2629843 | 0.907496 | 0 | 0 | 12.40093 | 0.013073 | -6.19533 | -6.33685 | -6.34072 | -6.34083 | -0.89309 | -0.917847097 | -0.91851 | -0.91853 | 0.202314 | 0.20773 | 0.207875 | 0.207879 | 2.996273 | 3.066788 | 3.068711868 | 3.068763399 | 0.009059779 | 0.009311712 | 0.009318458 | 0.009318639 |
| 2 | 33.09987338 | 44.03447049 | 0.959222 | 0 | 0 | 13.16493 | 0.015392 | -6.48196 | -6.62512 | -6.62904 | -6.62915 | -0.94372 | -0.969810342 | -0.9705 | -0.97052 | 0.21337 | 0.219035 | 0.219186 | 0.21919 | 3.139325 | 3.211155 | 3.213113076 | 3.213165077 | 0.009575019 | 0.009840612 | 0.009847665 | 0.009847853 |
| 2.25 | 31.44906365 | 43.79301776 | 1.013763 | 0 | 0 | 13.96497 | 0.017842 | -6.77127 | -6.91469 | -6.91864 | -6.91874 | -0.99707 | -1.024552569 | -1.02527 | -1.02529 | 0.224928 | 0.230841 | 0.230997 | 0.231002 | 3.284779 | 3.357384 | 3.359364611 | 3.359416659 | 0.010118085 | 0.010397929 | 0.010405287 | 0.010405482 |
| 2.5 | 29.72586913 | 43.5379338 | 1.071247 | 0 | 0 | 14.80154 | 0.02043 | -7.06027 | -7.20213 | -7.20607 | -7.20617 | -1.05325 | -1.082188354 | -1.08294 | -1.08296 | 0.236983 | 0.243137 | 0.243299 | 0.243303 | 3.431456 | 3.504102 | 3.506092314 | 3.506143879 | 0.010690151 | 0.010984821 | 0.010992476 | 0.010992677 |
| 2.75 | 27.93075124 | 43.26849771 | 1.131795 | 0 | 0 | 15.67479 | 0.023165 | -7.34499 | -7.48286 | -7.48675 | -7.48684 | -1.11239 | -1.142827726 | -1.14361 | -1.14363 | 0.249518 | 0.255902 | 0.256068 | 0.256072 | 3.577761 | 3.649461 | 3.65144612 | 3.651496545 | 0.011292347 | 0.011602383 | 0.01161032 | 0.011610526 |
| 3 | 26.06529124 | 42.98396109 | 1.195526 | 0 | 0 | 16.58442 | 0.026054 | -7.62017 | -7.75079 | -7.75460 | -7.75470 | -1.17457 | -1.206572481 | -1.20738 | -1.2074 | 0.262505 | 0.269095 | 0.269264 | 0.269269 | 3.721554 | 3.790988 | 3.792952175 | 3.793000643 | 0.011925717 | 0.012251602 | 0.01225979 | 0.012260001 |
| 3.25 | 24.13255602 | 42.68355005 | 1.262546 | 0 | 0 | 17.52952 | 0.029104 | -7.8788 | -7.99789 | -8.00161 | -8.00169 | -1.23991 | -1.273510951 | -1.27433 | -1.27435 | 0.27589 | 0.28265 | 0.282822 | 0.282826 | 3.859978 | 3.925387 | 3.92731893 | 3.927364401 | 0.012591163 | 0.012933284 | 0.012941679 | 0.012941892 |
| 3.5 | 22.13757727 | 42.36646853 | 1.332949 | 0 | 0 | 18.50839 | 0.032324 | -8.11166 | -8.21356 | -8.21718 | -8.21725 | -1.30848 | -1.343710518 | -1.34455 | -1.34457 | 0.289591 | 0.296464 | 0.296636 | 0.29664 | 3.98924 | 4.048289 | 4.050186291 | 4.050227358 | 0.013289362 | 0.013647958 | 0.013656488 | 0.013656702 |
| 3.75 | 20.08797756 | 42.03190352 | 1.4068 | 0 | 0 | 19.51824 | 0.035722 | -8.30659 | -8.38386 | -8.38744 | -8.38750 | -1.38033 | -1.417206752 | -1.41804 | -1.41806 | 0.303479 | 0.310376 | 0.310549 | 0.310553 | 4.104317 | 4.153923 | 4.155810274 | 4.155844786 | 0.014020642 | 0.014395723 | 0.01440428 | 0.014404493 |
| 4 | 17.99478186 | 41.67903286 | 1.484128 | 0 | 0 | 20.55489 | 0.039307 | -8.44768 | -8.49059 | -8.49435 | -8.49439 | -1.45548 | -1.493987473 | -1.49481 | -1.49483 | 0.317357 | 0.324147 | 0.324318 | 0.324321 | 4.19861 | 4.234737 | 4.236689333 | 4.236713404 | 0.014784792 | 0.015176018 | 0.015184442 | 0.015184653 |
| 4.25 | 15.87345029 | 41.3070371 | 1.564904 | 0 | 0 | 21.61231 | 0.043086 | -8.5143 | -8.51037 | -8.51477 | -8.51476 | -1.53387 | -1.573969 | -1.57475 | -1.57477 | 0.330928 | 0.337408 | 0.337578 | 0.337581 | 4.263539 | 4.280978 | 4.283176532 | 4.283181909 | 0.015580784 | 0.015987271 | 0.015995326 | 0.015995535 |
| 4.5 | 13.74514432 | 40.9151172 | 1.649007 | 0 | 0 | 22.68211 | 0.047066 | -8.48026 | -8.41387 | -8.41987 | -8.41977 | -1.61537 | -1.656960355 | -1.65766 | -1.65769 | 0.343741 | 0.349602 | 0.349779 | 0.349781 | 4.288164 | 4.280385 | 4.283211169 | 4.283178423 | 0.016406318 | 0.016826334 | 0.016833669 | 0.016833883 |
| 4.75 | 11.63816403 | 40.50252114 | 1.736186 | 0 | 0 | 23.75288 | 0.051256 | -8.31348 | -8.16619 | -8.17563 | -8.17532 | -1.69972 | -1.742608936 | -1.74318 | -1.7432 | 0.355111 | 0.359882 | 0.360084 | 0.360083 | 4.259043 | 4.218301 | 4.222488908 | 4.222370507 | 0.017257108 | 0.017687573 | 0.017693685 | 0.017693922 |
| 5 | 9.589312401 | 40.0685839 | 1.825982 | 12.08901 | 0.036992 | 24.80967 | 0.055661 | -6.71031 | -6.50402 | -6.51893 | -6.51814 | -1.58358 | -1.619796357 | -1.62009 | -1.62012 | 0.360621 | 0.364462 | 0.364721 | 0.364715 | 3.243023 | 3.175983 | 3.182303099 | 3.181986873 | 0.020184762 | 0.016407566 | 0.016430213 | 0.016430398 |
| 5.25 | 7.952880785 | 39.66510639 | 1.91697 | 11.90754 | 0.036437 | 25.60724 | 0.059923 | -6.28927 | -6.00445 | -6.02742 | -6.02583 | -1.65976 | -1.696507558 | -1.69657 | -1.69661 | 0.3677 | 0.369684 | 0.370064 | 0.370046 | 3.11159 | 3.012153 | 3.021710594 | 3.021069779 | 0.021183283 | 0.017156531 | 0.017178237 | 0.017178533 |
| 5.5 | 6.437095611 | 39.24250113 | 2.009355 | 11.73705 | 0.035915 | 26.36559 | 0.064383 | -5.71496 | -5.352 | -5.38653 | -5.38348 | -1.73666 | -1.773441314 | -1.77319 | -1.77326 | 0.370795 | 0.370178 | 0.370794 | 0.370749 | 2.916472 | 2.784565 | 2.798771057 | 2.797542327 | 0.022186287 | 0.017892826 | 0.01791324 | 0.017913729 |
| 5.75 | 5.079782996 | 38.80070222 | 2.102 | 11.57642 | 0.035424 | 27.06895 | 0.069038 | -4.99622 | -4.56891 | -4.61790 | -4.61250 | -1.81315 | -1.849306046 | -1.84864 | -1.84877 | 0.368462 | 0.364477 | 0.365512 | 0.365406 | 2.660842 | 2.501877 | 2.521891431 | 2.519713789 | 0.023175575 | 0.018595439 | 0.018614645 | 0.018615397 |
| 6 | 3.913852495 | 38.33995947 | 2.193411 | 11.42469 | 0.03496 | 27.70345 | 0.07388 | -4.17006 | -3.70841 | -3.77207 | -3.76350 | -1.88779 | -1.922489623 | -1.92136 | -1.92157 | 0.359368 | 0.351515 | 0.353186 | 0.352969 | 2.3594 | 2.185455 | 2.211339227 | 2.207880762 | 0.024126473 | 0.019237266 | 0.01925635 | 0.019257315 |
| 6.25 | 2.959913693 | 37.86091493 | 2.281817 | 11.28102 | 0.03452 | 28.26015 | 0.078895 | -3.30298 | -2.849 | -2.92302 | -2.91114 | -1.95885 | -1.991224126 | -1.98967 | -1.98997 | 0.342935 | 0.331425 | 0.333876 | 0.333492 | 2.03898 | 1.867065 | 1.897042712 | 1.892257191 | 0.025008887 | 0.01978799 | 0.019809573 | 0.01981037 |
| 6.5 | 2.21999088 | 37.36463964 | 2.365443 | 11.14469 | 0.034103 | 28.73763 | 0.084063 | -2.47732 | -2.07247 | -2.14851 | -2.13439 | -2.02466 | -2.053946006 | -2.05211 | -2.0525 | 0.320141 | 0.306215 | 0.309358 | 0.308783 | 1.732967 | 1.579946 | 1.610633999 | 1.604956577 | 0.025792378 | 0.020222011 | 0.020249925 | 0.020249739 |
| 6.75 | 1.67608777 | 36.85258656 | 2.442946 | 11.01507 | 0.033706 | 29.14259 | 0.089354 | -1.76504 | -1.43634 | -1.50548 | -1.49105 | -2.08395 | -2.109755457 | -2.10789 | -2.10832 | 0.293835 | 0.279508 | 0.28297 | 0.282256 | 1.470669 | 1.347565 | 1.375373025 | 1.369589742 | 0.026456382 | 0.020530593 | 0.020567992 | 0.020565885 |
| 7 | 1.295266217 | 36.32643829 | 2.513823 | 10.89158 | 0.033328 | 29.48785 | 0.094738 | -1.20515 | -0.95916 | -1.01561 | -1.00273 | -2.13629 | -2.158701831 | -2.15704 | -2.15745 | 0.267889 | 0.255108 | 0.258401 | 0.257656 | 1.26809 | 1.177672 | 1.200308158 | 1.195158575 | 0.027002042 | 0.020730975 | 0.020777887 | 0.020773506 |
| 7.25 | 1.038706972 | 35.78788686 | 2.578513 | 10.77374 | 0.032968 | 29.78865 | 0.100187 | -0.79911 | -0.62639 | -0.66871 | -0.65839 | -2.18219 | -2.201670776 | -2.20035 | -2.20069 | 0.245568 | 0.235446 | 0.238211 | 0.237541 | 1.126091 | 1.064661 | 1.081597554 | 1.077474846 | 0.027456341 | 0.020862394 | 0.020915295 | 0.020909251 |
| 7.5 | 0.870053047 | 35.23843154 | 2.638114 | 10.66111 | 0.032623 | 30.05932 | 0.105684 | -0.52308 | -0.40697 | -0.43688 | -0.42921 | -2.22277 | -2.239964121 | -2.239 | -2.23926 | 0.228419 | 0.221104 | 0.223221 | 0.22268 | 1.035327 | 0.996282 | 1.008235207 | 1.005172824 | 0.027861612 | 0.020968818 | 0.021022943 | 0.021016395 |
| 7.75 | 0.760053377 | 34.67926721 | 2.693937 | 10.55329 | 0.032293 | 30.31138 | 0.11122 | -0.34432 | -0.26805 | -0.28849 | -0.28303 | -2.25932 | -2.274873501 | -2.2742 | -2.27439 | 0.216344 | 0.211388 | 0.212917 | 0.21251 | 0.982846 | 0.959527 | 0.967686494 | 0.965510999 | 0.028256892 | 0.021081877 | 0.021133819 | 0.021127748 |
| 8 | 0.687534653 | 34.11127306 | 2.747164 | 10.44993 | 0.031977 | 30.55317 | 0.116796 | -0.23245 | -0.18248 | -0.19631 | -0.19250 | -2.29304 | -2.307442485 | -2.30698 | -2.30712 | 0.208362 | 0.205137 | 0.206213 | 0.205917 | 0.956602 | 0.943629 | 0.949148583 | 0.947628659 | 0.02866562 | 0.021215587 | 0.021264103 | 0.021258967 |
| 8.25 | 0.638262993 | 33.53506439 | 2.798705 | 10.35072 | 0.031673 | 30.79024 | 0.122416 | -0.16393 | -0.13059 | -0.14008 | -0.13739 | -2.3248 | -2.338412953 | -2.3381 | -2.33819 | 0.203308 | 0.201247 | 0.202006 | 0.201791 | 0.947265 | 0.940793 | 0.944580612 | 0.943508698 | 0.029095466 | 0.021371115 | 0.021416484 | 0.021412308 |

## C.5.4. MULTIPLE PARAMETER NON-LINEAR LEAST SQUARES FIT OF MODEL PREDICTION TO EXPERIMENTAL DATA FOR 50-50 G.L$^{-1}$ G-X FERMENTATION

The fitting of the kinetic model to the experimental data was performed by combining the numerical solutions estimated by the 4$^{th}$ order Runga-Kutta methods with a goal-attaining iterative tool. In this work, Excel$^{TM}$ 's Solver function was used as the goal attaining tool, with the multi-objective goal defined by equation 6.16. The simulation program was designed to achieve a goal of minimizing the total residuals sum of squares ($RSS_{total}$) with the kinetic parameters bound by their biological relevance. The ethanol inhibition constants were obtained from Rogers *et al.,* 2001 and Rogers *et al.,* 1983.

***Table 38:*** *Sample calculation of the least squares fit of the kinetic parameters to the model prediction using Excel's Solver as the goal-attaining iterative tool.*

| Experimental Data, Recycle_1 | | | | | | |
|---|---|---|---|---|---|---|
| Time | $S_1$ (g/IL) | $S_2$ (g/IL) | X (g/IL) | P (g/IL) | Acetate (g/IL | Productivity |
| 0 | 43.843 | 45.552 | 0.614 | 7.984 | 0.000 | - |
| 8 | 2.886 | 35.167 | 2.803 | 28.548 | 0.000 | - |
| 18 | 0.000 | 6.177 | 4.348 | 40.845 | 0.000 | 1.095 |
| 30.75 | 0.000 | 1.343 | 4.727 | 43.495 | 0.654 | 0.935 |
| 50 | 0.602 | 0.995 | 5.670 | 42.425 | 1.313 | 0.707 |
| 69 | 0.099 | 0.880 | 5.647 | 41.712 | 1.693 | 0.684 |
| 103 | 0.000 | 0.064 | 5.503 | 41.086 | 1.980 | 0.638 |
| 110 | 0.000 | 0.075 | 5.594 | 40.799 | 1.932 | 0.604 |

| Ethanol Inhibition Constants | | | |
|---|---|---|---|
| Threshold | | Maximum | |
| $P_{ix\_1}$ | 28.9 | $P_{mx\_1}$ | 86 |
| $P_{ix\_2}$ | 26.6 | $P_{mx\_2}$ | 86 |
| $P_{is\_1}$ | 42.6 | $P_{ms\_1}$ | 127 |
| $P_{is\_2}$ | 53.1 | $P_{ms\_2}$ | 127 |
| $P_{ip\_1}$ | 42.6 | $P_{mp\_1}$ | 127 |
| $P_{ip\_2}$ | 53.1 | $P_{mp\_2}$ | 127 |

| Productivity | | |
|---|---|---|
| Time | Exp | Model |
| 18 | 1.09527395 | 1.037196965 |
| 30.75 | 0.9349581 | 0.932702118 |
| 50 | 0.7068228 | 0.789189219 |
| 69 | 0.68363585 | 0.708438648 |
| 103 | 0.63807969 | 0.622324031 |
| 110 | 0.60405313 | 0.609550762 |

| Multiple Parameter Non-Linear Least Squares Fit | | | | | | | | | | | | | | | | | | | |
|---|---|---|---|---|---|---|---|---|---|---|---|---|---|---|---|---|---|---|---|
| Substrate_1 (Glucose) | | | | Substrate_2 (Xylose) | | | | Biomass (CDW) | | | | Product (Ethanol Conc) | | | | Acetate | | | |
| Time | $S_{1\_exp}$ | $S_{1\_Pred}$ | $(Exp-Pred)^2$ | Time | $S_{2\_exp}$ | $S_{2\_Pred}$ | $(Exp-Pred)^2$ | Time | $S_{2\_exp}$ | $S_{2\_Pred}$ | $(Exp-Pred)^2$ | Time | $S_{2\_exp}$ | $S_{2\_Pred}$ | $(Exp-Pred)^2$ | Time | $S_{2\_exp}$ | $S_{2\_Pred}$ | $(Exp-Pred)^2$ |
| 0 | 43.843 | 43.843 | 0 | 0 | 45.552 | 45.552 | 0 | 0 | 0.614 | 0.614 | 0 | 0 | 7.984 | 7.984 | 0 | 0 | 0.000 | 0.000 | 0 |
| 8 | 2.886 | 0.688 | 0.002513919 | 8 | 35.167 | 34.111 | 0.0005371 | 8 | 2.803 | 2.747 | 9.75149E-05 | 8 | 28.548 | 30.553 | 0.00212598 | 8 | 0.000 | 0.117 | 0.003480983 |
| 18 | 0.000 | 0.287 | 4.29372E-05 | 18 | 6.177 | 8.106 | 0.0017932 | 18 | 4.348 | 4.302 | 6.54943E-05 | 18 | 40.845 | 41.332 | 0.000125 | 18 | 0.000 | 0.375 | 0.035852538 |
| 30.75 | 0.000 | 0.211 | 2.31656E-05 | 30.75 | 1.343 | 0.606 | 0.0002616 | 30.75 | 4.727 | 4.945 | 0.001479088 | 30.75 | 43.495 | 43.556 | 1.9708E-06 | 30.75 | 0.654 | 0.721 | 0.001161348 |
| 50 | 0.602 | 0.164 | 9.99595E-05 | 50 | 0.995 | 0.457 | 0.0001398 | 50 | 5.670 | 5.362 | 0.002948748 | 50 | 42.425 | 42.374 | 1.3695E-06 | 50 | 1.313 | 1.184 | 0.004246243 |
| 69 | 0.099 | 0.142 | 9.48453E-07 | 69 | 0.880 | 0.390 | 0.0001157 | 69 | 5.647 | 5.550 | 0.000296594 | 69 | 41.712 | 41.633 | 3.2418E-06 | 69 | 1.693 | 1.573 | 0.003649257 |
| 103 | 0.000 | 0.123 | 7.84172E-06 | 103 | 0.064 | 0.335 | 3.561E-05 | 103 | 5.503 | 5.595 | 0.000262779 | 103 | 41.086 | 40.846 | 3.0495E-05 | 103 | 1.980 | 2.128 | 0.005624745 |
| 110 | 0.000 | 0.121 | 7.55414E-06 | 110 | 0.075 | 0.329 | 3.114E-05 | 110 | 5.594 | 5.576 | 9.13321E-06 | 110 | 40.799 | 40.735 | 2.1172E-06 | 110 | 1.932 | 2.223 | 0.021584816 |
| | | $RSS_{s1}$ | 0.002696326 | | | $RSS_{s2}$ | 0.0029142 | | | $RSS_x$ | 0.005159352 | | | $RSS_P$ | 0.00229018 | | | $RSS_{Ac}$ | 0.075599929 |
| Goal Term | | $RSS_{total}$ | 0.088660028 | | | | | | | | | | | | | | | | |